5-3-2018

Formulation Design and Evaluation of Amorphous and Crystalline Nanoparticles of BCS Class II and II/IV Drugs

Rajan Jog
University of Connecticut - Storrs, rajanjog2020@gmail.com

Formulation Design and Evaluation of Amorphous and Crystalline Nanoparticles of BCS Class II and II/IV Drugs

Rajan Jog, Ph.D.

University of Connecticut, 2018

In the last few decades, the pharmaceutical industry has employed a quality by design (QbD) approach for conventional drug product development to minimize errors in product optimization and validation. Lately, this has been extended to novel pharmaceutical drug products (such as nanocrystalline and nanoamorphous drug products). The present research emphasizes the design and development of stable nanocrystalline and nanoamorphous formulations of BCS class II and II/IV drugs *via* a comprehensive QbD approach. This approach was used to identify, optimize, validate and control different critical process parameters and critical formulation parameters of solid nano-formulations. The objectives of this research were to: *(1)* investigate any correlation between critical process parameters and critical formulation parameters as well as critical quality attributes using a comprehensive QbD approach; *(2)* investigate the effect of temperature and relative humidity during accelerated and/or long term stability studies; and *(3)* investigate drug-stabilizer interaction mechanisms.

Based on proof-of-concept studies, BCS class II and II/IV drugs with different physicochemical properties were utilized for the successful development of stable and robust nanocrystalline and nanoamorphous formulations. Different top-down and bottom-up manufacturing techniques: wet media milling (nanocrystalline formulations); and sonoprecipitation (nanoamorphous formulations) followed by spray drying were used to prepare the solid nanoformulations. Based on the pre-formulation studies, drug-stabilizer interaction mechanisms were investigated *via* different solid-state tools (DSC, FTIR and PXRD). The DSC data was used to determine whether drug-stabilizer interactions occurred and the type of interaction was investigated using FTIR. PXRD was used to detect the solid-state form and any polymorphic transition in the drug-stabilizer complexes. Low and intermediate molecular weight polymers, high glass transition (Tg) sugars and anionic surfactants were determined to be the strong stabilizers during processing and storage

stability of the solid nanoformulations. A quality by design approach was used to establish a correlation between critical process parameters, critical formulation parameters and critical quality attributes for the development of the robust solid nanoformulations. Critical process parameters related to manufacturing techniques: wet media milling (milling speed, milling time, pump speed); sonoprecipitation (ultra-sonication speed, time); and spray drying (inlet temperature, aspirator rate, feed flow rate) were investigated. Critical formulation parameters: drug and stabilizer concentrations were investigated. The process speed, time, inlet temperature, flow rates, drug concentrations and stabilizer concentration significantly affected the particle size and total product yield of the solid nanoformulations. Following the DoE studies, validation was performed to ensure reproducibility and robustness of different CQAs (particle size, total product yield, drug loading, moisture content and zeta potential) of solid nanoformulations prepared using the optimized and predicted process and formulation parameters. Stability studies were performed at three different conditions: 4°C, 25°C/60% RH and 40°C/75% RH for different time-points (1, 3, 6 and 12 month/s) to investigate the effect of temperature and relative humidity on the nanoamorphous and nanocrystalline formulations. Stability studies revealed the following trend: 4°C (most stable) > 25°C/60% RH > 40°C/75% RH (least stable) for the optimized spray-dried nanocrystalline and nanoamorphous formulations in terms of physicochemical attributes, crystallinity and *in vitro* dissolution testing. An array of orthogonal solid-state tools (DSC, ATR-FTIR, PLM, PXRD and AFM) were utilized to characterize the solid-state form (crystalline, amorphous, semi-crystalline and semi-amorphous) and polymorphic transitions in the freshly prepared solid nanoformulations and those stored at different stability conditions. Particle size distribution and moisture content analysis were performed *via* Zetasizer (ZS90) and Karl fisher titration, respectively. RP-HPLC was used to detect drug loading in the solid nanoformulations. The solid nano-formulations prepared *via* the comprehensive QbD approach resulted in a remarkably high total product yield (~70-80% w/w) with small, uniform and homogenous particle size (200-300 nm, 0.05-0.2 PDI). *In vitro* dissolution testing were performed to investigate the effect of pH, solid-state form, particle size, temperature and relative humidity on drug release from the solid nano-formulations. USP apparatus I and II were utilized to study and differentiate the drug release from the nanoamorphous and nanocrystalline formulations based on their solid-state form and particle size. Drug release from the solid nanoformulations followed a particle size

dependent dissolution trend. Nanoamorphous and nanocrystalline formulations showed a high dissolution rate/kinetic solubility compared to the macro-sized formulations.

To sum up, the comprehensive QbD approach performed in the present research delineates an important and time-saving strategy to develop successful, robust and stable solid nanoamorphous and nanocrystalline formulations with the desired physicochemical attributes/CQAs, solid-state form and *in vitro* and/or *in vivo* performance.

Formulation Design and Evaluation of Amorphous and Crystalline Nanoparticles of BCS Class II and II/IV Drugs

Rajan Jog

M.S. Pharm., National Institute of Pharmaceutical Education and Research, Mohali, India [2010]

B. Pharm., L. M. College of Pharmacy, Ahmedabad, India [2008]

A Dissertation

Submitted in Partial Fulfillment of the

Requirements for the Degree of Doctor of Philosophy

at the

University of Connecticut

[2018]

APPROVAL PAGE

Doctor of Philosophy Dissertation

Formulation Design and Evaluation of Amorphous and Crystalline Nanoparticles of BCS Class II and II/IV Drugs

Presented by

Rajan Jog, B. Pharm., M.S. Pharm.

Major Advisor_____
Diane J. Burgess

Associate Advisor_____
Rajeev Gokhale

Associate Advisor_____
Bodhi Chaudhuri

Associate Advisor_____
Xiuling Lu

University of Connecticut

[2018]

Dedication

To my wife, parents and grandparents

[2018]

Acknowledgements

It gives me an honor to express my earnest gratitude and deepest respect to my major advisor Dr. Diane J. Burgess. I would like to sincerely thank her for continuous motivation, enthusiasm, immense knowledge and patience. I am cordially indebted to her for providing me with this wonderful opportunity to work with her. In this journey of five years, I have learnt analytical thinking skills, leadership skills, as well as writing and presentation skills through her enriching scientific expertise. Her unimaginable passion for science has provided invaluable encouragement and strong support while working towards my dissertation. I cannot believe that five years passed so quickly, it feels like I was interviewed by her for Ph.D. just yesterday. I could not have imagined having a better advisor and mentor for my Ph.D.

I am deeply thankful to my associate advisors Dr. Rajeev Gokhale, Dr. Bodhisattwa Chaudhuri and Dr. Xiuling Lu for their valuable scientific input during my research. They are very passionate scientists, inspiring educators and encouraging mentors. Their constructive criticism, constant support, and valuable scientific guidance have provided tremendous help towards the completion of this dissertation.

I would like to thank the faculty members of the Pharmaceutics discipline, Dr. Michael Pikal, Dr. Robin Bogner, Dr. Devendra Kalonia and Dr. Raman Bahal for their support, the courses they offered and their valuable scientific input. I also would like to thank Dr. Robin Bogner and Dr. Xiuling Lu for generously providing me with access to their laboratory instruments. I am grateful for the help and support of Dean James Halpert, Dr. José Manatou (Interim Department Head), and the administrative staff of the School of Pharmacy: Ms. Leslie Lebel, Mr. Mark Armati, Ms. Kathleen Koji, Mr. Francis (Skip) Copeland, Mr James Reimen, Ms. Jacqueline Maliga, Ms. Karen Buske, Ms. Susan Corbin, and Ms. Sharon Giovenale during the course of my graduate studies.

I would like to acknowledge financial support received from the AbbVie Inc., Food and Drug Administration, and Juvenile Diabetes Research Foundation for my research projects. I am thankful to the University of Connecticut for supporting my graduate studies with assistantships and tuition waivers.

I would like to acknowledge the assistance and friendship from my past and present project-team members: Dr. Sumit Kumar, Dr. Jie Shen and Dr. Lokesh Kumar. I would also like to acknowledge the assistance from my past and present undergraduate students: Mr. Kenechi Unachukwu, Mr. Eric Pan, Ms. Belinda Sam, Ms. Helena Newandee, and Ms. Linh Ho. Their research, health and life suggestions and recommendations has helped me develop a lot.

I am grateful to the help, support, and friendship from my past and present lab-mates: Dr. Sumit Kumar, Dr. Jie Shen, Dr. Michail Kastellorizios, Dr. Bing Gu, Dr. Antonio Costa, Mr. Minsung Suh, Ms. Namita Tipnis, Ms. Janki Andhariya, Dr. Quanying Bao, Dr. Nitin Swarnakar, Ms. Carmen Zhang, Mr. Anand Gupta, Ms. Tingting Li, Ms. Jia He, and Mr. Gowtham Yenduri. They have provided a great home-like environment for me to learn, grow, and have fun along the way.

I would also like to acknowledge the support I received from my inter/intra department past and present friends: Dr. Japneet Kaur, Dr. Elizabeth Zecca, Ms. Arushi Manchanda, Ms. Laura Gonzales-Fajardo, Ms. Lauren Fontana, Mr. Derek Hargrove, Dr. Raj Mukherjee, Dr. Rui Fang, Ms. Shreya Kulkarni, Ms. Bruna Minatovicz, Mr. Andre Beringhs and Ms. Koyel Sen. Their interesting Pharmaceutics seminar feedbacks, AAPS-UCONN student chapter coffee hours and fun activities, research discussions in lab and in the 4th floor corridor and atrium are the beautiful memories that I will cherish throughout my life.

I would also like to sincerely thank my summer internship supervisor Dr. Mohamed ElSayed at Eli Lilly and company for his constant motivation and support. In addition, I would like to sincerely thank my colleagues at Eli Lilly: Dr. Huyen Tran and Ms. Alisa Klepach for their help in and out of lab. Thank you so much god for providing such motivational and supportive mentors and friends in my life. Be it academia or industry, I have been always inspired by them who has helped me to evolve as a better research scientist and overall as a better human being.

I would also like to sincerely thank my friends in USA: Dr. Lavanya Iyer, Dr. Jainik Panchal, Mr. Varun Mehta, Mr. Rishabh Kejriwal, Dr. Huseini Patanwala, Dr. Inseyah Bagasrawala, Dr. Sahil Vora, Ms. Joseline Raja and Dr. Vamsi Mudhivarthi for their support, motivation and hospitality.

I would sincerely appreciate efforts from my friends in India: Ms. Yogita Bhanwaria, Mr. Umang Jha and Mr. Sanket Shah who has constantly helped me face the worst situations in my life. I would also like to sincerely thank my second family in USA: Mr. Naresh Patel, Mrs. Saroj Patel, Ms. Ayushi Patel and Dr. Nishant Patel for their support and hospitality.

I am deeply indebted to my grandparents: Gauri and Govind Vaghela, my parents: Kusum and Trikam Vaghela, brother and sister-in-law: Swaraj and Divya Jog for their unconditional love, blessing and support. Last but not least, I am genuinely grateful to my wife and best friend, Janki Andhariya and her family for their patience, great support, affection and unconditional love.

I believe life is a journey and we are travelers with different destinations. I would like to quote few lines from the poem "Stopping by woods on a snowy evening" by Robert Frost:

"The woods are lovely, dark and deep,
But I have promises to keep,
And miles to go before I sleep,
And miles to go before I sleep."

To conclude, I would like to thank everyone, once again. Stay healthy and happy. Hope to cross paths in this beautiful journey of life.

REFERENCE:

Jon Snow *et. al. "*My watch has ended" – S6E3, Game of Thrones, 2016.

Table of Contents

LIST OF FIGURES

LIST OF TABLES

Chapter 1

Introduction, Objectives, and Specific Aims

1.1. Introduction

There has been an incredible increase in the identification of potential drug candidates based on the application of high throughput screening techniques, genomics, combinatorial chemistry and *in-silico* computational approaches [1-6]. Out of these potential drug candidates, about 70% do not have "drug-like" properties, such as good aqueous solubility and/or dissolution rates [6-9]. There are a number of approaches that are utilized to increase the dissolution rate and/or solubility and thus oral bioavailability of poorly soluble drugs. Traditional approaches to improve drug dissolution rate and/or solubility include: salt formation, as well as the use of solubilizing excipients and complexation agents. However, the success of these traditional approaches has been limited due to the taxing process of selection of highly soluble salts, as well as the requirement for large quantities of solubilizing excipients and complexation agents [10].

Crystalline or amorphous nanoparticles are an attractive alternative approach to enhance the rate of dissolution and/or the solubility of poorly soluble drugs. Discrete drug particles in the range of 100–1000 nm are defined as pharmaceutical nano-particles [11]. An increase in the exposed surface area (or surface area-to-volume ratio) by particle size reduction causes an increase in the dissolution rate and thus the oral bioavailability [12, 13]. In addition, according to the Kelvin equation, saturation solubility (in terms of vapor pressure) of the drug is dependent on the drug particle size (which translates to the curvature effect). Theoretically, reduction in particle size will cause an increase in drug solubility [14]. However, the actual increase in saturation solubility for "nanocrystalline suspensions" (colloidal size range 100–1000 nm) is marginal, approximately 2 - 10% compared to un-milled particles. Thus, nano-sized crystalline powders may not be a useful approach for solubility-limited drugs (*i.e.* solubility is rate limiting for oral bioavailability) [15]. In the case of amorphous formulations, the solubility of the drug is increased over the crystalline form due to its high-energy state (higher Gibbs' free energy) [16-18]. However, amorphous formulations are unstable and will convert to the stable crystalline form over pharmaceutically relevant timescales [19]. Generally, amorphous drugs have been formulated as micro-sized solid dispersions prepared using techniques such as spray drying and hot melt extrusion. For both of these techniques the drug is stabilized in a polymer matrix with a higher glass transition temperature than the neat polymer. Recently, nano-

sized amorphous formulations, namely "nano-amorphous" have been utilized to enhance the dissolution rates and solubilities of poorly soluble drugs. Theoretically, combining nanotechnology and amorphization approaches may offer absolute or synergistic effects in terms of solubility and dissolution rates. The advantage of amorphous versus crystalline nanoparticles is the considerably higher kinetic solubility of amorphous nanoparticles, which can be as much as 10 to 1600 fold. Although, a significant amount of research has been carried out on amorphous nanoparticles, there are no marketed drug products available, till date. The major formulation challenge associated with amorphous nanoparticles is their stability, which depends on: API properties such as the melting temperature (T_m), T_m/T_g ratio, and the properties of the polymer or stabilizer utilized [20-24]. Amorphous systems have higher free volume or enthalpy as well as high Gibbs-free energy. Accordingly, these systems are unstable and tend to crystallize to a stable polymorph of the drug, which typically would have lower solubility. The crystallization time of an amorphous drug is a kinetically controlled process (which can vary from seconds to years) and depends on several factors such as, storage temperature and moisture content. Various approaches have been used to stabilize the amorphous form of drugs. For example, crystallization inhibitors (high Tg polymers/sugars) can be added and/or the formulation may be stored at low temperature (50°C below the drug Tg) and at low moisture/humidity conditions [17].

Broadly, there are two basic methods to manufacture nanoparticles; (i) a "top-down approach" (*i.e.* milling/grinding of the particles to achieve the required size) and (ii) a "bottom-up approach" (*i.e.* precipitation of drug from a solvent to an anti-solvent system) [12]. The top-down approach is very time consuming and usually leads to crystalline particles whereas the bottom-up approach is less time consuming and usually leads to amorphous particles due to fast evaporation of the solvent and thus precipitation of the API as amorphous particles.

The mechanism by which nanoparticles improve the dissolution rate and bioavailability of poorly water-soluble active pharmaceutical ingredients (APIs) [BCS class II and II/IV] is the enhanced surface area to volume ratio as described by the Noyes-Whitney equation [25]. According to the Noyes-Whitney equation the dissolution rate J is given by the following equation;

$$J = \frac{DA}{h}\,(C_s - C)$$

[J = dissolution rate, D = diffusion coefficient of drug, A = surface area of the dissolving solid, h = thickness of the diffusion layer, C_s = saturation solubility of the compound in the dissolution medium, C = concentration of the drug in the medium at different time points during dissolution]

Increase in the surface-to-volume ratio and thus the dissolution rate of nanoparticles improves their pharmacokinetic properties in terms of: increased rate and extent of release and absorption; rapid onset of action; reduced side effects and improved clinical performance [12, 25, 26]. Concurrently, the drug saturation solubility is increased as theoretically predicted by the Ostwald–Freundlich equation as below;

$$ln\frac{C_{s,r}}{C_{s,\infty}} = \frac{2\gamma V_m}{rRT}$$

[$C_{s,r}$ and $C_{s,\infty}$ (g/L) = solubility of drug particles with radii r and r =∞ (m), respectively, c = interfacial tension between the drug particles and the medium (N/m), V_m = drug molar volume (m^3/mol), R = gas constant (8.314 J/ mol K), T = absolute temperature (K)]

The importance of crystalline nanosuspensions to the pharmaceutical industry can be judged by the fact that seventeen formulations are already on the market and approximately 10 - 15 are in different stages of clinical trials [27]. However, one of the major concerns with nanosuspension formulations is the preservation of their physical and chemical stability in aqueous medium [28, 29]. Experimental and computational approaches to estimate solubility and permeability in drug discovery and development settings are being investigated. Being a liquid dosage form, nanosuspensions are more susceptible to both physical instability (due to crystal growth and agglomeration) and to chemical instability (due to degradation of the active pharmaceutical ingredient(s)), when compared to solid dosage forms. In fact, of all the marketed formulations, only Megace ES is in the suspension form (nano-particulate suspension of megesterol acetate). All others are prepared as nanosuspension-based solid dosage forms, as a way to overcome instability problems. Liquid nanosuspensions can be converted into solid dosage forms by drying to obtain a powder of nano-sized drug particles, which can be processed into conventional dosage forms such as tablets or capsules. Spray and freeze-drying are the most common methods of removing water from aqueous systems [28, 29].

In this proposed research, different processes (wet media milling, sonoprecipitation and spray drying) were used to prepare robust and stable nanoamorphous and nanocrystalline

formulations (BCS class II and II/IV drugs) *via* a comprehensive QbD approach. Multiple linear regression and statistical ANOVA studies were applied to establish whether correlations exists between the different critical process parameters, critical formulation parameters and critical quality attributes. Several QbD approaches have been applied to conventional drug products (tablet, capsule, *etc.*), however, no comprehensive QbD has been reported till date to understand novel drug product development (such as amorphous and crystalline nanoparticles). There are individual process and formulation QbD studies reported in literature but comprehensive QbD including multiple manufacturing process optimization in combination with formulation QbD has not been reported for solid nano-formulations.

1.2. Objectives

The objectives of this research are to: *(1)* investigate whether correlations can be established between critical process parameters (wet media milling – speed, time; sonoprecipitation – speed, time; spray drying – inlet temperature, aspirator rate, feed flow rate) and critical formulation parameters (drug and stabilizer concentrations) as well as critical quality attributes (particle size, total product yield, moisture content, drug loading) using a comprehensive QbD approach; *(2)* investigate the effect of temperature and relative humidity (4°C, 25°C/60% RH and 40°C/75% RH) during accelerated and/or long term stability studies (1, 3, 6, and 12 month/s); and *(3)* investigate the drug-stabilizer interaction mechanism *via* an array of orthogonal solid-state tools (DSC, ATR-FTIR and PXRD). This information will aid in developing robust and stable nanoamorphous/nanocrystalline drug products with an improved shelf-life. This research will further help in minimizing the risks of product failure in terms of physicochemical attributes governing the therapeutic efficacy of poorly soluble compounds.

1.3. Specific Aims

The following specific aims were developed to achieve the objectives mentioned above:

Specific Aim I: (Chapter 2)

Solid state drug-polymer miscibility studies using the model drug ABT-102

Specific Aim II: (Chapter 3)

Formulation design and evaluation of amorphous ABT-102 nanoparticles

Specific Aim III: (Chapter 4)

Comprehensive quality by design approach for stable nanocrystalline drug products

Specific Aim IV: (Chapter 5)

Nanoamorphous drug products – design and development

*The stability studies were performed based on the ICH Q1A(R2) guidelines. The measured relative humidity at 4°C was 6-6.5%.

1.4. References:

1. Lipinski C. Poor aqueous solubility-an industry wide problem in drug discovery. *Am Pharm Rev*. 2002;5(3):82-85.
2. Lipinski CA, Lombardo F, Dominy BW, Feeney PJ. Experimental and computational approaches to estimate solubility and permeability in drug discovery and development settings. *Advanced Drug Delivery Reviews*. 2012;64:4-17.
3. Lipinski CA. Drug-like properties and the causes of poor solubility and poor permeability. *Journal of pharmacological and toxicological methods*. 2000;44(1):235-249.
4. Gribbon P, Andreas S. High-throughput drug discovery: what can we expect from HTS? *Drug Discovery Today*. 2005;10(1):17-22.
5. Hann MM, Oprea TI. Pursuing the leadlikeness concept in pharmaceutical research. *Current Opinion in Chemical Biology*. 2004;8(3):255-263.
6. Yamashita S. *In vitro-in vivo* correlations: Application to water insoluble drugs. *BULLETIN TECHNIQUE-GATTEFOSSE*. 1998:25-32.
7. Caldwell GW, Ritchie DM, Masucci JA, Hageman W, Yan Z. The new pre-preclinical paradigm: compound optimization in early and late phase drug discovery. *Current topics in medicinal chemistry*. 2001;1(5):353-366.
8. Prentis RA, Lis Y, Walker SR. Pharmaceutical innovation by the seven UK-owned pharmaceutical companies (1964-985). *British journal of clinical pharmacology*. 1988;25(3):387-396.
9. Hartmann T, Schmitt J, Rohring C, Nimptsch D, Noller J, Mohr C. ADME related profiling in 96 and 384 well plate format-a novel and robust HT-assay for the determination of lipophilicity and serum albumin binding. *Current drug delivery*. 2006;3(2):181-192.
10. http://www.accessdata.fda.gov/drugsatfda_docs/label/2009/020966s022lbl.pdf.

11. Verma S, Huey BD, Burgess DJ. Scanning probe microscopy method for nanosuspension stabilizer selection. *Langmuir*. 2009;25(21):12481-12487.
12. Merisko-Liversidge E, Liversidge GG, Cooper ER. Nanosizing: a formulation approach for poorly-water-soluble compounds. *European Journal of Pharmaceutical Sciences*. 2003;18(2):113-120.
13. Merisko-Liversidge EM, Liversidge GG. Drug nanoparticles: formulating poorly water-soluble compounds. *Toxicologic pathology*. 2008;36(1):43-48.
14. Thomson W. 4. On the Equilibrium of Vapour at a Curved Surface of Liquid. *Proceedings of the Royal Society of Edinburgh*. 1872;7:63-68.
15. Van Eerdenbrugh B, Vermant J, Martens JA, Froyen L, Humbeeck JV, Van den Mooter G, Augustijns P. Solubility increases associated with crystalline drug nanoparticles: methodologies and significance. *Molecular pharmaceutics*. 2010;7(5):1858-1870.
16. Chiou WL, Riegelman S. Oral absorption of griseofulvin in dogs: Increased absorption viasolid dispersion in polyethylene glycol 6000. *Journal of pharmaceutical sciences*. 1970;59(7):937-942.
17. Hancock BC, Parks M. What is the true solubility advantage for amorphous pharmaceuticals? *Pharmaceutical research*. 2000;17(4):397-404.
18. Leuner C, Dressman J. Improving drug solubility for oral delivery using solid dispersions. *European journal of Pharmaceutics and Biopharmaceutics*. 2000;50(1):47-60.
19. Serajuddin A. Solid dispersion of poorly water-soluble drugs: Early promises, subsequent problems, and recent breakthroughs. *Journal of pharmaceutical sciences*. 1999;88(10):1058-1066.
20. Chen X, Young TJ, Sarkari M, Williams RO, Johnston KP. Preparation of cyclosporine A nanoparticles by evaporative precipitation into aqueous solution. *International journal of pharmaceutics*. 2002;242(1):3-14.
21. Lindfors L, Skantze P, Skantze U, Rasmusson M, Zackrisson A, Olsson U. Amorphous drug nanosuspensions. 1. Inhibition of Ostwald ripening. *Langmuir*. 2006;22(3):906-910.

22. Zhang J-Y, Shen Z-G, Zhong J, Hu T-T, Chen J-F, Ma Z-Q, Yun J. Preparation of amorphous cefuroxime axetil nanoparticles by controlled nanoprecipitation method without surfactants. *International journal of pharmaceutics*. 2006;323(1):153-160.
23. Wang J-X, Zhang Q-X, Zhou Y, Shao L, Chen J-F. Microfluidic synthesis of amorphous cefuroxime axetil nanoparticles with size-dependent and enhanced dissolution rate. *Chemical Engineering Journal*. 2010;162(2):844-851.
24. Zhu W-Z, Wang J-X, Shao L, Zhang H-x, Zhang Q-x, Chen J-F. Liquid antisolvent preparation of amorphous cefuroxime axetil nanoparticles in a tube-in-tube microchannel reactor. *International journal of pharmaceutics*. 2010;395(1):260-265.
25. Liversidge GG, Cundy KC. Particle size reduction for improvement of oral bioavailability of hydrophobic drugs: I. Absolute oral bioavailability of nanocrystalline danazol in beagle dogs. *International journal of pharmaceutics*. 1995;125(1):91-97.
26. Pilcer G, Sebti T, Amighi K. Formulation and characterization of lipid-coated tobramycin particles for dry powder inhalation. *Pharmaceutical research*. 2006;23(5):931-940.
27. Kumar S, Burgess DJ. Nanosuspensions. In Wright JC, Burgess DJ, editors. Long acting injections and implants, ed., New York: Springer.2012; p 239-261.
28. Lee J. Drug nano- and microparticles processed into solid dosage forms: physical properties. *Journal of pharmaceutical sciences*. 2003;92(10):2057-2068.
29. Van Eerdenbrugh B, Froyen L, Van Humbeeck J, Martens JA, Augustijns P, Van den Mooter G. Drying of crystalline drug nanosuspensions - the importance of surface hydrophobicity on dissolution behavior upon redispersion. *European Journal of Pharmaceutical Sciences*. 2008;35(1):127-135.

Chapter 2

Solid-State Drug-Polymer Miscibility Studies Using the Model Drug ABT-102

ABSTRACT

Amorphous solid dispersions typically suffer storage stability issues due to: their amorphous nature, high drug loading, uneven drug:stabilizer ratio and plasticization effects as a result of hygroscopic excipients. An extensive solid state miscibility study was conducted to aid in understanding the mechanisms involved in drug/stabilizer interactions. ABT-102 (model drug) and nine different polymers with different molecular weights and viscosities were selected to investigate drug/polymer miscibility. Three different polymer:drug ratios (1:3, 1:1 and 3:1, w/w) were analyzed using: DSC, FTIR and PXRD. Three different techniques were used to prepare the amorphous solid dispersions: serial dilution, solvent evaporation and spray drying. Spray drying was the best method to obtain amorphous solid dispersions. However, under certain conditions amorphous formulations could be obtained using solvent evaporation. Melting point depression was used to calculate interaction parameters and free energy of mixing for the various drug polymer mixtures. The spray dried solid dispersions yielded a negative free energy of mixing which indicated strong drug-polymer miscibility compared to the solvent evaporation and serial dilution method. Soluplus was the best stabilizer compared to PVP and HPMC, which is probably a consequence of strong hydrogen bonding between the two C=O moieties of soluplus and the drug N-H moieities.

2.1. INTRODUCTION

Drug dissolution and gastrointestinal permeability are the important factors controlling the rate and extent of drug absorption. This forms the basis of the biopharmaceutics drug classification scheme (BCS class I, II, III and IV), which correlates *in vitro* drug product dissolution and *in vivo* bioavailability [1]. Dissolution is the rate-limiting step for gastrointestinal absorption for most BCS class II drugs [2]. There are different approaches (solid dispersion, solid lipid nanoparticles, crystalline nanoparticles, liposomes, cyclodextrin complexes, *etc.*) in the pharmaceutical world to enhance the dissolution rate and increase the oral bioavailability of these poorly soluble drugs. Solid dispersion technology is a well-established method to prepare the most stable solid formulations [3, 4].

Solid dispersion incorporate one or more crystalline or amorphous active ingredient in a solid matrix provided by an inert carrier [5]. These formulations increase the dissolution rate and oral bioavailability of poorly soluble drugs, with an added advantage of high drug loading [6]. Commercially, three different methods are used to prepare solid dispersions (*i.e.* spray drying, hot melt extrusion and co-precipitation) [7-9]. Additionally, solid dispersions can be prepared using solvent evaporation and fusion techniques [10, 11]. Generally, all these methods result in the production of amorphous solid dispersions (ASDs), which significantly enhance the solubility and bioavailability compared to the crystalline form of the drug [12]. Additionally, these methods might also result in formation of semi-crystalline or crystalline systems. The amorphous form of drug has drawn considerable attention, as theoretically it represents the most energetic solid state, and may provide the advantages in terms of solubility and bioavailability [13]. Recently, amorphous solid dispersions have been successfully developed to thermodynamically or kinetically stabilize the amorphous form of drugs and yield drug products with enhanced bioavailability [14-16]. Among the various techniques for preparing solid dispersions, hot-melt extrusion (HME) has stood out with obvious advantages due to its single-step, simple and organic solvent-free preparation process, and gained increasing popularity [6, 17]. However, the elevated processing temperature has certainly limited the application of HME for heat-sensitive drugs, and so far only a few number of studies focused on this problem [18-20]. Furthermore, amorphous solid dispersions have associated physical and chemical instability issues which become particularly apparent on scale up [21]. Selection of the best excipient at the formulation development stage may prevent the risk associated with these instabilities. Hence, it is very important to study drug stabilizer interactions (strong/weak) at the molecular level to predict the stability/miscibility of the drug in a given polymer matrix. Such understanding would allow a significant improvement over the conventional trial and error strategies for stabilizer selection.

Interactions between different stabilizers and poorly soluble drugs, has been reported in the literature for amorphous solid dispersions. Different solid state analytical tools such as DSC, FTIR and PXRD have been used to characterize both strong and weak interactions [22-27]. In the present study the effect of the molecular weight of three different polymers (PVP, HPMC and soluplus) on interaction with the drug – ABT-102 (BCS class II) were

investigated. Nine different polymers (PVP K-17, PVP K-25, PVP K-30, PVP K-90, HPMC E3, HPMC E5, HPMC E15, HPMC E50 and soluplus) with different molecular weights and viscosities were selected to investigate drug-polymer miscibility. Three different ratios of drug:polymer (1:3, 1:1 and 3:1, w/w) were studied using solid state characterization tools (DSC, FTIR and PXRD).

2.2. MATERIALS

Poly (1-vinyl-2-pyrrolidone) (PVP) – K17 and K90 were gifted by Sigma Chemicals. Poly (1-vinyl-2-pyrrolidone) (PVP) – K25, K30 (USP, JP, EP) and soluplus (polyvinyl caprolactam-polyvinyl acetate-polyethylene glycol graft copolymer) were gifted by BASF. Hydroxy propyl methyl cellulose (Methocel premium LV) – E3, E5, E15 and E50 were donated by the Dow Chemical Company. The chemical structures of the polymers and drug are shown in **Table 2.1**. Methanol HPLC grade was purchased from Fisher Scientific. ABT-102 was provided by AbbVie Pte. Ltd. The molecular weights and viscosities of the different polymers are shown in **Table 2.2**.

2.3. METHODS

2.3.1. Method of preparation of the solid dispersions

Nine different polymers (*i.e.* PVP K-17, PVP K-25, PVP K-30, PVP K-90, HPMC E3, HPMC E5, HPMC E15, HPMC E50 and soluplus) were selected to investigate drug-polymer miscibility. Based on the knowledge that polymers with carbonyl groups have a strong interaction ability with drugs containing amine groups, polymers containing carbonyl groups (PVPs) were selected. Additionally, polymers devoid of carbonyl groups (HPMCs) were selected to facilitate understanding of drug-polymer interactions. Furthermore, a polymer containing two carbonyl groups (soluplus) was also selected to investigate whether a better drug-polymer interaction may occur with additional carbonyl moieties. A wide range of PVPs and HPMCs (different molecular weights of both polymers) were selected for this study to compare the interaction of low, intermediate and high molecular weight polymers with the drug. The model drug selected for the study was ABT-102 which contains three –NH groups.

2.3.1.1. Spray drying

The polymer and drug were accurately weighed using an analytical balance. The mixtures were transferred into 250 mL Schott glass bottles. 37.5 mL, 25 mL and 12.5 mL of methanol were added to the polymer:drug ratios 1:3, 1:1 and 3:1, w/w, respectively to completely dissolve the mixtures. The solutions were spray dried using a Buchi B-290, bench-top spray dryer to prepare the amorphous solid dispersions. Briefly, the spray drier was equilibrated using 100% methanol. Once equilibrated, the solutions were pumped into the drying chamber using a peristaltic pump (feed rate about 20 mL/min). All the samples were spray dried at inlet and outlet temperatures of 75°C and 55°C, respectively. Gas flow (atomizing air) was kept constant at 40 mm Hg (air flow approximately 600 L/h) for all the samples. The dried samples were immediately transferred from the collection chamber and analyzed using solid state characterization tools (DSC, FTIR and PXRD). All samples were prepared in triplicate. Additionally, the standards of neat polymers and neat drug were also dissolved in appropriate volumes of methanol and these were spray dried to obtain standards for spray dried neat polymers and drug.

2.3.1.2. Solvent evaporation

The polymer and drug were accurately weighed using an analytical balance. The mixtures were transferred into uncapped glass tubes. A fixed volume of methanol was added to the polymer:drug mixtures as follows: 3.75 mL, 2.5 mL and 1.25 mL of methanol were added to the polymer:drug ratios 1:3, 1:1 and 3:1, w/w, respectively to completely dissolve the mixtures. The tubes were placed in a nitrogen evaporator assembly for approximately 2-3 h to remove the solvent. After complete solvent removal, the dry films were analyzed using the solid state characterization tools (DSC, FTIR and PXRD). All samples were prepared in triplicate. The samples were vacuum dried for 12 h and stored in uncapped glass tubes at 40°C for 12 h. Additionally, standards of neat polymers and drug were also dissolved in appropriate volumes of methanol and post solvent removal, the samples were vacuum dried for 12 h and stored in uncapped glass tubes at 40°C for 12 h.

2.3.1.3. Physical mixtures

The polymer and drug were accurately weighed using an analytical balance and mixed homogeneously *via* serial dilution. The mixture was transferred into uncapped glass tubes. For each polymer, three different polymer to drug ratios were mixed; 1:3, 1:1 and 3:1, w/w. The powder mixtures were vacuum dried for 12 h and following that stored in uncapped glass tubes at 40°C for a further 12 h. The samples were analyzed using the solid state characterization tools (DSC, FTIR and PXRD). All samples were prepared in triplicate. Additionally, standards of neat polymers and drug were similarly vacuum dried for 12 h and stored in uncapped glass tubes at 40°C for 12 h.

2.3.2. Characterization

2.3.2.1. Differential scanning calorimetry

DSC was performed using a TA Q1000 calorimeter (TA instruments, New Castle, DE, USA) equipped with a refrigerated cooling accessory. The instrument was calibrated for enthalpy and heat capacity using indium and sapphire, respectively. A constant weight of 10 mg of the samples were sealed in non-hermetic pans and analyzed. The heating rate was maintained at 10 °C/min from 0°C to 235 °C. Nitrogen gas was used for purging at a flow rate of 50 mL/min. Data were analyzed using TA universal analysis software.

2.3.2.2. Fourier transform infrared spectroscopy

IR spectroscopy was performed using a Nicolet FTIR (iS5 FTIR, Thermo Scientific) spectrometer attached with an attenuated total reflectance (ATR) accessory. The samples were placed on the crystal window (Germanium) and compressed lightly using the pressure clamp. Spectra were recorded over a range of 400–4000 cm^{-1} with a resolution of 4 cm^{-1}, for 128 parallel scans. Data analysis was performed using Omnic® 6.0a software (Thermo Nicolet Corporation).

2.3.2.3. Powder X-ray diffraction

PXRD (wide-angle X-ray scattering) was used to study the presence of crystallinity in the samples prepared using the above three methods. X-ray diffraction patterns were obtained using an X-ray diffractometer (Model D5005, Bruker AXS Inc., Madison, WI) with Cu-kα

radiation, a voltage of 40 kV, and a current of 40 mA. All the scans were performed with a scanning rate of 2°/minute from 5° to 40° at 2θ ranges.

2.4. RESULTS & DISCUSSIONS

The polymer:drug physical mixtures were easily retrieved for solid state analysis. However, the neat polymers and polymer:drug ratio of 3:1, w/w (exception - soluplus:drug) were difficult to retrieve post solvent evaporation due to the formation of a rigid glassy structure on the walls of the glass tubes, thus solid state analysis for these samples could not be performed. All physical mixtures showed drug in the crystalline form, dispersed in the polymer matrix. Samples prepared by solvent evaporation showed drug in crystalline form, dispersed in the polymer matrix at a higher drug:polymer ratio (3:1, w/w). However, all spray dried samples resulted in molecular level amorphous dispersions. Solid state analysis of the other samples were performed using DSC, FTIR and PXRD.

2.4.1. Differential scanning calorimetry

When the chemical potential of the pure crystalline drug is equal to the chemical potential of the molten drug, an endothermic event (the melting point) is observed in the DSC thermogram [30]. It has been established that strong interactions produce large melting point depressions while weak interactions, result in smaller melting point depressions [31]. However, if the drug-polymer mixtures are immiscible, the chemical potential of the molten drug remains unchanged in the presence of polymer, resulting in no melting point depression.

2.4.1.1. PVP

PVP is a carbonyl group containing polymer. The melting point depression of polymer-drug mixtures using three different manufacturing methods (serial dilution, solvent evaporation and spray drying) and three different PVPs:drug ratios are shown in figure 2.1. Lower molecular weight PVP (PVP K17) resulted in a significant shift (lowering) in the melting point peak (229.81±0.19°C) compared to the higher molecular weight PVP (PVP K90), for all three polymer:drug ratios (1:3, 1:1 and 3:1, w/w). Furthermore, the intermediate molecular weight PVP's (PVP K25 and PVP K30) also resulted in melting point depression, indicating possible interaction between the polymer and the drug. It was observed that for

polymer:drug mixtures prepared using all three methods (spray drying, solvent evaporation and physical mixture), the lower molecular weight PVP's showed a greater ability to interact with the drug compared to the higher molecular weight PVP. The presence of the carbonyl group (C=O) in PVP (PVP K17, K25 and K30) enhances interaction with drugs containing N-H groups, resulting in strong hydrogen bonding. In the case of the high molecular weight PVP (PVP K90), the high viscosity of this polymer is probably an inhibiting factor, limiting drug-polymer interaction. For the spray drying experiments, the DSC thermograms showed the absence of melting endotherms for polymer to drug ratios of 1:3 and 1:1, w/w. Similarly, for the solvent evaporation experiment, the DSC thermograms showed the absence of melting endotherms for the polymer to drug ratio of 3:1, w/w. This indicates a complete conversion from the crystalline to the amorphous form.

2.4.1.2. HPMC

HPMC is devoid of carbonyl groups. The melting point depression using three different manufacturing methods (serial dilution, solvent evaporation and spray drying) and three different HPMCs:drug ratios are shown in figure 2.2. For the physical mixtures, lower molecular weight HPMC's (HPMC E3 and E5) resulted in a minor shift (~224-227°C) in the drug melting peak (229.81±0.19°C) compared to the higher molecular weight HPMC's (HPMC E15 and E50) which showed no melting peak shift (~228-230°C), for two polymer:drug ratios (1:3 and 1:1, w/w). The minor shifts in the drug melting peak in the presence of low molecular weight HPMCs may be due to weak hydrogen bonding interactions between the OH group of the polymer and NH group of the drug. However, at the polymer:drug ratio of 3:1, w/w the drug melting peak shift was significant (~ 10°C lower than the drug melting point) for the lower molecular weight HPMC's (HPMC E3 and E5) indicating a strong interaction between the polymer and the drug. In addition, a minor shift in the melting peak was observed for the higher molecular weight HPMC's (HPMC E15 and E50) (~224°C). For the solvent evaporation experiment, the melting endotherm of the polymer:drug mixture (3:1, w/w) resulted in a significant shift in the drug melting endotherm for the lower molecular weight HPMC's (HPMC E3 and E5) (~216°C) indicating a strong interaction between the polymer and the drug. Again the high molecular weight HPMC's (HPMC E15 and E50) resulted in a minor shift in the melting peak

(~223°C). The 1:3 and 1:1, w/w drug:polymer ratios showed a minor shift (~224°C) for the lower molecular weight HPMC's (HPMC E3 and E5) and no shift (~227°C) for the higher molecular weight HPMC's (HPMC E15 and E50). For the spray dried samples, it was observed that the polymer:drug ratio of 3:1, w/w resulted in a significant shift in the drug melting endotherm for all molecular weight HPMC's. Again, the interaction appeared to be stronger for the low molecular weight HPMCs with melting point depressions of ~15-20°C compared to the high molecular weight HPMCs (~10°C). The polymer:drug ratio of 1:3, w/w did not show any significant change in the melting point for lower and higher molecular weight HPMCs. However, for the polymer:drug ratio of 1:1, w/w, HPMC E3 showed the strongest interaction with the drug, reducing the melting point to ~212°C. HPMC E5 and E50 also shifted the drug melting to ~215°C. HPMC E15 resulted in the weakest interaction with the drug at the polymer:drug ratio of 1:1, w/w, shifting the melting to ~217°C.

2.4.1.3 Soluplus

Soluplus contains two carbonyl moieities. The melting point depression observed for the three different manufacturing methods (serial dilution, solvent evaporation and spray drying) and the three different soluplus:drug ratios are shown in figure 2.3. No interactions were observed in the polymer:drug physical mixtures. This was confirmed by no change in the melting endotherms ~227-229°C for the three polymer:drug ratios of; 3:1, 1:1 and 1:3, w/w, compared to the neat drug melting endotherm (~229.81°C). In the case of polymer:drug samples prepared *via* solvent evaporation interactions were observed. However, these were significantly less compared to those observed between the drug and the HPMCs for soluplus:drug ratios of 1:1 and 1:3, w/w. The polymer:drug ratio of 3:1, w/w resulted in the strongest interaction as observed by a greater shift in the melting endotherm (to ~216°C) compared to the 1:3 and 1:1, w/w ratios (~222-223°C). The polymer-drug interactions appeared to be strongest in the case of solid dispersions prepared using spray drying for all three polymer:drug ratios. However, for the polymer:drug ratio of 3:1, w/w a melting endotherm was not observed, indicating that the polymer:drug mixture completely converted from the crystalline to the amorphous form at this ratio. The melting peak shifted to ~ 207 and ~ 216°C for polymer:drug ratios of 1:1 and 1:3, w/w, respectively. These were the strongest interactions observed between the drug and soluplus. The presence of two

carbonyl groups (C=O) in soluplus may result in a strong interaction with the multiple N-H moieities present in the drug, allowing for strong hydrogen bonding.

2.4.2 Thermodynamics of mixing

In amorphous solid dispersions containing a drug-polymer system, miscibility is defined as formation of the single phase amorphous system through drug-polymer mixing. A totally miscible system will achieve molecular level mixing of the drug and the polymer leading to a significant increase in the physical stability of the drug. Such molecular level mixing of the drug and the polymer will decrease the chemical potential of the drug, thus minimizing/preventing the thermodynamic driving force for crystallization [32-34].

2.4.2.1 Melting Point Depression Approach

The Flory-Huggins equations for polymer-solvent system interaction can be extended to drug-polymer systems, in order to calculate the polymer-drug interaction parameter from the melting point depression of the drug by the polymer [35]. Equation 1 represents the relationship between melting point depression of drug and the polymer-drug interaction parameter.

$$\left(\frac{1}{T^{mix}{}_{M}} - \frac{1}{T^{pure}{}_{M}}\right) = -\frac{R}{\Delta H_{fus}}\left[ln\emptyset_{drug} + \left(1 - \frac{1}{m}\right)\emptyset_{polymer} + \chi\emptyset^{2}{}_{polymer}\right] \quad (1)$$

where, $T^{mix}{}_{M}$ is the melting temperature of the drug in the presence of the polymer, $T^{pure}{}_{M}$ is the melting temperature of the drug in the absence of the polymer, ΔH_{fus} is the heat of fusion of the pure drug, and m is the ratio of the volume of the polymer to that of the lattice site (volume of the drug), χ is the interaction parameter (unit less), ϕ_{drug} and $\phi_{polymer}$ are the volume fractions of the drug and polymer, respectively. χ has an enthalpy component (defining the relative strength of adhesive and cohesive interactions) and an entropic component (which varies with composition and temperature) [30, 36, 37].

The equation for the free energy of mixing (ΔG_m in joules) for an API-polymer system can be described according to equation 2, on adding the Flory-Huggins interaction parameter, χ to account for the enthalpy of mixing. The Flory-Huggins interaction parameter was estimated using the melting point depression method.

$$\frac{\Delta G_{M}}{RT} = n_{drug}ln\emptyset_{drug} + n_{polymer}ln\emptyset_{polymer} + n_{drug}\emptyset_{polymer}\chi \quad (2)$$

where, n_{drug} is the number of moles of drug, $n_{polymer}$ is the number of moles of polymer, ϕdrug is the volume fraction of the drug, $\phi_{polymer}$ is the volume fraction of the polymer, χ is the interaction parameter, R is the gas constant, and T is the absolute temperature.

The interaction parameters and free energy of mixing for the different polymer-drug mixtures prepared via spray drying, solvent evaporation and serial dilution were calculated as follows;

2.4.2.1.1 Spray drying

The drug-polymer systems which exhibits a negative interaction parameter value, indicates strong miscibility. Furthermore, the free energy of mixing is positive for large positive interaction parameters indicating immiscibility, whereas the free energy of mixing is negative for small values of the interaction parameter, indicating miscibility [38]. As observed from figure 2.4(a), the low (PVP K17) and intermediate (PVP K25 and K30) molecular weight PVPs, all four grades of HPMCs and soluplus resulted in negative interaction parameter values, indicating strong miscibility with ABT-102 at polymer:drug ratio of 1:3, w/w. This result is reflected in the free energy of mixing data (figure 2.4(b)), as negative free energy of mixing was observed for drug-polymer mixtures that exhibited small interaction parameter values. The blends of ABT-102 and PVP K90 showed a positive interaction parameter value and a positive free energy of mixing predicting immiscibility. A plot of interaction parameter *vs*. the volume fraction of the polymers, as shown in figure 2.4c, yielded a linear relationship at low polymer weight fractions for low and intermediate molecular weight PVPs and soluplus, with a slope equal to χ. However, for all four HPMC grades and for the high molecular weight PVP, a non-linear relationship was observed with increase in the volume fraction of polymer. The non-linearity over the entire concentration range indicates escalating unfavorable kinetics of drug-polymer interaction and that the interaction parameter is composition dependent [30].

2.4.2.1.2 Solvent evaporation

As observed in Figure 2.5(a and b), samples prepared via solvent evaporation using PVP K17 and soluplus at a polymer:drug ratio of 1:3, w/w showed a negative interaction parameter and a negative free energy of mixing indicating strong miscibility of ABT-102

with the two polymers (PVP K17 and soluplus). The plot of interaction parameter *vs*. volume fraction of polymers (figure 2.5c) resulted in a non-linear relationship with increase in the volume fraction of the polymers.

2.4.2.1.3 Physical mixture

As observed in Figure 2.6(a and b), the samples prepared *via* serial dilution using PVP K17 at a polymer:drug ratio of 1:3, w/w showed a negative interaction parameter and a negative free energy of mixing indicating strong miscibility of ABT-102 with the two polymers (PVP K17 and soluplus). This indicates that even in the physical mixture for low molecular weight PVP, a strong interaction is observed. This result was different from the other polymers used to prepare the physical mixture samples *via* serial dilution. The other polymers resulted in a higher interaction parameter value and a positive free energy of mixing indicating weak miscibility or absence of miscibility. The plot of interaction parameter *vs*. volume fraction of polymers (figure 2.6c) resulted in a non-linear relationship with increase in the volume fraction of the polymers.

2.4.3. Fourier transform infrared spectroscopy

FTIR has been extensively used to study polymer-drug miscibility. Any change in the absorbance (shift in the wavenumber or change in the intensity) observed in the formulations compared to the neat drug or drug-polymer physical mixtures provides information that there is interaction between the drug and the polymer. These interactions can be of various types: hydrogen bonding, covalent bonding, ionic interaction, *etc*. The presence of hydrogen bonding in solid dispersions can be confirmed using FTIR by comparing the FTIR spectra of solid dispersions (formulations) with those of the neat drug and polymers. Polymer-drug miscibility was studied for the nine different polymers as described in section 2.3.1. The characteristic FTIR absorbance bands for ABT-102, PVP, soluplus and HPMC are listed in **Table 2.3**. Figure 2.7, 2.8, 2.9, 2.10, 2.11, 2.12, 2.13, 2.14 and 2.15 are shown in supplementary material.

2.4.3.1. Spray drying

The miscibility of the polymer:drug samples prepared using spray drying were superior compared to those prepared using the serial dilution and solvent evaporation techniques.

The polymer and drug in solution form precipitate together to form a solid powder with superior homogeneity due to rapidity of the spray drying process, compared to the solvent evaporation and serial dilution methods. In spray drying, the organic solvent containing the polymer:drug mixture (in dissolved state) is sprayed into fine droplets. The consequent evaporation of the organic solvent from the dispersed droplets, results in the conversion of the crystalline drug to mostly amorphous solid dispersions, due to the rapid precipitation. As a result of the higher free energy and higher molecular mobility of amorphous systems, interaction between the drug and the polymer is enhanced. The type of polymer and the polymer:drug ratio play an important role in maximizing stability. Different types of molecular level interactions such as hydrogen bonding and other weak hydrophobic interactions have been reported in the literature for spray dried solid dispersions [33, 43].

2.4.3.1.1. PVP

From figure 2.7, it can be observed that, with increase in the PVP:drug ratio from 1:3 to 3:1, w/w, band broadening was observed between 3700-3100 cm^{-1} compared to the sharp peak associated with the neat drug. This band broadening may be a result of: 1) the high level of interaction obtained in the drug:polymer solid dispersion; and/or 2) masking of the drug peak by the high concentration of the polymer. This interaction appears to be H-bonding, since N-H stretching and O-H stretching are observed in the drug and PVP, respectively. Additionally, with increase in the PVP:drug ratio from 1:3 to 3:1, w/w, there was a decrease in the absorption intensity between: 1600-1500 cm^{-1} (due to C-C stretching – aromatic); 1400-1200 cm^{-1} (due to C-H bending); and 1100-600 cm^{-1} (due to C-H aromatic out of plane bending and C-C stretching). These reductions in the absorption intensities indicate the presence of weak hydrophobic interactions between the drug and PVP. The spray dried PVP:drug mixtures showed similar FTIR spectra for all four grades of PVP, due to the high level of interaction between the drug and the polymer in these solid dispersion formulations. Additionally, the FTIR data is supportive of the DSC thermograms observed for the amorphous solid dispersions in the previous section.

2.4.3.1.2. Soluplus

As shown in figure 2.8, band broadening was observed between 3700-3000 cm^{-1} (due to N-H stretching in the drug and O-H stretching in soluplus), compared to the sharp peak

observed for the neat drug. The band broadening became more pronounced with increase in the soluplus:drug ratio from 1:3 to 3:1, w/w. Additionally, a decrease in the absorption intensity between 1700-1500 cm^{-1} was observed with increase in the polymer concentration, due to C-C aromatic stretching in the drug and C=O stretching (amide group) in soluplus. These observations suggest that there is strong hydrogen bonding between the drug and soluplus. Moreover, the decrease observed in the absorption intensity between 1000-600 cm^{-1} (C-H aromatic out of the plane bending) with the increase in polymer concentration indicated that there was weak hydrophobic interactions between the drug and polymer.

2.4.3.1.3. HPMC

According to Figure 2.9, for the spray dried dispersions prepared using HPMC as the stabilizer, all the different molecular weight HPMCs showed similar FTIR spectra. This indicated that there was strong miscibility between the drug and the HPMCs in the spray dried dispersions. With increase in the HPMC:drug ratio from 1:3 to 3:1, w/w, band broadening was observed between: 3680-3100 cm^{-1} (O-H stretching); and 3000-2800 cm^{-1} (C-H aliphatic stretch) compared to the neat drug. This indicates that there is intermolecular hydrogen bonding between the drug and all grades of HPMC. Additionally, with the increase in the HPMC concentration from 1:3 to 3:1, w/w (HPMC:drug), there was a decrease in the absorption intensity between: 1700-1500 cm^{-1} (C-C aromatic stretching); 1400-1200 cm^{-1} (symmetric bending of OCH3 and C-O-C stretching); and band broadening was observed between 1000-600 cm^{-1} (C-H aromatic out of plane bending), compared with the neat drug. Moreover, with the increase in the HPMC concentration from 1:3 to 3:1, w/w (HPMC:drug), there was increase in the absorption intensity between 1200-1000 cm^{-1}, mainly due to C-O-C stretching, for all four different molecular weights of HPMC. These observations suggests hydrogen bonding and hydrophobic interactions between the drug and polymer.

2.4.3.2. Solvent evaporation

The FTIR spectra indicated that the samples prepared *via* solvent evaporation were more homogenous compared to the physical mixtures. However, the spray dried solid dispersions showed superior miscibility between the drug and polymer compared to the solvent evaporation and serial dilution methods. Hydrogen bonding and other types of interactions

are more likely to occur in samples prepared *via* spray drying, followed by intermediate interactions observed in samples prepared *via* solvent evaporation and minimal/no interactions in the samples prepared *via* serial dilution. Since the solvent evaporation method is a slow drying process, one of the components (the drug or the polymer), precipitates before the other, resulting in a less homogeneous mixture compared to the spray drying process.

2.4.3.2.1. PVP

With increase in the PVP:drug ratio from 1:3 to 3:1, w/w, band broadening was observed between 3625-3150 cm^{-1} (figure 2.10) for the low and intermediate molecular weight PVPs. The broadening at 3600-3450 cm^{-1} is characteristic of O-H stretching (polymer, PVP) and N-H stretching (drug). Therefore, the observed broadening indicates hydrogen bonding between the aromatic group of the drug and the hydroxyl group of the low and intermediate PVPs. Additionally, with increase in the PVP:drug ratio from 1:3 to 3:1, w/w, there was a decrease in the absorbance intensity between 1600-1500 cm^{-1} and a broadening of the absorbance band between 1700-1600 cm^{-1} for the samples prepared using low and intermediate PVP's. This indicates that the low and intermediate molecular weight PVPs have strong miscibility with the drug due to the observed C-C stretching (aromatic moiety) and C=O stretching. The low and intermediate PVP's showed a characteristic decrease in the absorbance intensity form 1000-500 cm^{-1}, indicating C-H aromatic out of the plane bending and C-C stretching, which points to possible weak hydrophobic interactions between the drug and PVP. For the low and intermediate PVPs, with increase in the polymer concentration, there is strong hydrogen bonding and hydrophobic interactions. However, the high molecular weight PVP (PVP K-90) had a similar absorbance band as the neat drug for all polymer:drug ratios, indicating that the high molecular weight PVP was immiscible and lacked interaction with the drug.

2.4.3.2.2. Soluplus

According to Figure 2.11, the soluplus:drug 3:1, w/w, ratio showed band broadening between 3625-3150 cm^{-1} (due to N-H stretching in the drug and O-H stretching in the soluplus). For all polymer:drug ratios, a decrease in the absorbance band intensity was observed between 1700-1500 cm^{-1} (due to C=O stretching in the soluplus and C-C aromatic

stretching in the drug). Additionally, all three polymer:drug ratios showed an increase in the absorbance band intensity between 1300-1200 cm^{-1} and a decrease between 1000-500 cm^{-1}. These two effects indicate an interaction between the drug and the polymer due to C-H aromatic out of plane bending in the drug and C-C stretching in soluplus. Accordingly, there appears to be strong hydrogen bonding between the drug and soluplus at the polymer:drug ratio of 3:1, w/w, whereas, there appears to be weak hydrophobic interactions in the polymer:drug 1:1 and 1:3, w/w ratios.

2.4.3.2.3. HPMC

According to Figure 2.12(A), with increase in the HPMC:drug ratio from 1:3 to 3:1, w/w, band broadening was observed between: 3680-3100 cm^{-1} (O-H stretching) and 3000-2800 cm^{-1} (C-H aliphatic stretch) compared to the neat drug. These changes were observed mainly with HPMC E3 and not with the intermediate molecular weight HPMC's (HPMC E5 and E15) and high molecular weight HPMC's (HPMC E50). This indicates that there is intermolecular hydrogen bonding between the drug and HPMC E3 (lower molecular weight HPMC), which was absent in the other HPMCs used in this study (HPMC E5, E15 and E50). Specifically, for the low molecular weight HPMC (E3), there was a decrease in the absorption intensity between: 1700-1500 cm^{-1} (C-C aromatic stretching); 1300-1200 cm^{-1} (C-O-C stretching); and 800-700 cm^{-1} (C-H aromatic out of plane bending), with increase in the HPMC:drug ratio from 1:3 to 3:1, w/w, indicating a hydrophobic interaction between the drug and the polymer. Moreover, for HPMC E3, E15 and E50, an increase in the absorption intensity between 1100-1000 cm^{-1} (ethereal C-O-C stretching) was observed with the increase in the HPMC:drug ratio from 1:3 to 3:1, w/w.

2.4.3.3. Physical mixture

It was difficult to interpret any interaction between the drug and polymer in samples prepared *via* serial dilution into physical mixtures. However, weak interactions in the polymer-drug physical mixtures were observed for all three polymers at the high polymer:drug ratio (3:1, w/w). The samples prepared *via* serial dilution were controls for the other two methods (spray drying and solvent evaporation), due to minimal interactions between the drug and polymers.

2.4.3.3.1. PVP

As observed in figure 2.13, the FTIR spectra of the 1:1 and 1:3 PVP:drug physical mixtures, did not show any significant change in comparison to the neat drug and neat polymer, indicating insufficient miscibility to allow interaction. However, in the case of the 3:1, w/w PVP:drug physical mixture, a slight decrease in the absorbance intensity was observed between 1500-1600 cm^{-1}. This corresponds to a C-C stretch for aromatic molecules, indicating that a weak hydrophobic interaction between drug and PVP may have occurred.

2.4.3.3.2. Soluplus

According to figure 2.14, the intensity of the absorbance band corresponding to C=O stretching (1700-1800 cm^{-1}) was reduced for all soluplus:drug physical mixtures compared to the neat soluplus. This indicates that there may be weak interactions between the drug and soluplus. However, no other significant changes (such as wavenumber shift or absorbance intensity change) were observed.

2.4.3.3.3. HPMC

As observed in figure 2.15, the intensity of the absorbance band corresponding to ethereal C-O-C stretching (1100-1000 cm^{-1}) increased when the HPMC:drug ratio increased from 1:3 to 3:1, w/w, indicating a weak hydrophobic interaction between the drug and the HPMC physical mixtures. However, no other significant changes were observed for all four HPMC grades.

2.4.4. Powder X-ray diffraction

Powder X-ray diffraction (PXRD) is an important solid state tool to identify the crystallinity present in solid dispersions. Minimal or absence of crystallinity in the finished formulation has a great impact in improving the dissolution characteristics of many poorly soluble drugs. Crystalline drugs or their formulations are characterized by sharp diffraction peaks, however amorphous drug or their formulations are represented by a halo pattern (absence of sharp diffraction peaks) in the PXRD profile. The conversion of a mixture of crystalline drug and amorphous/crystalline polymer into a completely amorphous solid dispersion indicates that there is a strong miscibility between the drug and polymer, since amorphization leads to an increase in the molecular mobility of both the drug and the polymer. Additionally, PXRD has a limitation in the detection of small crystals (< 5%), which do not show strong

diffraction peaks. In this study, PXRD was used to characterize the amorphous formulations and understand the effect of increase in polymer concentration (different molecular weights) on the drug-polymer mixtures. Figure 2.16, 2.17 and 2.18 are shown in supplementary material.

2.4.4.1. PVP

The characteristic diffraction peaks of neat crystalline ABT-102 are 6.3°, 9.2°, 12°, 14.7°, 16.3°, 18.2°, 19.9°, 22.8°, 24.9° and 26.8°. According to figure 2.16A, it was observed that, after serial dilution of drug and PVP K17, all the PVP K17:drug physical mixtures were crystalline. However, in the formulations prepared *via* solvent evaporation, it was observed that with increase in the polymer concentration from 1:3 to 3:1, w/w (polymer:drug), there was complete transformation from crystalline to amorphous form. The crystalline diffraction peaks were only observed in the PVP K17:drug physical mixture 1:3 and 1:1, w/w, which transformed into the amorphous form for the 3:1, w/w PVP K17:drug physical mixtures.

According to figure 2.16 B,C,D, it was observed that all physical mixtures of PVP K25:drug, PVP K-30:drug and PVP K-90:drug showed characteristic crystalline diffraction peaks, similar to the neat crystalline drug. Additionally, for the formulation prepared using solvent evaporation, the halo pattern was only observed at the 3:1, w/w polymer:drug ratio. However, the other two polymer:drug ratios *i.e.* 1:1 and 1:3, w/w, showed the presence of diffraction peaks with less intensity, indicating low crystallinity. These observations were evident for all drug:PVP mixtures (intermediate and high molecular weight; PVP K25, PVP K30 and PVP K90), indicating that the 3:1, polymer:drug ratio resulted in completely amorphous material.

In the case of spray dried formulations, a halo pattern was observed for all three ratios of PVP:drug, indicating complete amorphization of the drug. The halo pattern was observed for low, intermediate and high molecular weight PVPs (PVP K17, PVP K25, PVP K30 and PVP K90), confirming their amorphous nature. Thus, spray drying was the best method to formulate amorphous dispersions, wherein the drug:polymer miscibility at all ratios was strong, compared to formulations prepared *via* the other methods.

2.4.4.2. Soluplus

According to figure 2.17, it was observed that for the physical mixtures prepared *via* serial dilution of drug and soluplus, all formulations were crystalline under PXRD, indicating minimal interaction between the drug and the polymer. For the formulations prepared using the solvent evaporation technique, the soluplus:drug ratio of 3:1, w/w showed a halo pattern in the PXRD, indicating its amorphous nature compared to the sharp crystalline peaks observed in the 1:1 and 1:3, w/w soluplus:drug mixtures. For the formulations prepared using spray drying, a halo pattern was observed for all three soluplus:drug ratios, indicating that the spray dried solid dispersions were amorphous.

2.4.4.3. HPMC

According to figure 2.18, formulations prepared *via* serial dilution showed sharp diffraction peaks under PXRD, indicating their crystalline nature. Amongst, the formulations prepared using solvent evaporation, the HPMC:drug ratios of 1:1 and 1:3, w/w, for the low molecular weight HPMCs (E3 and E5) showed less intense crystalline peaks, whereas, the 3:1, w/w was completely amorphous. However, for the high molecular weight HPMCs; E15 and E50, all polymer:drug ratios showed less intense crystalline peaks under PXRD. In the case of the spray dried solid dispersions, it was observed that all ratios of the HPMC:drug (all grades of HPMC) showed a halo pattern in the PXRD, confirming their amorphous nature. Thus, the spray drying method was the best method to formulate amorphous dispersions, since the interaction between the drug and the polymer is strong in these molecular dispersion.

2.5. CONCLUSIONS

Spray drying was determined to be the best method out of those investigated (spray drying, solvent evaporation and serial dilution) to formulate amorphous solid dispersions. This is due to the formation of solid state molecular dispersions during the rapid precipitation of the drug and the polymer in the spray drying process. In this study, nine different polymers (PVP K17, PVP K25, PVP K30, PVP K90, soluplus, HPMC E3, HPMC E5, HPMC E15 and HPMC E50) were used to investigate drug-polymer interactions. Soluplus, low molecular weight PVP K17, and HPMC E3 resulted in the best interactions with ABT-102, compared to the other polymers. Amongst these three polymers, soluplus showed the

strongest interaction due to the presence of two carbonyl groups on soluplus which were able to interact with the three N-H groups of ABT-102. PVP K17 showed the second best interaction with the N-H groups of ABT-102, due to its low viscosity and single C=O stretching, followed by HPMC E3, which interacted with the drug through multiple O-H stretching. It is important to characterize solid dispersions using a combination of solid state tools including; DSC, FTIR and PXRD. These different analytical techniques provide diverse information on drug-polymer interactions. The melting point depression observed in the DSC thermograms, along with the change in the intensity or shift in the absorbance bands (FTIR) and the absence of crystalline diffraction peaks (PXRD) are suggestive of drug-polymer interactions. DSC and PXRD only provide information on the presence of strong/weak interactions, whereas the type of interactions (hydrogen bonding, hydrophobic interactions) are provided *via* the supportive FTIR results. Hence, a combination of these three methods is necessary to understand the level and type of interactions between the drug and the polymer in amorphous solid dispersions as described here. A mechanistic approach was utilized to understand the drug-polymer interactions. The interaction parameters and free energy of mixing obtained using the Flory Huggins principle and the melting point depression approach confirmed that the solid dispersions prepared *via* spray drying resulted in the strongest miscibility between ABT-102 and the polymers compared to the solvent evaporation and serial dilution method. The present research describes the detailed mechanisms involved in the interactions between the drug ABT-102 and polymeric stabilizers. This study will aid pre-formulation scientists in screening stabilizers for formulation development of similar solid dispersion formulations compared to the conventional trial and error methods.

2.6. Tables

Table 2.1. Chemical structures of the active and excipients [28-30]

Polyvinyl pyrrolidone K17, K25, K30 and K90 **(Kollidon)**	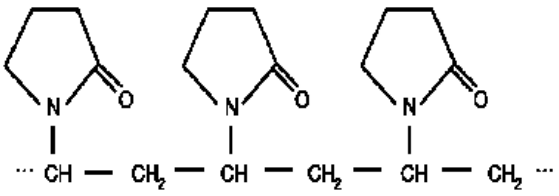
Hydroxypropyl methyl cellulose E3, E5, E15 and E50 **(Methocel)**	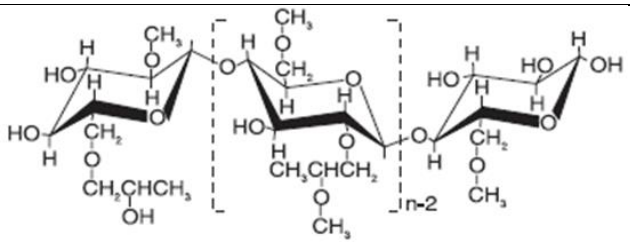
Polyvinyl caprolactam-polyvinyl acetate-polyethylene glycol graft copolymer **(Soluplus)**	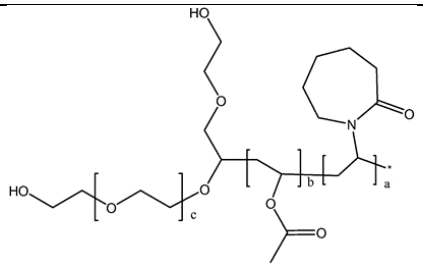
ABT-102 **(drug)**	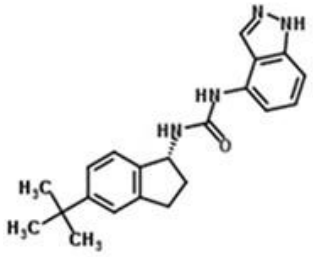

Table 2.2. Average molecular weights and viscosities of the polymers [28, 29]

Polymers	Average Molecular weight (Dalton)	Viscosity (mPa.s)
PVP K-17	9200	1.5-3.5
PVP K-25	26000	3.5-5.5
PVP K-30	42000	5.5-8.5
PVP K-90	1100000	300-700
HPMC E3	18000	2.4-3.6
HPMC E5	22000	4-6
HPMC E15	52000	12-18
HPMC E50	91300	40-60
Soluplus	118000	125

Table 2.3. Characteristic FTIR absorbance bands

	Characteristic FTIR absorbance bands (cm^{-1})	**Ref**
ABT-102	3300 (N-H stretch), 3000-2800 (C-H aliphatic stretch), 1625-1575 (C-C stretch aromatic), 900-650 (C-H aromatic out of plane bend)	[39]
PVP	3469 (O-H stretching), 1698 (C=O stretching-pyrrolidone group), 2987 (C-H asymmetric stretching-CH_2), 1427 (C-H bending), 1260 (C-N stretching), 931 (C-C stretching)	[40]
Soluplus	3448.72 (O-H stretching), 2927.98 (aromatic C-H stretching), 1735.93 -$OC(O)CH_3$ or ester group, 1635.23-C(O)N or amide group (C=O stretching), 1477.21 (C-O-C stretching)	[41]
HPMC	3500-3400 (intermolecular H-bonding), 2550-2500 (intramolecular H-bonding) (O-H stretching), 2900 (C-H symmetric stretching), 1650-1600 (C-O stretching – 6 membered cyclic ring), 1500-1450 (asymmetric bending – OCH_3), 1400-1350 (symmetric bending – OCH_3, C-O-C stretching – cyclic anhydride), 1300-1250 (C-O-C stretching – cyclic epoxide), 1100-1000 (ethereal C-O-C stretching), 1000-950 (asymmetrical stretching – pyranose), 850-800 (rocking CH_2)	[42]

2.7. Figures

GRAPHICAL ABSTRACT:

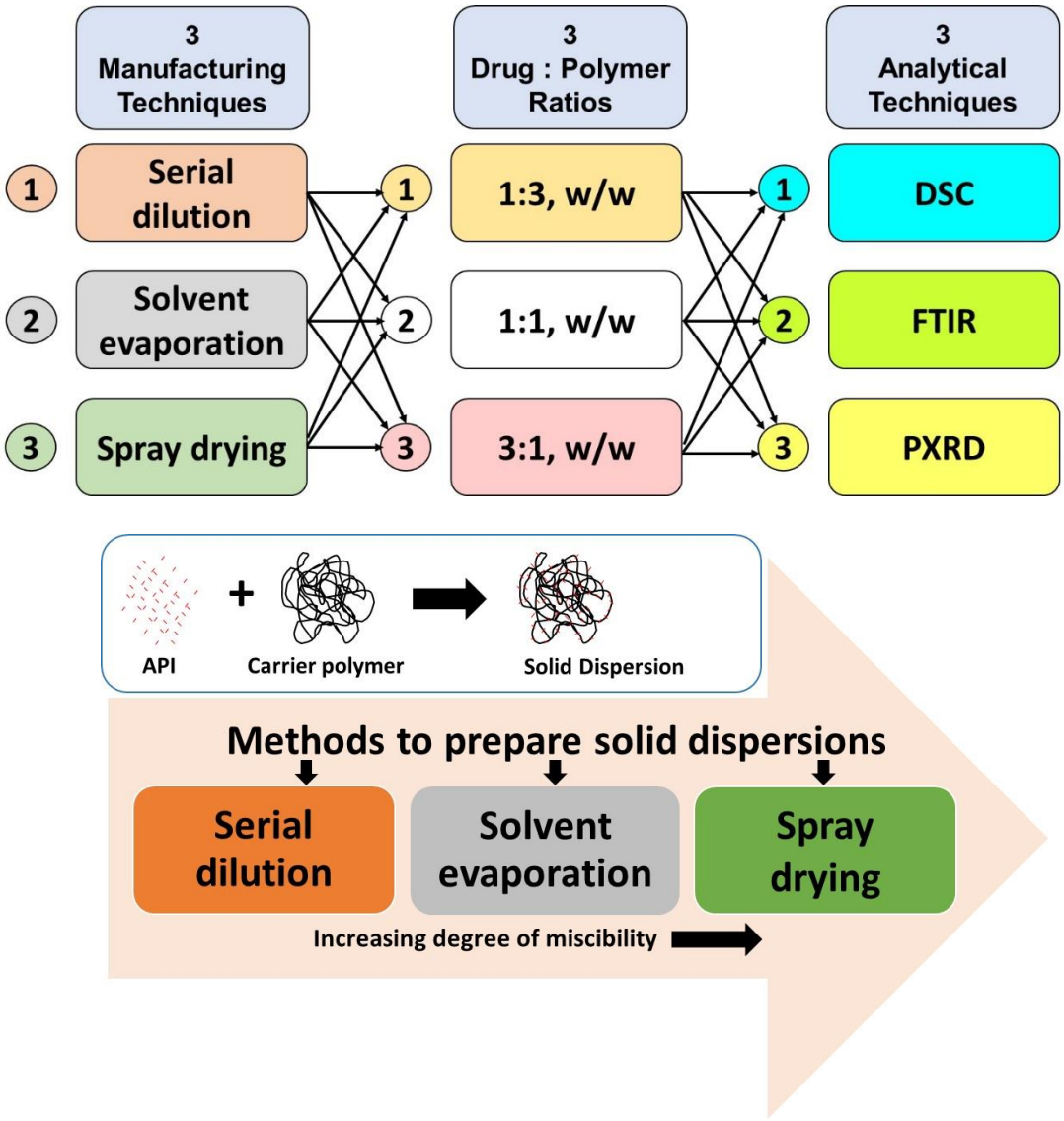

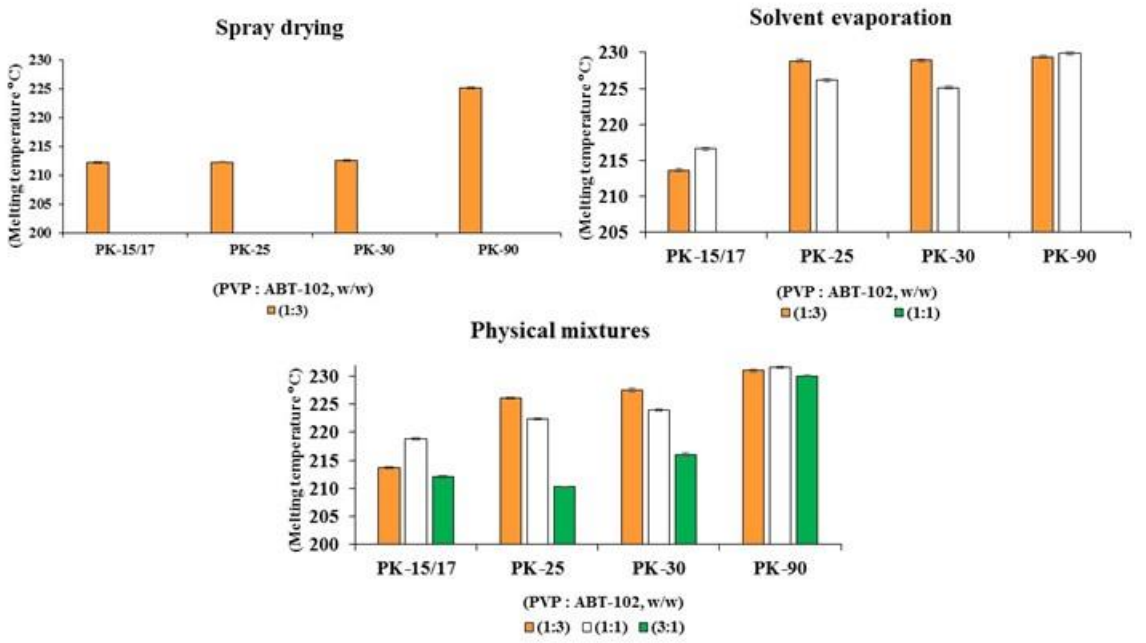

Figure 2.1: Comparison of melting temperature *vs.* PVPs:drug ratio (four grades of PVP). Samples were prepared using three different methods: (a) spray drying, (b) solvent evaporation and (c) physical mixture.

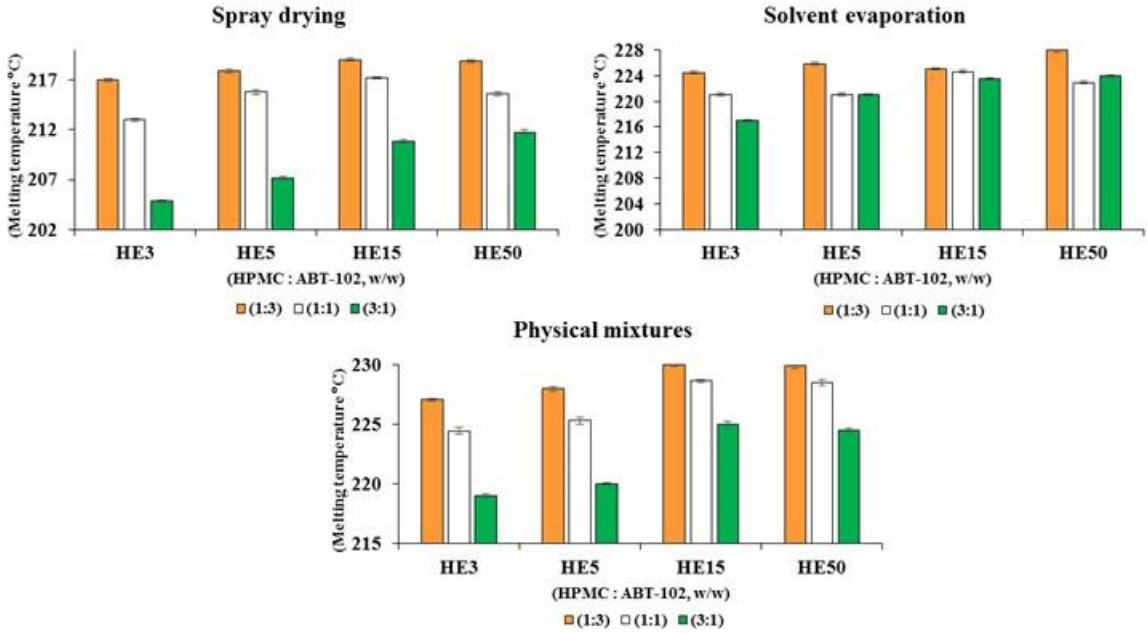

Figure 2.2: Comparison of melting temperature *vs.* HPMCs:drug ratio (four grades of HPMC). Samples were prepared using three different methods; (a) spray drying, (b) solvent evaporation and (c) physical mixture.

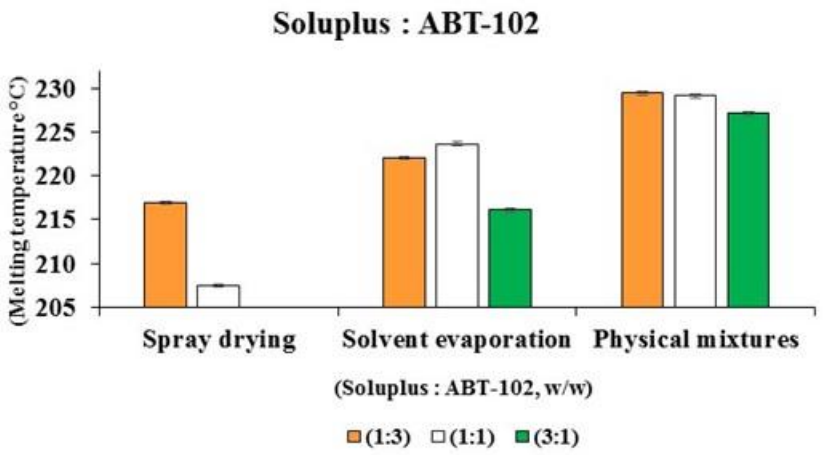

Figure 2.3: Comparison of melting temperature *vs.* soluplus:drug ratios. Samples were prepared using three different methods; (a) spray drying, (b) solvent evaporation and (c) physical mixture.

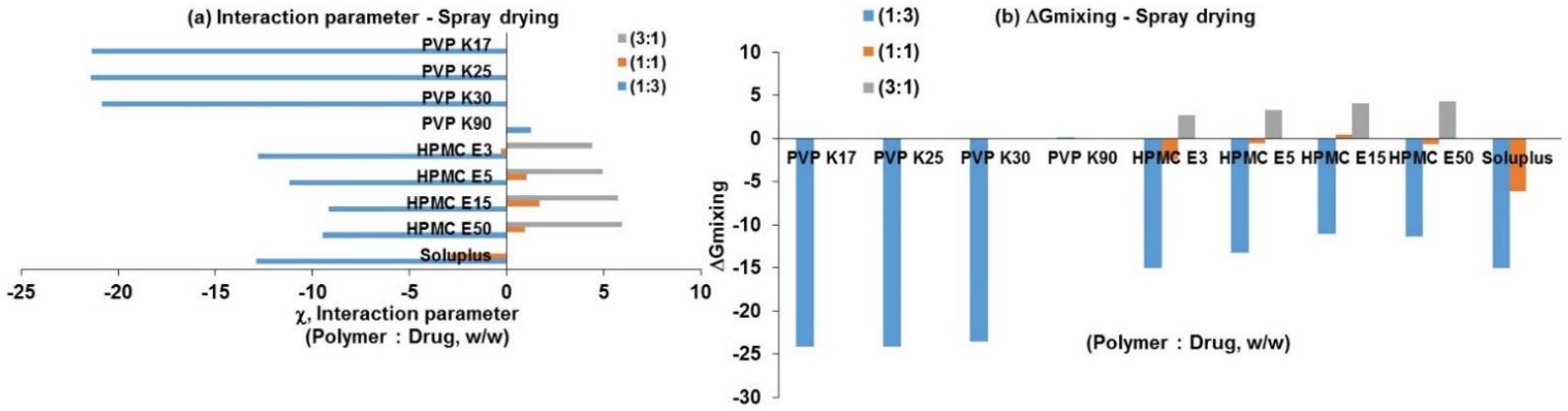

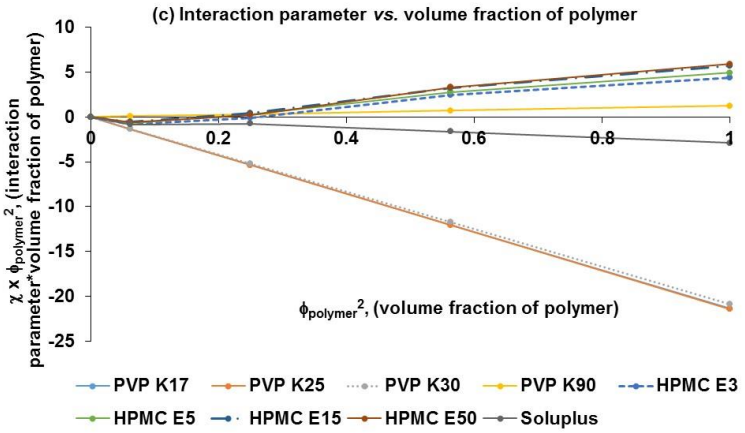

Figure 2.4: (a) interaction parameter; (b) free energy of mixing; and (c) interaction parameter *vs*. volume fraction of the nine different polymers along with the ABT-102 in the spray dried solid dispersions.

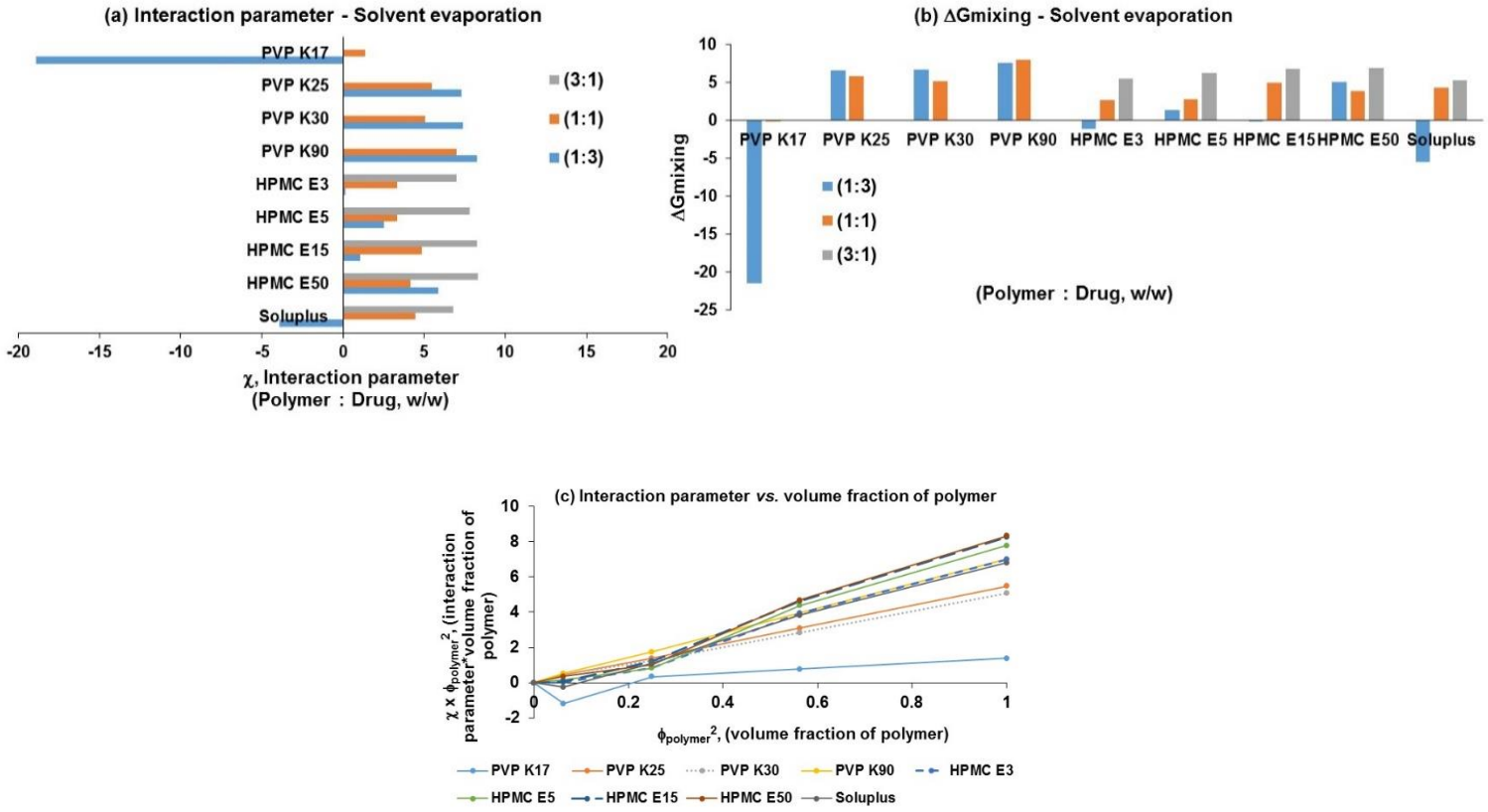

Figure 2.5: (a) interaction parameter; (b) free energy of mixing; and (c) interaction parameter *vs*. volume fraction of nine different polymers with ABT-102 for samples prepared using solvent evaporation.

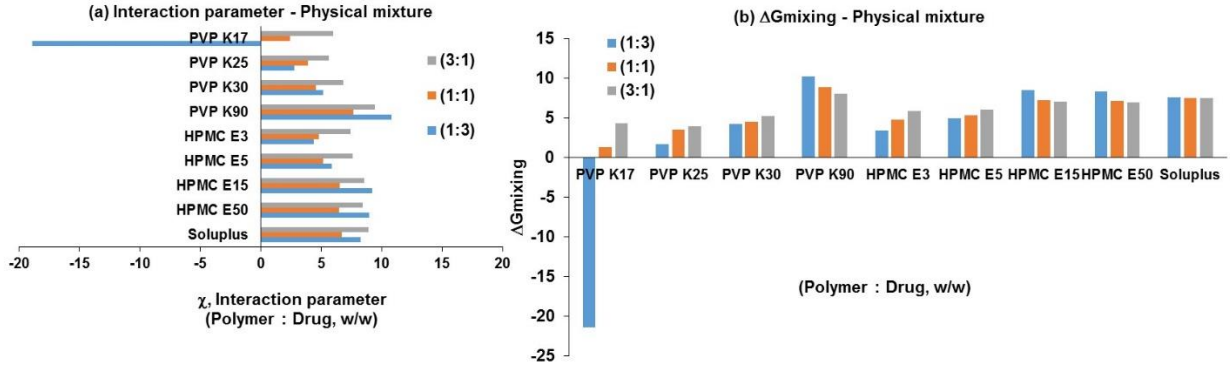

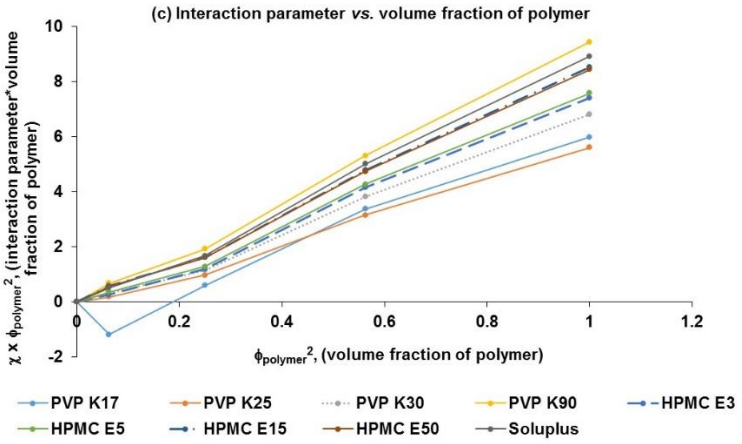

Figure 2.6: (a) interaction parameter; (b) free energy of mixing; and (c) interaction parameter *vs*. volume fraction of the nine different polymers with ABT-102 in samples prepared using serial dilution.

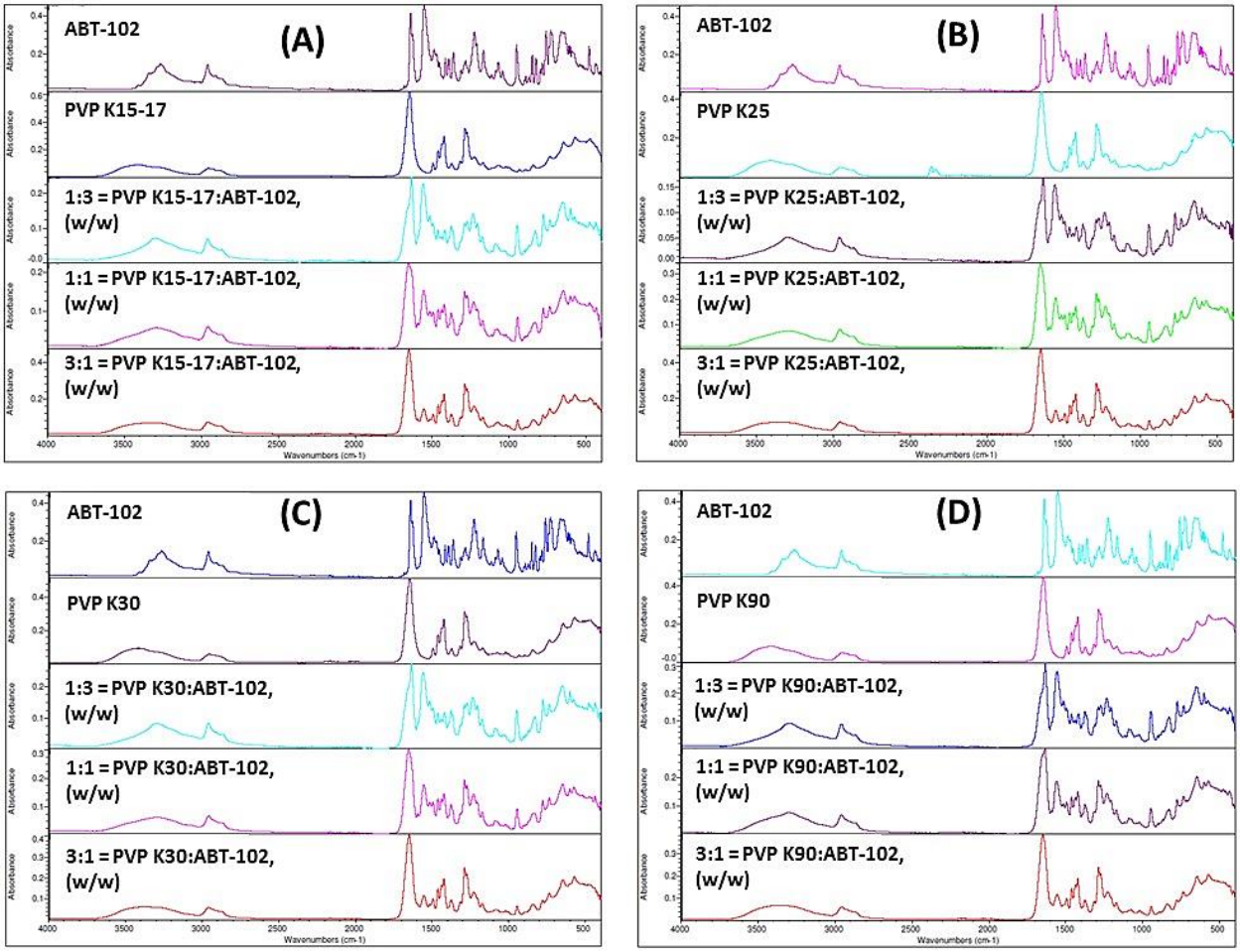

Figure 2.7: FTIR spectra of: (A) neat drug, neat PVP K17 and the 1:3, 1:1 and 3:1, w/w ratios of PVP K17:drug; (B) neat drug, neat PVP K25 and the 1:3, 1:1 and 3:1, w/w ratios of PVP K25:drug; (C) neat drug, neat PVP K30 and the 1:3, 1:1 and 3:1, w/w ratios of PVP K30:drug; and (D) neat drug, neat PVP K90 and the 1:3, 1:1 and 3:1, w/w ratios of PVP K90:drug.

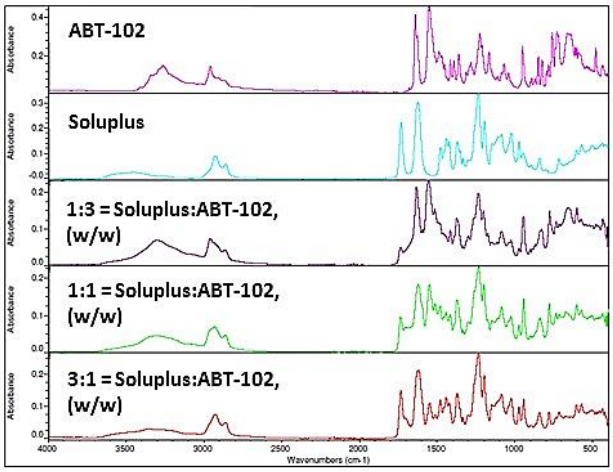

Figure 2.8: FTIR spectra showing; neat drug, neat soluplus and the 1:3, 1:1 and 3:1, w/w ratios of soluplus:drug.

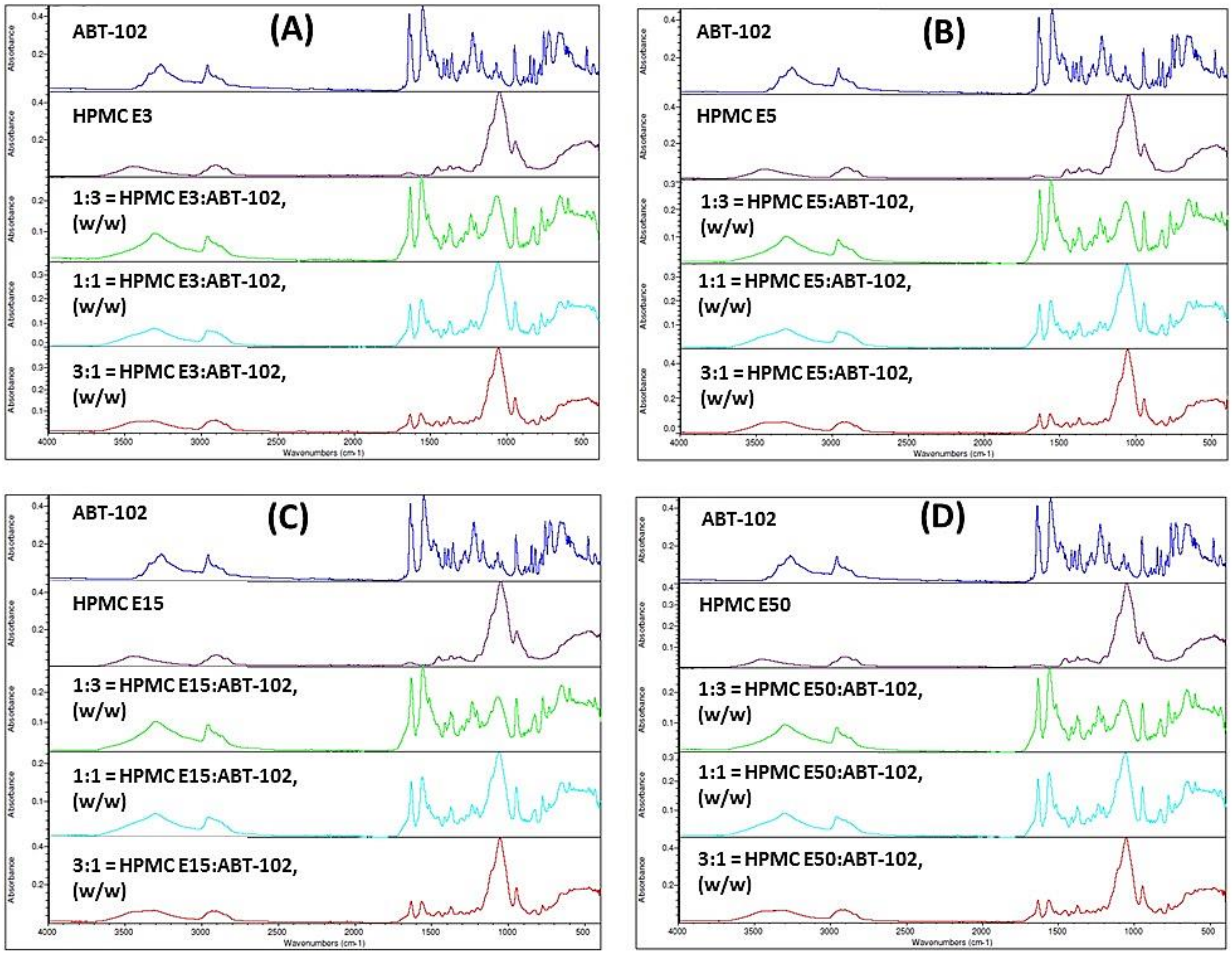

Figure 2.9: FTIR spectra of: (A) neat drug, neat HPMC E3 and the 1:3, 1:1 and 3:1, w/w ratios of HPMC E3:drug; (B) neat drug, neat HPMC E5 and the 1:3, 1:1 and 3:1, w/w ratios of HPMC E5:drug; (C) neat drug, neat HPMC E15 and the 1:3, 1:1 and 3:1, w/w ratios of HPMC E15:drug; and (D) neat drug, neat HPMC E50 and the 1:3, 1:1 and 3:1, w/w ratios of HPMC E50:drug.

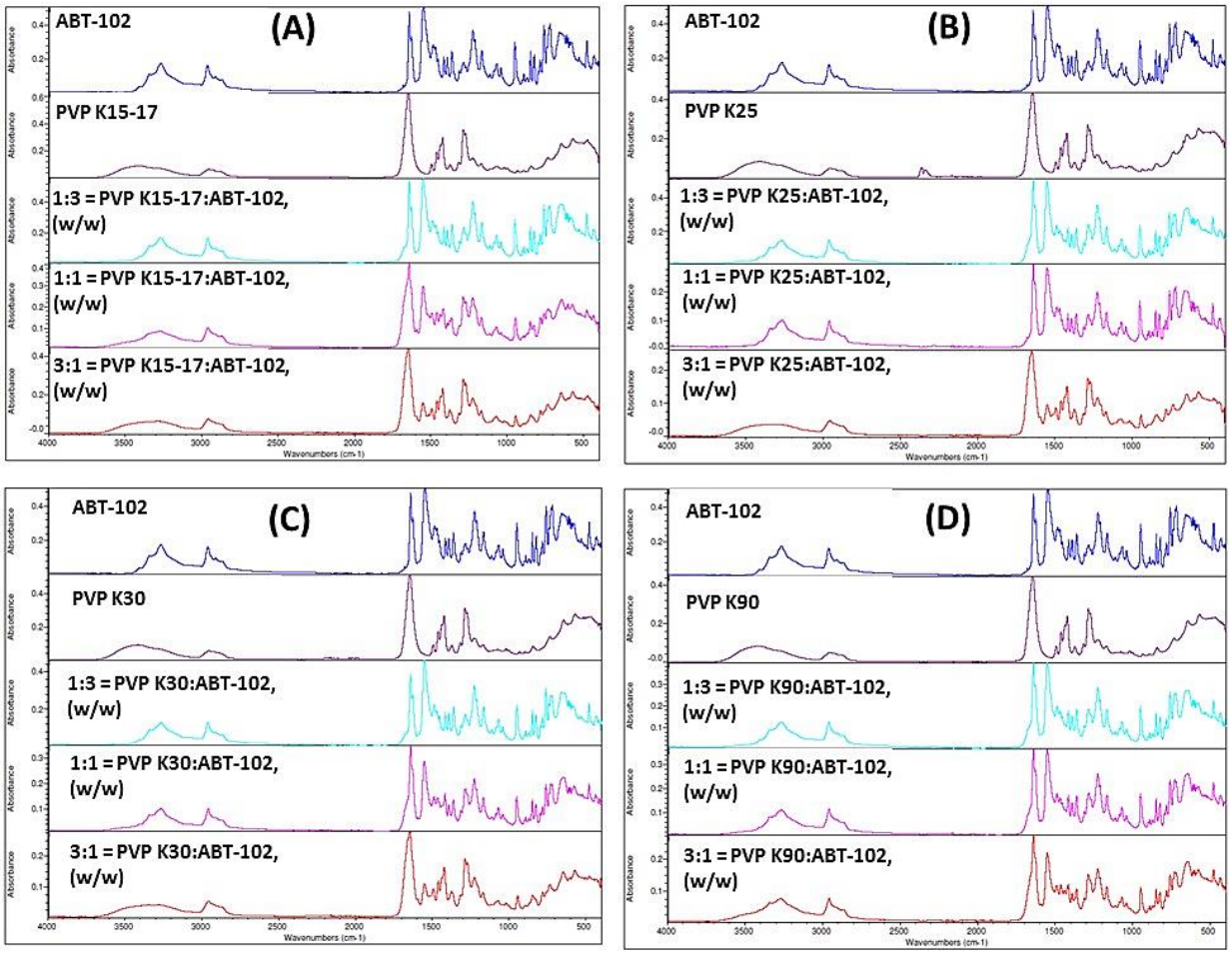

Figure 2.10: FTIR spectra of: (A) neat drug, neat PVP K17 and the 1:3, 1:1 and 3:1, w/w ratios of PVP K17:drug; (B) neat drug, neat PVP K25 and the 1:3, 1:1 and 3:1, w/w ratios of PVP K25:drug; (C) neat drug, neat PVP K30 and the 1:3, 1:1 and 3:1, w/w ratios of PVP K30:drug; and (D) neat drug, neat PVP K90 and the 1:3, 1:1 and 3:1, w/w ratios of PVP K90:drug.

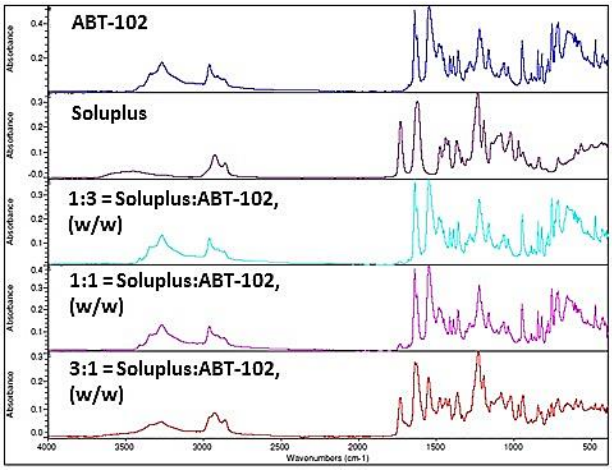

Figure 2.11: FTIR spectra showing; neat drug, neat soluplus and the 1:3, 1:1 and 3:1, w/w ratios of soluplus:drug.

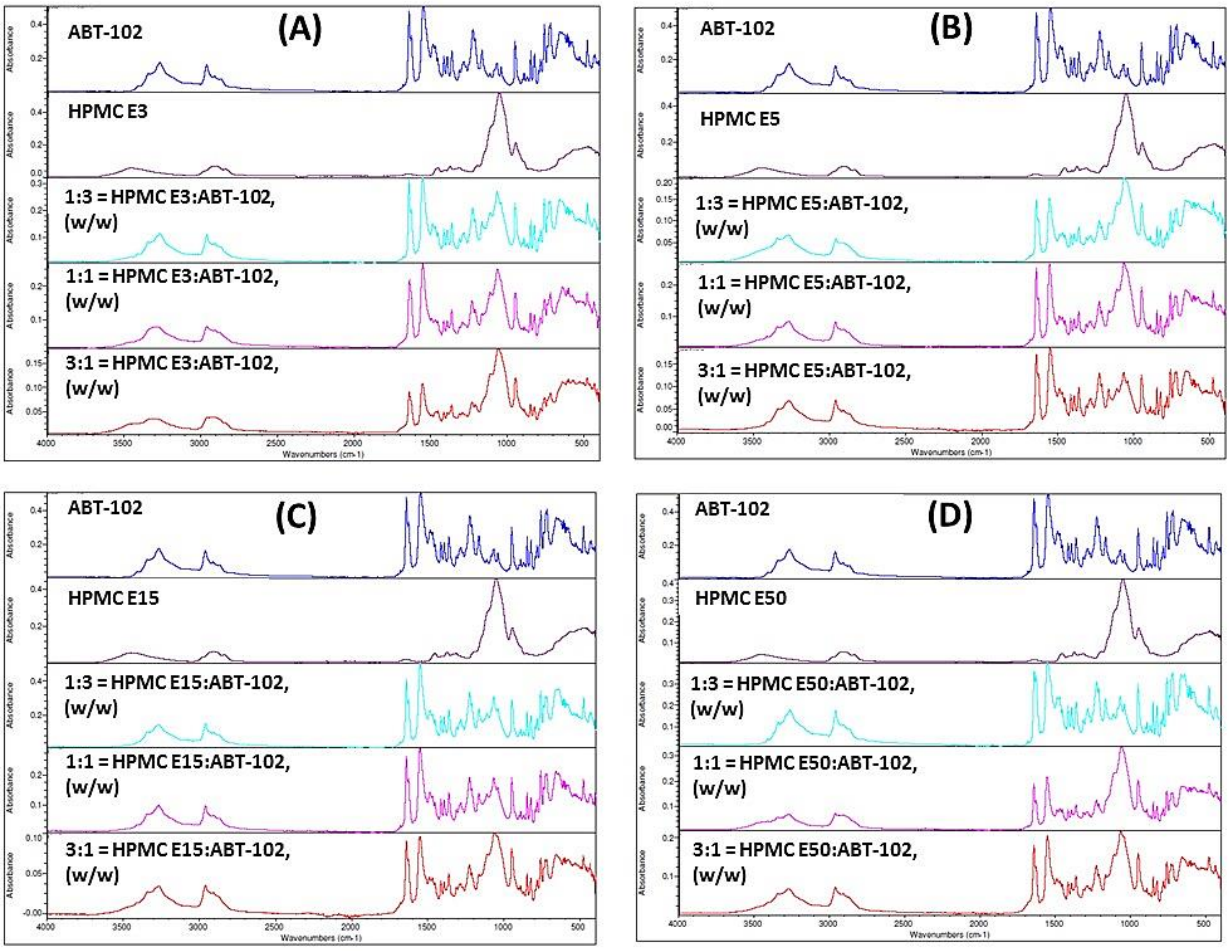

Figure 2.12: FTIR spectra of: (A) neat drug, neat HPMC E3 and the 1:3, 1:1 and 3:1, w/w ratios of HPMC E3:drug; (B) neat drug, neat HPMC E5 and the 1:3, 1:1 and 3:1, w/w ratios of HPMC E5:drug; (C) neat drug, neat HPMC E15 and the 1:3, 1:1 and 3:1, w/w ratios of HPMC E15:drug; and (D) neat drug, neat HPMC E50 and the 1:3, 1:1 and 3:1, w/w ratios of HPMC E50:drug.

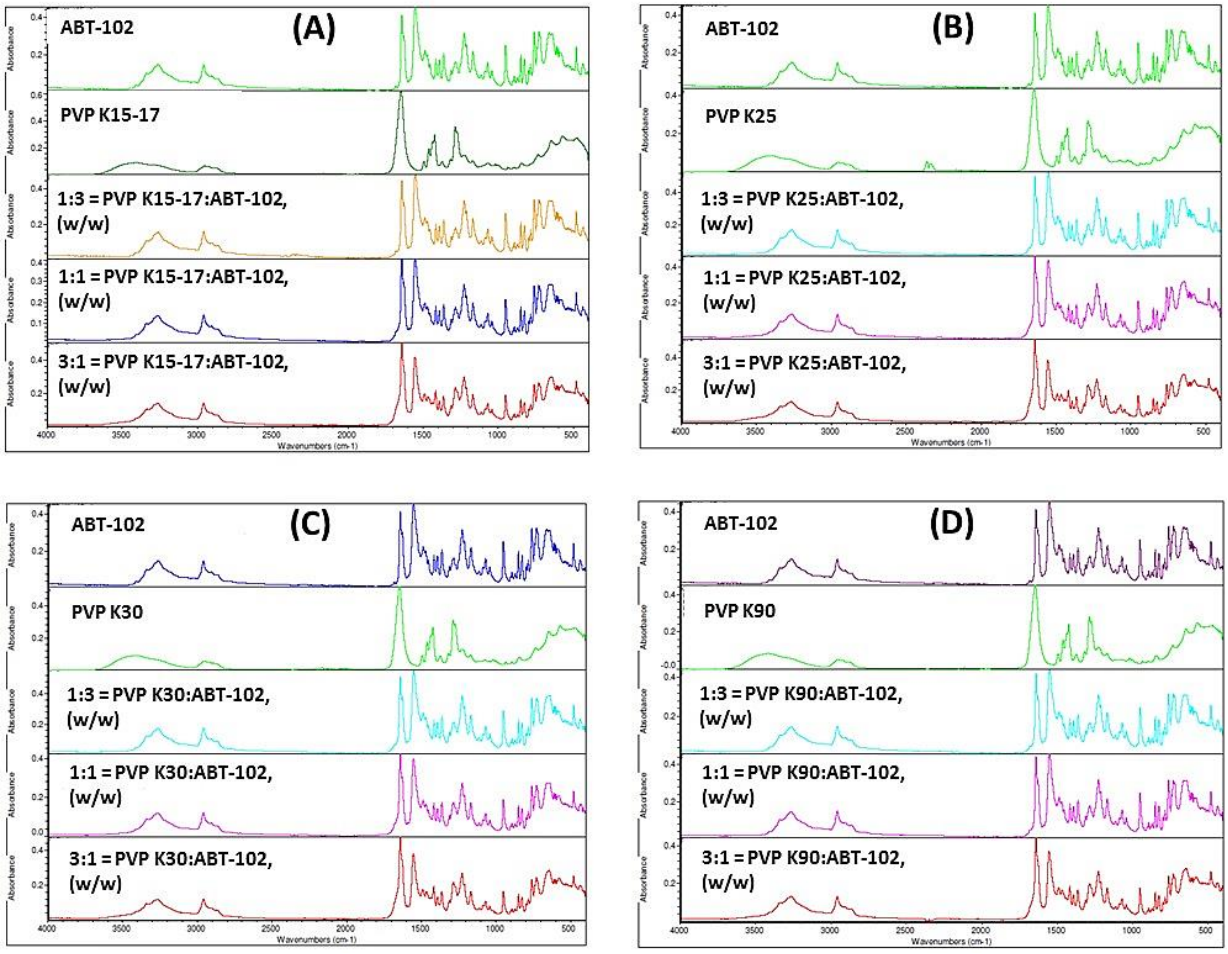

Figure 2.13: FTIR spectra of: (A) neat drug, neat PVP K17 and the 1:3, 1:1 and 3:1, w/w ratios of PVP K17:drug; (B) neat drug, neat PVP K25 and the 1:3, 1:1 and 3:1, w/w ratios of PVP K25:drug; (C) neat drug, neat PVP K30 and the 1:3, 1:1 and 3:1, w/w ratios of PVP K30:drug; and (D) neat drug, neat PVP K90 and the 1:3, 1:1 and 3:1, w/w ratios of PVP K90:drug.

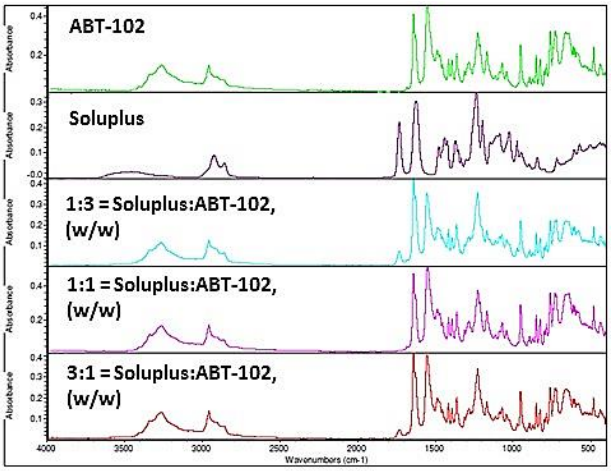

Figure 2.14: FTIR spectra showing; neat drug, neat soluplus and the 1:3, 1:1 and 3:1, w/w ratios of soluplus:drug.

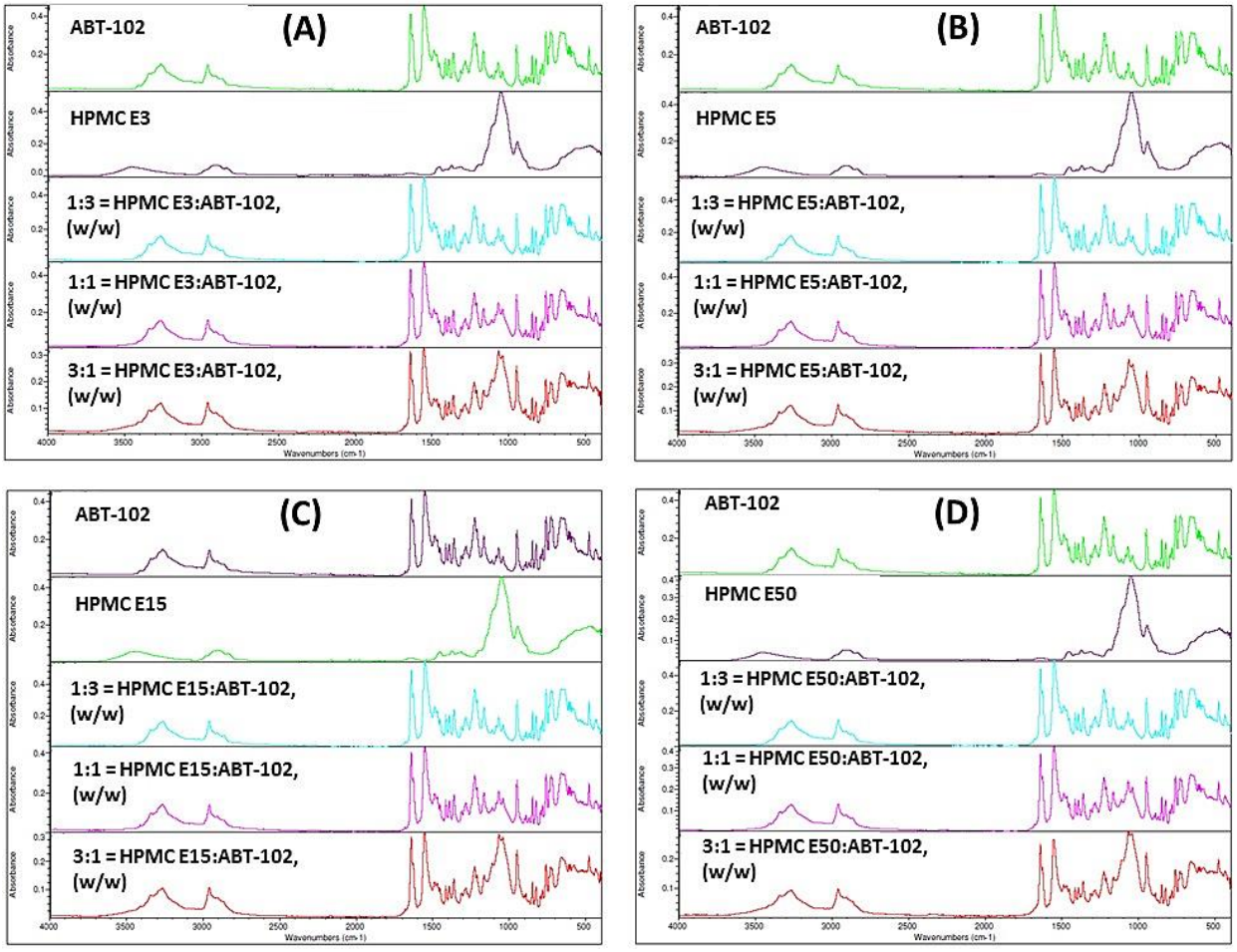

Figure 2.15: FTIR spectra of: (A) neat drug, neat HPMC E3 and the 1:3, 1:1 and 3:1, w/w ratios of HPMC E3:drug; (B) neat drug, neat HPMC E5 and the 1:3, 1:1 and 3:1, w/w ratios of HPMC E5:drug; (C) neat drug, neat HPMC E15 and the 1:3, 1:1 and 3:1, w/w ratios of HPMC E15:drug; and (D) neat drug, neat HPMC E50 and the 1:3, 1:1 and 3:1, w/w ratios of HPMC E50:drug

(A) PVP K17

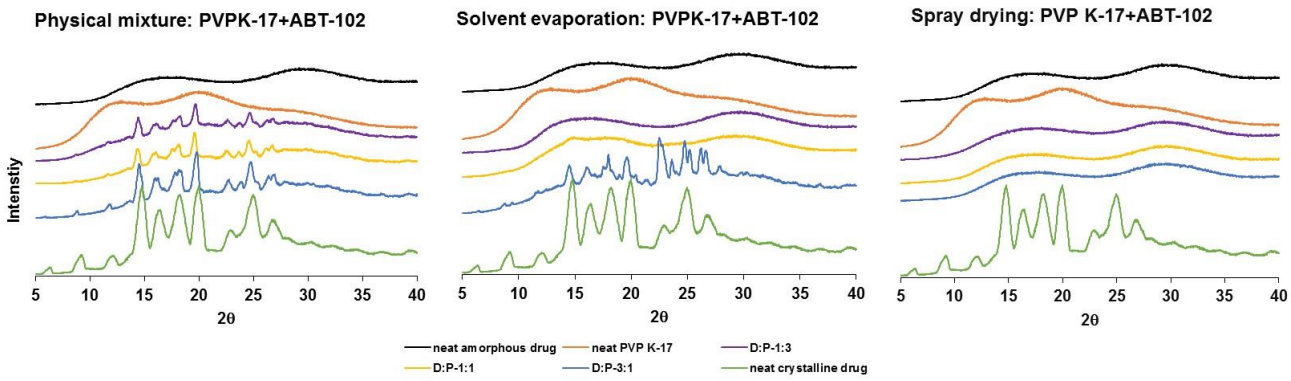

(B) PVP K25

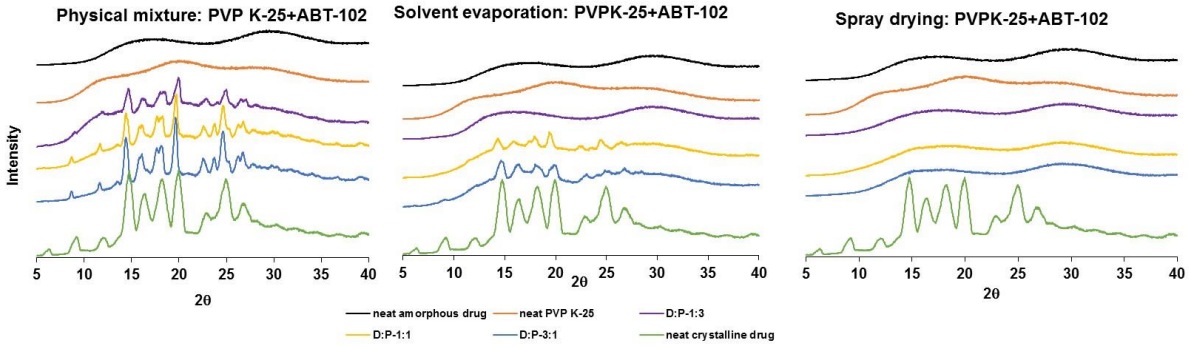

(C) PVP K30

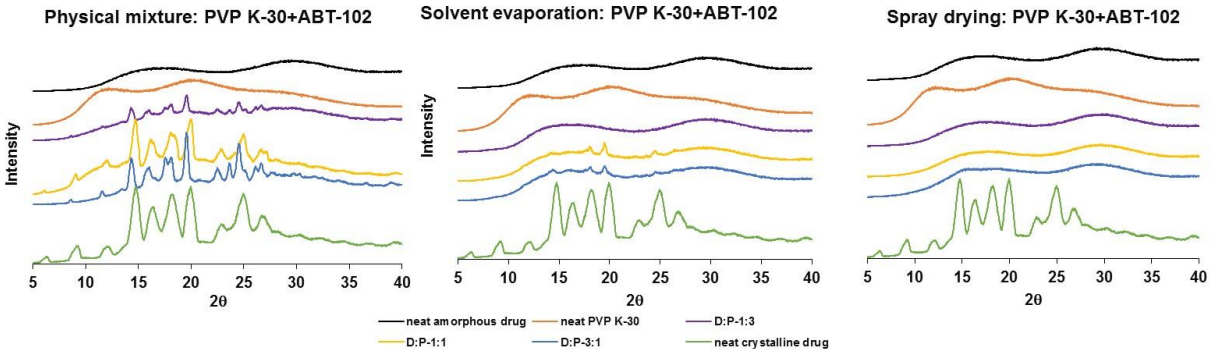

(D) PVP K-90

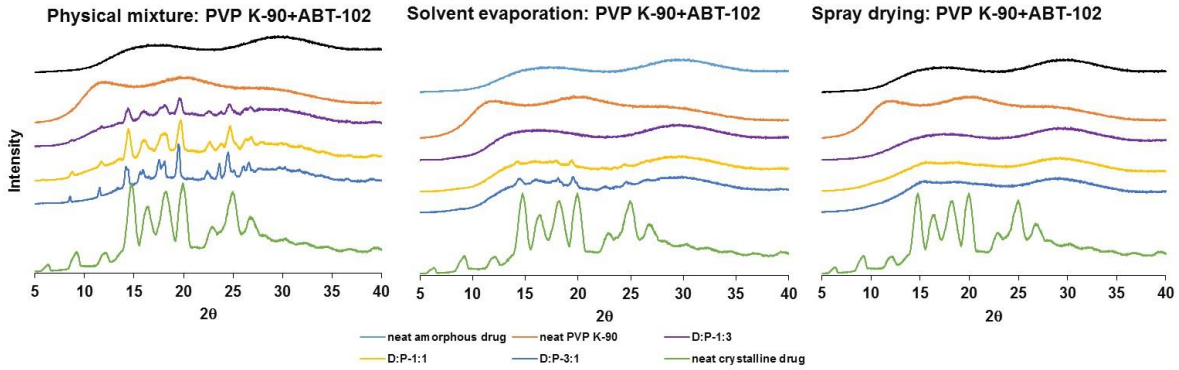

Figure 2.16: PXRD diffractograms showing: (A) PVP K17 (B) PVP K25 (C) PVP K30 and (D) PVP K90; neat amorphous drug (black), neat polymer (orange), drug:polymer mixtures 1:3 (purple), 1:1 (yellow) and 3:1 (blue), w/w and neat crystalline drug (green), (formulations are prepared using three different methods: (1) physical mixtures by serial dilution; (2) solvent evaporation; and (3) spray drying).

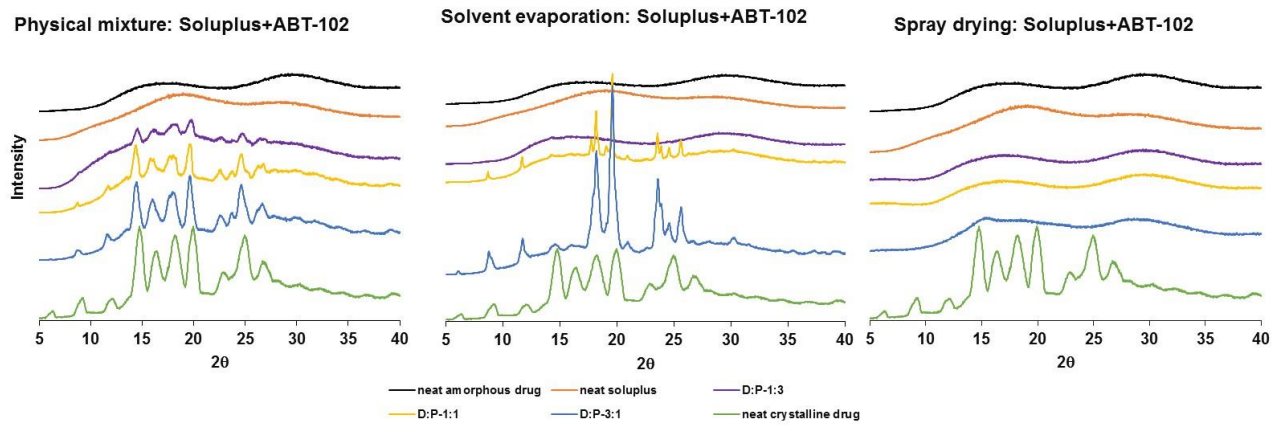

Figure 2.17: PXRD diffractograms showing: neat amorphous drug (black), neat soluplus (orange), drug:polymer mixtures 1:3 (purple), 1:1 (yellow) and 3:1 (blue), w/w and neat crystalline drug (green), (formulations were prepared using three different methods: (1) physical mixtures by serial dilution; (2) solvent evaporation; and (3) spray drying).

(A) HPMC E3

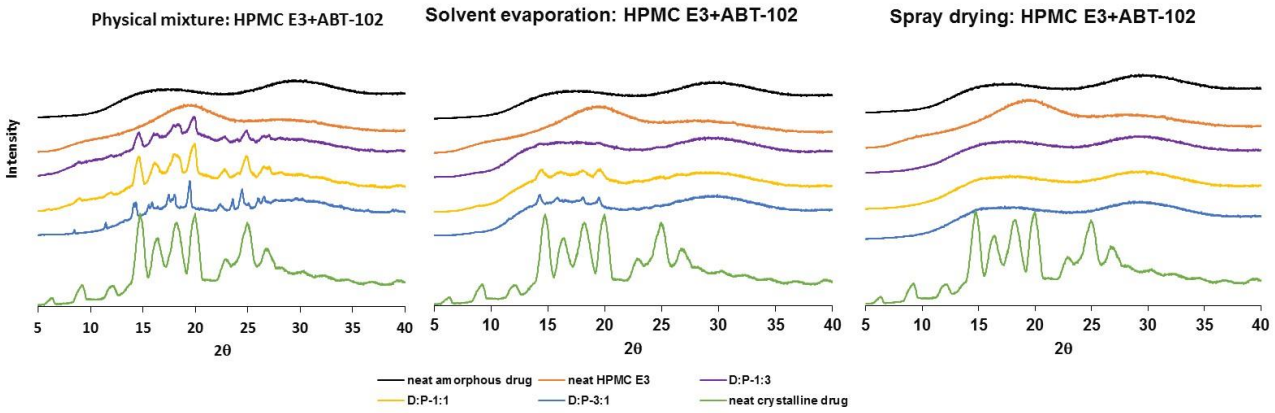

(B) HPMC E5

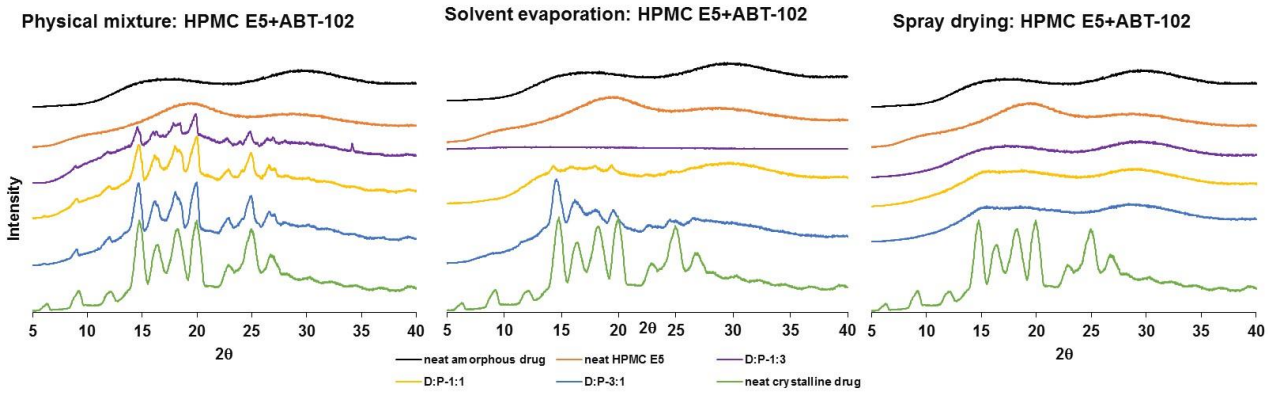

(C) HPMC E15

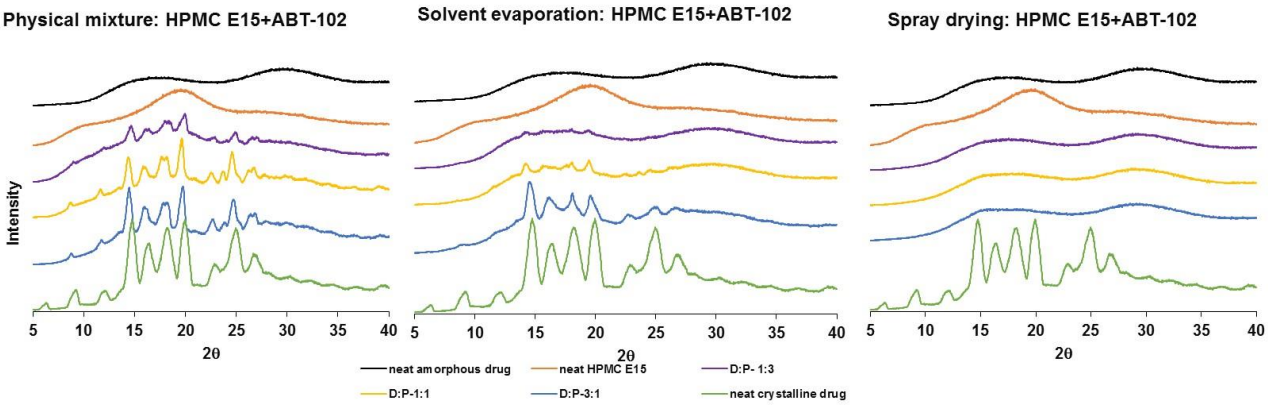

(D) HPMC E50

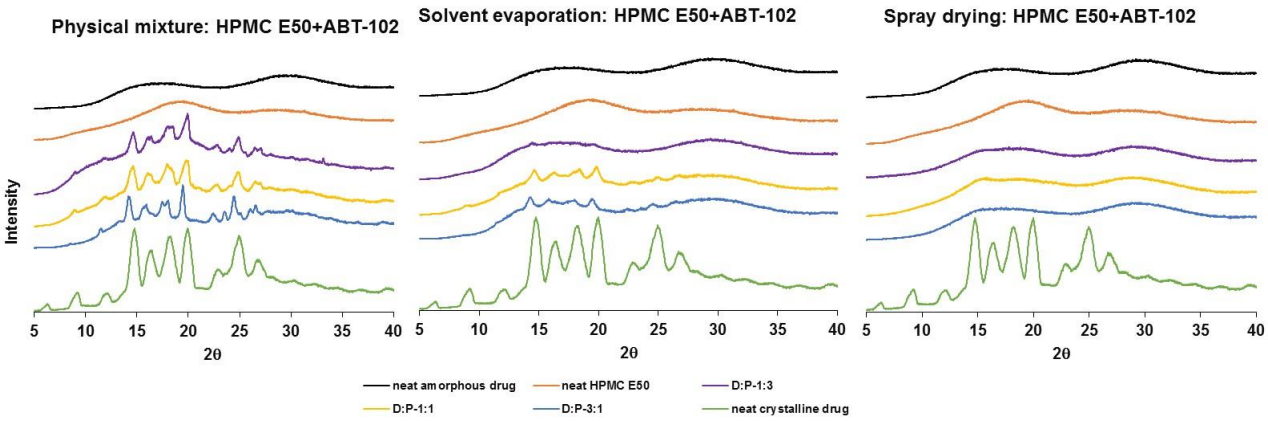

Figure 2.18: PXRD diffractograms showing: (A) HPMC E3 (B) HPMC E5 (C) HPMC E15 (D) HPMC E50; neat amorphous drug (black), neat polymer (orange), drug:polymer mixtures 1:3 (purple), 1:1 (yellow) and 3:1 (blue), w/w and neat crystalline drug (green), (formulations were prepared using three different methods: (1) physical mixtures by serial dilution; (2) solvent evaporation; and (3) spray drying).

2.8. REFERENCES

[1]Amidon, G. L., Lennernas, H., Shah, V. P. and Crison, J. R., 1995. A theoretical basis for a biopharmaceutic drug classification: the correlation of in vitro drug product dissolution and in vivo bioavailability. Pharm. Res. 12, 413-420.

[2]Cook, J., Addicks, W. and Wu, Y. H., 2008. Application of the biopharmaceutical classification system in clinical drug development-an industrial view. The AAPS J. 10, 306-310.

[3]Lindenberg, M., Kopp, S. and Dressman, J. B., 2004. Classification of orally administered drugs on the World Health Organization Model list of Essential Medicines according to the biopharmaceutics classification system. Eur. J. Pharm. Biopharm. 58, 265-278.

[4]Hauss, D. J., 2007. Oral lipid-based formulations: enhancing the bioavailability of poorly water-soluble drugs, In: (Eds.), CRC Press, Florida, 1-339.

[5]Bajaj, H., Bisht, S., Yadav, M. and Singh, V., 2011. Bioavailability enhancement: a review. Int. J. Pharm. Biosci. 2, 209-216.

[6]L Chaves, L., Cc Vieira, A., Reis, S., Sarmento, B. and C Ferreira, D., 2014. Quality by Design: Discussing and Assessing the Solid Dispersions Risk. Curr. Drug Deliv. 11, 253-269.

[7]Shah, S., Maddineni, S., Lu, J. and Repka, M. A., 2013. Melt extrusion with poorly soluble drugs. Int. J. Pharm. 453, 233-252.

[8]Paudel, A., Worku, Z. A., Meeus, J., Guns, S. and Van den Mooter, G., 2013. Manufacturing of solid dispersions of poorly water soluble drugs by spray drying: formulation and process considerations. Int. J. Pharm. 453, 253-284.

[9]Shah, N., Iyer, R. M., Mair, H. J., Choi, D. S., Tian, H., Diodone, R., Fahnrich, K., Pabsta Ravot, A., Tang, K. and Scheubel, E., 2013. Improved human bioavailability of

vemurafenib, a practically insoluble drug, using an amorphous polymer-stabilized solid dispersion prepared by a solvent-controlled coprecipitation process. J. Pharm. Sci. 102, 967-981.

[10]Leuner, C. and Dressman, J., 2000. Improving drug solubility for oral delivery using solid dispersions. Eur. J. Pharm. Biopharm. 50, 47-60.

[11]Weuts, I., Kempen, D., Verreck, G., Decorte, A., Heymans, K., Peeters, J., Brewster, M. and Van den Mooter, G., 2005. Study of the physicochemical properties and stability of solid dispersions of loperamide and PEG6000 prepared by spray drying. Eur. J. Pharm. Biopharm. 59, 119-126.

[12]WY Lee, T., A Boersen, N., Hui, H. W., Chow, S. F., Wan, K. Y. and Hl Chow, A., 2014. Delivery of poorly soluble compounds by amorphous solid dispersions. Current Pharm. Des. 20, 303-324.

[13]Hancock, B. C. and Parks, M., 2000. What is the true solubility advantage for amorphous pharmaceuticals? Pharm. Res. 17, 397-404.

[14]Baghel, S., Cathcart, H. and O'Reilly, N. J., 2016. Polymeric Amorphous Solid Dispersions: A Review of Amorphization, Crystallization, Stabilization, Solid-State Characterization, and Aqueous Solubilization of Biopharmaceutical Classification System Class II Drugs. J. Pharm. Sci. *In press.*

[15]Jackson, M. J., Kestur, U. S., Hussain, M. A. and Taylor, L. S., 2015. Dissolution of Danazol Amorphous Solid Dispersions: Supersaturation and Phase Behavior as a Function of Drug Loading and Polymer Type. Mol. Pharm. 13, 223-231.

[16]Savjani, K. T., Gajjar, A. K. and Savjani, J. K., 2012. Drug solubility: importance and enhancement techniques. ISRN Pharm. 2012.

[17]Wu, K. E., Li, J., Wang, W. and Winstead, D. A., 2009. Formation and characterization of solid dispersions of piroxicam and polyvinylpyrrolidone using spray drying and precipitation with compressed antisolvent. J. Pharm. Sci. 98, 2422-2431.

[18]Tres, F., Patient, J. D., Williams, P. M., Treacher, K., Booth, J., Hughes, L. P., Wren, S. A. C., Aylott, J. W. and Burley, J. C., 2015. Monitoring the dissolution mechanisms of amorphous bicalutamide solid dispersions via real-time raman mapping. Mol. Pharm. 12, 1512-1522.

[19]Li, Y., Pang, H., Guo, Z., Lin, L., Dong, Y., Li, G., Lu, M. and Wu, C., 2014. Interactions between drugs and polymers influencing hot melt extrusion. J. Pharm. Pharmacol. 66, 148-166.

[20]Wilson, M., Williams, M. A., Jones, D. S. and Andrews, G. P., 2012. Hot-melt extrusion technology and pharmaceutical application. Ther. Deliv. 3, 787-797.

[21]Karanth, H., Shenoy, V. S. and Murthy, R. R., 2006. Industrially feasible alternative approaches in the manufacture of solid dispersions: a technical report. AAPS PharmSciTech. 7, E31-E38.

[22]Guo, Z., Lu, M., Li, Y., Pang, H., Lin, L., Liu, X. and Wu, C., 2014. The utilization of drug-polymer interactions for improving the chemical stability of hot-melt extruded solid dispersions. J. Pharm. Pharmacol. 66, 285-296.

[23]Surwase, S. A., Itkonen, L., Aaltonen, J., Saville, D., Rades, T., Peltonen, L. and Strachan, C. J., 2015. Polymer incorporation method affects the physical stability of amorphous indomethacin in aqueous suspension. Eur. J. Pharm. Biopharm. 96, 32-43.

[24]Dian, L., Yu, E., Chen, X., Wen, X., Zhang, Z., Qin, L., Wang, Q., Li, G. and Wu, C., 2014. Enhancing oral bioavailability of quercetin using novel soluplus polymeric micelles. Nanoscale Res. Lett. 9, 1-11.

[25]Homayouni, A., Sadeghi, F., Varshosaz, J., Garekani, H. A. and Nokhodchi, A., 2014. Comparing various techniques to produce micro/nanoparticles for enhancing the dissolution of celecoxib containing PVP. Eur. J. Pharm. Biopharm. 88, 261-274.

[26]Wlodarski, K., Sawicki, W., Haber, K., Knapik, J., Wojnarowska, Z., Paluch, M., Lepek, P., Hawelek, L. and Tajber, L., 2015. Physicochemical properties of tadalafil solid dispersions-impact of polymer on the apparent solubility and dissolution rate of tadalafil. Eur. J. Pharm. Biopharm. 94, 106-115.

[27]Liu, J., Zou, M., Piao, H., Liu, Y., Tang, B., Gao, Y., Ma, N. and Cheng, G., 2015. Characterization and Pharmacokinetic Study of Aprepitant Solid Dispersions with Soluplus®. Molecules. 20, 11345-11356.

[28]DOW, 2002. METHOCEL cellulose ethers in aqueous systems for tablet coating. Published literature - The Dow Chemical Company.

[29]BASF, 2013. Soluble Kollidon grades. Technical information - BASF the chemical company.

[30]Flory, P. J., 1953. Principles of polymer chemistry, In: (Eds.), Cornell University Press, .

[31]Marsac, P. J., Li, T. and Taylor, L. S., 2009. Estimation of drug-polymer miscibility and solubility in amorphous solid dispersions using experimentally determined interaction parameters. Pharm. Res. 26, 139-151.

[32]Law, D., Krill, S. L., Schmitt, E. A., Fort, J. J., Qiu, Y., Wang, W. and Porter, W. R., 2001. Physicochemical considerations in the preparation of amorphous ritonavir-poly (ethylene glycol) 8000 solid dispersions. J. Pharm. Sci. 90, 1015-1025.

[33]Chiou, W. L. and Riegelman, S., 1971. Pharmaceutical applications of solid dispersion systems. J. Pharm. Sci. 60, 1281-1302.

[34]Six, K., Leuner, C., Dressman, J., Verreck, G., Peeters, J., Blaton, N., Augustijns, P., Kinget, R. and Van den Mooter, G., 2002. Thermal properties of hot-stage extrudates of itraconazole and eudragit E100. Phase separation and polymorphism. J. Therm. Anal. Calorim. 68, 591-601.

[35]Hoei, Y., Yamaura, K. and Matsuzawa, S., 1992. A lattice treatment of crystalline solvent-amorphous polymer mixtures on melting point depression. J. Phys. Chem. A. 96, 10584-10586.

[36]Bawn, C. E. H., Freeman, R. F. J. and Kamaliddin, A. R., 1950. High polymer solutions. Part I.Vapour pressure of polystyrene solutions. T. Faraday Soc. 46, 677-684.

[37]Newing, M. J., 1950. Thermodynamic studies of silicones in benzene solution. T. Faraday Soc. 46, 613-620.

[38]Marsac, P. J., Shamblin, S. L. and Taylor, L. S., 2006. Theoretical and practical approaches for prediction of drug-polymer miscibility and solubility. Pharm. Res. 23, 2417-2426.

[39]Frank, K. J., Westedt, U., Rosenblatt, K. M., Holig, P., Rosenberg, J., Magerlein, M., Fricker, G. and Brandl, M., 2012. The amorphous solid dispersion of the poorly soluble ABT-102 forms nano/microparticulate structures in aqueous medium: impact on solubility. Int. J. Nanomedicine. 7, 5757-5768.

[40]Sivaiah, K., Kumar, K. N., Naresh, V. and Buddhudu, S., 2011. Structural and optical properties of Li+: PVP & Ag+: PVP polymer films. Mater. Sci. Appl. 2, 1688-1696.

[41]Shamma, R. N. and Basha, M., 2013. Soluplus®: A novel polymeric solubilizer for optimization of Carvedilol solid dispersions: Formulation design and effect of method of preparation. Powder Technol. 237, 406-414.
[42]Sahoo, S., Chakraborti, C. K. and Behera, P. K., 2011. Spectroscopic investigations of a ciprofloxacin/hpmc mucoadhesive suspension. Int. J. App. Pharm. 4, 1-8.
[43]Surikutchi, B. T., Patil, S. P., Shete, G., Patel, S. and Bansal, A. K., 2013. Drug-excipient behavior in polymeric amorphous solid dispersions. J. Excip. Food Chem. 4, 70-94.

Chapter 3

Formulation Design and Evaluation of Amorphous ABT-102 Nanoparticles

ABSTRACT

Amorphous nanoparticles are able to enhance the kinetic solubility and concomitant dissolution rates of BCS class II and BCS class II/IV molecules due to their characteristic increased supersaturation levels, smaller particle size and greater surface area. A DoE approach was applied to investigate formulation and spray drying process parameters for the preparation of spray dried amorphous ABT-102 nanoparticles. Stability studies were performed on the optimized formulations to monitor physical and chemical changes under different temperature and humidity conditions. SLS/soluplus® and SLS/PVP K25 were the best stabilizer combinations. Trehalose was used to prevent nanoparticle aggregation during spray drying. Particle size distribution, moisture content, PXRD, PLM, FTIR and *in vitro* dissolution were utilized to characterize the spray dried nanoparticle formulations. The formulations prepared using soluplus® showed enhanced dissolution rate compared to those prepared using PVP K25. Following three months storage, it was observed that the formulations stored at 4°C were stable in terms of particle size distribution, moisture content, and crystallinity, whereas those stored at 25°C/60%RH and 40°C/75%RH were unstable. A predictive model to prepare stable solid spray dried amorphous ABT-102 nanoparticles, incorporating both formulation and process parameters, was successfully developed using multiple linear regression analysis.

3.1. INTRODUCTION

There has been a tremendous revolution in the field of nanotechnology, resulting in nano-medicines for diagnosis and therapy [1]. One application of nano-medicines is to improve drug dissolution and bioavailability. Such systems are of importance since most of the recent drug molecules coming out of the drug discovery pipeline are water insoluble and may pose bioavailability challenges[2]. Drug nanoparticles (amorphous and crystalline) are one of the novel nano-medicine tools to resolve the issues of solubility and bioavailability, associated with brick-like BCS class II and II/IV molecules [3]. Two basic methods to manufacture such nanoparticles: (i) a "top-down approach" (*i.e.* milling/grinding of the particles to

achieve the required size) and (ii) a "bottom-up approach" (*i.e.* precipitation of solubilized drug by adding an anti-solvent system) are commonly utilized [4]. The top-down approach is very time consuming and usually leads to crystalline particles whereas the bottom-up approach is less time consuming and usually leads to amorphous particles due to fast solvent evaporation and thus precipitation of the API as amorphous particles [5].

Amorphous drug nanoparticles are sub-micron colloidal dispersions of discrete drug particles, stabilized with polymers, surfactants or a mixture of both polymers and surfactant [6-8]. Amorphous nanoparticles through their combined mechanisms of enhancing dissolution rates (due to nano-size range and amorphous solid state form) and increasing supersaturation levels (due to amorphous solid state form) can significantly enhance solubility and bioavailability of poorly water-soluble active pharmaceutical ingredients (APIs) [BCS class II and II/IV] [9-15]. Amorphous nanoparticles of itraconazole have been shown to have improved dissolution and enhanced bioavailability compared to crystalline nanoparticles and amorphous macroparticles. For example, Kumar *et. al.* have reported that nano-amorphous itraconazole resulted in a 2.5-fold and 18-fold increase in bioavailability compared to macro-amorphous (melt quench) and macro-crystalline formulations respectively [16]. Similarly in another study, Dhumal *et. al*. showed that nano-amorphous cefuroxime resulted in a 2-fold increase in bioavailability compared to a macro-crystalline formulation [17]. However, until now, only a few nano-crystalline products have been successfully marketed for improved drug bioavailability [18]. Additionally, the technology to manufacture amorphous nanoparticles has been limited to only the nutraceutical and cosmetic industries [19]. Accordingly, it is important to optimize formulation and process parameters to achieve stable amorphous nanoparticles with desired properties of enhanced dissolution and bioavailability.

In the current study, we have prepared stable spray dried amorphous nanoparticles of ABT-102 (log P-5.2, aqueous solubility ~ 0.05 µg/mL in buffer [20]), a hydrophobic BCS class II molecule. A DoE approach was applied to investigate the spray drying process and formulation parameters. A three month stability study (40°C/75%RH, 25°C/60%RH and 4°C) was conducted to monitor the stability of the amorphous nanoparticles in terms of particle size distribution, *in vitro* dissolution and crystallinity. Based on the DoE approach

and stability studies, a predictive model to prepare stable solid spray dried ABT-102 amorphous nanoparticles, incorporating both formulation and process parameters, was successfully developed using multiple linear regression analysis.

3.2. MATERIALS

Crystalline ABT-102 (greater than 99% purity) was provided by AbbVie Pte. Ltd., Singapore. Soluplus®, PVP K-25 (polyvinyl pyrrolidone Kollidon®-25) and HPMC (hydroxy propyl methyl cellulose) were gifted by Dow Chemical Company. Sodium lauryl sulfate was purchased from Sigma Aldrich. Trehalose was gifted by Gattefose. The chemical structures are shown in **Table 3.1**. HPLC (high pressure liquid chromatography) grade solvents were purchased from Fisher Scientific. Inspire C18 column (4.6 mm x 100 mm, 5μm) was gifted by Dikma Technologies Inc.

3.3. METHODS

3.3.1. Sonoprecipitation of ABT-102

Amorphous nanoparticles were prepared using the sonoprecipitation approach. Briefly, 400 mg of the ABT-102 was completely dissolved in a 25 mL of methanol (16 mg/mL). Drug solution in methanol was injected (using a syringe with a 22.1G needle) into an aqueous phase (275 mL) containing stabilizers (soluplus®+SLS and PVP K-25+SLS) at a rate of 10 mL/min under probe sonication. A sonic dismembrator (Fisher scientific model 550) using a probe tip diameter of 13 mm at a frequency of 20 KHz was used. The probe tip was immersed a distance of 5 mm into the antisolvent solution and sonication was carried out for the optimized time of 4 minutes. The entire process was conducted at 2-8°C to prevent any drug degradation due to thermal stress. The resultant nanosuspensions were kept under magnetic stirring until further use.

3.3.2 Design of Experiments

Two different polymers (soluplus® and PVP K-25) in combination with SLS were evaluated for stabilization of the ABT-102 amorphous nanoparticles, based on results of screening studies for different stabilizers and the preliminary probe sonication studies. Two different

DoE design templates were drawn and studied for optimization of the formulation and spray drying process parameters.

3.3.2.1 Formulation parameters

Optimization of different formulation parameters [*e.g.* concentration of polymer (soluplus® and PVP K-25), surfactant (SLS) and sugar (trehalose)] for the preparation of amorphous ABT-102 nanoparticles was performed using a central composite design. Three critical factors that may affect the preparation of spray-dried formulations were selected (concentration of polymer, concentration of surfactant and amount of sugar). Six different responses were monitored namely: particle size, PDI, drug loading, yield of spray-dried powder, moisture content and zeta potential. The data obtained were evaluated using Design Expert statistical software version 9 (Stat-ease, Minneapolis, USA). For the polymer concentration, the minimum and maximum levels (concentrations) were 0.3 %w/v and 0.7 %w/v, respectively with 0.5 %w/v as the center point and 0.16 %w/v and 0.84 %w/v were the star or alpha points. For the surfactant concentration, the minimum and maximum levels (concentrations) were 0.03 %w/v and 0.07 %w/v, respectively with 0.05 %w/v as the center point and 0.016 %w/v and 0.084 %w/v were the star or alpha points. For the amount of sugar, the minimum and maximum levels were 600 mg and 1000 mg, respectively with 800 mg as the center point and 464 mg and 1136 mg were the star or alpha points. The critical quality attributes were total yield and particle size distribution of the spray dried product. A DoE for formulation parameters was carried out using soluplus soluplus® (table 3.2) and PVP K-25 (table 3.3) as the stabilizers. A total of 20 spray drying experiments post sonoprecipitation were performed.

3.3.2.2 Spray drying process parameters

Optimization of different spray-drying process parameters (*e.g.* temperature, aspirator setting, and feed rate) for the preparation of amorphous ABT-102 nanoparticles was performed using a central composite design. Three critical factors that may affect the preparation of spray-dried formulations were selected, namely the inlet temperature, aspirator rate and feed flow rate. Six different responses were monitored: outlet temperature (temperature at the connection between the spray drying chamber and cyclone); drug

loading; yield of spray-dried powder; particle size; PDI; and moisture content. The data obtained was evaluated using Design Expert statistical software version 9 (Stat-ease, Minneapolis, USA). For the inlet temperature, the minimum and maximum levels (temperatures) were 95°C and 130°C, respectively with 110°C as the center point and 83°C and 142°C were the star or alpha points. For the aspirator rate, the minimum and maximum levels (rate of dry air flow) were 55% and 75%, respectively with 65% as the center point and 48% and 82% were the star or alpha points. For the feed flow rate, the minimum and maximum levels (rate of feed flow) were 15% and 25%, respectively with 20% as the center point and 12% and 28% were the star or alpha points. The critical quality attributes were total yield and particle size distribution of the spray dried product. A DoE for the spray drying process parameters was carried out using soluplus® as the stabilizer (**Table 3.4**). A total of 20 spray drying experiments post sonoprecipitation were performed.

Based on the above DoE studies, for the spray drying process and formulation parameters, optimized formulations (n=3) were prepared and stored at three different storage conditions (4°C, 25°C/60%RH and 40°C/75%RH) for stability testing of the amorphous ABT-102 nanoparticles for 1 and 3 month/s.

3.3.3 Spray drying

The liquid ABT-102 nanosuspensions were converted to solid ABT-102 amorphous nanoparticles using a Buchi B-290 spray dryer (Buchi Labortechhnik AG, Switzerland). The spray drier was equilibrated using distilled water at the following conditions (inlet temperature 110°C, feed rate 5 ml/min and aspiration rate -30 mbar). The outlet temperature was approximately 75°C. The inlet temperature of 110°C was selected based on a proof of concept study to ensure maximum dry gas for the efficient removal of solvent at high evaporation rates without affecting the nanoparticle integrity, therefore minimizing the moisture content in the final product. Upon equilibration of the spray dryer, the distilled water was replaced with nanosuspension formulation. In order to prevent nanoparticles from aggregating, drug:trehalose (1:2, w/w) was added to each formulation before spray drying. The final products, in the form of spray-dried powders, were collected from the collection chamber and immediately analyzed for particle size and crystallinity.

3.3.4. Particle size measurement

Particle size measurements were performed using a Zetasizer Nano ZS90 (Malvern Instruments, UK). Briefly, the liquid or spray-dried samples were suspended in a saturated and filtered (0.2 μm PVDF membrane filter) solution of ABT-102 in 30% glycerin solution to avoid any discrepancy resulting from dissolution of the nano-particles during measurement. The viscosity of this dispersant solution was measured *via* a Brookfield viscometer (Model DV-III) and used to calculate the particle size of the re-dispersed and liquid nano-crystalline suspensions. All samples were analyzed in triplicate.

3.3.5. Powder X-Ray Diffraction (PXRD)

PXRD was utilized to determine the crystallinity of the spray-dried samples. X-ray diffraction patterns were obtained using an X-ray diffractometer (Model D5005, Bruker AXS Inc., Madison, WI) with Cu-kα radiation, a voltage of 40 kV, and a current of 40 mA. All the scans were performed with a scanning rate of 2°/minute with steps of 0.02° from 5° to 40° at 2θ ranges.

3.3.6. HPLC analytical method

The quantification of ABT-102 was conducted using a Perkin Elmer-HPLC system (USA) with a UV detector. The absorbance wavelength was set at 267 nm. The mobile phase was a mixture of 0.1% trifluoro acetic acid in water and acetonitrile at a isocratic 50:50 %v/v ratio. A C18 Inspire 5μ analytical column (4.6 mm × 100 mm) was used with a flow rate of 1 ml/min.

3.3.7 Transmission electron microscopy (TEM)

The morphology of the amorphous ABT-102 nanoparticles were observed using TEM. TEM images were obtained using FEI Tecnai G2 Spirit BioTWIN Lab6 20-120 kV TEM, with a 4 megapixel AMT 2k XR40 CCD camera (Oregon, USA). The samples were negatively stained using Uranyl acetate. One drop of the sample was transferred onto a copper TEM grid and dried under vacuum. The samples on the TEM grid were analyzed at 80 kV.

3.3.8 Attenuated Total Reflectance - Fourier Transform Infrared Spectroscopy (ATR-FTIR)

IR spectroscopy was performed using a Nicolet FTIR (iS5 FTIR, Thermo Scientific, USA) spectrometer with an attenuated total reflectance (ATR) accessory. Spray-dried powders were placed on the crystal window (Germanium) and compressed lightly using a pressure clamp. Spectra were recorded over a range of 400–4000 cm^{-1} with a resolution of 4 cm^{-1}, for 128 parallel scans. Data analysis was performed on Omnic® 6.0a software (Thermo Nicolet Corporation, USA).

3.3.9 Polarized Light Microscopy (PLM)

The spray-dried samples were dispersed in the immersion oil and placed on microscope slides. The samples were analyzed using an Olympus BH2 polarized microscope, USA with a Q-imaging camera, accessories and software. All the pictures were obtained at 10X resolution.

3.3.10. Stability

All the spray-dried powder formulations were stored at three different storage conditions *i.e.* 4°C, 25°C/60%RH and 40°C/75%RH for 3 months. Samples were withdrawn at 1 and 3 month/s and analyzed for particle size distribution, zeta potential, moisture content and crystallinity.

3.3.11. *In vitro* dissolution testing

USP apparatus I (basket apparatus) (Distek Inc. 2100C, NJ, USA) was utilized for the *in vitro* dissolution experiments. In the case of spray-dried powders, the samples were filled into hard gelatin capsules (size 000, Torpac) for *in vitro* dissolution studies. All the dissolution experiments were conducted at 37°C in 900 ml (sink conditions and non-sink conditions) of 0.1 N HCl and 0.025 %w/w Tween 80 (pH 1.2) at a speed of 100 rpm. At each time point, 2 ml samples were withdrawn from the dissolution chamber and replaced with fresh dissolution media. The samples were filtered using 0.1 μm PVDF filters to avoid any erroneous results from un-dissolved nano-particulates. All samples were analyzed using

the HPLC method as described above. The samples were analyzed initially and after storing for one month storage at three different conditions 4°C, 25°C/60%RH and 40°C/75%RH.

3.4. RESULTS & DISCUSSION

3.4.1. Selection of stabilizer/s

3.4.1.1 Selection of polymers and surfactants

Different polymers and surfactants were screened for the preparation of spray dried amorphous ABT-102 nanoparticles. The polymers investigated were PVP 40, PVP K-15/17, PVP K-25, PVP K-30, PVP K-90, HPMC E3, HPMC E5, HPMC E15, HPMC E50 and soluplus®. The surfactants investigated were Dowfax2A1, SLS, Triton X® and Pluronic F127. None of the above polymers and surfactants were able to stabilize the amorphous nanoparticles, both before and after spray drying, when used individually. The instabilities observed were both particle aggregation and change from the amorphous to the crystalline state. However, combinations of polymers and surfactants were able to stabilize the amorphous ABT-102 nanoparticles. Based on a preliminary study, PVP K-25 or soluplus® in combination with SLS were the best combinations of stabilizers (data not shown). Accordingly, these combinations were selected for the DoE study. The concentration ranges for the design study (0.3 – 0.7 %w/v for PVP K-25/soluplus® and 0.03 – 0.07 %w/v for SLS) were also based on the preliminary stabilization data.

3.4.1.2 Selection of solvents

The solubility of ABT-102 in different solvents (chloroform, hexane, PEG 400, tetra butyl methyl ether, ethyl ether, acetone, acetic acid, dichloromethane, methanol and acetonitrile) was investigated at room temperature. ABT-102 was insoluble in chloroform, hexane, PEG 400, tetra butyl methyl ether, ethyl ether, acetone, and acetic acid. The solubility of ABT-102 in dichloromethane and acetonitrile was below 1 mg/mL and that in methanol and ethanol it was around 16 mg/mL (data not shown). However, the yield of the spray dried powder when using ethanol as the solvent was significantly lower (10 %w/w) compared to that when using methanol (70 %w/w) as the solvent. Ethanol increases the hygroscopicity and therefore caused sticking of the nanoparticles to the walls of the spray dryer chamber.

Accordingly, methanol was selected as the solvent for the preparation of the amorphous nanoparticles.

3.4.1.3 Selection of sugars

Five different sugar molecules namely: mannitol, sucrose, lactose, trehalose and maltose were screened. For the selection of sugars, one polymer must be selected, which stabilizes the spray dried formulation. It has been previously reported that both PVP and HPMC are crystallization inhibitors and have been used for the preparation of amorphous solid dispersions [21]. In particular, PVP K-25 is a well-known crystallization inhibitor [22]. Accordingly, the PVP K-25/SLS stabilizer combination was used in the sugar screening study. As shown in Table 3, formulations containing higher concentrations of PVP K-25 (0.5%, w/v) appeared to be more stable before and after spray drying, compared to formulations containing lower concentrations of PVP K-25 (0.05%, w/v). Only trehalose and lactose were able to prevent nanoparticle aggregation during the spray drying process. Due to its high Tg (106°C), trehalose was selected for further investigation. The high Tg of trehalose, indicates less hygroscopicity as well as the absence of internal hydrogen bonding [23]. Accordingly, trehalose should be able to readily hydrogen bond with the nanoparticles during the spray drying process. In addition, these hydrogen bonds will facilitate removal of trehalose from nanoparticle surfaces when exposed to aqueous environment *in vivo* and during drug dissolution testing *in vitro* [24].

3.4.2. Design of Experiments

According to the results from the spray drying process DoE studies, as shown in Table 3.2, it was determined that certain responses (*i.e.* moisture content and drug loading) were not significantly affected by the spray drying process parameters investigated. However, other responses such as outlet temperature, yield, particle size and homogeneity of the spray-dried amorphous nanoparticles were significantly affected by the spray drying process parameters. Moreover, according to the results from the formulation DoE studies as shown in the Table 3.3, it was determined that certain responses (*i.e.* zeta potential and drug loading) were not significantly affected by the formulation parameters investigated. However, other responses (*i.e.* particle size, PDI, yield, and moisture content) were significantly affected by the formulation parameters investigated.

3.4.2.1 Optimization of formulation parameters of spray dried amorphous ABT-102 nanoparticles using soluplus®

1) Particle size

As observed from Table 3.5, it was evident that the surface cubic model was significant indicating that the model obtained (Table 3.6) was significant for the response (*i.e.* particle size of the spray-dried powder). The final equation, based on the three factors and the interaction terms for the prediction of the particle size of the spray-dried powder, is shown in Table 3.6. According to the contour plots (Figures 3.1(a) and 3.1(b)), it was observed that high polymer concentration and high amounts of sugar can prevent particle aggregation during the drying process, thus the particle size did not increase. However, the surfactant concentration had minimal effect on the particle size. The particle size was smaller (<200 nm) when the polymer concentration was >0.55% and the sugar amount was >800 mg.

2) Yield of the spray-dried powder

As observed from the Table 3.7, it was evident that the surface cubic model was significant indicating that the model (Table 3.8) was significant for the response (*i.e.* the yield of the spray-dried powder). The final equation, based on the three factors and the interaction terms for the prediction of the yield of the spray-dried powder, is shown in Table 3.8. According to the contour plots (Figure 3.2(a)), it was observed that the yield of the spray-dried powder increased with increase in the polymer and surfactant concentrations. Furthermore, it was observed that the yield of the spray-dried powder decreased with increase in the amount of sugar (Figure 3.2(b)). This may be due to the sticky nature of sugar in the presence of residual moisture resulting in more particle adhesion to the walls of the cyclone separator. As shown in Tables 3.7 and 3.8, as well as Figure 3.2, the yield was >70% when the polymer concentration was >0.5% and the surfactant concentration was >0.048%. However, the amount of sugar used had a significant effect on the yield of the spray-dried formulations.

Based on the DoE study for optimizing the formulation parameters, the statistical software recommended the optimized formulation parameters as shown in Table 3.15.

3.4.2.2 Optimization of formulation parameters of spray dried amorphous ABT-102 nanoparticles using PVP K25

1) Particle size

As observed from Table 3.9, it was evident that the surface cubic model was significant indicating that the model obtained (Table 3.10) was significant for the response (*i.e.* particle size of the spray-dried powder). The final equation, based on the three factors and the interaction terms for the prediction of the particle size of the spray-dried powder, is shown in Table 3.10. According to the contour plots (Figures 3.3), it was observed that the particle size of the spray-dried powder decreased with increase in the polymer concentration and the amount of sugar. However, the surfactant concentration had a minimal effect on the particle size. Increased polymer concentration and sugar amount can prevent particle aggregation during the drying process, thus the particle size did not increase. The particle size was smaller (<170 nm) when the polymer concentration was >0.5% and the sugar amount was >750 mg.

2) Yield of the spray-dried powder

As observed from the Table 3.11, it was evident that the surface cubic model was significant indicating that the model (Table 3.12) was significant for the response (*i.e.* the yield of the spray-dried powder). The final equation, based on the three factors and the interaction terms for the prediction of the yield of the spray-dried powder, is shown in Table 3.12. According to the contour plots (Figure 3.4(a)), it was observed that the yield of the spray-dried powder increased with increase in the polymer concentration, however the surfactant concentration had minimal effect on the yield of the spray dried powder. Furthermore, it was observed that the yield of the spray-dried powder decreased with increase in the amount of sugar (Figure 3.4(b)). This may be due to the sticky nature of sugar in the presence of the residual moisture resulting in more particle adhesion on the walls of the cyclone separator. As shown in Tables 3.11 and 3.12, as well as Figure 3.4, the yield was ≥80 % w/w when the polymer concentration and amount of sugar was >0.5% w/v and 800-900 mg respectively. However, the surfactant concentration had a minimum effect on the yield of the spray-dried formulations. Based on the DoE study for optimizing the formulation parameters, the statistical software recommended the optimized formulation parameters as shown in Table 3.15.

3.4.2.2 Optimization of spray drying process parameters

1) Particle size

As shown in Table 3.13, it was evident that the surface cubic model was significant indicating that the model was significant for the responses (*i.e.* particle size of the spray-dried powder). The final equation based on the three factors and the interaction terms for the prediction of the particle size of the spray dried powder is given in Table 3.14. As shown in Figure 3.5(a), the particle size of the spray-dried powder decreased with increase in the inlet temperature. However, the effect of aspirator rate on the particle size was minimal. Furthermore, it was observed that the particle size of the spray-dried powder decreased with decrease in the feed flow rate and increase in the inlet temperature (Figure 3.5(b)). Increased inlet temperature can increase the evaporation rate of the solvent from the nanosuspension droplets, which can reduce the particle size and consequently the homogeneity. In addition, a higher feed flow rate means that less liquid is evaporated from the nanoparticle surfaces, which in turn decreased the outlet temperature and both these factors resulted in particle aggregation. Based on the spray drying process parameter DoE, the particle aggregation was prevented when the inlet temperature and the aspirator rate were maintained above 115°C and 65%, respectively, while maintaining a low flow rate (<19%). Similarly total product yield was optimized for the spray drying process.

Based on the spray drying process parameter DoE study, the statistical software recommended the optimized process parameters (Table 3.15). These optimized process parameters were implemented in the DoE study for optimizing the formulation parameters.

3.4.3. Spray drying

The ABT-102 nanosuspensions were spray dried as mentioned in the methods section using trehalose as an ancillary excipient. All DoE formulations (spray drying process parameters and formulation parameters) were evaluated for drug loading, total spray dried powder yield, particle size and zeta potential. The optimized spray drying process parameters (inlet temperature: 110°C, aspirator rate: 80 and feed flow rate: 20), were used to perform the DoE studies for the formulation parameters of the ABT-102 spray dried powder prepared using the stabilizer combinations (PVP K25+SLS and soluplus®+SLS). The contour plots of the amorphous spray dried nanoparticles are shown in section 4.2. No polymorphic changes were observed for any of the DoE formulations as determined by PXRD (data not shown). Based on the formulation parameters DoE, a combination of 0.6% w/v soluplus®, 0.05%

w/v SLS and ~ 860 mg of trehalose was selected for the amorphous ABT-102 nanoparticle formulation. Additionally, based on the formulation parameters DoE, a combination of 0.3% w/v PVP K25, 0.07% w/v SLS and ~ 1000 mg of trehalose was selected for the amorphous ABT-102 nanoparticle formulation.

3.4.4. Stability studies

The optimized formulations prepared based on the parameters obtained from the formulation parameter DoE studies were stored at three different stability conditions; 4°C, 25°C/60%RH and 40°C/75%RH for one and three months. After one and three months, the formulations were analyzed for particle size distribution, moisture content and zeta potential. Additionally, the formulations were also analyzed using PXRD (to monitor any polymorphic transformation *i.e.* conversion of amorphous to crystalline form), ATR-FTIR (for interaction between drug and polymer), PLM (to monitor any generation of crystallinity) and *in vitro* dissolution testing (to observe the effect of temperature and humidity on drug release).

3.4.4.1 Particle size distribution

As shown in Table 3.16 (a and b) and Figure 3.6, the particle size and PDI of the prepared spray-dried nanosuspensions increased following one and three month/s storage under 40°C/75%RH conditions. On the other hand, the optimized formulation stored at 4°C and 25°C/75%RH were determined to be stable in terms of particle size distribution and zeta potential over the three month study period.

3.4.4.2 Moisture content

As observed in Figure 3.7, the moisture content increased for the formulations stored at 40°C/75%RH compared to those stored at 4°C and 25°C/60%RH. The formulations stored at 4°C and 25°C/60%RH were determined to be stable even after 3 months. It was also observed that the moisture content for the optimized formulation prepared using PVP K25 was higher compared to those prepared using soluplus® for all storage conditions, except at 4°C. The higher moisture content of the optimized formulation prepared using PVP K25 can be attributed to the low viscosity (hydrophilic nature) of PVP K25, which results in

water entrapment into the formulations. This can be compared to the high viscosity (combined hydrophilic and lipophilic nature) of soluplus®, which limits water entrapment.

3.4.4.3 Powder X-ray diffraction

The characteristic diffraction peaks of neat crystalline ABT-102 are 6.3°, 9.2°, 12°, 14.7°, 16.3°, 18.2°, 19.9°, 22.8°, 24.9° and 26.8°. As shown in Figure 3.8 (a and b), the optimized formulation prepared using soluplus® and PVP K25 showed a distinct halo pattern in PXRD after one and three month/s exposure at 4°C, 25°C/60%RH and 40°C/75%RH, indicating the amorphous nature of the formulations. However, the physical mixture containing the drug and polymer (soluplus® or PVP K25) resulted in distinct diffraction peaks, indicating the crystalline nature of the drug.

3.4.4.4 Attenuated total reflectance – Fourier transform infrared spectroscopy

According to Figure 3.9 (a and b), there was a band broadening between 3000-3500 cm^{-1} in the FTIR spectra for the spray-dried amorphous nanoparticles stored for one and three month/s under all conditions (*i.e.* 4°C, 25°C/60%RH, and 40°C/75%RH). However, there was no band broadening in the case of the crystalline raw drug and the physical mixture of the drug-polymer when stored under similar conditions. It was hypothesized that there may be hydrogen bonding between the N-H moiety of ABT-102 and the C=O group of the polymer (*i.e.* soluplus® or PVP K25). In case of the physical mixture of the drug and the polymer, a sharp peak was observed at 3380 cm^{-1}, indicating the absence of hydrogen bonding in the physical mixture.

3.4.4.5 Polarized light microscopy

As observed in Figure 3.10, there was no birefringence observed for the optimized formulation stored at 25°C/60%RH and 4°C after three months. However, those stored at 40°C/75%RH for three months showed extensive birefringence. The amorphous nanoparticles will absorb moisture under accelerated stress at 40°C/75%RH which in turn causes plasticization and consequent recrystallization. However, the PXRD diffractograms for the optimized formulations stored under all three stability conditions showed a halo pattern (Figure 3.10), indicating PXRD was not able to detect this phase transformation due to limitations in the sensitivity of this instrument (<= 5% of crystallinity). Additionally, it was observed that the optimized formulation prepared using soluplus® crystallized after only

one month storage at 40°C/75%RH, indicating that PVP K25 is a better crystallization inhibitor for this drug.

3.4.4.6 Transmission electron microscopy

As observed in Figure 3.11, the TEM images of the spray dried amorphous ABT-102 nanoparticles prepared using soluplus® showed the presence of the hydrophilic PEG chains of soluplus® extending from the particle surfaces. However, the TEM images of the spray dried amorphous ABT-102 nanoparticles prepared using PVP K25 did not show any tail like moieities on the exterior, instead the PVP appeared to be in a globular form on the surface of the drug particles.

3.4.5. *In vitro* dissolution testing

All the dissolution experiments were conducted as described in the methods section, under non sink conditions (20 times the sink condition). As observed from Figure 3.12, the spray dried amorphous ABT-102 nanoparticles prepared using soluplus® showed a four times increase in drug solubility (8-9 µg/mL) and were able to maintain supersaturation levels for 5 hours. The optimized formulations prepared using PVP K25 increased the drug solubility by three fold (6 µg/mL) and also maintained supersaturation levels for 5 hours after which the drug crystallized out.

The mechanism behind the enhanced solubility of amorphous ABT-102 nanoparticles compared to the macro-crystalline dug could be attributed to the better dispersibility of drug nanoparticles in soluplus®, due to the proper miscibility of the drug with the polycaprolactam moieties (hydrophobic region) of soluplus®. When the amorphous nanoparticles are exposed to the aqueous dissolution media, the polyethylene glycol moieties (hydrophilic region) undergoes rapid hydration into the aqueous solution, ultimately leading to enhanced solubility of the dispersed amorphous ABT-102 nanoparticles [25, 26]. The physical mixture of drug and polymer have slightly higher solubility compared to the macro-crystalline drug, due to the formation of a viscose gel of soluplus® around drug particles, which results in low miscibility between drug and the polymer, and ultimately increases the solubility of the physical mixture compared to the macro-crystalline drug. Similarly, the enhanced wettability of the drug nanoparticles in PVP

K25, resulted in increased solubility of the amorphous ABT-102 nanoparticles compared to the macro-crystalline drug. Although, PVP K25 is a strong crystallization inhibitor, the polymer was not as good as stabilizer for the amorphous ABT-102 nanoparticles, resulting in crashing out of the drug (recrystallization) after five hours of *in vitro* dissolution.

3.5. CONCLUSIONS

A novel sonoprecipitation method (a combination of ultrasonication and solvent-antisolvent precipitation) followed by spray drying for the preparation of the stable amorphous ABT-102 nanoparticles was developed. Based on the spray drying process and formulation DoE studies, two responses (particle size and total yield of spray dried amorphous ABT-102 nanoparticles) were significant, while the other responses (moisture content and drug loading) were not significant. Two polymers, PVP K25 and soluplus® were effective stabilizers for the preparation of the amorphous ABT-102 nanoparticles. FTIR data showed that the C=O moieities of these polymers interacted with the N-H moiety of the drug *via* hydrogen bonding to facilitate nanoparticle stabilization. Soluplus® possesses two carbonyl groups and therefore is able to form stronger hydrogen bonds with the drug. In addition, the lipophilic PVC region of soluplus® is able to interact with the drug, while the hydrophilic PEG region resulted in enhanced wettability of the amorphous nanoparticles, thus increasing the dissolution rate and maintaining higher supersaturation levels (four fold) compared to PVP K25 (three fold). PLM was a better solid state characterization tool compared to PXRD for the analysis of the amorphous ABT-102 nanoparticles stability. The stability studies carried out in the present study indicated that the storage conditions for the amorphous ABT-102 nanoparticles should be 4°C for long term stability. This study shows that amorphous nanoparticles prepared using sonoprecipitation followed by spray drying have an enhanced dissolution rate and may enhance bioavailability compared to macro-crystalline drug.

3.6. Tables

Table 3.1. Chemical structures of the active pharmaceutical ingredient and excipients

Materials	Chemical structures
ABT-102	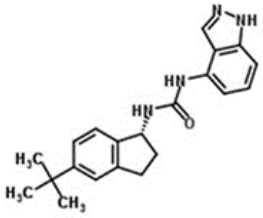
Soluplus® (polyvinyl caprolactam-polyvinyl acetate-polyethylene glycol graft copolymer)	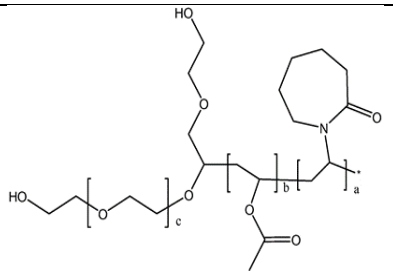
Polyvinyl pyrrolidone K25 (PVP K25 - Kollidon®)	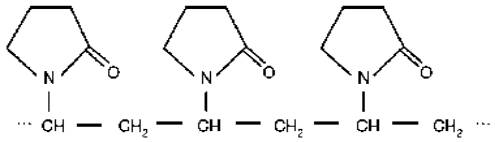
Sodium lauryl sulfate (SLS)	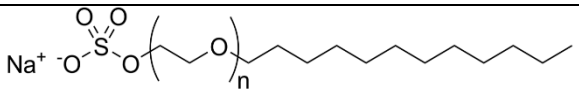
Trehalose	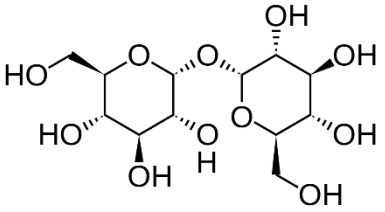

Table 3.2. Design space for the optimization of formulation parameters for the preparation of stable spray dried amorphous ABT-102 nanoparticles using soluplus® (3 Factors x 6 Responses).

No.	Factors			Responses					
	Polymer concentration	Surfactant concentration	Sugar	Particle size	PDI	Drug loading	Yield	Moisture content	Zeta potential
	%	%	mg	nm	-	%	%	%	mV
-	0.3-0.7	0.03-0.07	600-1000						
1	0.7	0.07	1200	159.3	0.186	11.76	75.63	2.566	-55.2
2	0.5	0.05	800	202.9	0.191	13.93	76.04	2.539	-61.6

3	0.5	0.05	800	194.6	0.187	13.91	71.09	2.256	-67.7
4	0.3	0.07	400	273.5	0.326	12.24	63.35	2.074	-75.7
5	0.5	0.05	800	190.7	0.172	13.95	70.81	2.279	-60.7
6	0.7	0.03	1200	191	0.216	12.84	74.22	2.676	-48.8
7	0.5	0.05	800	175.5	0.196	13.97	73.26	2.459	-57.5
8	0.5	0.05	800	202.9	0.178	13.8	69.16	2.382	-63
9	0.5	0.05	800	208.5	0.165	13.86	72.77	2.522	-59.6
10	0.5	0.08	800	211.9	0.225	13.93	68.18	2.418	-68.5
11	0.5	0.05	1473	202.5	0.136	13.75	69.15	3.093	-63.6
12	0.3	0.07	1200	214.2	0.3	13.91	52.69	3.113	-87.4
13	0.7	0.07	400	223	0.244	13.92	49.77	2.059	-71.7
14	0.3	0.03	400	537.4	0.488	12.39	67.49	2.507	-62.5
15	0.7	0.03	400	153.9	0.205	13.57	66.02	2.519	-39.9
16	0.84	0.05	800	193.4	0.11	11.85	64.15	2.535	-69.7
17	0.5	0.05	127	312.5	0.402	13.88	58.97	1.915	-69.2
18	0.16	0.05	800	261.4	0.415	13.38	42.91	4.008	-85.2
19	0.5	0.02	800	231.8	0.263	13.2	53.95	2.926	-61.8
20	0.3	0.03	1200	78.57	0.208	13.91	32.63	3.69	-79.3

Table 3.3. Design space for the optimization of formulation parameters for the preparation of stable spray dried amorphous ABT-102 nanoparticles using PVP K25 (3 Factors x 6 Responses).

No.	Factors			Responses					
	Polymer concentration	Surfactant concentration	Sugar	Particle size	PDI	Drug loading	Yield	Moisture content	Zeta potential
	%	%	mg	nm	-	%	%	%	mV
-	0.3-0.7	0.03-0.07	600-1000						
1	0.5	0.084	800	153.2	0.171	8.820	72.72	4.133	-72.6
2	0.5	0.05	800	162.1	0.177	10.430	79.06	2.053	-85.9
3	0.3	0.03	1000	161.8	0.168	11.730	81.86	2.801	-84.6
4	0.5	0.05	800	166.2	0.131	10.490	75.88	2.108	-66.9
5	0.5	0.05	800	162.6	0.183	10.670	80.12	4.663	-76.6
6	0.84	0.05	800	179.8	0.163	7.710	78.95	4.698	-62.0
7	0.5	0.05	800	165.0	0.142	9.840	74.24	4.289	-80.7
8	0.16	0.05	800	185.1	0.266	13.660	84.32	2.284	-84.6
9	0.5	0.05	800	159.4	0.155	10.660	76.73	3.408	-79.1
10	0.5	0.05	464	165.2	0.146	12.200	68.79	4.451	-76.4
11	0.5	0.016	800	170.5	0.112	10.750	78.80	3.634	-89.2
12	0.3	0.03	600	172.7	0.194	13.960	62.33	3.497	-81.1
13	0.7	0.03	600	179.7	0.228	8.750	81.90	4.604	-61.9
14	0.7	0.03	1000	169.2	0.142	8.380	76.83	3.865	-76.9

15	0.5	0.05	1136	150.9	0.205	8.940	64.85	3.693	-62.9
16	0.7	0.07	600	169.8	0.191	8.950	66.25	4.914	-73.3
17	0.3	0.07	1000	151.0	0.166	11.530	69.29	2.988	-90.3
18	0.7	0.07	1000	156.8	0.122	8.290	87.19	4.43	-79.2
19	0.5	0.05	800	169.8	0.170	9.730	78.57	3.615	-84.7
20	0.3	0.07	600	183.0	0.248	13.16	78.71	3.125	-87.4

Table 3.4. Design space for optimization of the spray drying process parameters for the preparation of stable ABT-102 amorphous spray dried nanoparticles (3 factors x 6 responses).

No.	Factors			Responses					
	Inlet temperature	Aspirator	Feed flow	Outlet temperature	Drug loading	Yield	Particle size	Moisture content	PDI
	°C	%	%	°C	% (w/w)	% (w/w)	nm	% (w/w)	-
-	95-130	55-75	15-25						
1	110	65	20	43	13.4	59.33	202.8	2.653	0.271
2	95	75	25	32	13.67	49.82	234.1	2.383	0.271
3	110	65	20	44	13.6	61.49	225.2	2.556	0.231
4	125	75	15	65	13.12	67.19	211.3	2.101	0.242
5	95	75	15	46	12.32	69.33	191	2.666	0.203
6	110	65	28	33	13.59	37.3	383.9	2.691	0.543
7	95	55	25	29	14.04	23.75	330.6	1.971	0.663
8	110	82	20	56	13.95	74.6	198.6	2.684	0.247
9	125	55	25	42	13.19	37.89	244.1	2.204	0.304
10	125	55	15	56	13.03	50.39	186.8	2.277	0.162
11	110	65	20	43	13.28	58.19	214.7	2.481	0.263
12	110	48	20	39	13.08	37.19	213	2.385	0.185
13	85	65	20	29	14.14	38.21	386	2.48	0.643
14	110	65	20	42	13.67	58.48	228.7	2.617	0.278
15	110	65	20	44	13.44	59.71	216.4	2.462	0.253
16	95	55	15	29	14.2	47.72	213.8	2.587	0.234
17	110	65	12	56	13.1	67.02	180.4	1.964	0.156
18	110	65	20	44	13.38	59.21	209.4	2.519	0.224
19	135	65	20	56	13.98	59.37	155.1	2.186	0.248
20	125	75	25	50	12.98	59.82	228.8	1.975	0.218

Table 3.5. ANOVA response table for particle size of the spray-dried powder.

ANOVA for response surface cubic model (Aliased)						
Analysis of variance table [partial sum of squares - Type III]						
	Sum of		**Mean**	**F**	**p-value**	
Source	**Squares**	**df**	**Square**	**Value**	**Prob > F**	
Model	1.472E+005	13	11326.73	70.20	< 0.0001	significant

A-Polymer	2312.00	1	2312.00	14.33	0.0091	
B-Surfactant	198.01	1	198.01	1.23	0.3104	
C-Sugar	6050.00	1	6050.00	37.49	0.0009	
Lack of Fit	266.50	1	266.50	1.90	0.2267	not significant
R-squared – 0.9935, Adjusted R-squared – 0.9793						

Table 3.6. Final equation to predict the response: particle size of the spray-dried powder.

Final equation in terms of coded factors:	
Particle size	=
+196.14	
-20.22	* A
-5.92	* B
-32.70	* C
+20.71	* AB
+61.44	* AC
+37.34	* BC
+9.23	* A^2
+7.26	* B^2
+19.87	* C^2
-62.54	* ABC
-5.44	* A^2B
-35.39	* A^2C
-26.84	* AB^2
A – concentration of polymer, B – concentration of surfactant, C – amount of sugar	

Table 3.7. ANOVA response table for total yield of the spray-dried powder.

ANOVA for response surface cubic model (Aliased)						
Analysis of variance table [partial sum of squares - Type III]						
	Sum of		**Mean**	**F**	**p-value**	
Source	**Squares**	**df**	**Square**	**Value**	**Prob > F**	
Model	2578.49	13	198.35	33.79	0.0002	significant
A-Polymer	225.43	1	225.43	38.40	0.0008	
B-Surfactant	101.29	1	101.29	17.26	0.0060	
C-Sugar	51.80	1	51.80	8.82	0.0249	
Lack of Fit	6.62	1	6.62	1.16	0.3310	not significant
R-squared – 0.9865, Adjusted R-squared – 0.9573						

Table 3.8. Final equation to predict the response: total yield of the spray-dried powder.

Final equation in terms of coded factors:	
Yield	=
+72.14	
+6.31	* A
+4.23	* B
+3.03	* C

-3.85	* AB
+9.95	* AC
+5.23	* BC
-6.29	* A^2
-3.63	* B^2
-2.57	* C^2
-0.82	* ABC
-4.10	* A^2B
-4.46	* A^2C
-0.13	* AB^2
A – concentration of polymer, B – concentration of surfactant, C – amount of sugar	

Table 3.9. ANOVA response table for particle size of the spray-dried powder.

ANOVA for response surface cubic model (Aliased)						
Analysis of variance table [partial sum of squares - Type III]						
	Sum of		**Mean**	**F**	**p-value**	
Source	**Squares**	**df**	**Square**	**Value**	**Prob > F**	
Model	1851.57	13	142.43	12.96	0.0024	significant
A-Polymer	13.87	1	13.87	1.26	0.3042	
B-Surfactant	150.80	1	150.80	13.72	0.0100	
C-Sugar	102.24	1	102.24	9.30	0.0225	
Lack of Fit	0.38	1	0.38	0.029	0.38	not significant
R-squared – 0.9656, Adjusted R-squared – 0.8911						

Table 3.10. Final equation to predict the response: particle size of the spray-dried powder.

Final equation in terms of coded factors:	
Particle size	=
+164.15	
-1.57	* A
-5.16	* B
-4.25	* C
-2.73	* AB
+2.41	* AC
-2.94	* BC
+6.53	* A^2
-0.74	* B^2
-2.09	* C^2
+2.33	* ABC
+2.32	* A^2B
-4.05	* A^2C
+2.45	* AB^2
A – concentration of polymer, B – concentration of surfactant, C – amount of sugar	

Table 3.11. ANOVA response table for total yield of the spray-dried powder.

ANOVA for response surface cubic model (aliased)						
Analysis of variance table [partial sum of squares - Type III]						
	Sum of		**Mean**	**F**	**p-value**	
Source	**Squares**	**df**	**Square**	**Value**	**Prob > F**	
Model	811.18	13	62.40	13.73	0.0021	significant
A-Polymer	14.41	1	14.41	3.17	0.1252	
B-Surfactant	18.47	1	18.47	4.06	0.0904	
C-Sugar	7.76	1	7.76	1.71	0.2391	
Lack of Fit	3.01	1	3.01	0.62	0.4665	not significant
R-squared – 0.9675, Adjusted R-squared – 0.8970						

Table 3.12. Final equation to predict the response: total yield of the spray-dried powder.

Final equation in terms of coded factors:	
Yield	=
+77.40	
-1.60	* A
-1.81	* B
-1.17	* C
-1.14	* AB
+0.72	* AC
-0.37	* BC
+1.69	* A^2
-0.39	* B^2
-3.55	* C^2
+6.87	* ABC
+1.62	* A^2B
+4.42	* A^2C
+4.09	* AB^2
A – concentration of polymer, B – concentration of surfactant, C – amount of sugar	

Table 3.13. ANOVA response table for particle size of the spray-dried powder.

ANOVA for response surface cubic model (Aliased)						
Analysis of variance table [partial sum of squares - Type III]						
	Sum of		**Mean**	**F**	**p-value**	
Source	**Squares**	**df**	**Square**	**Value**	**Prob > F**	
Model	1.477E-005	13	1.136E-006	25.55	0.0004	significant
A-Inlet temperature	7.437E-006	1	7.437E-006	167.22	< 0.0001	
B-Aspirator	6.101E-011	1	6.101E-011	1.372E-003	0.9717	
C-Feed flow rate	2.751E-006	1	2.751E-006	61.85	0.0002	

Lack of Fit	5.211E-008	1	5.211E-008	1.21	0.3209	not significant
R-squared – 0.9823, Adjusted R-squared – 0.9438						

Table 3.14. Final equation to predict the response: particle size of the spray dried powder.

Final equation in terms of coded factors:	
1/(Particle size)	=
+4.629E-003	
+1.147E-003	* A
+3.284E-006	* B
-6.974E-004	* C
-2.405E-004	* AB
+1.532E-004	* AC
+1.694E-004	* BC
-1.335E-005	* A^2
+5.075E-005	* B^2
-2.755E-004	* C^2
-2.703E-006	* ABC
+2.075E-004	* A^2B
+1.965E-004	* A^2C
-1.007E-003	* AB^2
A = Inlet temperature, B = Aspirator rate, C = Feed flow rate	

Table 3.15. Statistically predicted factors and responses based on the DoE studies.

DoE studies	**Inlet temperature (°C)**	**Aspirator rate (%)**	**Feed flow rate (%)**	**Outlet temperature (°C)**	**Yield (%)**	**Particle size (nm)**	**PDI**	**Desirability**		
Spray drying process parameters	110	80	20	53.65	72.80	190.45	0.164	0.868		
Formulation parameters (using soluplus)	**Polymer concentration (% w/v)**	**Surfactant concentration (% w/v)**	**Amount of sugar (mg)**	**Particle size (nm)**	**PDI**	**Drug loading (%)**	**Yield (%)**	**Moisture content (%)**	**Zeta potential (mV)**	**Desirability**
	0.584	0.054	860	188.54	0.145	13.62	75.02	2.32	-61.16	0.86
Formulation parameters (using PVP K25)	0.3	0.069	1000	150.9	0.165	11.43	68.92	2.84	-84.6	0.823

Table 3.16. Physicochemical properties of the optimized formulations prepared using: (a) soluplus®; and (b) PVP K25. Following one and three month/s exposure under different storage conditions.

(a) Nanoparticles prepared using soluplus®						
No.	**Testing formulation**	**Storage conditions**	**Particle size (nm)**	**PDI**	**Moisture content (%)**	**Zeta potential (mV)**
Predicted values			**188.6**	**0.145**	**2.32**	**-61.2**

Experimental values						
1	**Optimized spray dried nanoparticles prepared using soluplus®**	**Initial**	**189.3**	**0.197**	**1.81**	**-55.1**
2		**40°C/75%RH – 1 month**	483.9	0.613	2.039	-67.8
3		**25°C/60%RH – 1 month**	196.8	0.177	2.225	-67.0
4		**4°C – 1 month**	175.6	0.183	2.313	-66.4
5		**40°C/75%RH – 3 months**	386.2	0.319	4.712	-71.4
6		**25°C/60%RH – 3 months**	162.1	0.211	2.231	-65.4
7		**4°C – 3 months**	186.5	0.222	2.197	-66.0

(b) Nanoparticles prepared using PVP K-25						
No.	**Testing formulation**	**Storage conditions**	**Particle size (nm)**	**PDI**	**Moisture content (%)**	**Zeta potential (mV)**
Predicted values			**150.9**	**0.165**	**2.84**	**-84.6**
Experimental values						
1	**Optimized spray dried nanoparticles prepared using PVP K25**	**Initial**	**148.9**	**0.15**	**2.27**	**-73.2**
4		**40°C/75%RH – 1 month**	79.94	0.173	2.86	-58.3
5		**25°C/60%RH – 1 month**	148.4	0.127	2.33	-87.4
6		**4°C – 1 month**	145.0	0.173	2.15	-84.9
7		**40°C/75%RH – 3 months**	307.2	0.489	4.42	-56.0
8		**25°C/60%RH – 3 months**	207.5	0.223	2.71	-76.3
9		**4°C – 3 months**	152.8	0.15	2.20	-93.2

3.7. Figures

GRAPHICAL ABSTRACT:

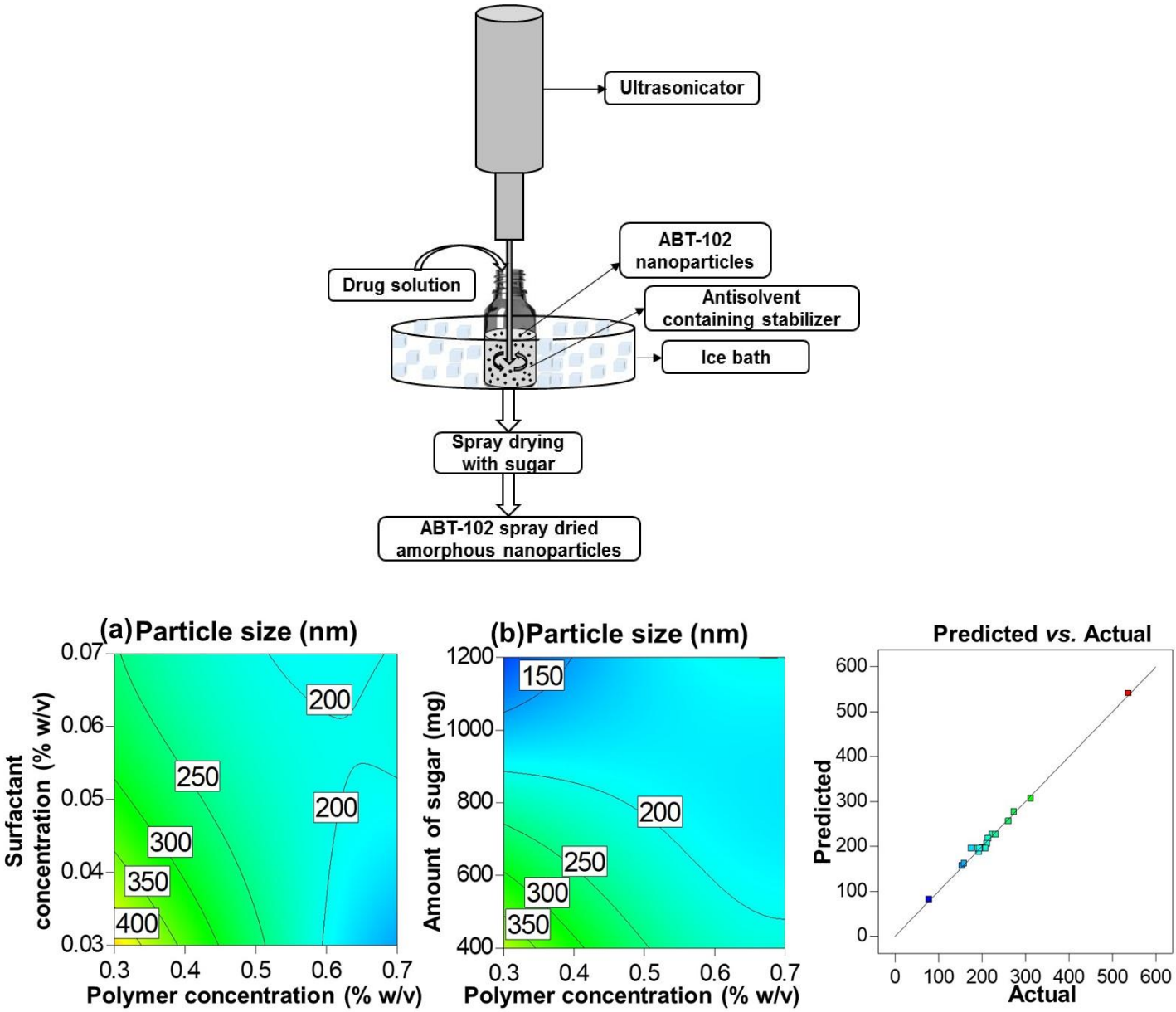

Figure 3.1. Contour plots for response: particle size of the spray-dried powder. (a) The effect of polymer concentration and surfactant concentration on the particle size of the spray-dried powder. (b) The effect of polymer concentration and amount of sugar on the particle size of the spray-dried powder. (polymer – Soluplus, surfactant – SLS, sugar – trehalose)

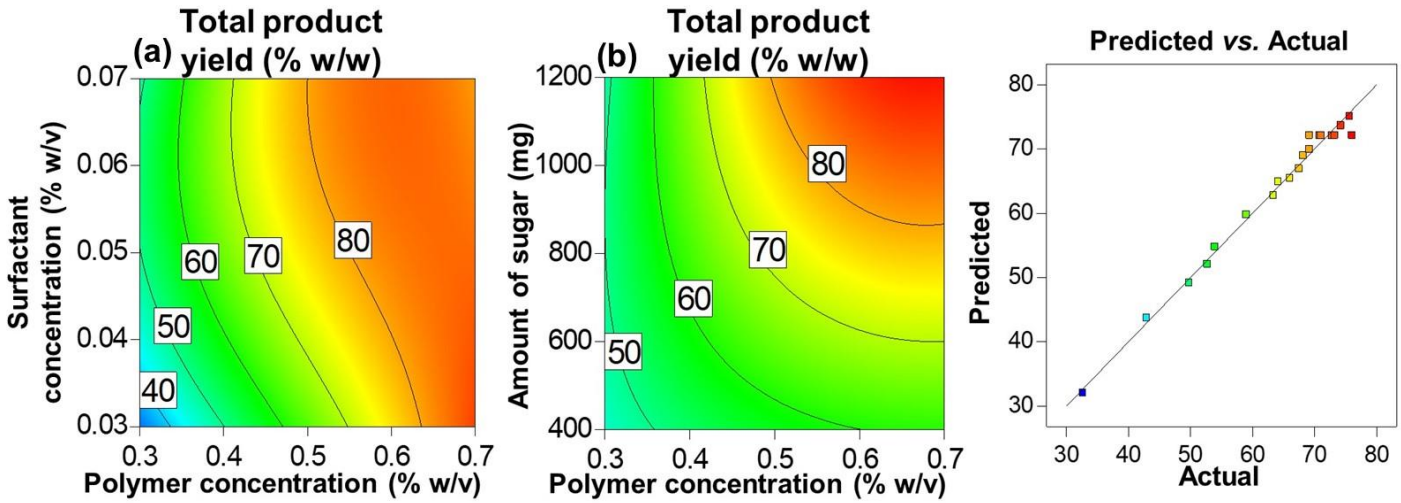

Figure 3.2. Contour plots for response: the yield of the spray-dried powder. (a) The effect of polymer concentration and surfactant concentration on the yield of the spray-dried powder. (b) The effect of polymer concentration and amount of sugar on the yield of the spray-dried powder. (polymer – Soluplus, surfactant – SLS, sugar – trehalose)

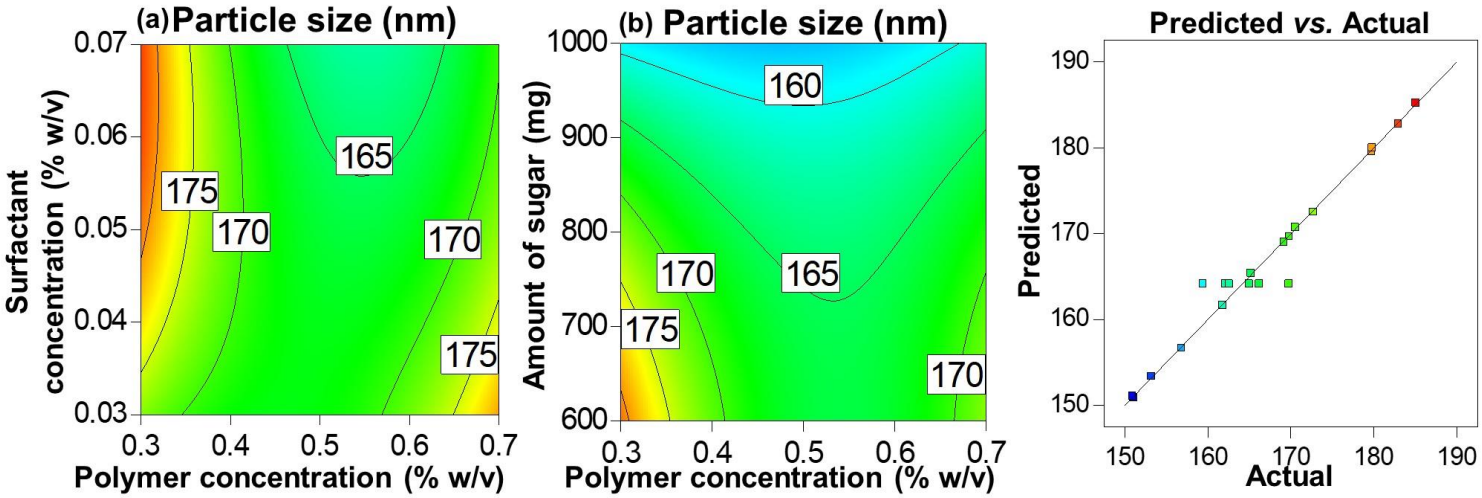

Figure 3.3. Contour plots for response: particle size of the spray-dried powder. (a) The effect of polymer concentration and surfactant concentration on the particle size of the spray-dried powder. (b) The effect of polymer concentration and amount of sugar on the particle size of the spray-dried powder. (polymer – PVP K25, surfactant – SLS, sugar – trehalose)

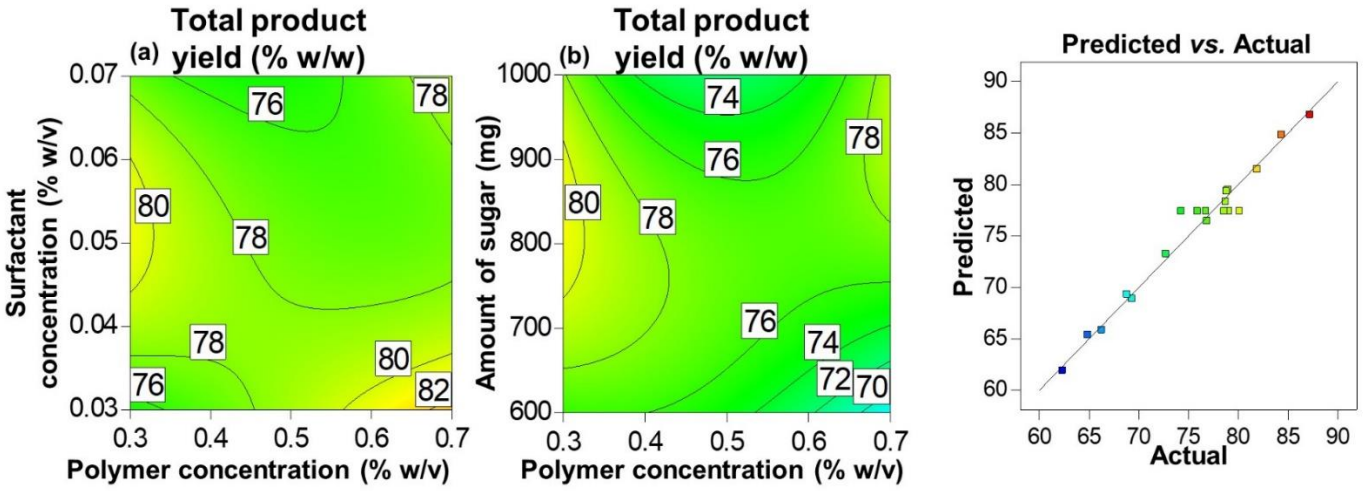

Figure 3.4. Contour plots for response: the yield of the spray-dried powder. (a) The effect of polymer concentration and surfactant concentration on the yield of the spray-dried powder. (b) The effect of polymer concentration and amount of sugar on the yield of the spray-dried powder. (polymer – PVP K25, surfactant – SLS, sugar – trehalose)

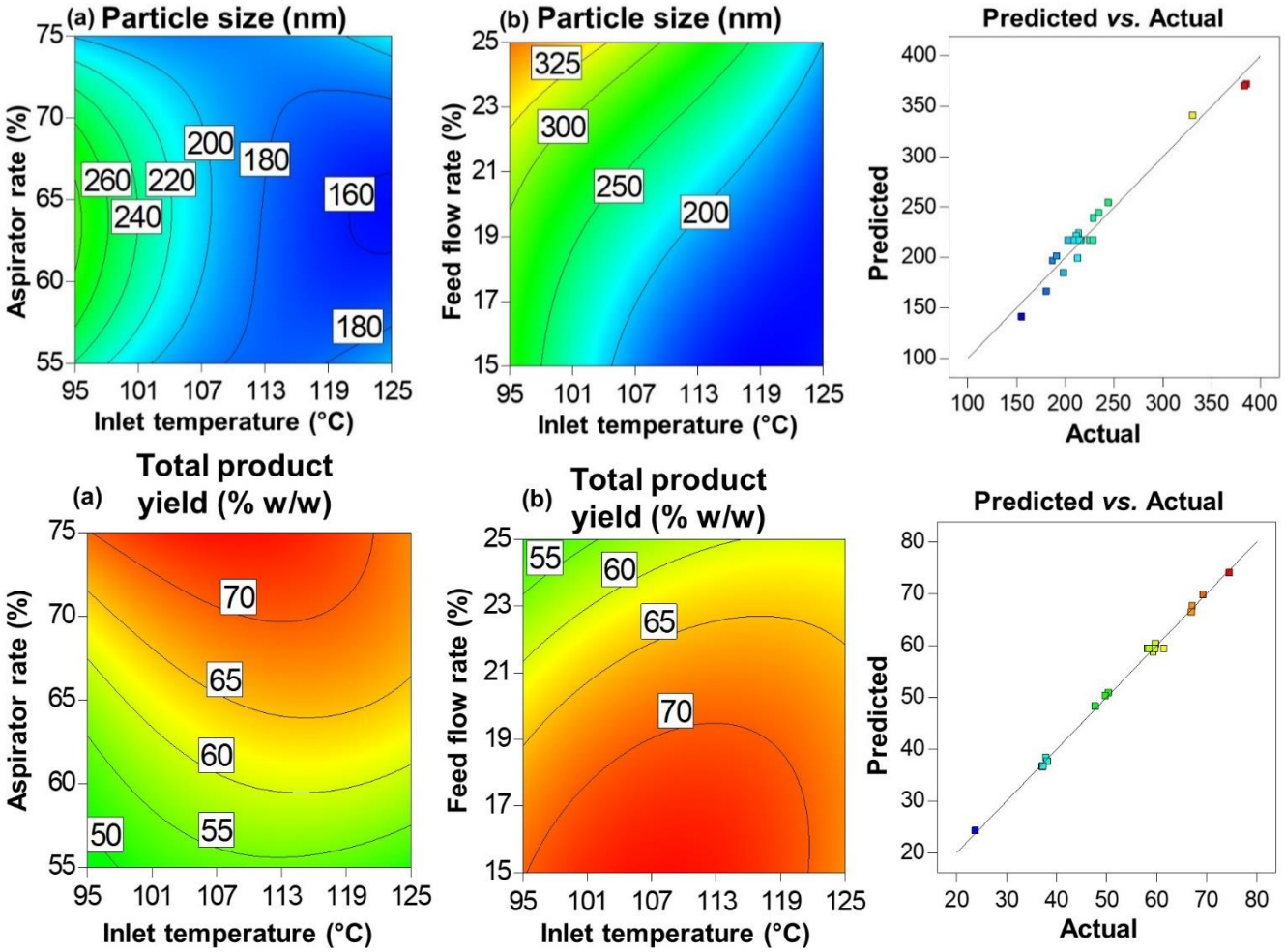

Figure 3.5. Contour plots for response: particle size of the spray-dried powder. (a) The effect of inlet temperature and aspirator rate on the particle size and total yield of the spray-dried powder. (b) The effect of inlet temperature and feed flow rate on the particle size and total yield of the spray-dried powder. (polymer – Soluplus, surfactant – SLS, sugar – trehalose)

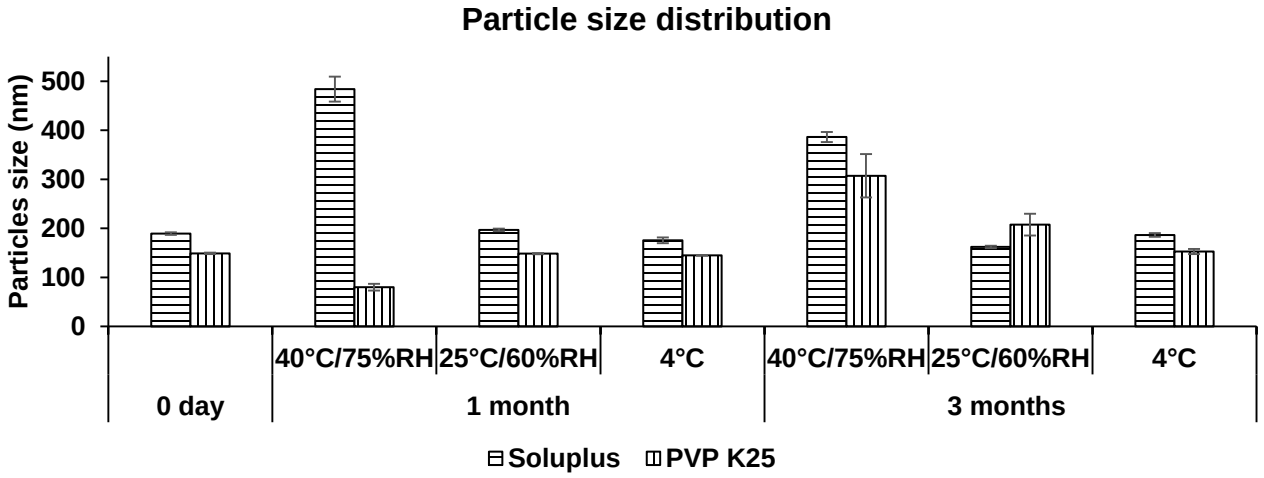

Figure 3.6. Particle size distribution of the optimized spray dried amorphous nanoparticle formulation prepared using soluplus® and PVP K25 stored for 1 and 3 month/s at (a) 4°C (b) 25°C/60%RH (c) 40°C/75%RH compared with zero day formulations.

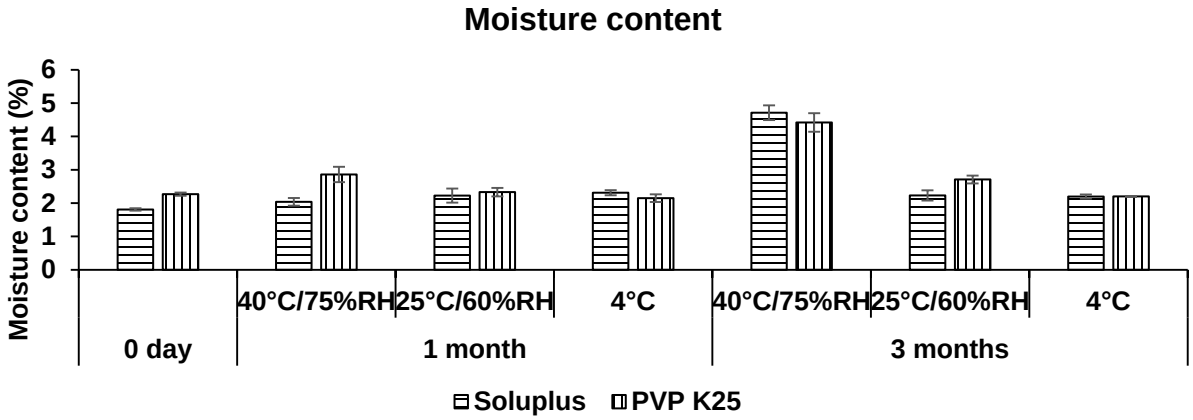

Figure 3.7. Moisture content of the optimized spray dried amorphous nanoparticle formulation prepared using soluplus® and PVP K25 stored for 1 and 3 month/s at (a) 4°C (b) 25°C/60%RH (c) 40°C/75%RH compared with the initial formulations.

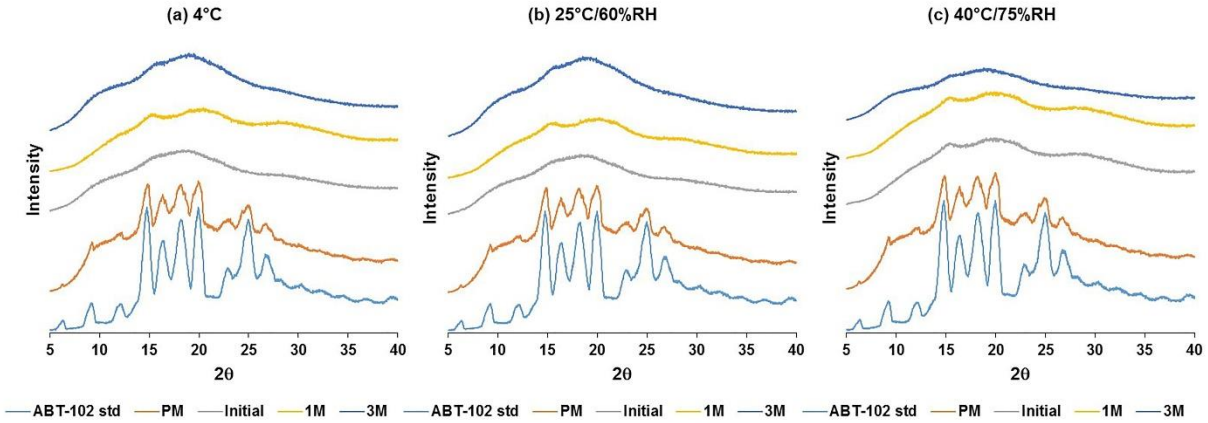

Figure 3.8 (a). PXRD diffraction profiles of the ABT-102 std (raw crystalline drug), physical mixture (PM) of the drug and the polymer (soluplus®) and the optimized formulation stored for 1 (1M) and 3 month/s (3M) at (a) 4°C (b) 25°C/60%RH and (c) 40°C/75%RH

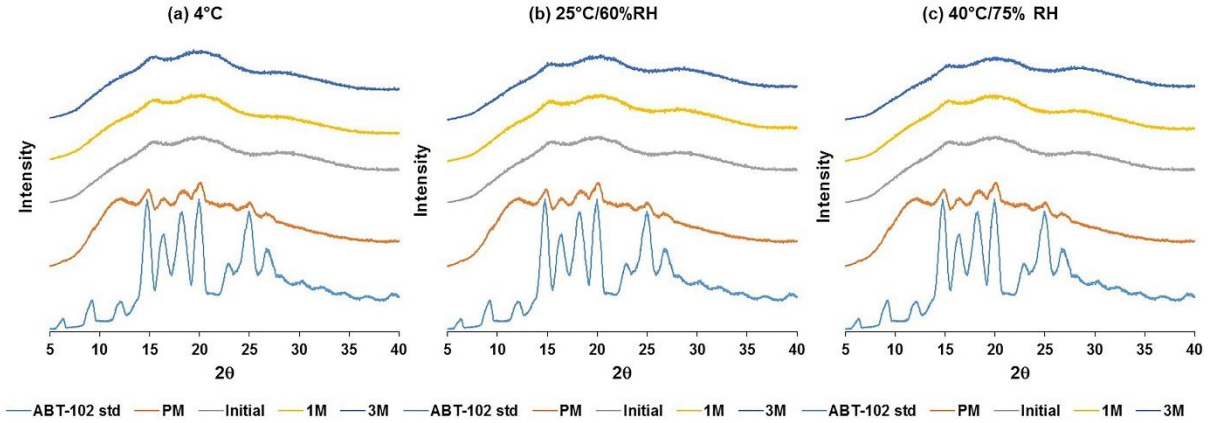

Figure 3.8 (b). PXRD diffraction profiles of the ABT-102 std (raw crystalline drug), physical mixture (PM) of the drug and the polymer (PVP K25) and the optimized formulation stored for 1 (1M) and 3 month/s (3M) at (a) 4°C (b) 25°C/60%RH and (c) 40°C/75%RH

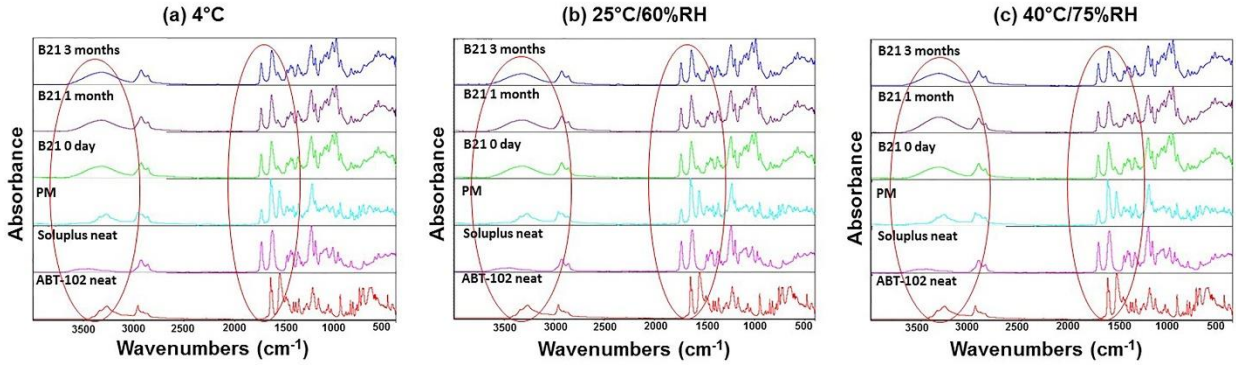

Figure 3.9 (a). FTIR spectra of the ABT-102 neat (raw crystalline drug), soluplus® neat (polymer), physical mixture (PM) of the drug and the polymer (soluplus®) and the optimized formulation stored for 1 month and 3 months at (a) 4°C (b) 25°C/60%RH and (c) 40°C/75%RH.

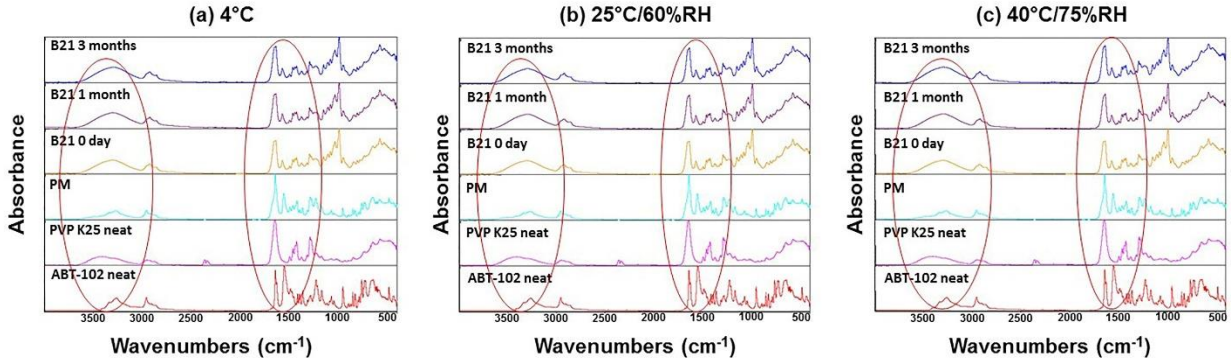

Figure 3.9 (b). FTIR spectra of the ABT-102 neat (raw crystalline drug), PVP K25 neat (polymer), physical mixture (PM) of the drug and the polymer (PVP K25) and the optimized formulation stored for 1 month and 3 months at (a) 4°C (b) 25°C/60%RH and (c) 40°C/75%RH.

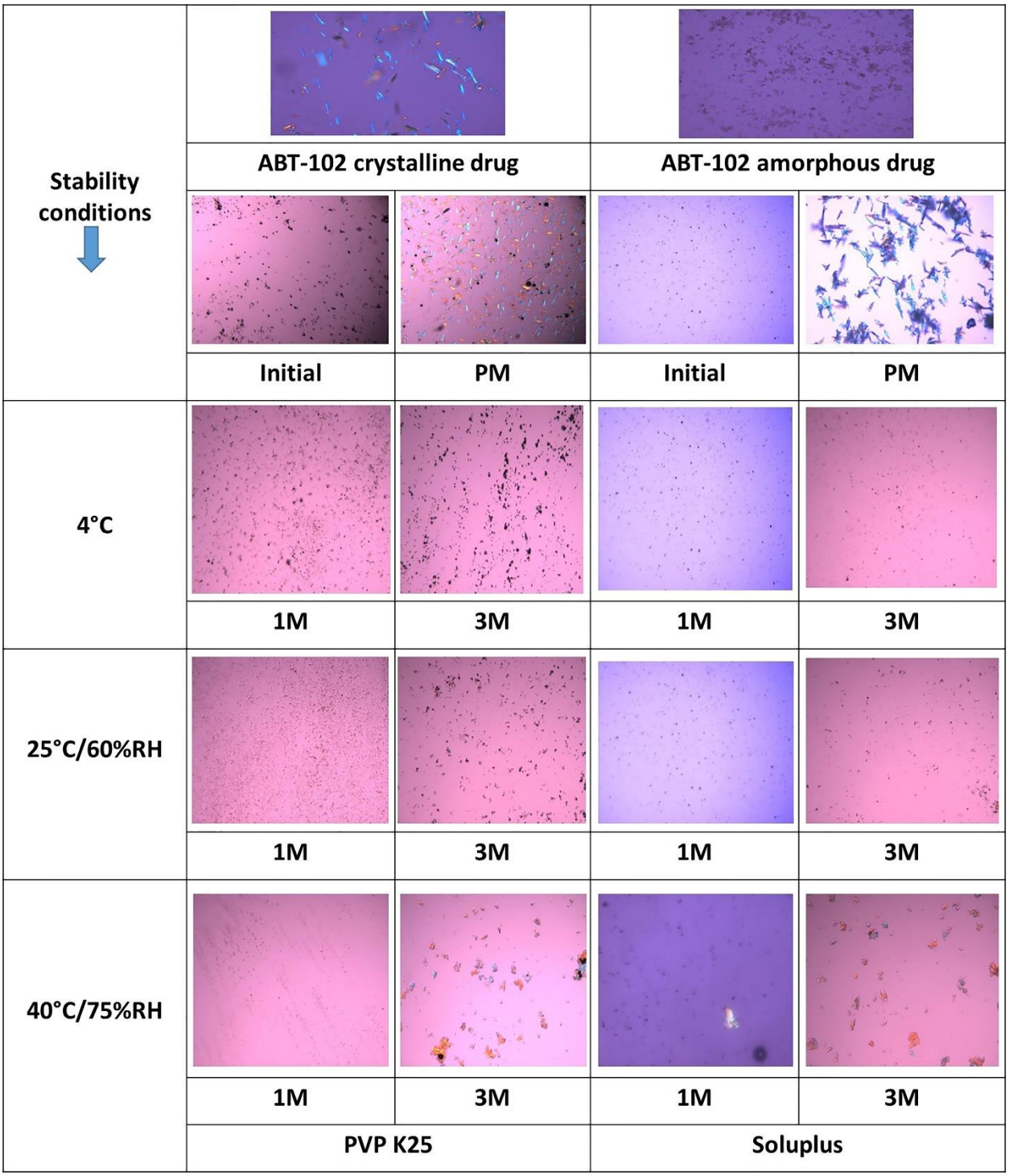

Figure 3.10. PLM images of ABT-102 crystalline drug, ABT-102 amorphous drug, day zero optimized formulations prior to accelerated stability tests (initial), physical mixture of drug and polymer (PM), optimized formulations stored at 4°C, 25°C/60%RH and 40°C/75%RH for one and three month/s (1M & 3M).

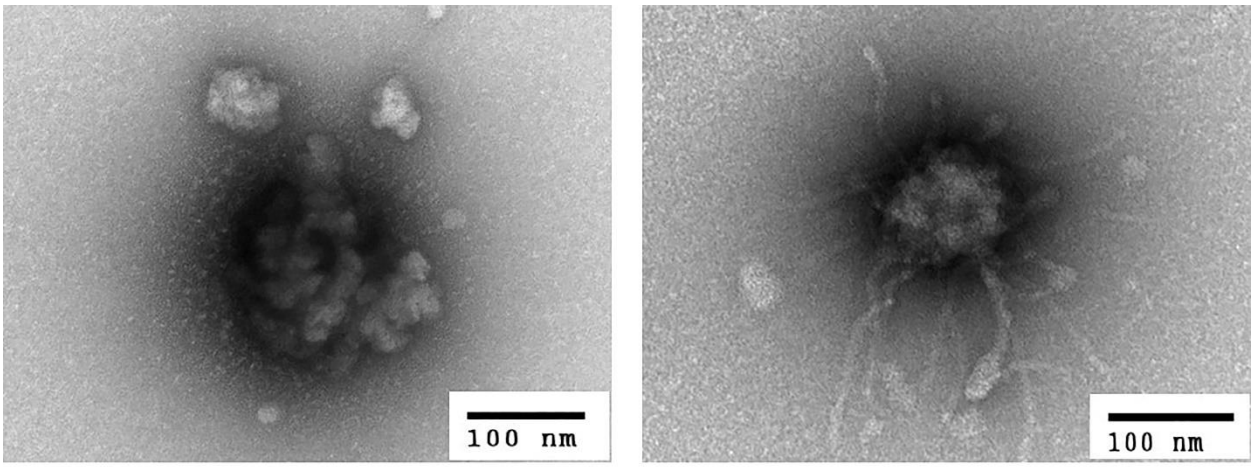

Figure 3.11. TEM images of the spray dried amorphous ABT-102 nanoparticles prepared using: (a) PVP K25 and (b) soluplus®

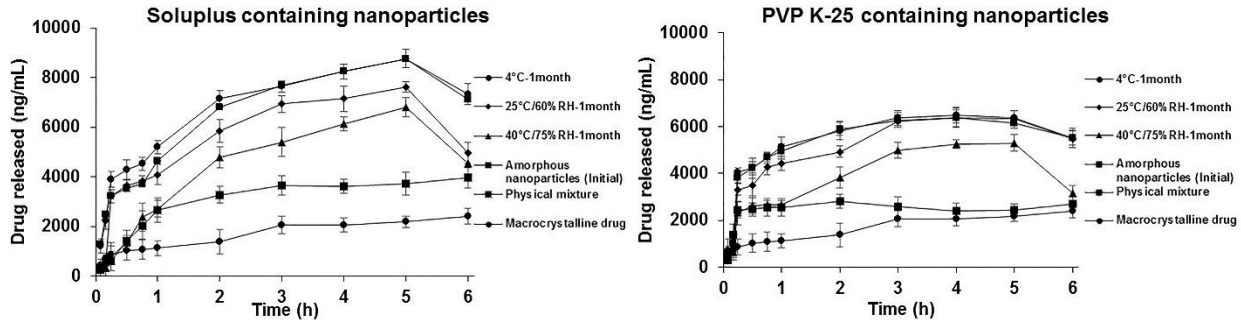

Figure 3.12. *In vitro* dissolution testing profiles (amount of drug release (ng/mL) *vs.* time (h)) of the ABT-102 crystalline drug, physical mixture of drug and polymer (PM), optimized spray-dried nanoparticle formulations prepared using: (a) soluplus® and (b) PVP K25. The formulations were filled into hard gelatin capsules and stored under 4°C, 25°C/60%RH and 40°C/75%RH for one month.

3.8. REFERENCES

[1]Mousa, S. A. and Bharali, D. J., 2011. Nanotechnology-based detection and targeted therapy in cancer: nano-bio paradigms and applications. Cancers. 3, 2888-2903.

[2]Hughes, J. P., Rees, S., Kalindjian, S. B. and Philpott, K. L., 2011. Principles of early drug discovery. British journal of pharmacology. 162, 1239-1249.

[3]Merisko-Liversidge, E. M. and Liversidge, G. G., 2008. Drug nanoparticles: formulating poorly water-soluble compounds. Toxicologic Pathology. 36, 43-48.

[4]Sun, B. and Yeo, Y., 2012. Nanocrystals for the parenteral delivery of poorly water-soluble drugs. Current Opinion in Solid State and Materials Science. 16, 295-301.

[5]Merisko-Liversidge, E., Liversidge, G. G. and Cooper, E. R., 2003. Nanosizing: a formulation approach for poorly-water-soluble compounds. European Journal of Pharmaceutical Sciences. 18, 113-120.
[6]Serajuddin, A., 1999. Solid dispersion of poorly waterâ€• soluble drugs: early promises, subsequent problems, and recent breakthroughs. Journal of pharmaceutical sciences. 88, 1058-1066.
[7]Hancock, B. C. and Parks, M., 2000. What is the true solubility advantage for amorphous pharmaceuticals? Pharmaceutical research. 17, 397-404.
[8]Leuner, C. and Dressman, J., 2000. Improving drug solubility for oral delivery using solid dispersions. European Journal of Pharmaceutics and Biopharmaceutics. 50, 47-60.
[9]Liversidge, G. G. and K.C. Cundy, 1995. Particle-size reduction for improvement of oral bioavailability of hydrophobic drugs.1. Absolute oral bioavailability of nanocrystalline danazol in beagle dogs. . International Journal of Pharmaceutics. 125, 91-97.
[10]Thomson, W., 1872. 4. On the Equilibrium of Vapour at a Curved Surface of Liquid. Proceedings of the Royal Society of Edinburgh. 7, 63-68.
[11]Chiou, W. L. and Riegelman, S., 1970. Oral absorption of griseofulvin in dogs: Increased absorption viasolid dispersion in polyethylene glycol 6000. Journal of pharmaceutical sciences. 59, 937-942.
[12]Chen, X., Young, T. J., Sarkari, M., Williams, R. O. and Johnston, K. P., 2002. Preparation of cyclosporine A nanoparticles by evaporative precipitation into aqueous solution. International Journal of Pharmaceutics. 242, 3-14.
[13]Peagram, R., Gibb, R. and Sooben, K., 2005. The rational selection of formulations for preclinical studies: An industrial perspective. Bulletin technique GattefossÃ©. 98, 53-64.
[14]Wang, J.-X., Zhang, Q.-X., Zhou, Y., Shao, L. and Chen, J.-F., 2010. Microfluidic synthesis of amorphous cefuroxime axetil nanoparticles with size-dependent and enhanced dissolution rate. Chemical Engineering Journal. 162, 844-851.
[15]Zhu, W.-Z., Wang, J.-X., Shao, L., Zhang, H.-x., Zhang, Q.-x. and Chen, J.-F., 2010. Liquid antisolvent preparation of amorphous cefuroxime axetil nanoparticles in a tube-in-tube microchannel reactor. International Journal of Pharmaceutics. 395, 260-265.
[16]Kumar, S., Shen, J. and Burgess, D. J., 2014. Nano-amorphous spray dried powder to improve oral bioavailability of itraconazole. Journal of Controlled Release. 192, 95-102.

[17]Dhumal, R. S., Biradar, S. V., Yamamura, S., Paradkar, A. R. and York, P., 2008. Preparation of amorphous cefuroxime axetil nanoparticles by sonoprecipitation for enhancement of bioavailability. European Journal of Pharmaceutics and Biopharmaceutics. 70, 109-115.

[18]Junghanns, J. A. H. and Muller, R. H., 2008. Nanocrystal technology, drug delivery and clinical applications. International journal of nanomedicine. 3, 295.

[19]Rainer H. M. and Junghanns, A. H., 2006. Drug nanocrystals/ nanosuspensions for the delivery of poorly soluble drugs, In: V. P. Torchilin (Eds.), Nanoparticulates as drug carriers. Imperial college press, London, 307-324.

[20]Narayan, P., Porter, W., Brackhagen, M. and Tucker, C., 2015. Polymers and Surfactants, In: A. Newman (Eds.), Pharmaceutical Amorphous Solid Dispersions. John Wiley & Sons, Inc., Hoboken, New Jersey, 42-84.

[21]Vaka S.R.K., Bommana M.M., Desai D., Djordjevic J., Phuapradit W. and N., S., 2014. Excipients for Amorphous Solid Dispersions, In: N. Shah, H. Sandhu, D. S. Choi, H. Chokshi, A.W. Malick and J. M. Rathbone (Eds.), Amorphous Solid Dispersions, Theory and Practice. Springer, Controlled Release Society, New York, 123-164.

[22]Bruce, C., Fegely, K. A., Rajabi-Siahboomi, A. R. and McGinity, J. W., 2007. Crystal growth formation in melt extrudates. International Journal of Pharmaceutics. 341, 162-172.

[23]Ohtake, S. and Wang, Y. J., 2011. Trehalose: current use and future applications. Journal of pharmaceutical sciences. 100, 2020-2053.

[24]Jain, N. K. and Roy, I., 2009. Effect of trehalose on protein structure. Protein Science. 18, 24-36.

[25]Homayouni, A., Sadeghi, F., Varshosaz, J., Garekani, H. A. and Nokhodchi, A., 2014. Promising dissolution enhancement effect of soluplus on crystallized celecoxib obtained through antisolvent precipitation and high pressure homogenization techniques. Colloids and Surfaces B: Biointerfaces. 122, 591-600.

[26]Patnaik, S., Aditha, S. K., Rattan, T. and Kamisetti, V., 2015. Aceclofenac-Soluplus® Nanocomposites for Increased Bioavailability. Soft Nanoscience Letters. 5, 13.

Chapter 4

Comprehensive Quality by Design Approach for Stable Nanocrystalline Drug Products

ABSTRACT

The novelty of the present research is application of a comprehensive quality by design (QbD) approach to minimize errors in product optimization and validation for the development of a stable nanocrystalline zileuton (BCS class II drug) formulation. A QbD approach was used to identify, optimize and validate the critical processes parameters (wet media milling and spray drying) and critical formulation parameters (drug and excipient concentrations). The milling time, milling speed, inlet temperature, aspirator rate, feed flow rate and drug concentration had a significant influence on the particle size and total product yield of the nanocrystalline zileuton. Trehalose compared to mannitol was determined to be a better stabilizer during spray drying processing. Stability studies revealed the following trend after 12 months: 4°C (most stable) > 25°C/60% RH > 40°C/75% RH (least stable) for the optimized spray-dried nanocrystalline zileuton in terms of physicochemical attributes, crystallinity and *in vitro* dissolution testing. Based on the comprehensive QbD approach, stable spray-dried nanocrystalline zileuton was obtained with exceptionally high total product yield (~80% w/w) and small particle size (276.4±27.54 nm) with low PDI (0.109±0.056 units). Drug release from the formulations followed a particle size dependent dissolution trend. Additionally, pH switch dissolution testing indicated that complete drug release from the nanoformulations was observed at intestinal pH (pH 6.8) within 1-2 h of the shift from the stomach pH (pH 1.2).

4.1. INTRODUCTION

The pharmaceutical world has undergone an unprecedented transformation in the last two decades in terms of novel strategies for drug product development [1-3]. Conventional drug product development involving high levels of resources (people, time, money and energy) is being replaced by cutting-edge and modern tools and technology that minimize the usage of resources and maximize the quality of the final drug product [4-8]. A QbD (quality by design) approach expedites product and process understanding and thereby can achieve high

quality and economical drug products [9-11]. QbD has replaced the traditional approach of "one factor/variable at a time" optimization of drug product development and manufacturing by screening and analyzing "multiple factors/variables at a time". Thus providing a scientific understanding of the entire design space in the drug product development cycle [12-17].

According to the International Conference on Harmonization (ICH) Q8 guideline (Pharmaceutical Development), QbD is defined as "a systematic approach to development that begins with predefined objectives and emphasizes on product and process understanding and process control, based on sound science and quality risk management" [18-21]. The important components of QbD include understanding and identification of the quality target product profile (QTPP) in order to define the precise design space for the identification of critical process parameters (CPPs), critical material attributes (CMAs), critical formulation parameters (CFPs), critical quality attributes (CQAs) and sources of variability (Figure 4.1) [22, 23]. The concept of QbD has been applied to diverse drug products ranging from conventional (tablets, capsules, injections) [24-26] to novel drug delivery systems (nanoparticles, liposomes) [27-32].

The majority of drug products are solid oral dosage forms due to their straightforward manufacturability, ease of administration and patient acceptability [33]. Oral nanoparticles are an important class of drug products which involve critical manufacturing processes and complex compositions [17]. Therefore, it is important to optimize the drug product constituents and manufacturing processes utilized in developing quality and robust nano-oral drug products, which can be achieved *via* a comprehensive QbD approach. Crystalline nanoparticles have significant advantages over other nano-oral dosage forms one of which is the enhancement in the rate of dissolution/kinetic solubility and the concurrent improvement in oral bioavailability of poorly soluble drugs (BCS class II and II/IV) (Figure 4.2) [29-31, 34-38]. Predominantly, drug nanocrystals are manufactured by two techniques: (1) top down approach (*i.e.* milling/grinding of the drug macrocrystals to microcrystals and further to nanocrystals) and; (2) bottom-up approach (solvent-antisolvent precipitation technique) [39, 40]. These techniques are followed by a suitable drying step (spray drying, freeze-drying, solvent evaporation, *etc.*) to develop a solid nanocrystalline drug product.

Drug nanocrystals are stabilized using functional excipients: polymers; surfactants; sugars; or a combination of these. Particle size reduction of macro-crystalline to nanocrystalline drug results in increase in the exposed surface area (or surface area-to-volume ratio), leading to increase in the drug dissolution rate/solubility and hence concomitant improvement in the oral bioavailability of poorly soluble drugs [41]. Enhanced dissolution rate/solubility and improved oral bioavailability unequivocally translates to tremendous improvement in the biopharmaceutical properties of nanocrystals: increased rate and extent of release and absorption; rapid onset of action; reduced side effects and improved clinical performance (Figure 4.3) [39, 41-44]. It is important to establish a correlation between different critical process parameters, critical formulation parameters and CQAs to develop a robust and quality nanocrystalline drug product. A comprehensive QbD helps in identifying and defining the critical *vs.* non-critical parameters (product and process) influencing drug product critical quality attributes.

Until now, individual DoEs (process or formulation) have been reported for nano-crystalline formulations [27, 30, 45-50]. Beg *et. al.* optimized the self-nanoemulsifying drug delivery system of lovastatin using only formulation DoE with amounts of lipid, surfactant and co-surfactant as the critical material attributes without focusing on any critical process parameters involved in the manufacturing of nanoemulsions of lovastatin SNEDDS, which can significantly influence the CQAs (globule size, lipid liquefaction time and emulsification time) [46].Ghosh *et. al.* investigated only critical process parameters involved in the naproxen nanosuspension formulation development *via* wet media milling without focusing on any critical formulation parameters (drug or polymer concentration) or other critical process parameters (drying techniques and related parameters) [48]. Baldinger *et. al.* and Kumar *et. al.* studied only the critical process parameters of the spray drying process (inlet temperature, aspirator rate and feed flow rate) for excipients (mannitol and trehalose) and nanocrystalline indomethacin, respectively. They investigated the influence of these critical process parameters on the CQAs such as particle size, total yield, particle morphology and crystallinity of the spray-dried powder. The pre-processing step involved in the investigation of other critical process parameters related to the manufacturing of the nano-formulations (microfluidization) or the critical formulation parameters (drug and excipient concentrations) were not studied which may have significant influence on the

CQAs [27, 45]. There are many similar published literature reports wherein the authors have described to perform DoE leading to successful QbD, however all of them have performed either one or two process DoE studies and not a comprehensive multi-process and formulation DoE study [47, 49, 50]. This can lead to errors in optimization of critical process parameters and critical formulation parameters significantly affecting CQAs or an important CQA may be neglected. Whereas, a comprehensive QbD approach will minimize the errors in product optimization through investigation of the entire range of important CQAs (defining an explicit design space) involved in process and formulation DoE models.

In the present research, a holistic QbD approach involving five DoE models (wet media milling, spray drying with sucrose, spray drying with trehalose, formulation post wet media milling and formulation post spray drying) was applied for the identification and optimization of the CQAs to achieve a stable spray-dried nanocrystalline zileuton formulation. Zileuton is an anti-asthmatic BCS class II drug (average molecular weight 236.3 g/mol, log P-0.9, aqueous solubility ~ 0.1 mg/mL) [51]. It is a selective inhibitor of 5-lipoxygenase, the enzyme that catalyzes the formation of leukotrienes from arachidonic acid in the eicosanoid synthesis pathway [52]. Multiple full factorial designs were applied to understand the critical process parameters [wet media milling (milling time, milling speed and pump speed) and spray drying (inlet temperature, aspirator rate and feed flow rate)] as well as the critical formulation parameters [drug and excipients (polymer – KollidonVA64 fine, surfactant – dowfax2A1, sugar – trehalose) concentrations]. Additionally, the interactions between these critical parameters which significantly influence the CQAs (particle size distribution (as Z-average), total product yield, outlet temperature of spray dryer, drug loading, moisture content, PDI and zeta potential) were monitored. Furthermore, a response surface analysis was performed to design a predictive model for the particle size distribution, total product yield and nanocrystal agglomeration. Detailed data interpretation using ANOVA and multifactor analysis was performed to: *(a)* identify and optimize the most important critical process parameters and critical formulation parameters significantly affecting the CQAs; *(b)* elucidate the interactions between multiple critical process parameters and critical formulation parameters and their influence on the CQAs; *(c)* develop the rank order of multiple critical process parameters and critical formulation parameters; and *(d)* design a predictive model for development of stable spray-dried nanocrystalline

zileuton. Following the exhaustive QbD approach, validation and stability studies were performed for the optimized solid nanocrystalline formulations. Stability studies (40°C/75% RH, 25°C/60% RH and 4°C) were conducted for one year to monitor the stability of the crystalline nanoparticles in terms of particle size distribution, *in vitro* dissolution and crystallinity. Based on the comprehensive QbD approach and stability studies, a predictive model to prepare stable solid spray-dried nanocrystalline zileuton, incorporating both formulation and process parameters, was successfully developed using multiple linear regression analysis.

4.2. MATERIALS

Crystalline zileuton (greater than 99% purity) was purchased from Beijing Mesochem Technology Co. Ltd., China. Trehalose was gifted by Gattefose. Mannitol was procured from Fisher Scientific. SLS (sodium lauryl sulfate) was gifted by Sigma Aldrich. PVP (poly (1-vinyl-2-pyrrolidone) K17, PVP K25, PVP K30, PVP K90, soluplus (polyvinyl caprolactam-polyvinyl acetate-polyethylene glycol graft copolymer), Kolliphor SLS fine, KollidonVA (vinyl acetate) 64, KollidonVA 64 fine and KollidonCLM were gifted by BASF. Dowfax 2A1, HPMC (hydroxy propyl methyl cellulose) E3, HPMC E5, HPMC E15, HPMC E50, HPMC K3, MC (methyl cellulose) A15 and EC (ethyl cellulose) 10 were gifted by Dow Chemical Company. Poloxamer P407 and Poloxamer 188 were purchased from Spectrum. The chemical structures of the ingredients used in the optimized spray-dried zileuton nanocrystalline formulation are shown in Table 4.1. HPLC grade solvents were purchased from Fisher Scientific. Inspire C18 column (4.6 mm x 100 mm, 5µm) was gifted by Dikma Technologies Inc.

4.3. METHODS

4.3.1. Solubility determination

Equilibrium solubility was determined in different excipient solutions under continuous shaking for 48 h at 37 °C. Briefly, 10 mg of the drug was added to each vial containing 10 mL of the stabilizer/excipient solution (0.2% w/v solution). After 48 h, 1 mL samples were withdrawn from each vial, filtered through 0.22 µm PVDF (polyvinylidene fluoride) filters, and analyzed using the RP-HPLC method described below.

4.3.2 Wet media milling

Nanocrystalline zileuton suspensions were manufactured using wet media milling. Three different design of experiments (DoEs) (process (wet media milling and spray drying) and formulation) were performed to investigate both critical process parameters (milling speed, milling time, pump speed, spray drying inlet temperature, aspirator rate, feed flow rate) and critical formulation parameters (drug concentration, polymer concentration, surfactant concentration and amount of sugar) affecting the critical quality attributes (CQAs) (particle size, zeta potential, drug loading and total yield). For wet media milling DoE: zileuton (1% w/v) was suspended in the distilled water containing stabilizers - KollidonVA64 (0.75% w/v) and Dowfax2A1 (0.05% w/v). The prepared suspensions were stirred for 30 min for complete wetting of the drug by the stabilizer solution. The micro-suspension (100 mL) was milled using a wet media mill (Microcer® Netzsch) based on the DoE detailed in the section 4.3.4.3.2. The temperature of the sample was maintained between 2 - 8 °C using two cooling bath re-circulators (one attached to the milling and the other to the suspension re-circulation chambers) (Figure 4.4) [53].

4.3.3 Spray drying

Solid dry powders of nanocrystalline zileuton were prepared *via* spray drying. For spray drying DoE: zileuton (1% w/v) was suspended in the aqueous stabilizer - KollidonVA64 (0.75% w/v) and Dowfax 2A1 (0.05% w/v). The micro-suspension (100 mL) was milled to nanosuspension using a wet media mill (Microcer® Netzsch) based on the optimized milling parameters from the wet media milling DoE detailed in section 4.3.4.3.2. The nanosuspension was spray-dried using a B-290 spray dryer (Buchi Labortechhnik AG) based on the DoE detailed in section 4.3.4.3.2. The spray dryer was equilibrated using distilled water. Once the spray dryer was equilibrated, distilled water was replaced with the nanosuspension formulations. Each formulation was spray-dried using trehalose as an excipient [drug–trehalose (1:1)] to prevent nanocrystal aggregation. Spray-dried powders were collected from the collection chamber and immediately analyzed for the CQAs (particle size, total yield and crystallinity) (Figure 4.5) [54].

4.3.4 Quality by Design (QbD)

The comprehensive QbD approach includes three important stages: *(1)* risk assessment; *(2)* design of experiments (process and formulation); and *(3)* process analytical tools (offline or inline).

4.3.4.1 Risk assessment

Risk identification, analysis and evaluation were performed for the different manufacturing process parameters (wet media milling and spray drying) and formulation parameters that can significantly influence the CQAs of zileuton nanocrystalline formulations. The process (wet media milling and spray drying) and formulation risk estimation matrix is summarized in Figure 4.6a. The risk estimation matrix were developed based on the preliminary results (data not shown) correlating different process and formulations parameters to different quality attributes of the nanocrystalline zileuton formulations in three major categories – high risk (red), medium risk (orange) and low risk (green). An Ishikawa diagram (fishbone diagram) shown in Figure 4.6b analyzes the risk associated with the preparation of stable nanocrystalline zileuton.

4.3.4.2 Design of Experiments

Three different design of experiments (DoEs) [process (wet media milling and spray drying) and formulation] were performed to investigate both critical formulation parameters (drug concentration, polymer concentration, surfactant concentration and amount of sugar) and critical process parameters (milling speed, milling time, pump speed, spray drying inlet temperature, aspirator rate and feed flow rate) affecting the critical quality attributes (CQAs) (particle size, polydispersity index, zeta potential, drug loading and total yield).

Wet media milling DoE

Three milling critical process parameters (milling speed, milling time, pump speed) were investigated against three different CQAs (particle size, PDI and zeta potential) monitored during the wet media milling DoE studies.

Optimization of different wet media milling critical process parameters (*e.g.* milling speed, milling time and pump speed) for the preparation of nanocrystalline zileuton was performed

using a central composite design. Three critical process parameters that may affect the preparation of milled formulations were selected, namely the milling speed, milling time and pump speed. Three different CQAs were monitored: particle size, PDI and zeta potential. The data obtained was evaluated using Design Expert® 11.0 and Minitab® 18.0 statistical software. For the milling speed, the minimum and maximum levels (speed) were 500 and 1500 rpm, respectively with 1000 rpm as the center point and 159 rpm and 1840 rpm were the star or alpha points. For the milling time, the minimum and maximum levels (time) were 15 and 30 min, respectively with 22.5 min as the center point and 10 min and 35 min were the star or alpha points. For the pump speed, the minimum and maximum levels (rpm) were 80 and 120 rpm, respectively with 100 rpm as the center point and 66 rpm and 134 rpm were the star or alpha points. The CQAs were particle size, PDI and zeta potential of milled nanosuspension. A DoE for the wet media milling was performed using KollidonVA 64 fine and Dowfax2A1 as the stabilizers. A total of 20 wet media milling experiments were performed. (Table 4.2)

Spray drying DoE

Following the wet media milling DoE study, the optimized milling critical process parameters (milling speed 1200 rpm; milling time 30 min; and pump speed 92 rpm) were used to prepare the formulations for the spray drying DoE. Three spray drying critical process parameters (inlet temperature, aspirator rate and feed flow rate) were investigated against seven different CQAs (outlet temperature, particle size, PDI, zeta potential, drug loading, total yield and moisture content) monitored during the spray drying DoE studies. Two different sugars (mannitol and trehalose) were used at drug:sugar - 1:1, w/w as stabilizers during spray drying.

Optimization of different spray drying critical process parameters (*e.g.* inlet temperature, aspirator rate and feed flow rate) for the preparation of nanocrystalline zileuton was performed using a central composite design. Three critical process parameters that may affect the preparation of spray-dried formulations were selected, namely inlet temperature, aspirator rate and feed flow rate. Seven different CQAs were monitored: outlet temperature, particle size, PDI, zeta potential, drug loading, total yield and moisture content. The data obtained was evaluated using Design Expert® 11.0 and Minitab® 18.0 statistical software.

For the inlet temperature during spray drying, the minimum and maximum levels (°C) were 105°C and 125°C, respectively with 115°C as the center point and 98°C and 132°C were the star or alpha points. For the aspirator rate (rate of dry air flow), the minimum and maximum levels (%) were 70 and 90%, respectively with 80% as the center point and 63% and 97% were the star or alpha points. For the feed flow rate (rate at which the milled nanosuspension is flowing through the nozzle of the spray dryer), the minimum and maximum levels (%) were 10 and 25%, respectively with 17.5% as the center point and 5% and 30% were the star or alpha points.

A DoE for the spray drying was performed using nanosuspension prepared using the optimized milling parameters in addition to two different sugar stabilizers (trehalose and mannitol) to prevent aggregation during spray drying. A total of 20 spray drying experiments were performed for each sugar (mannitol and trehalose). (Table 4.3a and 4.3b)

F*ormulation DoE*

Following the wet media milling and spray drying DoE study, the optimized milling critical process parameters (milling speed 1200 rpm; milling time 30 min; and pump speed 92 rpm) and optimized spray drying critical process parameters (inlet temperature:125 °C, aspirator rate:90 % and feed flow rate: 10 %) were used to prepare the solid nanocrystalline zileuton for the formulation DoE. Three critical formulation parameters (drug concentration, polymer concentration and surfactant concentration) were investigated against three different CQAs post wet media milling (particle size, PDI and zeta potential) and seven CQAs post spray drying (outlet temperature, particle size, PDI, zeta potential, drug loading, total yield and moisture content) monitored during the DoE studies. KollidonVA 64 fine and Dowfax2A1 were used as stabilizers during wet media milling. Trehalose was used at drug:sugar - 1:1, w/w as the stabilizer during spray drying.

Optimization of critical formulation parameters [*e.g.* concentration of drug (zileuton), polymer (KollidonVA 64 fine), surfactant (Dowfax2A1) and sugar (trehalose)] for the preparation of nanocrystalline zileuton was performed using a central composite design. The data obtained were evaluated using Design Expert® 11.0 and Minitab® 18.0 statistical software. For the drug concentration, the minimum and maximum levels (concentrations)

were 0.35% w/v and 1% w/v, respectively with 0.675% w/v as the center point and 0.025% w/v and 1.325% w/v were the star or alpha points. For polymer concentration, the minimum and maximum levels (concentrations) were 0.3% w/v and 0.8% w/v, respectively with 0.55% w/v as the center point and 0.05% w/v and 1.05% w/v were the star or alpha points. For the surfactant concentration, the minimum and maximum levels (concentrations) were 0.03% w/v and 0.08% w/v, respectively with 0.055% w/v as the center point and 0.005% w/v and 0.105% w/v were the star or alpha points. For the amount of sugar, the minimum and maximum levels were 850 mg and 2000 mg, respectively with 1425 mg as the center point and 275 mg and 2575 mg were the star or alpha points. The CQAs were particle size distribution (post wet media milling) and total yield (post spray drying). A DoE for formulation parameters was carried out using wet media milling (Table 4.4a) and spray drying (Table 4.4b) as the stabilizers. A total of 30 wet media milling and spray drying experiments were performed.

Based on the above DoE studies, for the critical process parameters (wet media milling process and spray drying process parameters) and critical formulation parameters (formulation parameters), the process validation was performed. The process and product validation was performed *via* preparation of optimized formulations (n=3). These formulations were stored at three different storage conditions (4°C, 25°C/60% RH and 40°C/75% RH) for stability testing of the nanocrystalline zileuton for 1, 6 and 12 month/s. The controls (neat zileuton, physical mixture of drug and excipients) were also loaded for stability testing.

4.3.4.3 Process Analytical Technology

For the characterization of the nanocrystalline zileuton formulations, different offline process analytical tools were used including the analytical and solid-state tools.

4.3.4.3.1 Particle size measurement

Particle size measurements were performed using a Zetasizer Nano ZS90 (Malvern Instruments). Briefly, the liquid or spray-dried samples were suspended in a saturated and filtered (0.2 μm PVDF membrane filter) solution of zileuton in 30% glycerin solution to avoid any discrepancy resulting from dissolution of the nano-particles during measurement.

The viscosity of this dispersant solution was measured *via* a Brookfield viscometer (Model DV-III) and used to calculate the particle size of the re-dispersed and liquid nano-crystalline suspensions. All samples were analyzed in triplicate and reported as the standard deviation.

4.3.4.3.2 Powder X-Ray Diffraction (PXRD)

PXRD was utilized to determine the crystallinity of the spray-dried samples. X-ray diffraction patterns were obtained using an X-ray diffractometer (Model D5005, Bruker AXS Inc., Madison, WI) with Cu-kα radiation, a voltage of 40 kV, and a current of 40 mA. All the scans were performed with a scanning rate of 2°/minute with steps of 0.02° from 5° to 40° at 2θ ranges.

4.3.4.3.3 HPLC analytical method

The quantification of zileuton was conducted using a Shimadzu-HPLC system with a UV detector. The absorbance wavelength was set at 260 nm. The mobile phase was a mixture of 0.1% trifluoro acetic acid in water and acetonitrile at a 40:60% v/v ratio. A C18 Inspire 5 μ analytical column (4.6 mm × 100 mm) was used with a flow rate of 1 mL/min and the column temperature was maintained at 40°C using a column heater. All samples were analyzed in triplicate and reported as the standard deviation.

4.3.4.3.4 Attenuated Total Reflectance - Fourier Transform Infrared Spectroscopy (ATR-FTIR)

IR spectroscopy was performed using a Nicolet FTIR (iS5 FTIR, Thermo Scientific) spectrometer with an attenuated total reflectance (ATR) accessory. Spray-dried powders were placed on the crystal window (Germanium) and compressed lightly using a pressure clamp. Spectra were recorded over a range of 400–4000 cm^{-1} with a resolution of 4 cm^{-1}, for 128 parallel scans. Data analysis was performed on Omnic® 6.0a software (Thermo Nicolet Corporation).

4.3.4.3.5 Polarized Light Microscopy (PLM)

The spray-dried samples were dispersed in the immersion oil and placed on microscope slides. The samples were analyzed using an Olympus BH2 polarized microscope with a Q-imaging camera, accessories and software. All the pictures were obtained at 10X resolution. All samples were analyzed in triplicate and reported as the standard deviation.

4.3.4.3.6 Differential Scanning Calorimetry

Differential scanning calorimetry (DSC) was performed using a TA Q1000 (TA instruments) calorimeter and calibrated using indium and sapphire discs. Approximately 5–10 mg of spray-dried formulations and neat drug (control) were sealed in hermetic pans and analyzed. The heating rate was maintained at 5 °C/min and the temperature was increased from room temperature to 190 °C. Nitrogen gas was used for purging at a flow rate of 50 mL/min. The data were analyzed using TA universal analysis software. All samples were analyzed in triplicate and reported as the standard deviation.

4.3.4.3.7 *In vitro* dissolution testing

USP apparatus I (basket apparatus for spray-dried powders) and USP apparatus II (paddle apparatus for nanosuspensions) (AT7 smart, Sotax AG Switzerland) were utilized for the *in vitro* dissolution experiments. In the case of spray-dried powders, the samples were filled into hard gelatin capsules (size 0, Torpac) for *in vitro* dissolution studies. All the dissolution experiments were conducted at 37°C in 900 mL (sink conditions and non-sink conditions) of pH 6.8 phosphate buffer at a speed of 100 rpm. At each time point, 2 ml samples were withdrawn from the dissolution chamber and replaced with fresh dissolution media. The samples were filtered using 0.1 μm PVDF filters to avoid any erroneous results from un-dissolved nano-particulates. All samples were analyzed using the HPLC method as described above. The samples were analyzed on zero day (initial) and after storing at different conditions 4°C, 25°C/60% RH and 40°C/75% RH for one, six and twelve month/s.

In addition, pH shift experiments were designed to mimic the *in vivo* conditions that the dosage form experience while transiting from stomach (pH 1.2) to intestine (pH 6.8) and understand the differences in the dissolution rate of the nanocrystalline zileuton formulations at different pH. The required volume of the zileuton nanosuspension was directly added to the USP II apparatus (paddle) with 0.1N HCl dissolution media (pH 1.2) (675 mL) and samples were collected at different times points until 2 h. After 2 h, pH was switched from 1.2 to 6.8 by addition of required volume (225 mL) of tribasic sodium phosphate. pH 6.8 was maintained for another 4 h and samples were withdrawn at different time points. The samples were filtered using 0.1μ PVDF filter membrane and the drug concentration was quantified using RP-HPLC. Similarly, the required quantity of spray

dried zileuton nanoparticles were directly added to the USP apparatus II (paddle) and pH shift experiments were performed. All formulations were tested in sextuplets (n=6) and reported as the standard deviation.

4.3.5 Storage stability testing

All the spray-dried powder formulations were stored at three different storage conditions *i.e.* 4°C, 25°C/60% RH and 40°C/75% RH for 12 months. Samples were withdrawn at 1, 6 and 12 month/s and analyzed for particle size distribution, zeta potential, moisture content and crystallinity. All samples were analyzed in triplicate and reported as the standard deviation.

4.4. RESULTS & DISCUSSION

4.4.1. Selection of stabilizer/s

4.4.1.1 Selection of polymers and surfactants

Different polymers and surfactants were investigated as potential stability enhancers. The polymers and surfactants were first screened to determine whether they caused any significant increase in the equilibrium solubility of the drug. These polymers and surfactants are present in different concentrations in the nanocrystalline formulations to stabilize the drug. Nanocrystalline formulations (small sized drug crystals) have significantly high Gibb's free energy due to high surface area to volume ratios resulting in thermodynamically unstable nanocrystalline suspensions. The advantage of nanocrystalline formulations over their microcrystalline counterparts is their significant enhancement in dissolution performance. However, nanocrystalline formulations suffer from a major instability issue involving aggregation as well as Oswald's ripening, which results in particle size changes eventually leading to a small number of very large particles causing a significant reduction in the dissolution rate of the formulations.

The polymers investigated were PVP K-17, PVP K-25, PVP K-30, PVP K-90, HPMC E3, HPMC E5, HPMC E15, HPMC E50, HPMC K3, MC A15, EC 10, KollidonVA64, KollidonVA64 fine and soluplus. The surfactants investigated were Dowfax2A1, SLS, Kolliphor SLS fine, Poloxamer P407 and Poloxamer 188. Drug solubility was measured in all of the above excipient solutions. All surfactants investigated (Dowfax2A1, SLS,

Poloxamer P407 and Poloxamer 188) were unable to increase the drug equilibrium solubility. EC 10, Kolliphor SLS fine and Kollidon CLM were able to increase the drug equilibrium solubility (1.5-fold) compared to the no excipient (control) sample as shown in Figure 4.8 and Table 4.7. PVPs (K-17, K-25, K-30, K-90), HPMC K3, KollidonVA64 and KollidonVA64 fine were able to increase the drug equilibrium solubility (2-fold) compared to the no excipient (control) sample as shown in Figure 4.7 and Table 4.5. HPMCs (E3, E5, E15, E50) and MC A15 were able to increase the drug equilibrium solubility (2.5-fold) compared to the no excipient (control) sample as shown in Figure 4.7 and Table 4.5. Soluplus was able to increase the drug equilibrium solubility (3-fold) compared to the no excipient (control) sample as shown in Figure 4.7 and Table 4.5.

The increase in the equilibrium solubility of the drug upon addition of excipient can result in Ostwald ripening. As a consequence, all excipients which result in significant increase in drug equilibrium solubility should not be selected for the next stage of formulation development of nanocrystalline suspensions. This eliminated the excipients: soluplus, HPMCs (E3, E5, E15, E50) and MC A15 from the screening studies. Furthermore, it was observed that there was a lot of sticking to the glass vessels (significantly affecting the product yield) and particle aggregation during spray drying of the formulations containing only surfactant excipients *viz.*, Poloxamer P407 and Poloxamer 188, and as a result these stabilizers were not selected. In addition, during the wet media milling of the formulations containing excipients: EC 10, Kolliphor SLS fine and Kollidon CLM, it was observed that the nanoparticles tend to aggregate as a result of poor stabilizing effect.

In the preliminary wet media milling experiments, the formulations containing excipients (PVPs, KollidonVA64 and KollidonVA64 fine) resulted in stable particle size nanocrystalline formulations. However, the nanocrystalline formulations prepared using KollidonVA64 fine resulted in unimodal particle size distribution and stable particle size compared to PVPs. The vinyl acetate moiety linked to the vinyl pyrrolidone chain present in the KollidonVA64 fine provided a strong stabilization effect to the nanoparticles, compared to PVPs. Consequently, KollidonVA64 fine was used as a stabilizer during wet media milling to prepare crystalline nanosuspensions. Post wet media milling, spray drying was performed to prepare powdered nanocrystalline formulations. It was observed that the

particle size post spray drying was in the range of 600-700 nm. Based on these observations, screening studies were performed for the addition of a small amount of surfactant (*viz*., Dowfax2A1 or sodium lauryl sulfate) along with KollidonVA64 fine. A combination of KollidonVA64 fine and Dowfax2A1 resulted in particle size <400 nm in 30 min of continuous milling (data not shown). It was observed that prolonging the milling time above 30 min led to significant particle aggregation. Accordingly, a combination of KollidonVA64 fine and Dowfax2A1 were used as stabilizers for the multiple DoE approach to optimize the process (wet media milling and spray drying) and formulation parameters (excipients and drug concentrations) for the preparation of a stable nanocrystalline zileuton.

4.4.1.2 Selection of sugars

Following the wet media milling process, it is required to add a sugar stabilizer to the nanocrystalline suspensions before spray drying in order to prevent nanoparticle aggregation (to maintain uniform particle size) and minimize sticking to the glass walls of the spray dryer (maximize the nanocrystalline powder yield). Based on the preliminary results, three different sugars: mannitol, sucrose and trehalose were screened. In the presence of sucrose, the nanoparticles tend to aggregate the most, compared to the other sugars. Furthermore, nano-formulations containing sucrose resulted in sticking to the glass walls of the spray dryer impacting the spray drying process and significantly reducing the total drug product yield. It has been reported that the high Tg of trehalose (106°C) results in less hygroscopicity, minimal/absence of internal hydrogen bonding between trehalose-trehalose molecules and strong hydrogen bonding between trehalose-nanoparticles during the spray drying process [38]. During the screening studies, the nano-formulations prepared using trehalose and mannitol had uniform particle size, minimal moisture content and high drug product yield. As a result, trehalose and mannitol were selected for the multiple DoE studies to prepare stable nanocrystalline zileuton formulations.

4.4.2. Design of Experiments

Following the pre-formulation studies, five sets of DoE studies [wet media milling, spray drying (comparing nano-formulations containing mannitol *vs.* trehalose), formulation parameters (post wet media milling) and formulation parameters (post spray drying)], were

investigated to optimize and prepare stable spray-dried nanocrystalline zileuton drug product.

4.4.2.1 Wet Media Milling DoE

Based on the wet media milling DoE, it was observed that the milling critical process parameters (especially milling time and milling speed) have a significant influence on the particle size of the nanocrystalline zileuton. According to Figure 4.8(A), with increase in milling speed >1100 rpm, there was a decrease in the particle size <200 nm of the nanocrystalline zileuton suspensions. According to Figure 4.8(B), with increase in milling speed >1100 rpm and milling time >24 min, there was a decrease in the particle size <200 nm of the nanocrystalline zileuton suspensions.

A particle size <200 nm for the nanocrystalline zileuton was obtained at a milling speed >1000 rpm, milling time <30 min and pump speed >120 rpm (Figure 4.8C). The surface plots clearly show this result with dark green shade correlating to the larger particle size (>250 nm) and the light green shade pattern correlates to the smaller particle size (<250 nm). Accordingly, the DoE study has achieved uniform and homogenous particle size as desired.

As can be observed in Table 4.6b, it is evident that the surface quadratic model was significant and the lack of fit for this model was not significant, indicating that the model was significant for the CQA (*i.e.* particle size of the nanocrystalline zileuton suspension). The final equation based on the three critical process parameters (milling time, milling speed and pump speed) and the interaction terms for the prediction of the particle size of the nanocrystalline zileuton suspension are provided in Table 4.6b.

It was observed that the particle size of the zileuton macro-suspension decreased with increase in the milling speed and milling time, due to strong shear force and attrition force of the yttrium-stabilized zirconium oxide grinding beads (50μ) in the wet media mill significantly impacting upon the macroparticles and breaking them into multiple microparticles. These microparticles are further broken into small uniform nanoparticles upon several passes of the zileuton suspension in the wet media mill. A high milling speed indicates strong shear and attrition force of the milling beads (zirconia beads) and a high

milling time defines the number of passes of the zileuton macro- and micro-suspensions to form nanocrystalline zileuton suspensions. Following the wet media milling DoE, the optimized critical process parameters and CQAs predicted by the DoE model are provided in Table 4.6c. The predicted critical process parameters were applied to the formulations prepared for the validation of spray drying DoE.

4.4.2.2 Spray drying DoE

Following the wet media milling DoE, the statistically predicted critical process parameters obtained were applied to the spray drying DoE formulations. For spray drying DoE, two different sugar stabilizers (mannitol and trehalose, drug:sugar – 1:1, w/w) were investigated to prevent nanoparticle aggregation and sticking to the walls of the spray dryer glass vessel, resulting in uniform particle size and maximum total drug product yield at the end of the process.

4.4.2.2.1 Spray drying DoE [Stabilizer:Mannitol]

Based on the spray drying DoE (using mannitol), it was observed that the spray drying critical process parameters (inlet temperature, aspirator rate and feed flow rate) had a significant influence on the total product yield and the particle size of the nanocrystalline zileuton.

According to Figure 4.9(A), with increase in the inlet temperature (>115°C) and the aspirator rate (>85%) of the spray dryer, there was increase in the total product yield (>70% w/w) of the nanocrystalline zileuton (solid powder). The influence of the inlet temperature and the aspirator rate on the total product yield as shown by the curved green lines (against yellow background) on the base of the 3D surface plot is shown in the contour plot on the left side. The curved light blue shade on the contour and 3D surface plots indicate low total product yield (65% w/w) and the yellow to light orange shade on the contour and 3D surface plots indicate high total product yield (75% w/w). Inlet temperature is the temperature of the dry gas (air or inert gas) flowing through the spray dryer chamber. Aspirator rate is the rate at which the dry gas (air or inert gas) flowing through the spray dryer chamber. An optimized combination of the inlet temperature and aspirator rate is important for complete drying of the spray-dried particles with uniform particle size and maximum total product

yield. A high inlet temperature indicates increase in the rate of surface evaporation from the atomized droplets formed at the spray dryer nozzle. A high aspirator rate maintains a completely dry environment in the spray dryer, thus minimizing sticking to the walls of the spray dryer glass vessel and maximizing the total product yield.

According to the Figure 4.9(B), with decrease in the feed flow rate (<20%) and increase in the inlet temperature (>115°C) of the spray dryer, there was an increase in the total product yield (≥ 75% w/w) of the nanocrystalline zileuton (solid powder). According to the 3D surface plot on the right side of the Figure 4.9(B), a yellow-orange shade (high total product yield (≥75% w/w)) at the top and aqua shade (low total product yield (≤65% w/w)) tapering at the bottom of the curve was observed. The influence of the inlet temperature and the feed flow rate on the total product yield as shown by the curved green lines (against yellow background) on the base of the 3D surface plot is shown in the contour plot on the left side. Feed flow rate is the flow rate of the nanosuspension flowing through the spray dryer with the first contact being with the spray dryer nozzle following which the nanosuspension atomizes into multiple tiny droplets resulting in increase in surface area and increase in rate of surface evaporation. An optimized combination of the inlet temperature, aspirator rate and feed flow rate is important for complete drying of the spray-dried particles with uniform particle size and maximum total product yield. A high inlet temperature indicates increase in the rate of surface evaporation from the atomized droplets formed at the spray dryer nozzle. A high feed flow rate results in the formation of large droplets following atomization from the spray dryer nozzle. These large droplets even under the influence of high inlet temperature and high aspirator rate will not dry completely due to their smaller surface area and decreased rate of surface evaporation. Thus multiple large droplets formed at high feed flow rates results in incomplete drying leading to sticking to the glass walls of the spray dryer, minimizing total product yield and maximizing nanoparticle aggregation significantly impacting product quality and stability. On the contrary, low feed flow rates indicate formation of multiple tiny droplets following atomization from the spray dryer nozzle resulting in increased rate of surface evaporation, better drying with minimal sticking to the glass walls of the spray dryer. This results in uniform particle size and maximum total product yield.

Aspirator rates >85%, feed flow rates <20% and inlet temperatures >115°C result in total product yield >70% w/w (Figure 4.9C). The surface plots clearly show this result with green shade (light to dark) correlating to high total product yield (>70% w/w) and the blue shade (light to dark) correlating to low total product yield (<70% w/w). Accordingly, the DoE study has achieved maximum total product yield as desired.

As can be observed in Table 4.7b, it is evident that the surface reduced cubic model was significant and the lack of fit for this model was not significant, indicating that the model was significant for the CQA (*i.e.* total product yield of the nanocrystalline zileuton solid powder). The final equation based on the three critical process parameters (inlet temperature, aspirator rate and feed flow rate) and the interaction terms for the prediction of the total product yield of the nanocrystalline zileuton solid powder are provided in Table 4.7b.

4.4.2.2.2 Spray drying DoE [Stabilizer:Trehalose]

Based on the spray drying DoE (using trehalose), it was observed that the spray drying critical process parameters (inlet temperature, aspirator rate and feed flow rate) had a significant influence on the total product yield and the particle size of the nanocrystalline zileuton.

According to the Figure 4.10(A), a high aspirator rate (>85%) lead to increase in the total product yield (>65% w/w) of the nanocrystalline zileuton (solid powder). The influence of the inlet temperature and the aspirator rate on the total product yield as shown by the curved green-orange lines (against the yellow background) on the base of the 3D surface plot is demonstrated in the contour plot on the left side. The curved light blue – green shade on the contour and 3D surface plots indicate low total product yield (60% w/w) whereas the yellow to light orange shade on the contour and 3D surface plots indicate high total product yield (65-70% w/w). An optimized combination of the inlet temperature and aspirator rate is important for complete drying of the spray-dried particles with uniform particle size and maximum total product yield. Spray drying of the nanocrystalline zileuton in the presence of trehalose resulted in lower total product yield (65-70% w/w) compared to the spray-dried nanocrystalline zileuton with mannitol (75-80% w/w). However, following the spray drying DoE, the optimized spray-dried nanocrystalline zileuton in the presence of trehalose had a

uniform and smaller particle size (300-350 nm) with minimal nanoparticle aggregation compared to the spray-dried nanocrystalline zileuton in the presence of mannitol (450-500 nm). One of the potential reasons for this could be recrystallization of mannitol into large particles along with the zileuton nanoparticles, meanwhile trehalose resulted in minimal to no change in the particle size of the zileuton nanoparticles during spray drying.

According to Figure 4.10(B), with decrease in the feed flow rate (<20%) and decrease in the inlet temperature (<120°C) of the spray dryer, there was increase in the total product yield (≥ 75% w/w) of the nanocrystalline zileuton (solid powder). According to the 3D surface plot on the right side of the Figure 4.10(B), a yellow-orange shade (high total product yield (≥70% w/w)) at the top and green-aqua shade (low total product yield (≤60% w/w)) tapering at the sides of the curve was observed. The influence of the inlet temperature and the feed flow rate on the total product yield as shown by the curved orange-green lines (against the yellow background) on the base of the 3D surface plot is shown in the contour plot on the left side. An optimized combination of the inlet temperature, aspirator rate and feed flow rate is important for complete drying of the spray-dried particles with uniform particle size and maximum total product yield. A low feed flow rate resulted in increased surface evaporation from the atomized droplets, maximizing the total product yield and producing uniform sized nanocrystalline zileuton solid powder.

Aspirator rates >90%, feed flow rates <15% and inlet temperatures:110-115°C resulted in total product yield >65% w/w (Figure 10C). The surface plots clearly show this result with dark green shade correlating to high total product yield (>65% w/w) and light green shade correlating to low total product yield (<65% w/w). Accordingly, the DoE study has achieved maximum total product yield as desired.

As can be observed in Table 4.8b, it is evident that the surface reduced cubic model was significant and the lack of fit for this model was not significant, indicating that the model was significant for the CQA (*i.e.* total product yield of the nanocrystalline zileuton solid powder). The final equation based on the three critical process parameters (inlet temperature, aspirator rate and feed flow rate) and the interaction terms for the prediction of the total product yield of the nanocrystalline zileuton solid powder are provided in Table 4.8b.

Following the spray drying DoE, the optimized critical process parameters and CQAs predicted by the DoE model are provided in Table 4.8c. The statistically predicted critical process parameters were applied for the validation of the formulation DoEs. The spray-dried nanocrystalline zileuton prepared using sugar stabilizer trehalose (drug:sugar-1:1, w/w) showed a uniform particle size distribution and maximum total product yield. Therefore, trehalose was used as a sugar stabilizer during spray drying for all further DoE studies maintaining high product quality of the nanocrystalline zileuton (solid powder).

4.4.2.3 Formulation DoE (wet media milling)

The statistically predicted critical process parameters based on the wet media milling DoE were used for the nanocrystalline zileuton formulations (nanosuspensions) DoE.

It was observed that the formulation critical formulation parameters (drug, polymer and surfactant concentration) have a significant influence on the particle size of the nanocrystalline zileuton. According to Figure 4.11(A), with increase in drug concentration >0.65% w/v and at polymer concentrations between 0.4-0.7% w/v, there was decrease in the particle size <300 nm of the nanocrystalline zileuton suspension. According to Figure 4.11(B), with increase in drug concentration >0.65% w/v and at surfactant concentration >0.045% w/v, there was decrease in particle size <300 nm of the nanocrystalline zileuton suspension.

Drug concentrations >0.5% w/v, at polymer concentrations between 0.4-0.7% w/v and surfactant concentrations between 0.04-0.07% w/v result in particle size <300 nm (Figure 4.11(C). Accordingly, the DoE study has achieved small and uniform particle size (<500 nm) as desired.

As can be observed in Table 4.9b, it is evident that the surface cubic model was significant and the lack of fit for this model was not significant, indicating that the model was significant for the CQA (*i.e.* particle size of the nanocrystalline zileuton suspension). The final equation based on the three critical formulation parameters (drug concentration, polymer concentration and surfactant concentration) and the interaction terms for the prediction of the particle size of the nanocrystalline zileuton suspension is provided in Table 4.9b.

In the preparation of the nanocrystalline zileuton suspension *via* wet media milling, the surfactant (Dowfax2A1) acts as a bridge between the drug (zileuton) and the polymer (KollidonVA64 fine). The polymer stabilizes the drug by forming hydrogen bonds between the carbonyl group of the polymer and the amino group of the drug. The combination of excipients (polymer and surfactants) stabilizes the drug in the nanoparticulate system by electrosteric stabilization (electrostatic and steric stabilization). A very low concentration of each ingredient (drug, polymer and surfactant) results in larger particle size distribution due to insufficient drug-stabilizer interaction leading to destabilization of the nanoparticulate system. A very high concentration of each ingredient (drug, polymer and surfactant) leads to nanoparticle aggregation significantly affecting the product quality and stability. An optimized concentration of the drug and stabilizers (polymer and surfactant) is desired for the preparation of stable nanocrystalline zileuton suspensions during wet media milling.

4.4.2.4 Formulation DoE (Spray drying)

The statistically predicted critical process parameters based on the wet media milling DoE and spray drying DoE (using trehalose) were used for the formulation DoE for the preparation of the nanocrystalline zileuton (solid powder). Based on the formulation DoE (spray drying using trehalose), it was observed that the critical formulation parameters (drug concentration, polymer concentration, surfactant concentration and amount of sugar) had a significant influence on the total product yield and the particle size of the nanocrystalline zileuton (solid powder).

According to Figure 4.12(A), a high drug concentration (>0.65% w/v) and a low polymer concentration (<0.4% w/v) leads to an increase in the total product yield (>75% w/w) of the nanocrystalline zileuton (solid powder). The influence of the drug concentration and the polymer concentration on the total product yield as shown by the curved green-orange lines (against the yellow background) on the base of the 3D surface can be observed in the contour plot on the left side. The curved light green shade on the contour and 3D surface plots indicate low total product yield (65% w/w) and the yellow to light orange shade on the contour and 3D surface plots indicate high total product yield (75-80% w/w). According to the formulation DoE (spray drying), a low concentration of polymer is sufficient to stabilize

the drug nanoparticles. The drug concentration does not significantly influence the total product yield.

According to Figure 4.12(B), with increase in the surfactant concentration (≥0.06% w/v) and increase in drug concentration (>0.65% w/v), there was increase in the total product yield (≥76% w/w) of the nanocrystalline zileuton (solid powder). The influence of the drug concentration and the surfactant concentration on the total product yield as shown by the curved orange-green lines (against the yellow background) on the base of the 3D surface plot can be seen in the contour plot on the left side. An optimized combination of drug, polymer and surfactant is desired to obtain spray-dried nanoparticles with uniform particle size and maximum total product yield. A high concentration of surfactant (≥0.06% w/v) provides a strong steric stabilization to the nanocrystalline drug-polymer system (which is stabilized electrostatically). The drug-polymer system has a tendency to aggregate, which upon addition of the surfactant, results in uniform and homogenous particle size due to the electrosteric stabilization effect. This electrosteric stabilization effect (drug-surfactant-polymer) in combination with the optimized critical process parameters from the spray drying process results in completely dry nanoparticles, therefore minimizing sticking to the glass walls of the spray dryer, maximizing the total product yield and producing uniform sized nanocrystalline zileuton solid powder.

According to Figure 4.12(C), with decrease in the amount of sugar (<1200 mg) and increase in drug concentration (>0.65% w/v), there was an increase in the total product yield (≥75% w/w) of the nanocrystalline zileuton (solid powder). The influence of the drug concentration and amount of sugar on the total product yield as shown by the curved orange-green lines (against the yellow background) on the base of the 3D surface plot is shown in the contour plot on the left side. Sugars are known to prevent nanoparticle aggregation during the drying process by the virtue of electrostatic repulsion. Sugars such as trehalose provide strong rigidity by coating the nanoparticles and thus preventing the attractive forces between the nanoparticles in presence of other stabilizers (surfactants and polymers) and maintaining sufficient repulsion to keep the nanoparticles apart [55]. An optimized ratio of the drug:sugar is desired to obtain stable spray-dried nanoparticles with uniform particle size and maximum total product yield. The low amount of sugar (<1200 mg) resulted in

significantly high total product yield (≥75% w/w), this indicates that the drug:sugar ratio (1:1, w/w) is sufficient to prevent nanoparticle aggregation during the spray drying process. A high sugar amount (>1600 mg) resulted in a decrease in total product yield (<65% w/w). A high amount of sugar significantly influences the particle morphology and also leads to increased hygroscopicity due to its hydrophilic nature (in combination with less drying of the nanoparticles), this leads to increased sticking of the partially dried nanoparticles to the glass walls of the spray dryer, significantly decreasing the total product yield.

Polymer concentrations <0.6% w/v, surfactant concentrations >0.05% w/v and amount of sugar <1400 mg, resulted in total product yield between 60-70% w/w (Figure 4.12D). The surface plots clearly show this result with dark green shade correlating to high total product yield (>70% w/w) and light green shade correlating to low total product yield (<70% w/w). Accordingly, the DoE study has achieved maximum total product yield as desired.

As can be observed in Table 4.10b, it is evident that the surface quadratic model was significant and the lack of fit for this model was not significant, indicating that the model was significant for the CQA (*i.e.* total product yield of the nanocrystalline zileuton solid powder). The final equation based on the four critical formulation parameters (drug concentration, polymer concentration, surfactant concentration and amount of sugar) and the interaction terms for the prediction of the total product yield of the nanocrystalline zileuton solid powder are provided in Table 4.10b.

The optimized critical formulation parameters and CQAs predicted by the DoE models (process and formulation) are detailed in Table 4.11. The predicted critical formulation parameters (post wet media milling and post spray drying) were applied for the validation of the DoE studies.

4.4.3. Validation of DoE studies

The DoE studies were validated by applying the statistically predicted critical process parameters and critical formulation parameters to prepare sextuplets batches (n=6) of the spray-dried nanocrystalline zileuton formulations. The average experimental physicochemical properties (Table 4.12) of the sextuplet formulations were compared with the statistically predicted CQAs (Table 4.11).

4.4.4 Stability studies

The optimized spray-dried nanocrystalline zileuton formulations prepared based on the statistically predicted critical process parameters and critical formulation parameters obtained from the DoE studies as described in the Table 4.20 were stored at three different stability conditions; 4°C, 25°C/60% RH and 40°C/75% RH for one, six and twelve month/s. The formulations were then analyzed for particle size distribution, moisture content, drug loading and zeta potential. Additionally, the formulations were also analyzed using: DSC and PXRD (to monitor any polymorphic transformation *i.e.* conversion of one crystalline form to other); ATR-FTIR (to study the interaction between drug and polymer); PLM (to monitor any generation of non-crystallinity or amorphous particles); and *in vitro* dissolution testing (to investigate the effect of pH, particle size, temperature and humidity on drug release).

4.4.4.1 Particle size distribution and Moisture content

As shown in Table 4.11 and Figure 4.13, the particle size, PDI and moisture content of the prepared spray-dried nanocrystalline zileuton increased following one, six and twelve month/s storage under: 25°C/60% RH and 40°C/75% RH. On the other hand, the optimized formulations stored at 4°C were determined to be stable in terms of particle size distribution, moisture content and zeta potential over the one year study period.

The particle size increase for the formulations stored at 25°C/60% RH and 40°C/75% RH conditions (3-3.5%) is considered to be due to high humidity causing aggregation of the nanocrystalline zileuton particles.

4.4.4.2 Powder X-ray diffraction

The characteristic diffraction peaks of neat macrocrystalline zileuton drug (most stable - anhydrous polymorphic form I) are 9.8°, 15.7°, 17.7°, 19.7°, 22.48°, 22.5°, 26.5°, 29°, and 31.3°. Figure 4.14 displays an overlay of the PXRD diffraction profiles of the neat macrocrystalline zileuton (raw crystalline drug), a physical mixture (zileuton, KollidonVA64 fine, Dowfax2A1 and trehalose) as well as the optimized spray-dried nanocrystalline zileuton formulation (day zero and those stored for 12 months at 4°C, 25°C/60% RH and 40°C/75% RH). As shown in Figure 4.14, the optimized spray-dried

nanocrystalline zileuton formulation (day zero) showed a similar diffraction pattern as the neat drug but with reduced intensity. The decrease in the intensity is characteristic of the nanoparticles, due to their small particle size. The optimized spray-dried nanocrystalline zileuton formulations stored at 4°C and 25°C/60% RH for 12 months showed similar diffraction patterns as the day zero formulations. However, the formulations stored at 40°C/75% RH for 12 months showed blunt diffraction peaks (compared to the sharp diffraction peaks for the formulations at day zero as well as the 12 months samples (at 4°C and 25°C/60% RH)). The increase in the particle size (as discussed above in section 4.4.1.1) and polymorphic transition (semi-crystallinity) as a result of the high humidity are the possible reasons for the blunt PXRD diffraction peaks with reduced intensity.

4.4.4.3 Attenuated total reflectance – Fourier transform infrared spectroscopy

According to Figure 4.15 (a and b), there is band broadening between 3000-3500 cm^{-1} in the FTIR spectra for the spray-dried nanocrystalline zileuton formulations at zero day as well as those stored for twelve months under all conditions (*i.e.* 4°C, 25°C/60% RH, and 40°C/75% RH). The band broadening is considered to be due to hydrogen bonding between the N-H moiety of zileuton and the C=O group of the polymer (KollidonVA64 fine). However, there is no band broadening in the case of the macrocrystalline zileuton (neat drug) and the physical mixture of the drug-stabilizers (drug-polymer-surfactant-sugar).

From Figure 4.15b, two additional peaks (2970 cm^{-1} (C-H antisymmetric stretching vibrations, N-H aromatic stretching) and 2905 cm^{-1} (C-H symmetric stretching vibration) – in CH_3) were observed in the nanocrystalline zileuton stored at 40°C/75% RH for 12 months compared to the other formulations and the neat drug as well as the physical mixture. It is reported that the methylene ($-CH_2$) stretching of ethylene glycol ($HO-CH_2-CH_2-OH$) molecules results in a peak at 2970 cm^{-1} [56]. The formulations stored at high humidity (75% RH) have physical instability due to the high moisture content causing degradation of KollidonVA64 fine through converting the ethylene side chains to ethylene glycol moieties.

The N-H stretching (present in the 1° amides) results in an absorbance peak at 3180 cm^{-1}. From Figure 4.15c, a broad band (3220 – 3140 cm^{-1}) with maximum intensity at 3180 cm^{-1} in both the neat drug and the physical mixture was observed, however this peak was absent

in all formulations (day zero and 12 months). The peak was not present in the day zero nanoformulations possibly due to the labile nature of the amide group in presence of aqueous media during manufacturing. This peak was not present in any formulation stored at different stability conditions. Another possible reason behind the absence of the peak at 3180 cm^{-1} could be due to the interaction (hydrogen bonding) between the drug-surfactant-polymer complex with sugar.

From Figure 4.15d, it was observed that there was hydrophobic interaction between the drug and the stabilizers in the nanocrystalline zileuton formulations (day zero and stability formulations (12 months)). The peaks between 1650-1550 cm^{-1} is mainly observed due to N-H bending and is stronger in amides than amines. The two sharp peaks between 1650-1550 cm^{-1} is characteristic of the amide moiety in the neat drug, which is also observed in the physical mixture. The intensity of these peaks reduced significantly in the formulations (both at day zero and those stored for 12 months) due to strong interactions (hydrophobic (C-C) and hydrogen bonding) between the drug and the stabilizers. The highlighted area (a) indicate that the sharp peaks 1350 – 1150 cm^{-1} are present in drug and physical mixture, however these peaks are absent in all formulations. It has been reported that the sharp peaks at 1350 and 1150 cm^{-1} are characteristics of C-O-C stretching vibration in acrylates and esters [57]. Furthermore the sharp peaks between 1350 and 1150 cm^{-1} are also associated with acyl group (C-O) [58]. This sharp peaks disappears due to the strong interaction between the drug and the stabilizers in solid formulations. The highlighted area (b) (1150-1050 cm^{-1}) is associated with the formation of the alkoxy group (CH_3-O-) and related C-O stretching vibrations in these groups during the preparation of the nanoparticles [59]. The neat drug and physical mixture of drug-stabilizers are devoid of these peaks, which is present only in the nanoparticle formulations. The polymer KollidonVA64 fine have number of –CH-CH_2 moieties both linked to the pyrrolidone and to the vinyl functional groups. The carbon atom of the –CH-CH_2 moieties interacts with the oxygen atom of the N-OH moieties present in the drug (hydrophobic interaction) during the preparation of the nanocrystalline zileuton, thus the two peaks are observed only in the nanocrystalline zileuton formulations and not in the drug or the physical mixture of the drug-stabilizers. The highlighted area (c) (1050-950 cm^{-1}) indicate the peak shift of one of the two peaks in the nanocrystalline zileuton formulations compared to those observed in the drug and the

physical mixture. The peak shifts from 1020 cm^{-1} as observed in the drug and the physical mixture to 980 cm^{-1} as observed in the nanocrystalline zileuton formulations. It has been reported that this peak shift is due to the C-H stretching in the monosubstituted alkene [57]. According to the highlighted area (d) a new peak was observed at 800 cm^{-1} in all nanoparticle formulations which was missing in the drug and physical mixture. This peak is a characteristics of the N-H bending in the amines and the C-H bending at the para position (para – carbon) of the aromatic ring. The hydrophobic interactions and the hydrogen bond formation between the drug and the stabilizers result in the appearance of the peak at 800 cm^{-1} only in the nanoparticles and not in the neat drug or the physical mixture. The hydrophobic interactions between the drug and the stabilizers result in the decreased intensity of the two peaks between 750-700 cm^{-1} in the nanocrystalline zileuton formulations compared to sharp peaks as observed in the neat drug and the physical mixture.

4.4.4.4 Polarized light microscopy

According to Figure 4.16, large rod and plate shaped crystals (sharp birefringence) was observed for the neat drug (macrocrystalline zileuton – 20 μ particle size). This sharp birefringence was also observed in the physical mixture. The birefringence was evident in the spray-dried nanocrystalline zileuton formulations both at day zero and following 12 months storage at 4°C. However, the large rod and plate shaped macrocrystals were converted to uniform sized nanocrystals during the milling process which was evident in the initial spray-dried nanocrystalline zileuton formulations as well as those stored for 12 months at 4°C. In agreement with the PXRD and the particle size results it is evident that there is no aggregation of the spray-dried nanocrystalline zileuton formulations at 4°C and significant aggregation at 40°C/75% RH. Additionally, it is evident that there is significantly more aggregation at 40°C/75% RH compared to 25°C/60% RH.

4.4.4.5 Differential Scanning Calorimetry

According to the DSC thermograms (Figure 4.17), there was no polymorphic transition of the zileuton (neat drug) after processing it into nanoparticles (nanocrystalline zileuton) *via* wet media milling and spray drying. This was also evident from the PXRD (Figure 4.12) and the PLM (Figure 4.14) results. The melting endotherm of neat zileuton

(macrocrystalline drug) is observed at 153.52°C. There was broadening of the melting endotherm peak in all nanocrystalline zileuton formulations (initial and stability formulations (12 months)) as observed in the DSC thermograms. The melting endotherm broadening in the zileuton nanoparticles at day zero and those stored at 4°C for 12 months was observed to be 140-155°C. The melting endotherm broadening in the zileuton nanoparticles stored at 25°C/60% RH and 40°C/75% RH (12 months) was observed to be 130-155°C. The melting endotherm broadening observed for all the nanoparticle formulations is considered to be due to the strong interactions (hydrogen bonding and hydrophobic) between the drug and the stabilizers. The glass transition temperature (Tg) is an important characteristic of the polymers and sugars. A single Tg is observed for all components (otherwise having different Tgs) in a true solid dispersion, indicating that the excipients are providing strong stabilization to the drug [60, 61]. The spray-dried nanocrystalline zileuton formulations showed a single Tg (~63.7°C) which correlated to the mixture of excipients compared to their separate Tgs (KollidonVA64 fine ~104°C and trehalose ~107°C). For the formulations stored at 40°C/75% RH for 12 months, two Tgs (~78.7°C and ~87.41°C) were observed. The appearance of two Tgs is due to the presence of high moisture/humidity, which has a plasticization effect on the nanoparticles causing the nanocrystalline zileuton to isolate from the excipients, leaving the nanoparticle vulnerable to the physical instability (particle aggregation). All other formulations were stable post 12 months.

4.4.5. *In vitro* dissolution testing

The *in vitro* dissolution testing was performed using sextuplet formulations (n=6). In addition to the optimized nanocrystalline zileuton suspensions (30 min milled (216 nm)), two additional formulations (10 min milled (630 nm) and unmilled (20 μm)) were investigated to determine the effect of particle size on the drug release profile (Figure 4.18a). The 216 nm showed the fastest dissolution rate and took only 45 min for complete drug release compared to 240 min and 480 min for the 630 nm and 20 μ formulations, respectively. The drug release or dissolution rate from the liquid crystalline zileuton formulations followed a particle size dependent dissolution trend.

For the spray-dried crystalline zileuton formulations, a similar particle size dependent trend in the dissolution profiles was observed (Figure 4.18b), except the rate was slower in comparison to the liquid crystalline formulations. The spray-dried formulations were filled into gelatin capsules and placed in USP apparatus I baskets. The slow dissolution rate is probably a result of gelatin capsule shell wetting, dissolution and erosion prior to the release of the spray dried powder in the dissolution media. The total time for complete drug dissolution from the spray dried crystalline zileuton – 276.4 nm, 738.2 nm and 22 μm was 2 h, 4 h and 8 h, respectively.

The formulations stored at 4°C showed the fastest dissolution rate similar to the freshly prepared samples. The formulations stored at 40°C/75% RH showed a slower dissolution rate compared to the other formulations. The slow dissolution rate for the formulations stored at 40°C/75% RH is attributed to the increase in particle size due to nanoparticle aggregation as evident from the solid-state and particle size characterization techniques. The *in vitro* dissolution rate trend for the stability formulations was: freshly prepared=4°C > 25°C/60% RH > 40°C/75% RH (post 12 months, Figure 4.18c). Complete drug release was achieved from the 4°C (and freshly prepared), 25°C/60% RH and 40°C/75% RH nanoparticle formulations in ~120 min, ~240 min and ~720 min, respectively.

The effect of different pH conditions – stomach (pH 1.2) and intestine (pH 6.8) on the drug release during the transit of the nanocrystalline formulations (liquid and spray-dried) through the GIT was investigated using the *in vitro* dissolution pH shift test. The liquid nanocrystalline zileuton formulations showed <10 % drug release at pH 1.2 compared to the spray-dried formulations (<8 % drug release) in the initial 2 h (Figure 4.18d(i)). Following the pH switch from pH 1.2 to 6.8, the liquid nanocrystalline zileuton reached complete drug release in 1 h (total time: 3 h) compared to 2 h (total time: 4 h) taken by spray dried nanocrystalline zileuton. Following the stability studies, the pH shift experiments during *in vitro* dissolution testing were performed for the nanoparticles stored at different stability conditions (4°C, 40°C and 40°C/75% RH for 12 months) and compared with the day zero formulations. In the case of liquid nanocrystalline zileuton, the day zero and those stored at 4°C showed <10% drug release at pH 1.2 in 2 h (Figure 4.18d(ii)). Switching the pH from 1.2 to 6.8, complete drug release was observed in 1 h (total time: 3h). However, the

nanoformulations stored at 40°C, showed a decrease in the drug dissolution rate and incomplete drug release (only 85% drug release in 4 h, total time: 6h) due to nanoparticle aggregation in these samples. In the case of spray dried nanocrystalline zileuton (powder formulations), the day zero and those stored at 4°C showed <8% drug release at pH 1.2 in 2 h (Figure 4.18d(iii)). Switching the pH from 1.2 to 6.8, complete drug release was observed in 2 h (total time: 4h). The spray-dried formulations stored at 40°C/75% RH showed a similar trend to the liquid formulations stored at 40°C for 12 months, except the rate was slower.

4.5. CONCLUSIONS

The present research manifests the benefits of a comprehensive QbD approach for the systematic design and development of stable nanoparticulate drug products. Using the example of the spray-dried nanocrystalline zileuton, the significant CQAs were determined to be particle size and total product yield. The remaining CQAs were non-significant. Typically, a lab-scale spray dryer have total product yield of ~50% w/w, however based on this research, the total product yield of the nanocrystalline zileuton solid powder was ~80% w/w. A remarkably high total product yield was obtained following the comprehensive QbD approach, which is difficult to achieve in the case of individual DoE studies. Trehalose compared to mannitol was determined to be a better stabilizer preventing nanoparticle aggregation during the spray drying process which is in agreement with previous reports on nanoparticle aggregation. Based on the pH switch *in vitro* dissolution test, it was evident that complete drug release from the nanocrystalline zileuton formulations is achieved at intestinal pH (6.8). Based on the stability data, it is concluded that the spray-dried nanocrystalline drug products should be stored and transported at 4°C to avoid any physicochemical instability. In addition, the manufacturing of such nanocrystalline drug products (lab-scale and pilot scale) requires strict temperature control (2-8°C) to prevent nanoparticle physicochemical instability as well as any API associated instability. It is important to utilize orthogonal techniques (solid-state and analytical) to investigate the physicochemical instability (such as nanoparticle aggregation, drug degradation, polymorphic transition, *etc.*) as well as drug-stabilizer interaction because the combined

critical information from these techniques helps to develop robust nanoparticulate drug products.

Till date, individual DoEs (either process or formulation) have been investigated for the development of nanocrystalline drug products. These isolated DoEs can resolve a specific physicochemical property (one or two) of the drug product, however, the optimized formulation composition or process parameters cannot be assured, since all possible process and formulation interactions are not investigated. The innovation in the present research is application of a comprehensive QbD approach for the identification, optimization, validation and control of the critical processes parameters and critical formulation parameters *via* multiple DoE models. The individual critical process parameters and critical formulation parameters as well as their interactions were analyzed for stable spray-dried nanocrystalline zileuton. In addition, this research investigated important CQAs (particle size and total product yield) to develop a precise design space. This research can be applied to other BCS class II and II/IV drugs for the successful development of robust spray-dried nanocrystalline drug products.

4.6. Tables

Table 4.1. Chemical structures of the active pharmaceutical ingredient and excipients

Materials	Chemical structures
Zileuton	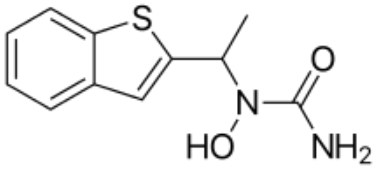
KollidonVA64 fine	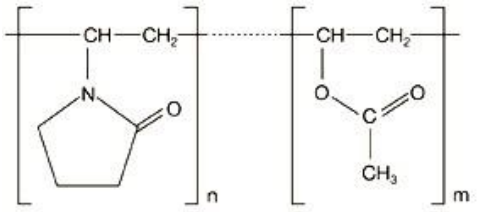
Dowfax 2A1	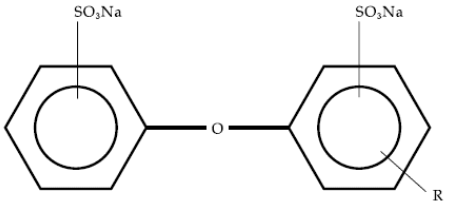
Trehalose	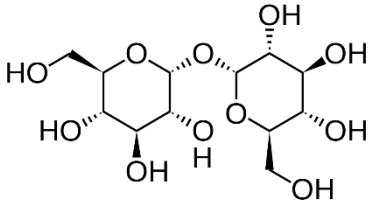

Table 4.2. A DoE Design space for optimization of the wet media milling critical process parameters for the preparation of stable nanocrystalline zileuton.

No.	CPPs (wet media milling)		
	Milling speed	Pump speed	Milling time
	rpm	rpm	min
-	500-1500	80-120	15-30
1	159	100	22.5
2	1500	80	30
3	1500	120	15
4	1500	120	30
5	1500	80	15
6	1000	100	22.5
7	1000	100	10
8	1000	100	22.5
9	1000	100	22.5
10	1000	134	22.5
11	1000	66	22.5
12	1841	100	22.5
13	500	120	15
14	1000	100	22.5
15	1000	100	35

16	500	120	30
17	1000	100	22.5
18	500	80	30
19	1000	100	22.5
20	500	80	15

Table 4.3a. A DoE Design space for optimization of the spray drying critical process parameters for the preparation of stable nanocrystalline zileuton using **mannitol** as the sugar stabilizer (drug:sugar – 1:1, w/w).

No.	CPPs (spray drying with mannitol)		
	Inlet temperature	Aspirator rate	Feed flow rate
	°C	%	%
-	**105-125**	**70-90**	**10-25**
1	115	80	18
2	132	80	18
3	115	80	18
4	105	70	25
5	115	80	18
6	115	80	30
7	105	90	25
8	115	63	18
9	105	70	10
10	115	80	18
11	115	80	5
12	98	80	18
13	125	70	25
14	105	90	10
15	125	90	25
16	115	80	18
17	115	80	18
18	115	97	18
19	125	90	10
20	125	70	10

Table 4.3b. A DoE Design space for optimization of the spray drying critical process parameters for the preparation of stable nanocrystalline zileuton using **trehalose** as the sugar stabilizer (drug:sugar – 1:1, w/w).

No.	CPPs (spray drying with trehalose)		
	Inlet temperature	Aspirator rate	Feed flow rate
	°C	%	%
-	**105-125**	**70-90**	**10-25**
1	115	80	18
2	132	80	18
3	115	80	18
4	105	70	25
5	115	80	18
6	115	80	30
7	105	90	25
8	115	63	18
9	105	70	10

10	115	80	18
11	115	80	5
12	98	80	18
13	125	70	25
14	105	90	10
15	125	90	25
16	115	80	18
17	115	80	18
18	115	97	18
19	125	90	10
20	125	70	10

Table 4.4a. A DoE Design space for the optimization of critical formulation parameters for the preparation of stable nanocrystalline zileuton post wet media milling.

No.	**CFPs**		
	Drug concentration	**Polymer concentration**	**Surfactant concentration**
	% w/v	**% w/v**	**% w/v**
-	**0.35-1**	**0.3-0.8**	**0.03-0.08**
1	1	0.3	0.08
2	0.675	0.55	0.005
3	1.325	0.55	0.055
4	0.675	0.55	0.055
5	1	0.3	0.08
6	1	0.3	0.03
7	0.675	1.05	0.055
8	0.675	0.55	0.055
9	0.675	0.55	0.055
10	0.35	0.8	0.08
11	0.675	0.55	0.055
12	1	0.8	0.08
13	0.675	0.55	0.055
14	0.675	0.55	0.105
15	0.35	0.3	0.03
16	0.675	0.05	0.055
17	0.35	0.8	0.08
18	1	0.8	0.03
19	0.35	0.8	0.03
20	0.35	0.3	0.08
21	0.35	0.3	0.03
22	0.025	0.55	0.055
23	0.675	0.55	0.055
24	0.35	0.8	0.03
25	1	0.3	0.03
26	1	0.8	0.08
27	0.35	0.3	0.08
28	0.675	0.55	0.055
29	0.675	0.55	0.055
30	1	0.8	0.03

Table 4.4b. A DoE Design space for the optimization of critical formulation parameters for the preparation of stable nanocrystalline zileuton post spray drying.

No.	CFPs			
	Drug concentration	**Polymer concentration**	**Surfactant concentration**	**Sugar amount**
	% w/v	**% w/v**	**% w/v**	**mg**
-	**0.35-1**	**0.3-0.8**	**0.03-0.08**	**850-2000**
1	1	0.8	0.03	2000
2	0.35	0.3	0.03	2000
3	0.35	0.3	0.08	850
4	0.675	0.55	0.055	1425
5	0.35	0.8	0.03	2000
6	0.35	0.3	0.03	850
7	1	0.3	0.03	2000
8	1	0.8	0.08	850
9	0.675	0.05	0.055	1425
10	0.675	0.55	0.055	2575
11	1	0.8	0.08	2000
12	0.675	0.55	0.055	1425
13	0.675	1.05	0.055	1425
14	0.35	0.8	0.08	2000
15	0.35	0.3	0.08	2000
16	0.675	0.55	0.055	1425
17	1	0.3	0.03	850
18	1	0.3	0.08	2000
19	0.675	0.55	0.055	275
20	0.35	0.8	0.08	850
21	0.675	0.55	0.105	1425
22	0.675	0.55	0.055	1425
23	1	0.3	0.08	850
24	0.675	0.55	0.055	1425
25	0.675	0.55	0.055	1425
26	1	0.8	0.03	850
27	0.025	0.55	0.055	1425
28	1.325	0.55	0.055	1425
29	0.35	0.8	0.03	850
30	0.675	0.55	0.005	1425

Table 4.5. Solubility of zileuton in different excipient solutions

Sample Number	Excipient solution (0.2% w/v)	Type of Stabilizer	Zileuton solubility (µg/mL)	Solubility (times X)
1	No excipient	N/A	130.2	-
2	Dowfax2A1	Anionic surfactant	165.2	1
3	SLS	Anionic surfactant	144.43	
4	Poloxamer P407	Nonionic surfactant	165.2	
5	Poloxamer 188	Nonionic surfactant	135.12	
6	EC 10	Nonionic polymer	187.905	1.5
7	Kolliphor SLS fine	Anionic surfactant	184.78	
8	Kollidon CLM	Nonionic polymer	197.97	
9	PVP K17	Nonionic polymer	241.41	2
10	PVP K25	Nonionic polymer	262.52	
11	PVP K30	Nonionic polymer	258.35	
12	PVP K90	Nonionic polymer	282.75	
13	HPMC K3	Nonionic polymer	258.94	
14	KollidonVA64	Nonionic polymer	254.74	
15	KollidonVA64 fine	Nonionic polymer	242.55	
16	HPMC E3	Nonionic polymer	319.32	2.5
17	HPMC E5	Nonionic polymer	327.01	
18	HPMC E15	Nonionic polymer	338.45	
19	HPMC E50	Nonionic polymer	344.9	
20	MC A15	Nonionic polymer	346.68	
21	Soluplus	Nonionic polymer	391.64	3

Table 4.6a. Results of DoE runs for optimization of the wet media milling critical process parameters for the preparation of stable nanocrystalline zileuton (3 CPPs x 3 CQAs).

Wet media milling DoE						
No.	CPPs			CQAs		
	Milling speed	Pump speed	Milling time	Particle size	PDI	Zeta potential
	rpm	rpm	min	nm	units	mV
-	500-1500	80-120	15-30			
1	159	100	22.5	212.3	0.26	-78.3
2	1500	80	30	29.16	0.322	-62.1
3	1500	120	15	135	0.235	-66.8
4	1500	120	30	65.7	0.156	-57.4
5	1500	80	15	85.24	0.145	-63.6
6	1000	100	22.5	214.5	0.187	-71.9
7	1000	100	10	431.3	0.112	-76.3
8	1000	100	22.5	200.4	0.237	-64.6
9	1000	100	22.5	214.3	0.136	-57.1
10	1000	134	22.5	130.5	0.219	-68.8
11	1000	66	22.5	174.2	0.121	-69.3
12	1841	100	22.5	37.13	0.228	-42.2
13	500	120	15	306	0.136	-82.9
14	1000	100	22.5	157.1	0.163	-72.8
15	1000	100	35	145.9	0.17	-74.9
16	500	120	30	182.1	0.13	-73.7

17	1000	100	22.5	245.4	0.459	-74.7
18	500	80	30	274.2	0.197	-47.2
19	1000	100	22.5	271.5	0.218	-77.6
20	500	80	15	269	0.136	-82

Table 4.6b. ANOVA table for CQA: Particle size of nanocrystalline zileuton post wet media milling

Particle size ➔ ANOVA for Response Surface Quadratic model						
Source	**Sum of Squares**	**df**	**Mean Square**	**F Value**	**p-value Prob > F**	
Model	1.563E+005	9	17362.87	6.73	0.0032	**significant**
A-Milling speed	74813.42	1	74813.42	28.99	0.0003	R^2=0.9519, Adjusted R^2=0.9478
B-Pump speed	130.98	1	130.98	0.051	0.8263	
C-Milling time	38388.65	1	38388.65	14.88	0.0032	
AB	2499.25	1	2499.25	0.97	0.3483	
AC	5.58	1	5.58	2.162E-003	0.9638	
BC	2531.87	1	2531.87	0.98	0.3453	
A^2	19311.12	1	19311.12	7.48	0.0210	
B^2	10378.25	1	10378.25	4.02	0.0727	
C^2	6560.44	1	6560.44	2.54	0.1419	
Lack of Fit	18150.64	5	3630.13	2.37	0.1826	***not significant***
Particle size (nm) = +217.80 – 74.01A – 3.1B – 53.02C + 17.68AB – 0.83AC – 17.79BC – $36.61A^2$ – $26.84B^2$ + $21.34C^2$						

Table 4.6c. Statistically predicted CPPs and CQAs based on the wet media milling DoE studies

CPPs			**CQAs**			**Desirability**
Milling speed (rpm)	**Milling time (min)**	**Pump speed (rpm)**	**Particle size (nm)**	**PDI (units)**	**Zeta potential (mV)**	
1200	30	92	225	0.198	-67.99	0.898

Table 4.7a. Results of DoE runs for optimization of the spray drying critical process parameters (stabilizer: mannitol) for the preparation of stable nanocrystalline zileuton (3 CPPs x 7 CQAs).

Spray drying DoE (Stabilizer: Mannitol)										
No.	**CPPs**			**CQAs**						
	Inlet temperature	**Aspirator rate**	**Feed flow rate**	**Outlet temperature**	**Particle size**	**PDI**	**Zeta potential**	**Drug loading**	**Yield**	**Moisture content**
	°C	**%**	**%**	**°C**	**nm**	**units**	**mV**	**% (w/w)**	**% (w/w)**	**%**
-	**105-125**	**70-90**	**10-25**							
1	115	80	18	51	1084.00	0.098	-95.200	38.554	64.174	0.850
2	132	80	18	60	1285.00	0.140	-73.600	33.764	66.957	0.745
3	115	80	18	48	748.30	0.521	-11.000	33.582	61.739	0.745
4	105	70	25	40	7259.00	0.866	-25.000	39.163	58.696	0.592
5	115	80	18	51	222.50	0.257	-20.000	35.611	56.348	1.013
6	115	80	30	46	169.50	0.125	-85.300	39.513	60.174	1.252
7	105	90	25	48	165.50	0.205	-99.600	40.656	64.348	0.684
8	115	63	18	47	180.70	0.289	-12.000	35.928	62.000	0.774
9	105	70	10	60	167.40	0.164	-13.000	43.318	75.478	0.828
10	115	80	18	51	1144.00	0.539	-24.000	35.656	62.696	0.980
11	115	80	5	74	1131.00	0.373	-20.000	34.833	67.043	0.518
12	98	80	18	37	5779.00	0.901	-36.000	37.959	60.174	0.767
13	125	70	25	51	515.00	0.509	-42.000	41.774	54.174	0.711
14	105	90	10	67	266.60	0.523	-37.000	37.438	84.000	0.815
15	125	90	25	58	158.50	0.241	-11.000	41.575	60.609	0.683
16	115	80	18	51	586.40	0.329	-15.000	36.752	74.522	1.208
17	115	80	18	50	1071.00	0.967	-19.000	40.331	57.391	1.133
18	115	97	18	60	172.70	0.306	-21.000	36.959	87.739	0.639
19	125	90	10	74	356.70	0.613	-35.000	42.574	75.652	0.424
20	125	70	10	68	191.10	0.421	-22.000	38.324	85.913	0.480

Table 4.7b. ANOVA table for CQA: Total product yield of nanocrystalline zileuton (solid powder) post spray drying (with mannitol)

Total product yield ➔ ANOVA for Response Surface Reduced Cubic model						
Source	**Sum of Squares**	**df**	**Mean Square**	**F Value**	**p-value Prob > F**	
Model	1684.42	10	168.44	5.94	0.0066	**significant**
A-Inlet temperature	23.00	1	23.00	0.81	0.3913	R^2=0.9694, Adjusted R^2=0.9622
B-Aspirator rate	331.25	1	331.25	11.68	0.0077	
C-Feed flow rate	23.60	1	23.60	0.83	0.3855	
AB	40.50	1	40.50	1.43	0.2626	
BC	23.90	1	23.90	0.84	0.3826	
B^2	310.54	1	310.54	10.95	0.0091	
ABC	47.85	1	47.85	1.69	0.2263	
A^2B	133.99	1	133.99	4.72	0.0578	
A^2C	231.58	1	231.58	8.17	0.0189	
AB^2	25.76	1	25.76	0.91	0.3654	
Lack of Fit	43.94	4	10.98	0.26	0.8919	***not significant***
Total product yield (% w/w) = +63.85 + 2.02A + 7.65B – 2.04C – 2.25AB +1.73BC +4.6B^2 + 2.45ABC – 6.36A^2B – 8.36A^2C – 2.79AB^2						

Table 4.8a. Results of DoE runs for optimization of the spray drying critical process parameters (stabilizer:trehalose) for the preparation of stable nanocrystalline zileuton (3 CPPs x 7 CQAs).

Spray drying DoE (Stabilizer:Trehalose)										
No.	**CPPs**			**CQAs**						
	Inlet temperature	**Aspirator rate**	**Feed flow rate**	**Outlet temperature**	**Particle size**	**PDI**	**Zeta potential**	**Drug loading**	**Yield**	**Moisture content**
	°C	**%**	**%**	**°C**	**nm**	**units**	**mV**	**% (w/w)**	**% (w/w)**	**%**
-	**105-125**	**70-90**	**10-25**							
1	115	80	18	54	161.70	0.216	-27.00	40.00	59.57	3.36
2	132	80	18	65	231.80	0.517	-29.00	41.25	67.57	3.21
3	115	80	18	56	200.30	0.743	-19.00	36.27	58.61	3.47
4	105	70	25	39	588.10	0.747	-33.00	40.31	58.96	3.45
5	115	80	18	55	152.90	0.235	-11.00	43.06	64.96	3.42
6	115	80	30	50	1316.00	0.779	-17.00	40.04	56.61	4.06
7	105	90	25	50	3646.00	0.569	-19.00	43.64	51.91	3.42
8	115	63	18	53	3069.00	0.741	-10.00	40.64	64.35	3.61
9	105	70	10	60	3223.00	1.000	-16.00	42.23	63.65	3.93
10	115	80	18	55	175.70	0.188	-20.00	45.30	63.30	3.78
11	115	80	5	73	423.20	0.454	-58.60	40.02	59.39	3.07
12	98	80	18	50	1523.00	0.351	-80.20	37.18	45.22	3.87
13	125	70	25	50	1248.00	0.611	-23.00	44.57	60.87	3.31
14	105	90	10	65	1054.00	0.681	-16.00	44.63	74.61	2.71
15	125	90	25	60	964.00	0.930	-14.00	42.83	58.26	3.19
16	115	80	18	55	117.70	0.485	-11.00	42.83	65.39	3.51
17	115	80	18	56	148.10	0.231	-29.00	44.99	70.09	3.37
18	115	97	18	60	284.30	0.595	-12.00	39.64	72.70	3.29
19	125	90	10	75	1221.00	0.424	-88.40	41.24	50.00	2.79
20	125	70	10	70	809.40	0.934	-15.00	38.22	60.00	2.98

Table 4.8b. ANOVA table for CQA: Total product yield of nanocrystalline zileuton (solid powder) post spray drying (with trehalose)

Total product yield ➔ ANOVA for Response Surface Reduced Cubic model						
Source	**Sum of Squares**	**df**	**Mean Square**	**F Value**	**p-value Prob > F**	
Model	907.60	13	69.82	4.57	0.0363	**significant**
A-Inlet temperature	249.71	1	249.71	16.33	0.0068	R^2=0.9082, Adjusted R^2=0.8993
B-Aspirator rate	34.84	1	34.84	2.28	0.1819	
C-Feed flow rate	3.87	1	3.87	0.25	0.6328	
AB	34.12	1	34.12	2.23	0.1859	
AC	166.73	1	166.73	10.90	0.0164	
BC	14.07	1	14.07	0.92	0.3745	
A^2	111.66	1	111.66	7.30	0.0355	
B^2	32.65	1	32.65	2.14	0.1943	
C^2	70.69	1	70.69	4.62	0.0751	
ABC	80.59	1	80.59	5.27	0.0615	
A^2B	42.20	1	42.20	2.76	0.1477	
A^2C	7.02	1	7.02	0.46	0.5234	

AB^2	277.07	1	277.07	18.12	0.0053	
Lack of Fit	3.36	1	3.36	0.19	0.6810	***not significant***
Total product yield (% w/w) = +63.69 + 6.64A + 2.48B – 0.83C – 2.07AB + 4.57AC – 1.33BC – $2.78A^2$ + $1.51B^2$ – $2.21C^2$ +3.17ABC – $3.57A^2B$ – $1.46A^2C$ – $9.41AB^2$						

Table 4.8c. Statistically predicted CPPs and CQAs based on the spray drying DoE studies

Spray drying DoE (drug:sugar-1:1, w/w)		**Mannitol**	**Trehalose**
CPPs	**Inlet temperature (°C)**	125	118
	Aspirator rate (%)	90	90
	Feed flow rate (%)	10	10
CQAs	**Outlet temperature (°C)**	70	67
	Particle size (nm)	499.24	326.97
	PDI (units)	0.28	0.12
	Zeta potential (mV)	-27.66	-58.18
	Drug loading (% w/w)	41.15	41.28
	Total yield (% w/w)	72.95	63.05
	Moisture content (%)	2.85	0.47
Desirability		0.807	0.967

Table 4.9a. Results of DoE runs for optimization of the critical formulation parameters (wet media milling) for the preparation of stable nanocrystalline zileuton (3 CFPs x 3 CQAs).

Formulation DoE (Wet Media Milling)						
No.	**CFPs**			**CQAs**		
	Drug concentration	**Polymer concentration**	**Surfactant concentration**	**Particle size**	**PDI**	**Zeta potential**
	% w/v	**% w/v**	**% w/v**	**nm**	**units**	**mV**
-	**0.35-1**	**0.3-0.8**	**0.03-0.08**			
1	1	0.3	0.08	174.1	0.266	-71.7
2	0.675	0.55	0.005	346.5	0.336	-68.1
3	1.325	0.55	0.055	125.8	0.224	-69.9
4	0.675	0.55	0.055	383.3	0.263	-79.2
5	1	0.3	0.08	182.8	0.277	-77.6
6	1	0.3	0.03	212.6	0.316	-80.6
7	0.675	1.05	0.055	356.8	0.499	-9.1
8	0.675	0.55	0.055	497.5	0.315	-81
9	0.675	0.55	0.055	397	0.213	-83.7
10	0.35	0.8	0.08	746.1	0.885	-83.2
11	0.675	0.55	0.055	426.6	0.313	-90.1
12	1	0.8	0.08	230.7	0.176	-59
13	0.675	0.55	0.055	434	0.202	-69.1
14	0.675	0.55	0.105	526.7	0.319	-89.8
15	0.35	0.3	0.03	732.8	0.394	-98.1
16	0.675	0.05	0.055	286.3	0.166	-129
17	0.35	0.8	0.08	621	0.462	-74.2
18	1	0.8	0.03	207.6	0.181	-69
19	0.35	0.8	0.03	703.3	0.483	-80.1
20	0.35	0.3	0.08	748.5	0.5	-109
21	0.35	0.3	0.03	613	0.419	-96.3
22	0.025	0.55	0.055	1536	0.45	-112

23	0.675	0.55	0.055	366.3	0.282	-81.3
24	0.35	0.8	0.03	756.2	0.478	-78.1
25	1	0.3	0.03	108.5	0.167	-78.2
26	1	0.8	0.08	133.3	0.225	-55.4
27	0.35	0.3	0.08	667.1	0.434	-107
28	0.675	0.55	0.055	230.9	0.363	-75.8
29	0.675	0.55	0.055	234.1	0.253	-82.6
30	1	0.8	0.03	117.3	0.278	-64.5

Table 4.9b. ANOVA table for CQA: Particle size of nanocrystalline zileuton post wet media milling

Particle size ➔ ANOVA for Response Surface Cubic model						
Source	**Sum of Squares**	**df**	**Mean Square**	**F Value**	**p-value Prob > F**	
Model	2.551E+006	22	1.160E+005	16.86	0.0004	**significant**
A-Drug concentration	9.943E+005	1	9.943E+005	144.60	< 0.0001	R^2=0.9815, Adjusted R^2=0.9233
B-Polymer concentration	2485.13	1	2485.13	0.36	0.5667	
C-Surfactant concentration	16236.02	1	16236.02	2.36	0.1683	
AB	184.28	1	184.28	0.027	0.8746	
AC	594.14	1	594.14	0.086	0.7773	
BC	1578.08	1	1578.08	0.23	0.6465	
A^2	2.911E+005	1	2.911E+005	42.33	0.0003	
B^2	16219.91	1	16219.91	2.36	0.1685	
C2	541.88	1	541.88	0.079	0.7870	
ABC	1711.89	1	1711.89	0.25	0.6331	
A^2B	883.23	1	883.23	0.13	0.7306	
A^2C	9310.26	1	9310.26	1.35	0.2827	
AB^2	41990.59	1	41990.59	6.11	0.0428	
Lack of Fit	8427.93	2	4213.97	0.53	0.6180	***not significant***
Particle size (nm) = +392.58 – 352.55A + 17.62B + 45.05C – 3.39AB + 6.09AC – 9.93BC +103.02A^2 – 24.32B^2 + 4.44C^2 + 10.34ABC – 12.87A^2B – 41.78A^2C + 88.73AB^2						

Table 4.10a. Results of DoE runs for optimization of critical formulation parameters (spray drying) for the preparation of stable nanocrystalline zileuton (4 CFPs x 7 CQAs).

Formulation DoE (spray drying)											
No.	CFPs				CQAs						
	Drug concentration	Polymer concentration	Surfactant concentration	Sugar amount	Outlet temperature	Particle size	PDI	Zeta potential	Drug loading	Total Yield	Moisture content
	% w/v	% w/v	% w/v	mg	°C	nm	units	mV	%	%	%
-	0.35-1	0.3-0.8	0.03-0.08	850-2000							
1	1	0.8	0.03	2000	72	494.1	1	-117	11.75377	48.69	3.68
2	0.35	0.3	0.03	2000	71	1718	0.065	-103	6.539006	63.69	3.456
3	0.35	0.3	0.08	850	68	1756	0.291	-113	12.5826	75.40	3.214
4	0.675	0.55	0.055	1425	68	1472	1	-109	11.98958	54.30	3.18
5	0.35	0.8	0.03	2000	71	658.7	0.855	-106	6.510985	49.85	3.649
6	0.35	0.3	0.03	850	71	1735	0.2	-99.1	10.98196	68.35	3.404
7	1	0.3	0.03	2000	68	1004	0.877	-123	11.00261	59.29	3.457
8	1	0.8	0.08	850	72	694.8	0.781	-107	21.56875	58.25	2.703
9	0.675	0.05	0.055	1425	70	1551	0.679	-101	16.41053	82.69	2.668
10	0.675	0.55	0.055	2575	70	1668	0.927	-114	14.89958	46.00	4.431
11	1	0.8	0.08	2000	72	137.9	0.323	-103	9.036766	52.06	3.82
12	0.675	0.55	0.055	1425	71	1668	0.927	-113	14.21775	65.96	3.611
13	0.675	1.05	0.055	1425	68	1593	1	-94.1	10.57662	40.16	3.858
14	0.35	0.8	0.08	2000	68	2880	0.956	-108	5.346451	42.95	3.729
15	0.35	0.3	0.08	2000	76	852.2	0.233	-99.9	5.612018	58.18	3.663
16	0.675	0.55	0.055	1425	70	1668	0.927	-50.2	11.90832	72.29	3.323
17	1	0.3	0.03	850	68	273.3	0.663	-94.7	31.19071	83.51	2.806
18	1	0.3	0.08	2000	70	171.9	0.177	-130	18.74133	64.15	3.433
19	0.675	0.55	0.055	275	71	1668	0.927	-91	12.25046	65.57	2.857
20	0.35	0.8	0.08	850	68	969.1	0.367	-80.3	9.417043	61.06	3.108
21	0.675	0.55	0.105	1425	68	102.4	0.692	-103	15.849	70.65	3.607
22	0.675	0.55	0.055	1425	71	1582	1	-101	16.11059	55.99	3.499
23	1	0.3	0.08	850	72	146.1	0.414	-43.2	14.40945	85.07	2.98
24	0.675	0.55	0.055	1425	72	898.7	0.786	-76.3	37.93154	52.89	2.728
25	0.675	0.55	0.055	1425	67	317.9	0.642	-90.7	16.26445	54.00	3.003
26	1	0.8	0.03	850	69	368.5	0.697	-86.9	27.06975	59.85	3.17
27	0.025	0.55	0.055	1425	71	3440	0.735	-111	2.75378	48.84	4.421
28	1.325	0.55	0.055	1425	71	196.9	0.455	-102	21.35168	49.52	3.146
29	0.35	0.8	0.03	850	75	1990	0.729	-92.8	8.798703	65.44	4.334
30	0.675	0.55	0.005	1425	72	1718	0.0656	-103	15.95752	73.25	3.166

Table 4.10b. ANOVA table for CQA: Total product yield of nanocrystalline zileuton (solid powder) post spray drying (with trehalose)

Total product yield ➔ ANOVA for Response Surface Quadratic model						
Source	**Sum of Squares**	**df**	**Mean Square**	**F Value**	**p-value Prob > F**	
Model	3492.06	14	249.43	6.19	0.0006	**significant**
A-Drug concentration	31.14	1	31.14	0.77	0.3931	R^2=0.9525, Adjusted R^2=0.9149
B-Polymer concentration	1743.67	1	1743.67	43.29	< 0.0001	
C-Surfactant concentration	1.90	1	1.90	0.047	0.8310	
D-Amount of sugar	1029.61	1	1029.61	25.56	0.0001	
AB	45.14	1	45.14	1.12	0.3065	
AC	20.07	1	20.07	0.50	0.4910	
AD	2.99	1	2.99	0.074	0.7890	
BC	19.09	1	19.09	0.47	0.5016	
BD	15.94	1	15.94	0.40	0.5387	
CD	2.90	1	2.90	0.072	0.7920	
A^2	117.96	1	117.96	2.93	0.1076	
B^2	26.79	1	26.79	0.67	0.4275	
C^2	359.40	1	359.40	8.92	0.0092	
D^2	4.88	1	4.88	0.12	0.7326	
Lack of Fit	285.94	10	28.59	0.45	0.8681	***not significant***
Total product yield (% w/w) = +59.24 + 1.14A – 8.52B – 0.28C – 6.55D – 1.68AB + 1.12AC – 0.43AD – 1.09BC + 1.00BD – 0.43CD – $2.07A^2$ + $0.99B^2$ + $3.62C^2$ – $0.42D^2$						

Table 4.11. Statistically predicted CPPs, CFPs and CQAs based on the formulation DoE

Comprehensive DoEs					
Wet media milling (CPPs)		**Spray drying (CPPs)**		**Formulation (CFPs)**	
Milling speed (rpm)	1200	**Inlet temperature (°C)**	118	**Drug concentration (% w/v)**	1
Milling time (min)	30	**Aspirator rate (%)**	90	**Polymer concentration (% w/v)**	0.3
Pump speed (rpm)	92	**Feed flow rate (%)**	10	**Surfactant concentration (% w/v)**	0.06
				Amount of sugar (mg)	850

CQAs	**Outlet temperature (°C)**	69
	Particle size (nm)	300.03
	PDI (units)	0.126
	Zeta potential (mV)	-80.84
	Drug loading (% w/w)	22.31
	Total yield (% w/w)	77.66
	Moisture content (%)	1.66
Desirability		0.904

Table 4.12. Physicochemical properties of the optimized spray-dried nanocrystalline zileuton formulations following one, six and twelve month/s exposure under different storage conditions.

Testing formulation : Optimized spray-dried nanocrystalline zileuton		**Particle size (nm)**	**PDI (units)**	**Zeta potential (mV)**	**Moisture content (%)**	**Drug loading (% w/w)**
Predicted values		**300.03**	**0.126**	**-80.84**	**1.66**	**22.31**
Experimental values						
0 month	**Initial (n=6)**	**276.4**	**0.109**	**-91.4**	**1.09**	**23.8**
1 month	**4°C**	273.1	0.115	-81.5	0.990	23.71
	25°C/60% RH	619.5	0.589	-103	1.17	23.25
	40°C/75% RH	996.4	0.791	-92.6	1.29	23.31
6 months	**4°C**	275.43	0.12	-79.63	0.994	23.84
	25°C/60% RH	648.91	0.723	-97.64	2.79	23.41
	40°C/75% RH	1013.19	0.817	-94.61	3.29	23.61
12 months	**4°C**	274.16	0.118	-81.2	0.989	23.82
	25°C/60% RH	694.37	0.653	-102	3.19	23.28
	40°C/75% RH	1209.43	0.923	-96.39	4.55	23.81

4.7. Figures

GRAPHICAL ABSTRACT

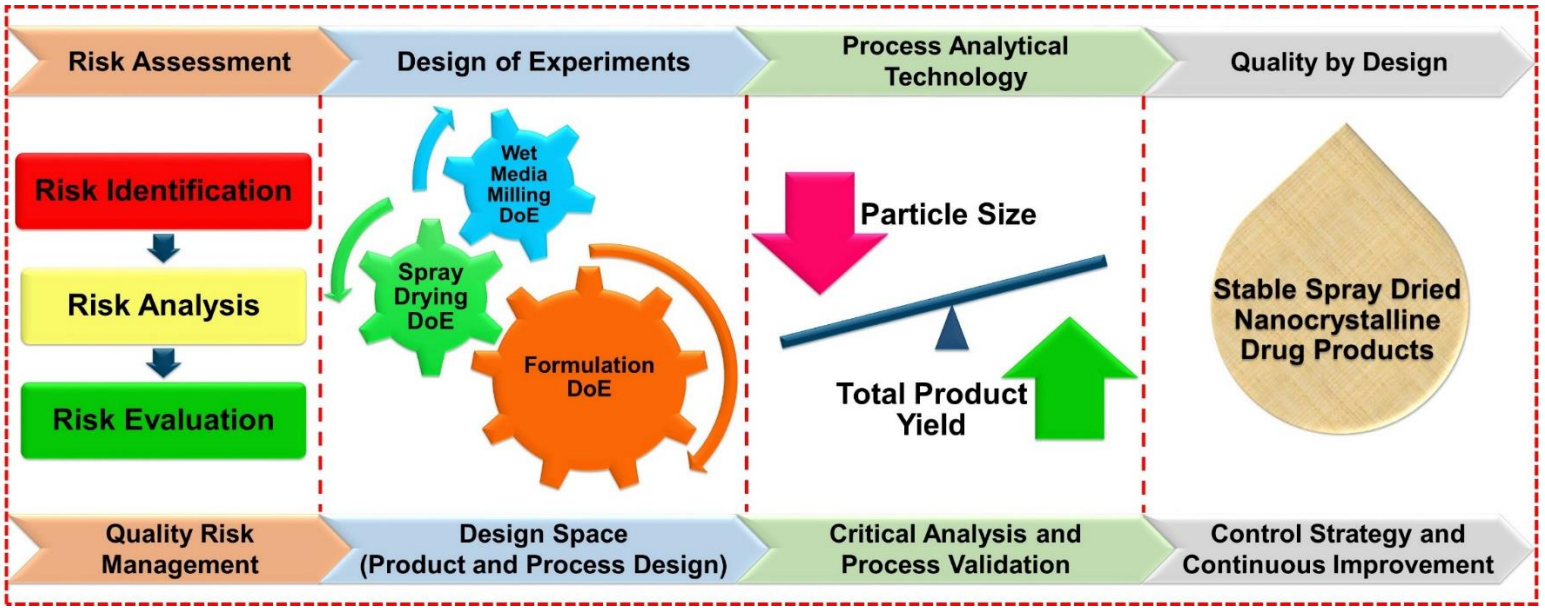

Graphical abstract: Comprehensive QbD process flow for the successful development of the robust nanocrystalline drug products

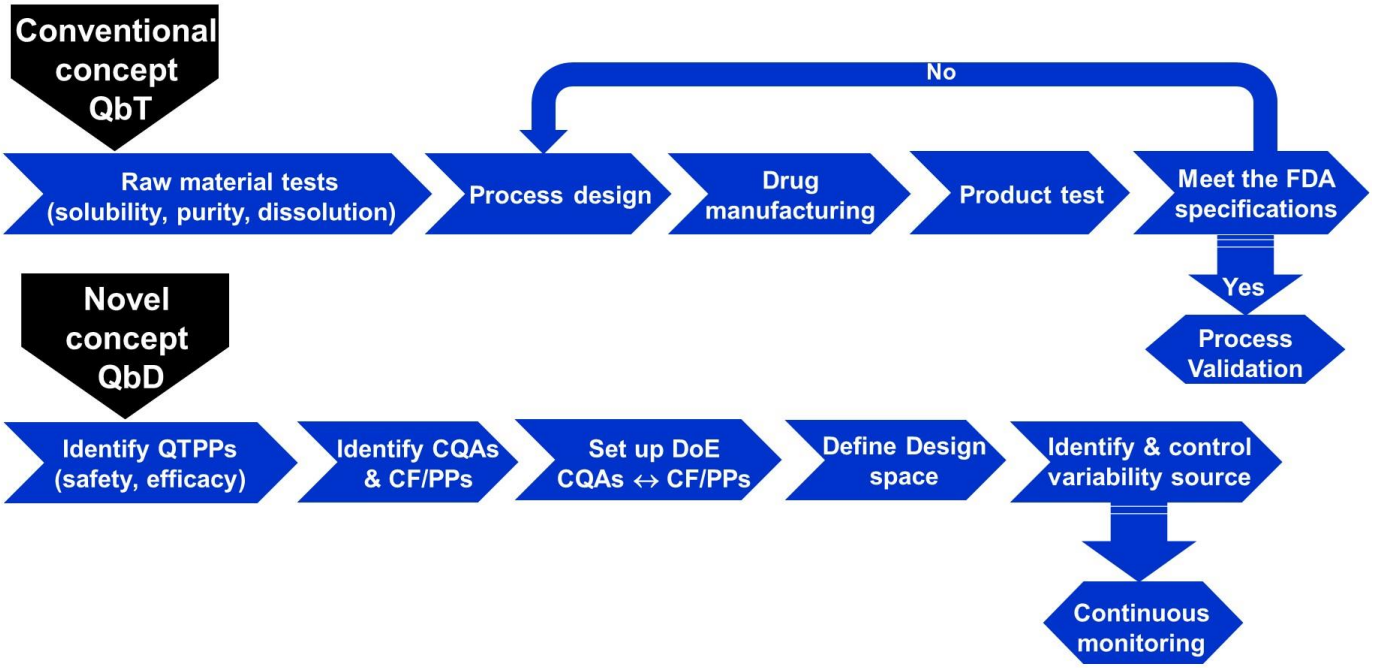

Figure 4.1. Flow diagram comparing conventional QbT (quality by testing) approach *vs.* novel QbD (quality by design) approach.

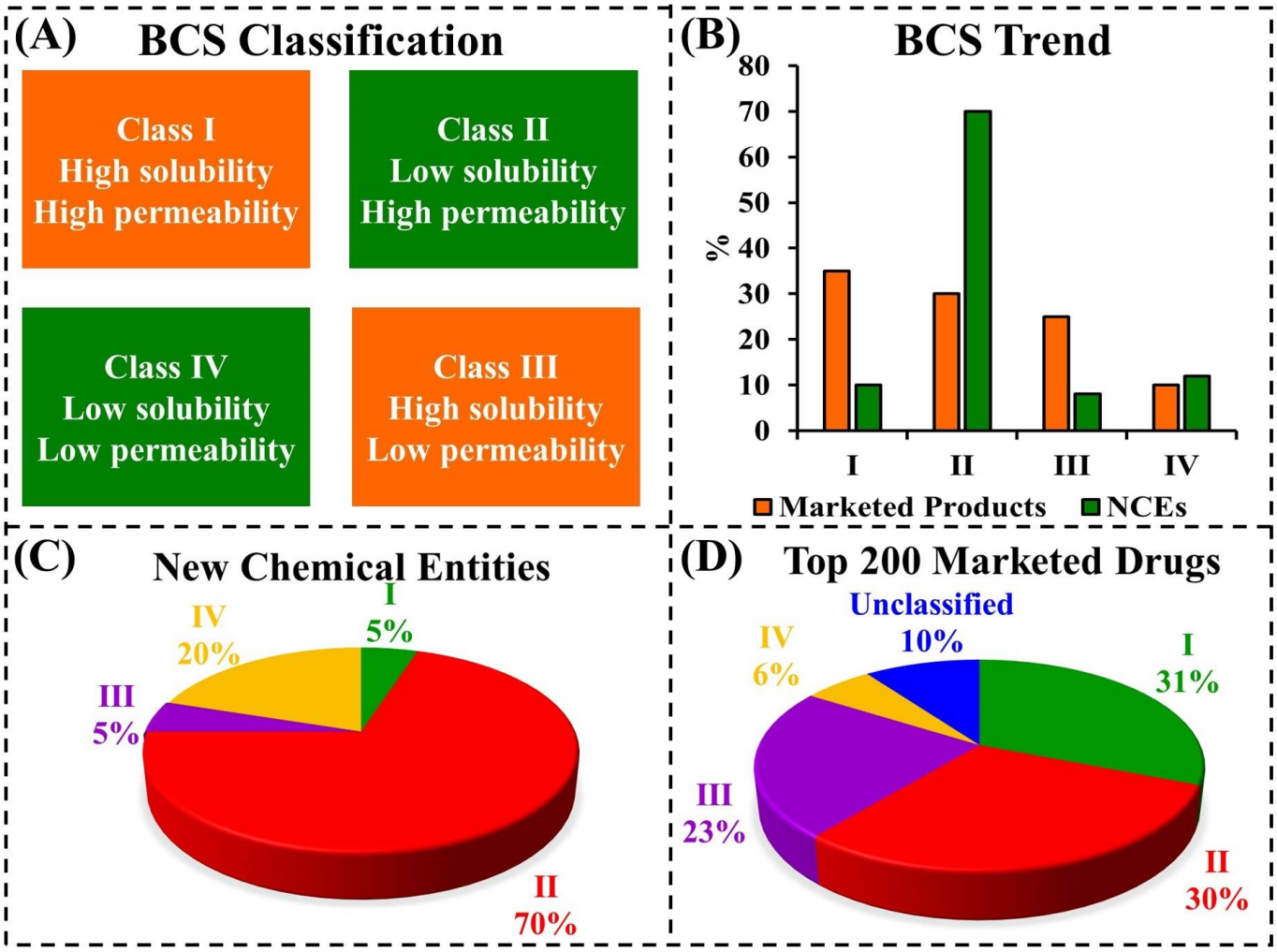

Figure 4.2: (A) Biopharmaceutical classification system (I-IV); (B) Current trend in the BCS; (C) % of the new chemical entities distributed amongst different BCS class (I-IV); (D) Top 200 marketed drugs categorized amongst different BCS class (I-IV).

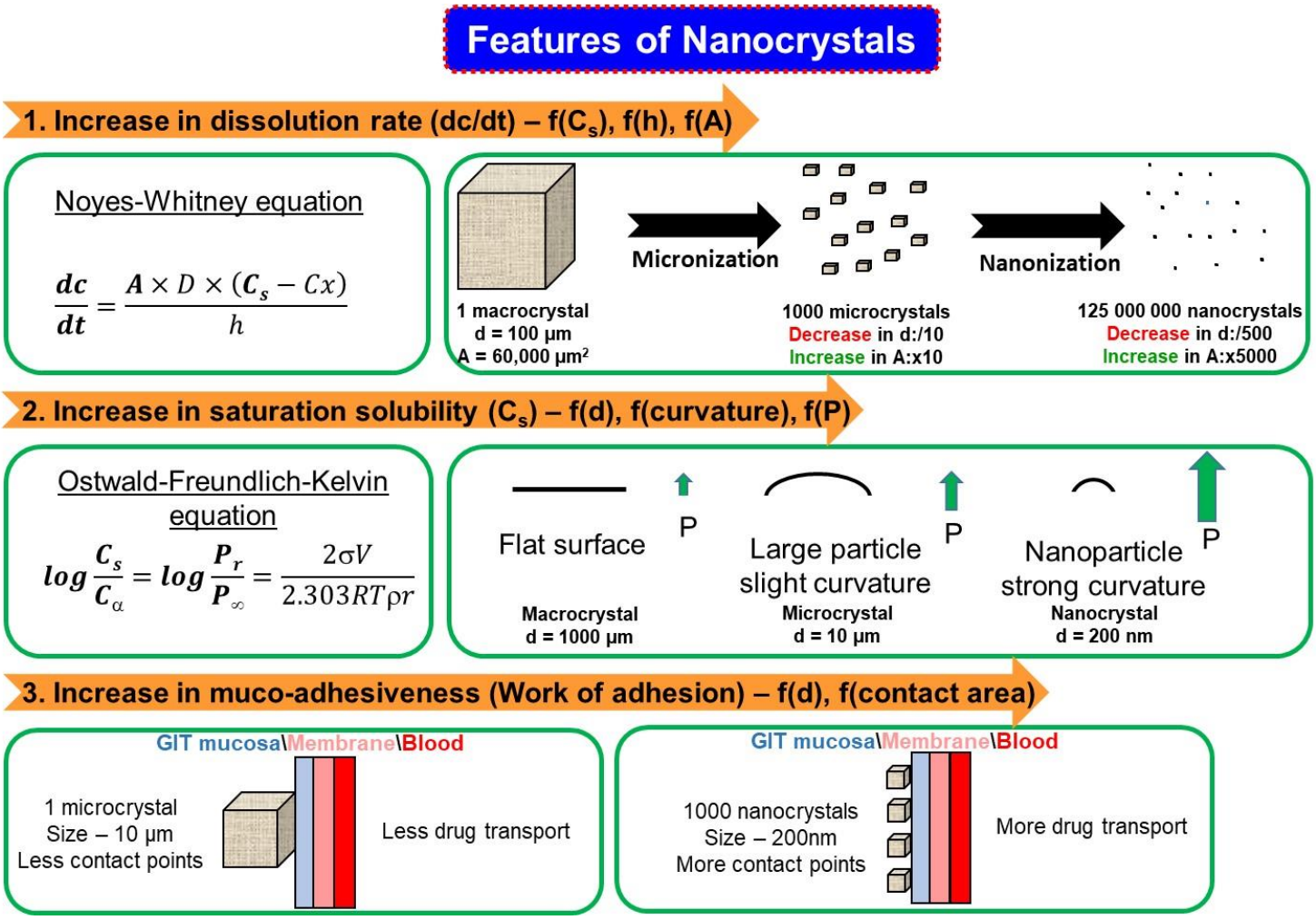

Figure 4.3: Features of nanocrystals: (1) increased dissolution rate (dc/dt) due to increased surface area (A); (2) increased apparent solubility (C_s) due to increased dissolution pressure (P) of strongly curved small nanocrystals; and (3) increased mucoadhesiveness of nanocrystals due to increased contact area of small versus large particles [(f(x)-function of x, D-diffusion coefficient, C_s-saturation solubility of drug, C_x-concentration around the particle/bulk concentration, h-diffusional distance, C_α-solubility of solid consisting of large particles, P_r-dissolution pressure of particle with radius r, P_∞-dissolution pressure of an infinitely large particle, σ-interfacial tension of substance, V-molar volume of the particle material, R-gas constant, T-absolute temperature, ρ-density of the solid, r-radius, d-diameter]

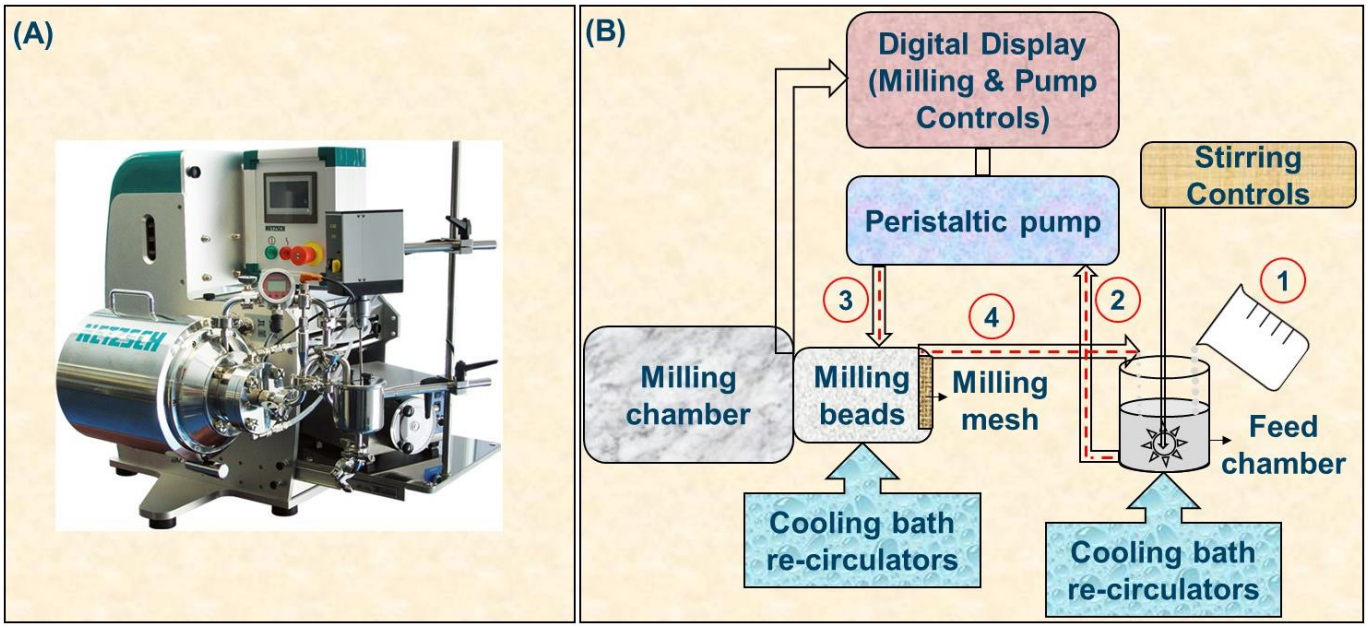

Figure 4.4. (A) Image of Microcer® Netzsch wet media mill **(B)** Schematic representation of wet media milling process: (1) Addition of micro-suspension to feed chamber; (2) Transfer of micro-suspension from feed chamber to peristaltic pump; (3) Transfer of micro-suspension from peristaltic pump to milling chamber in the presence of grinding media (zirconia milling beads – 0.05 mm diameter) for nano-milling; and (4) Transfer of nanosuspension from milling chamber to feed chamber].

(A)

(B)

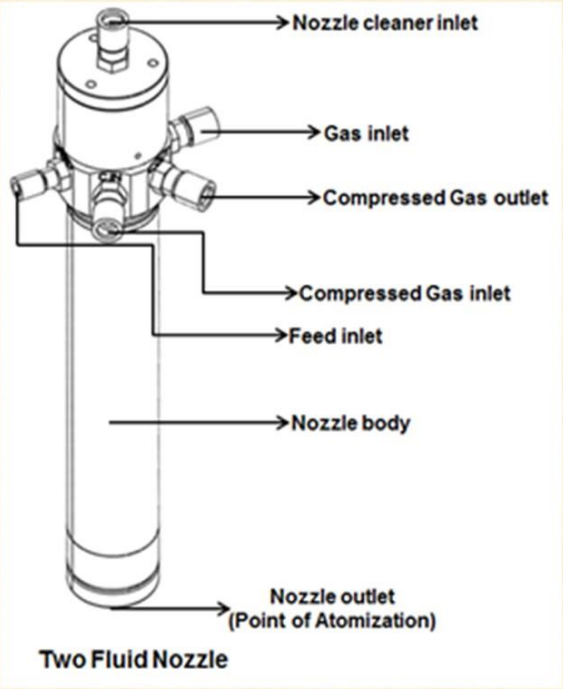

Two Fluid Nozzle

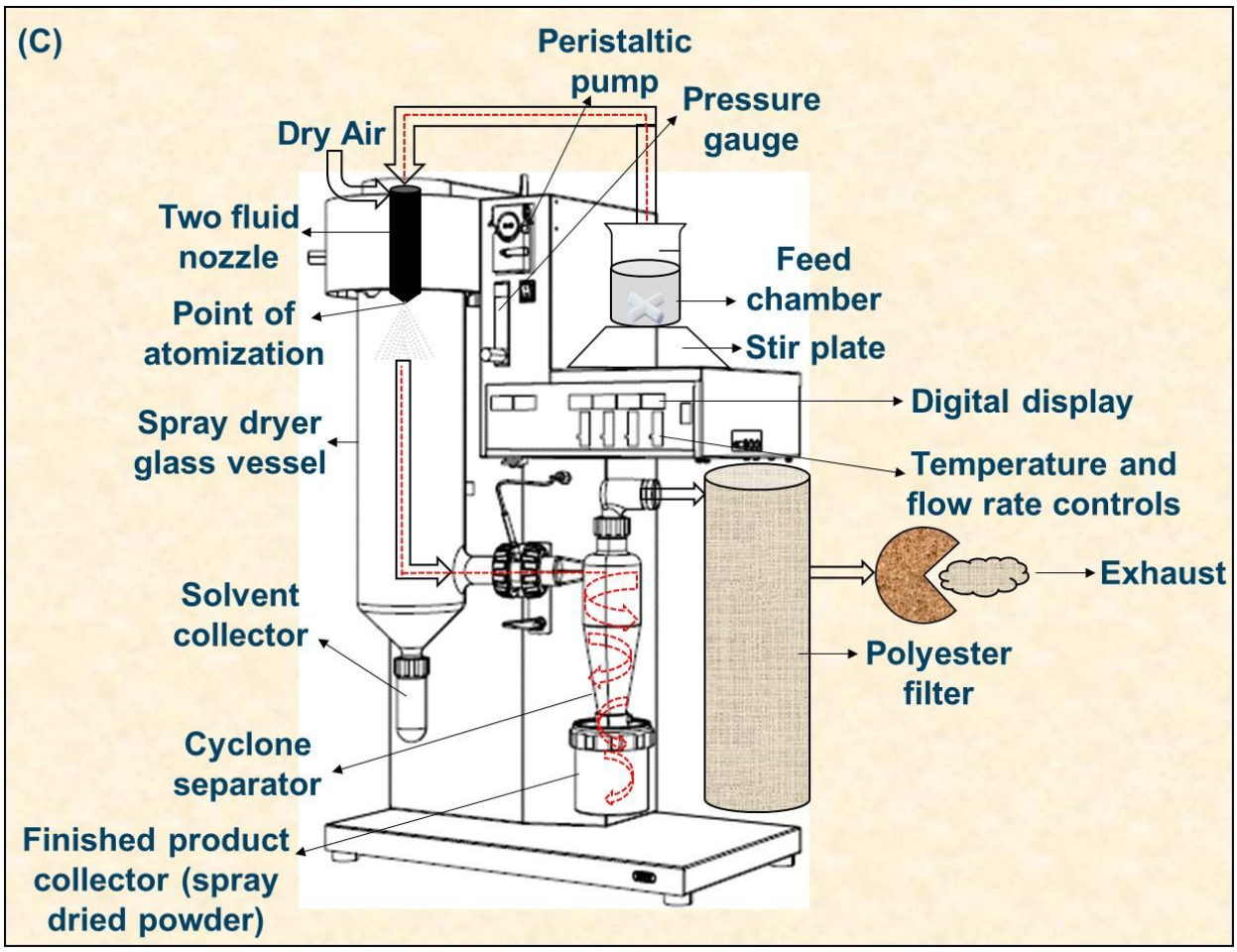

Figure 4.5. (A) Image of Buchi Mini Spray Dryer B-290 **(B)** Two fluid Nozzle (Atomization tool) **(C)** Schematic representation of Buchi Mini Spray Dryer B-290 and particle spray flow pattern (the vertical inverted cone (grey dotted lines) at point of atomization followed by red dotted lines)

(A) Drug product CQAs ↓	Risk Estimation Matrix									
	Milling speed	Milling time	Pump speed	Milling beads size	Milling beads volume	Inlet temperature	Aspirator rate	Feed flow rate	Outlet temperature	Nozzle diameter
Particle size	High	High	Low	High	Medium	High	High	High	High	High
Total yield	Low	Low	Low	High	High	High	High	High	Medium	Medium
Moisture content	Low	Low	Low	Low	Medium	High	High	High	Medium	Medium
Drug loading	Low	Low	Low	High	Medium	High	Medium	High	Medium	Low
Drug release	Low	Low	Low	Low	Low	Low	Low	Low	Low	Low
CFP/CPPs →	Wet Media Milling					Spray drying				
	Process risks									

(B) Drug product CQAs ↓	Risk Estimation Matrix				
	Conc. of drug	Conc. of polymer	Conc. of surfactant	Conc. of sugar	Water
Particle size	High	High	Medium	High	Medium
Total yield	High	High	Low	High	Medium
Moisture content	Low	Low	Medium	Low	High
Drug loading	High	Low	Low	Low	Medium
Drug release	High	High	High	High	Medium
CFP/CPPs →	Formulation risks				

High risk parameter
Medium risk parameter
Low risk parameter

Figure 4.6a. Risk estimation matrix for **(A)** process risks and **(B)** formulation risks

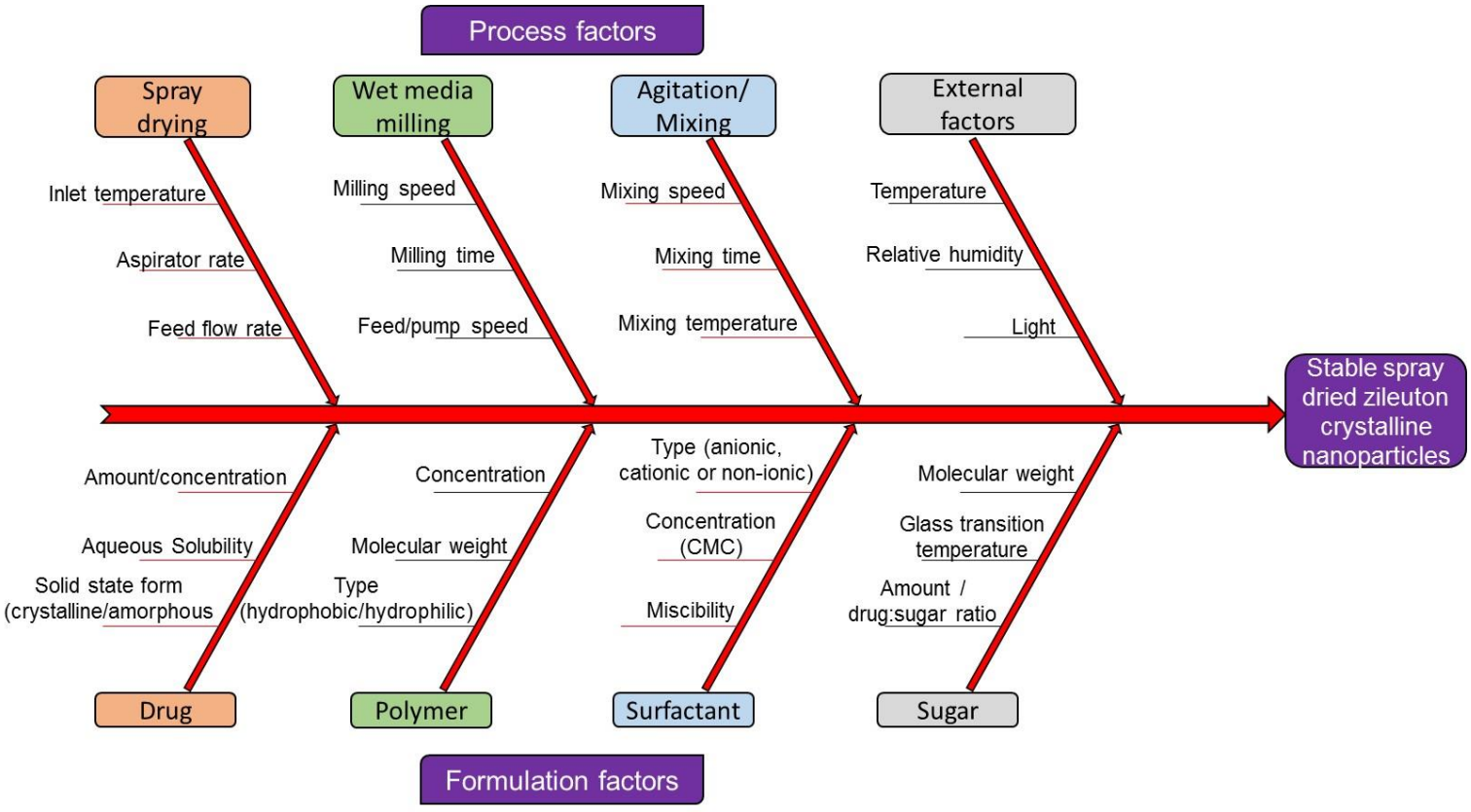

Figure 4.6b. Ishikawa/Fishbone diagram for preparation of stable spray-dried nanocrystalline zileuton (risk assessment tool)

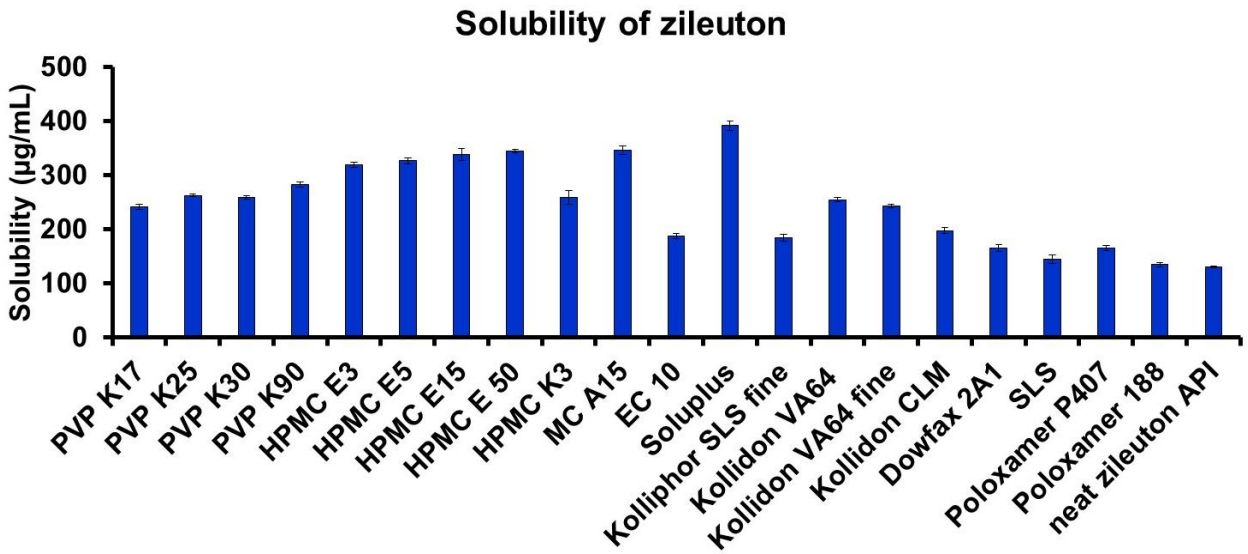

Figure 4.7. Bar chart displaying solubility of zileuton in different excipients

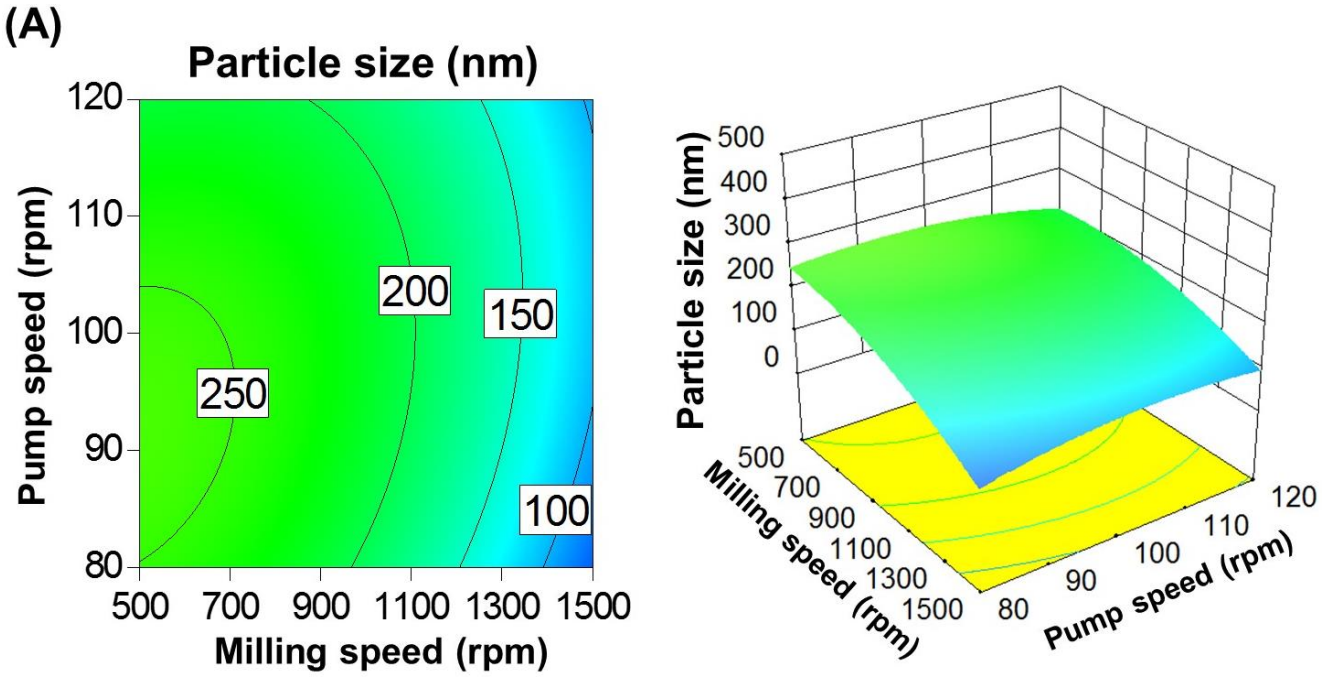

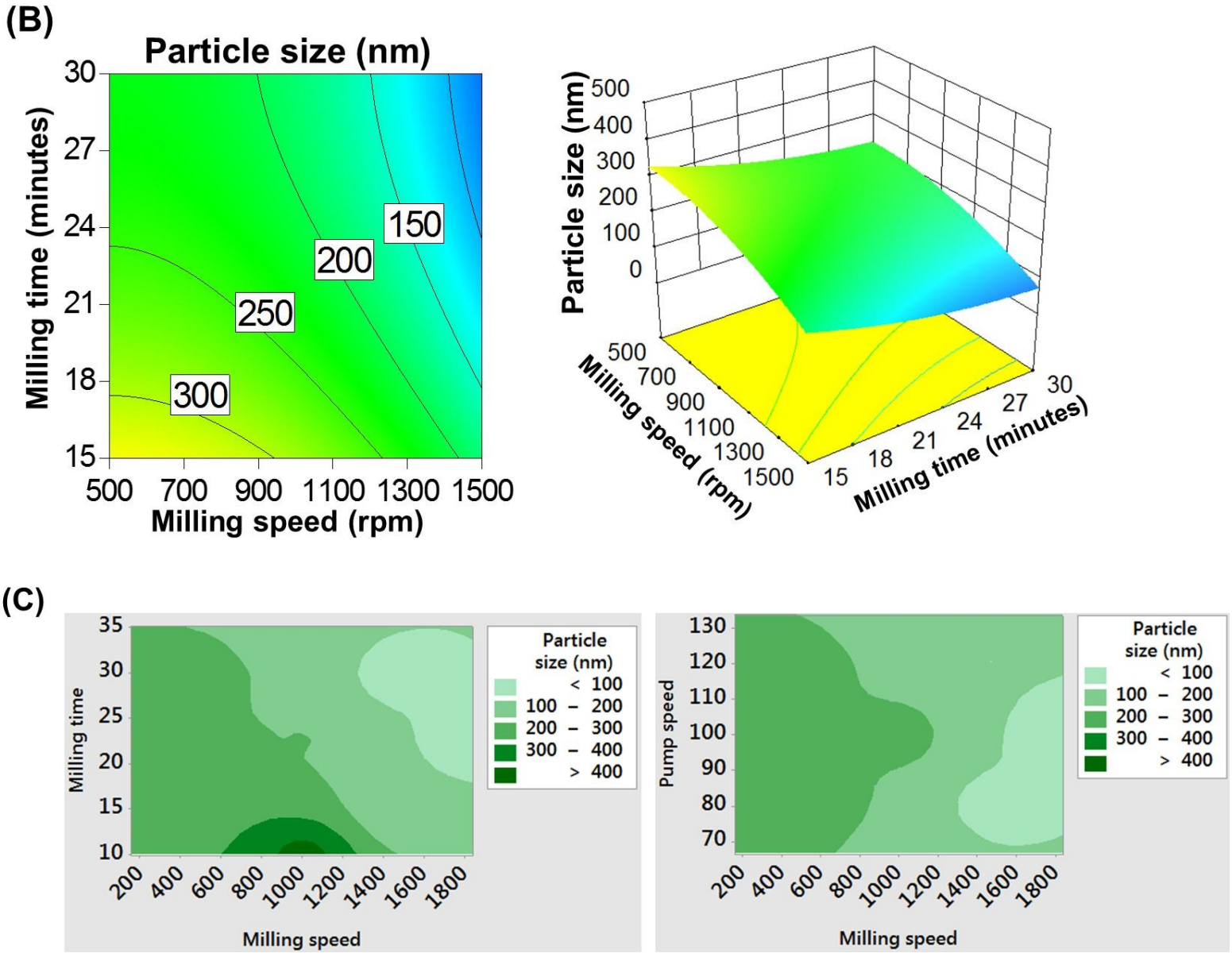

Figure 4.8. Contour plots and 3D surface plots for CQA: particle size comparing: (A) effect of milling speed and pump speed on the particle size; (B) effect of milling time and milling speed on the particle size; and (C) comparative surface plots: milling speed *vs.* milling time (left) and milling speed *vs.* pump speed (right).

(A)

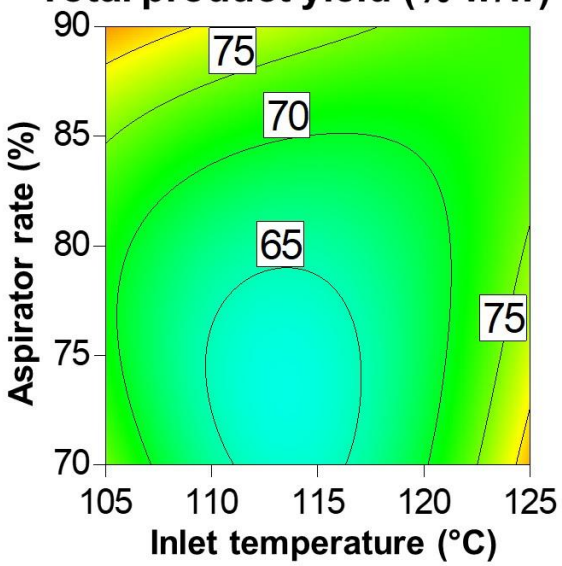
Total product yield (% w/w)
Aspirator rate (%)
Inlet temperature (°C)
90
85
80
75
70
105
110
115
120
125
75
70
65
75

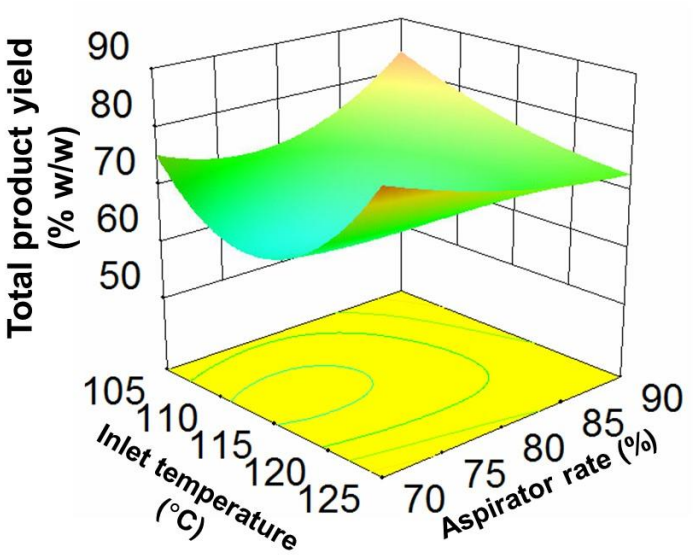
Total product yield (% w/w)
90
80
70
60
50
105
110
115
120
125
Inlet temperature (°C)
70
75
80
85
90
Aspirator rate (%)

(B)

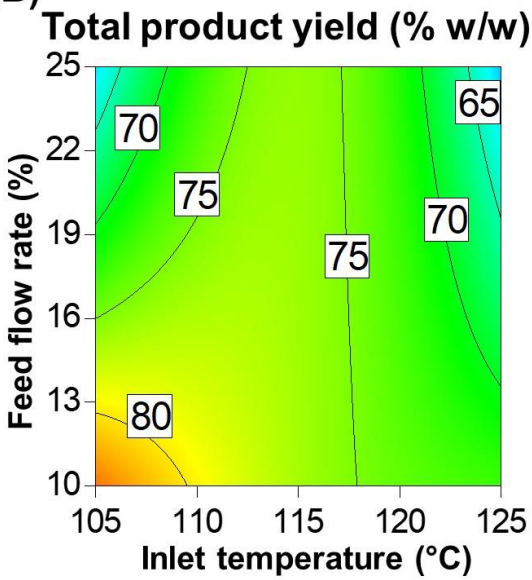
Total product yield (% w/w)
Feed flow rate (%)
Inlet temperature (°C)
25
22
19
16
13
10
105
110
115
120
125
70
75
65
70
75
80

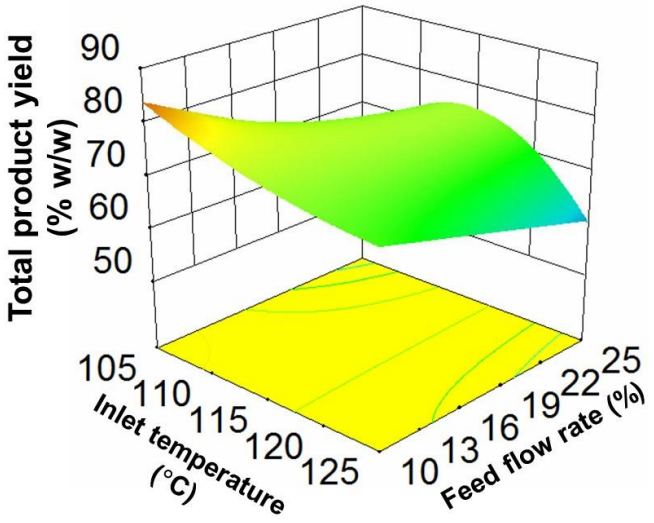
Total product yield (% w/w)
90
80
70
60
50
105
110
115
120
125
Inlet temperature (°C)
10
13
16
19
22
25
Feed flow rate (%)

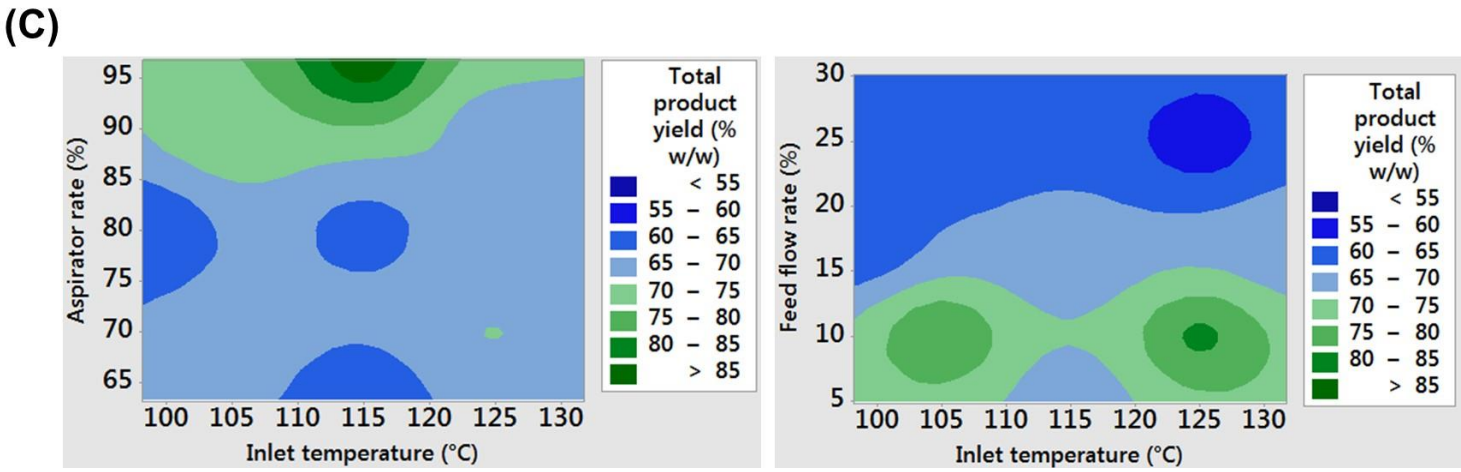

Figure 4.9. Contour plots and 3D surface plots for CQA: total product yield of spray-dried nanocrystalline zileuton (stabilizer: mannitol) comparing: (A) effect of inlet temperature and aspirator rate on the total product yield; (B) effect of inlet temperature and feed flow rate on the total product yield; and (C) comparative surface plots: inlet temperature *vs.* aspirator rate (left) and inlet temperature *vs.* feed flow rate (right)

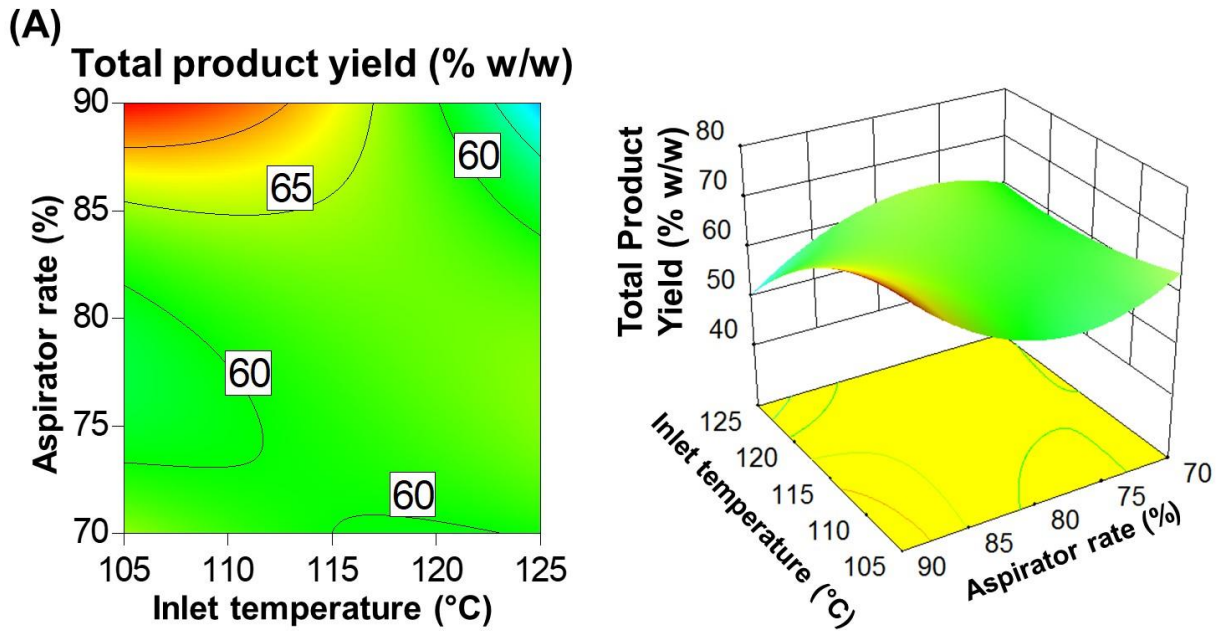

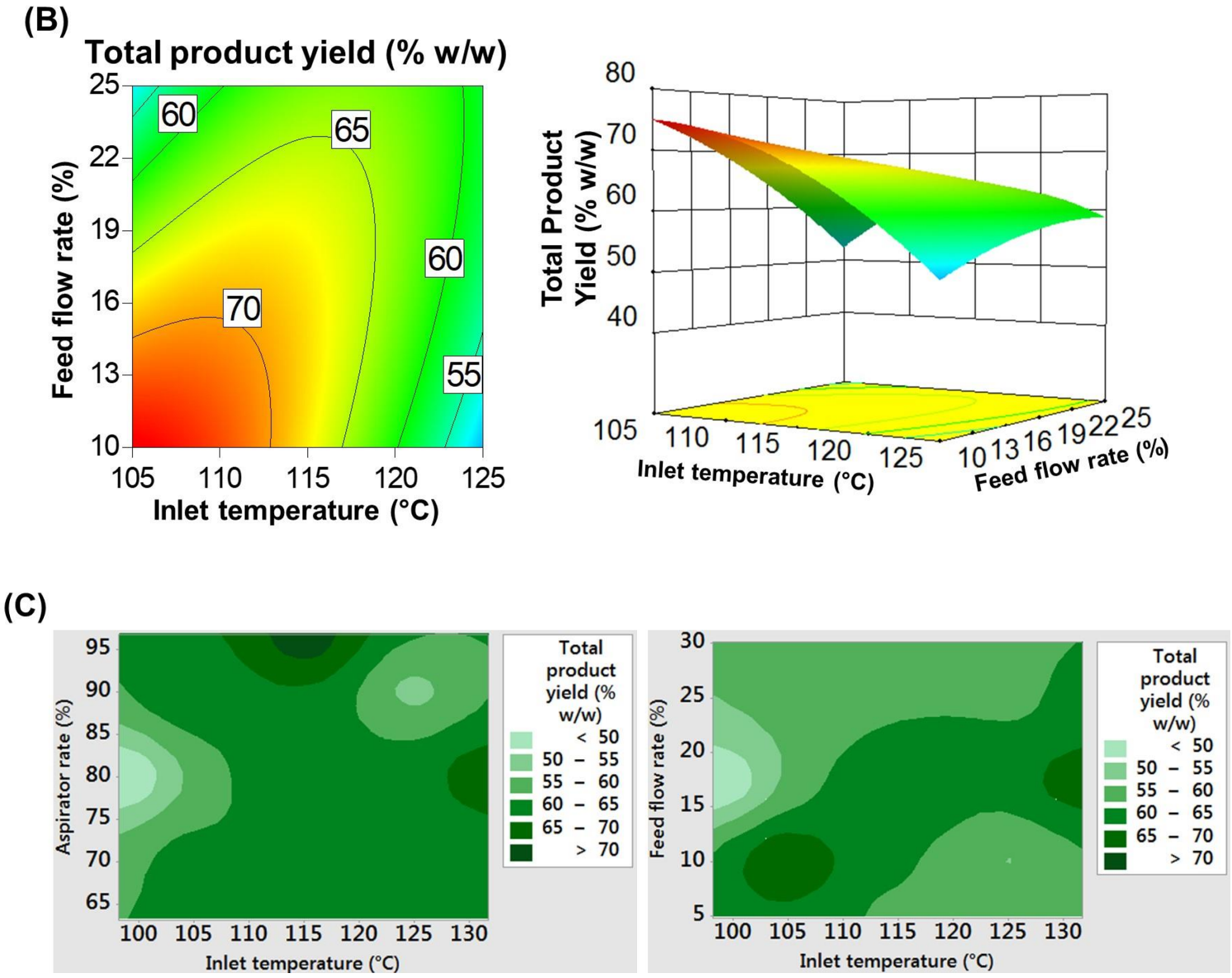

Figure 4.10. Contour plots and 3D surface plots for CQA: total product yield of spray-dried nanocrystalline zileuton (stabilizer: trehalose) comparing: (A) effect of inlet temperature and aspirator rate on the total product yield; (B) effect of inlet temperature and feed flow rate on the total product yield; and (C) comparative surface plots: inlet temperature *vs.* aspirator rate (left) and inlet temperature *vs.* feed flow rate (right)

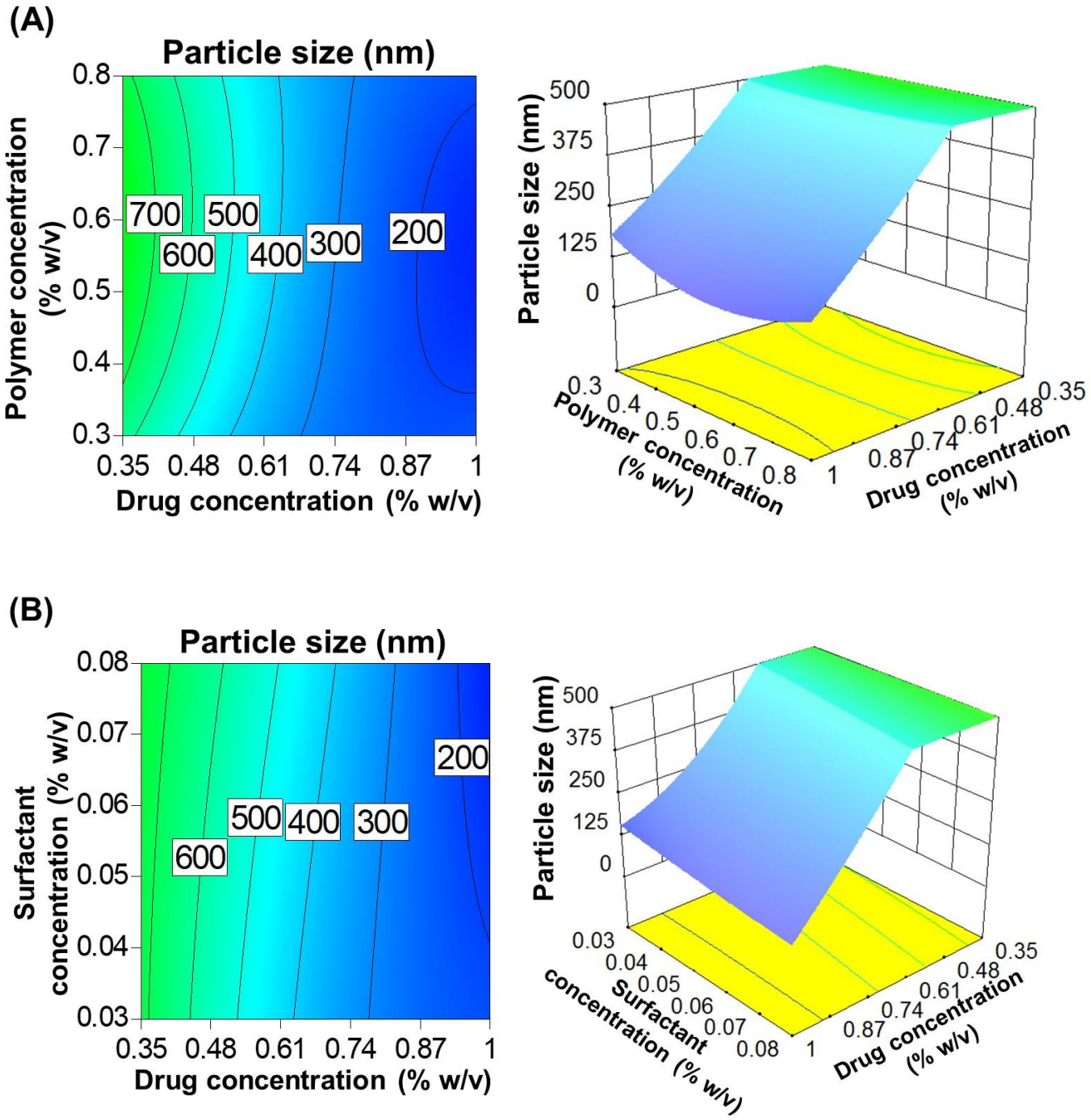
(A)
Particle size (nm)
Polymer concentration (% w/v)
Drug concentration (% w/v)
700
600
500
400
300
200
Particle size (nm)
Polymer concentration (% w/v)
Drug concentration (% w/v)
(B)
Particle size (nm)
Surfactant concentration (% w/v)
Drug concentration (% w/v)
Particle size (nm)
Surfactant concentration (% w/v)
Drug concentration (% w/v)

(C)

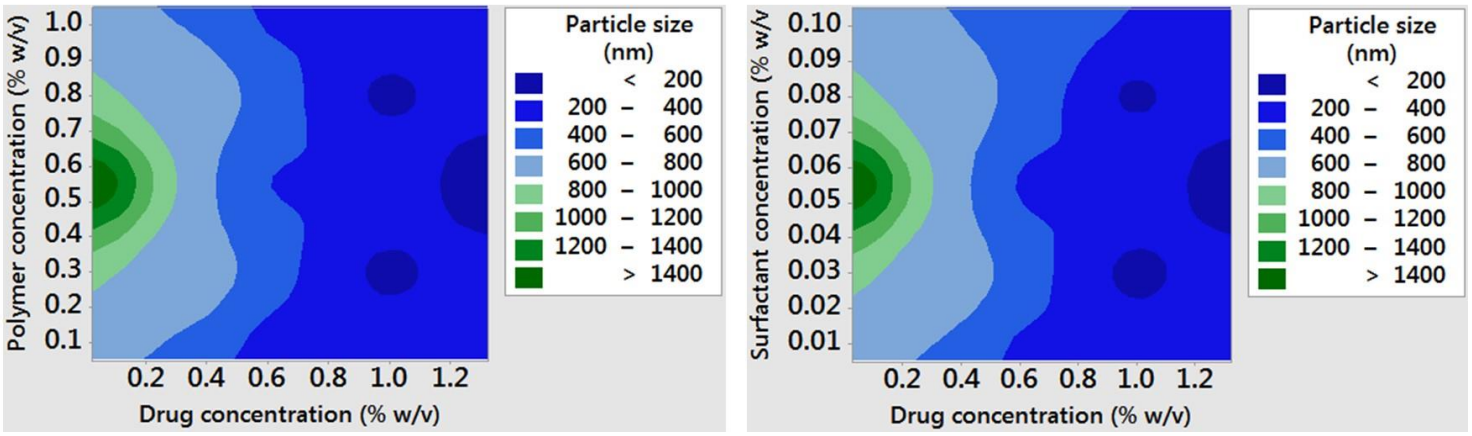

Figure 4.11. Contour plots and 3D surface plots for CQA: particle size comparing: (A) effect of drug concentration and polymer concentration on the particle size; (B) effect of drug concentration and surfactant concentration on the particle size; and (C) comparative surface plots: drug concentration *vs.* polymer concentration (left) and drug concentration *vs* surfactant concentration (right)

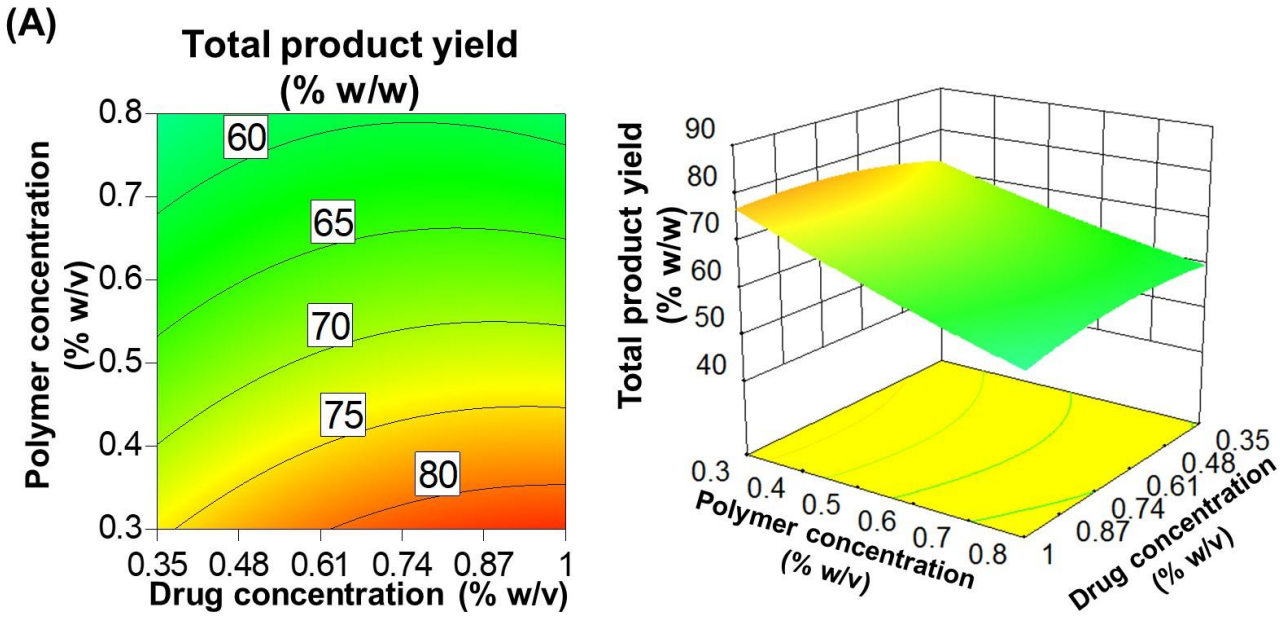

(B)

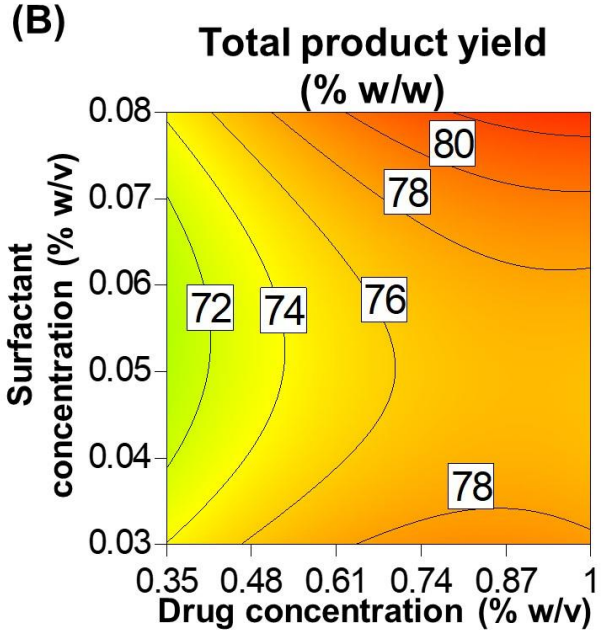
Total product yield
(% w/w)
Surfactant concentration (% w/v)
Drug concentration (% w/v)
0.08
0.07
0.06
0.05
0.04
0.03
0.35 0.48 0.61 0.74 0.87 1
80
78
76
74
72
78

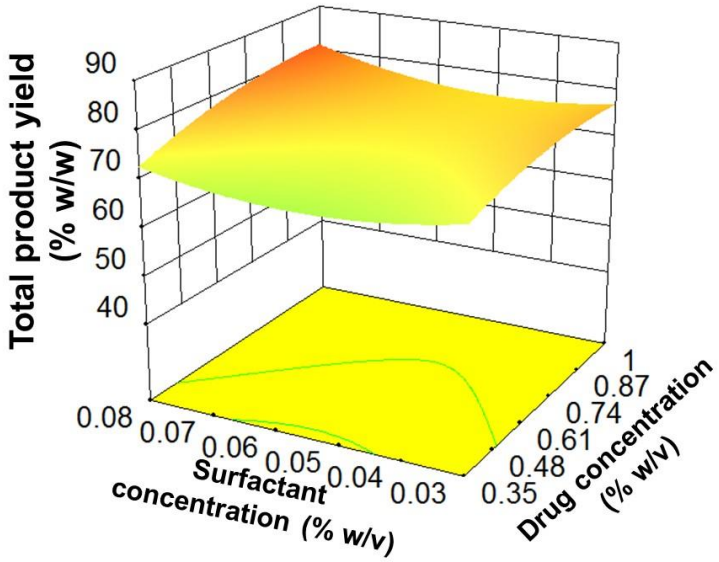
Total product yield
(% w/w)
90
80
70
60
50
40
Surfactant concentration (% w/v)
0.08 0.07 0.06 0.05 0.04 0.03
Drug concentration (% w/v)
0.35 0.48 0.61 0.74 0.87 1

(C)

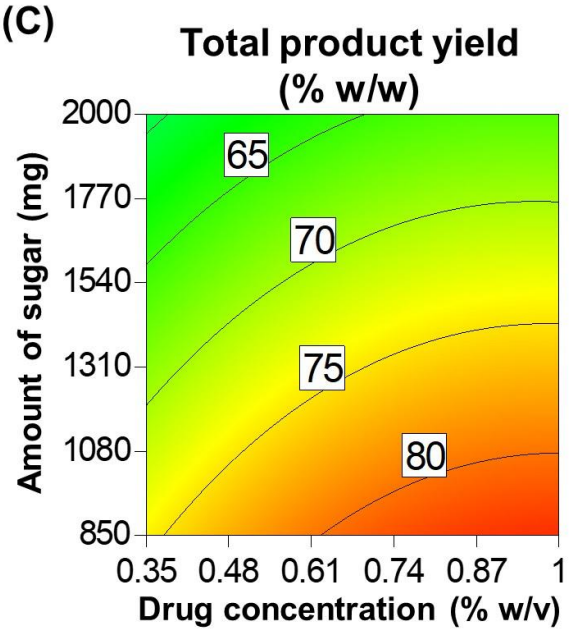
Total product yield
(% w/w)
Amount of sugar (mg)
Drug concentration (% w/v)
2000
1770
1540
1310
1080
850
0.35 0.48 0.61 0.74 0.87 1
65
70
75
80

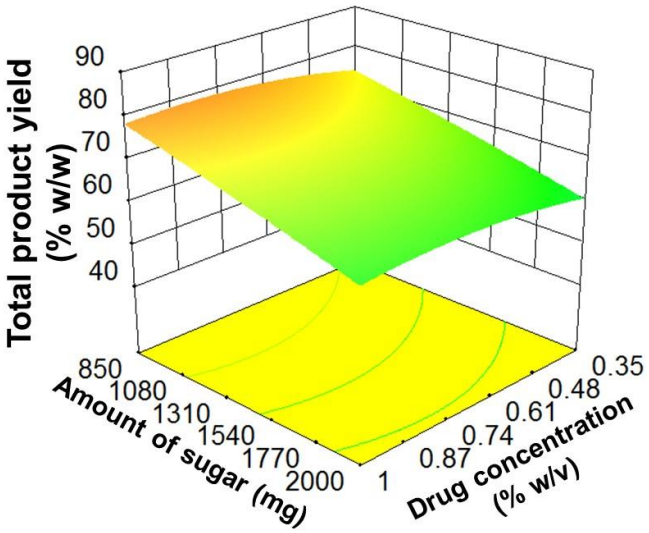
Total product yield
(% w/w)
90
80
70
60
50
40
Amount of sugar (mg)
850 1080 1310 1540 1770 2000
Drug concentration (% w/v)
1 0.87 0.74 0.61 0.48 0.35

(D)

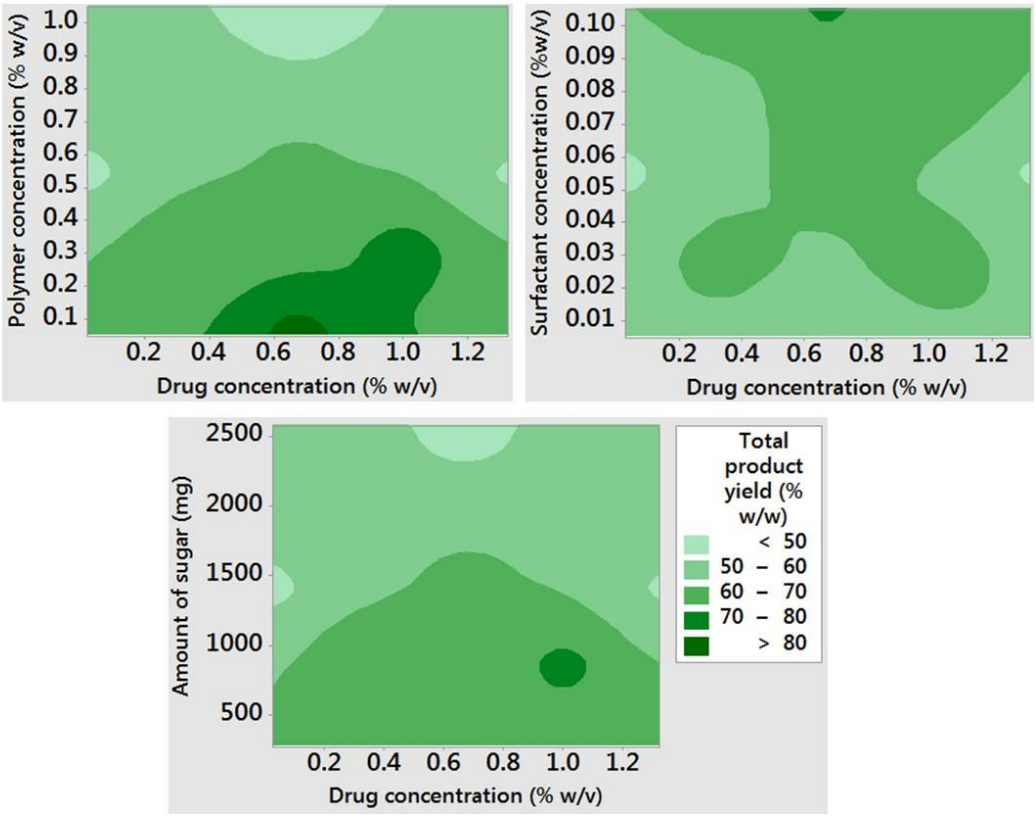

Figure 4.12. Contour plots and 3D surface plots for CQA: total product yield of spray-dried nanocrystalline zileuton (stabilizer:trehalose) comparing: (A) effect of drug concentration and polymer concentration on the total product yield; (B) effect of drug concentration and surfactant concentration on the total product yield; (C) effect of drug concentration and amount of sugar on the total product yield; and (D) comparative surface plots: drug concentration *vs.* polymer concentration (top left); drug concentration *vs.* surfactant concentration (top right) and; drug concentration *vs.* amount of sugar (bottom center)

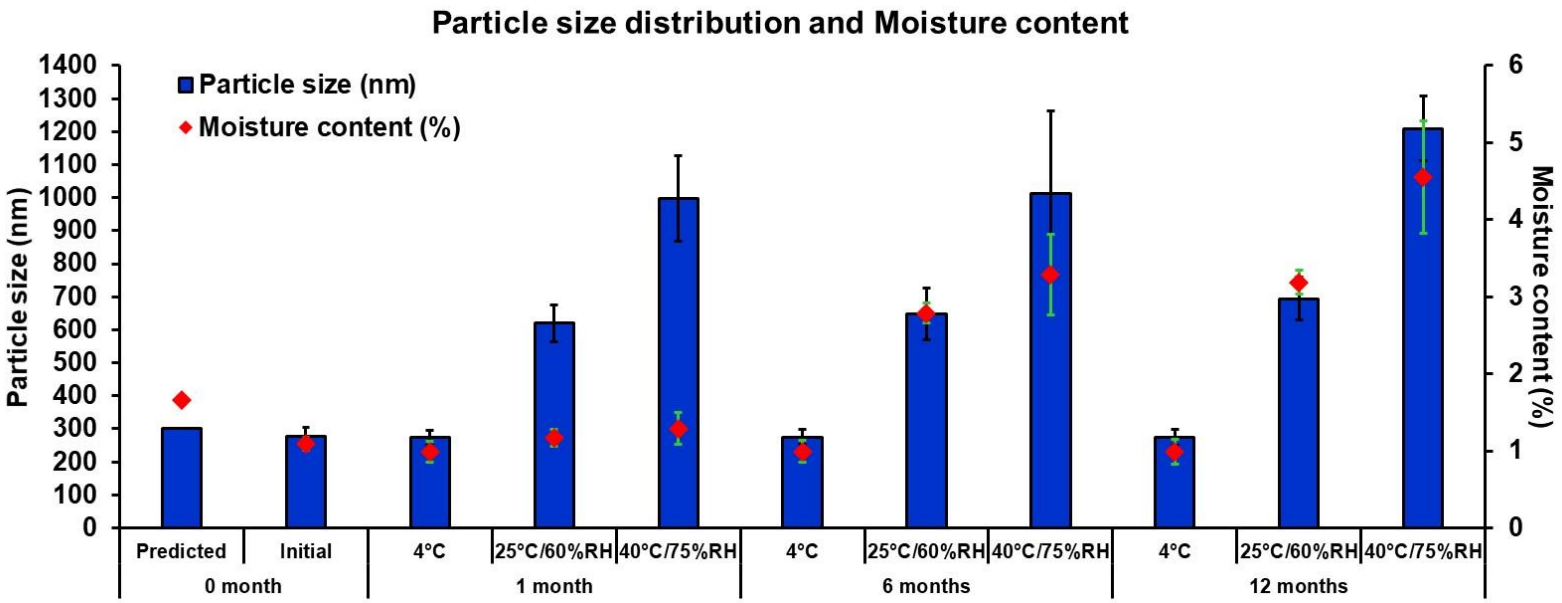

Figure 4.13. Particle size distribution and moisture content of the optimized spray-dried nanocrystalline zileuton formulations stored for 1, 6 and 12 month/s at: (a) 4°C; (b) 25°C/60% RH; and (c) 40°C/75% RH compared with zero month formulations.

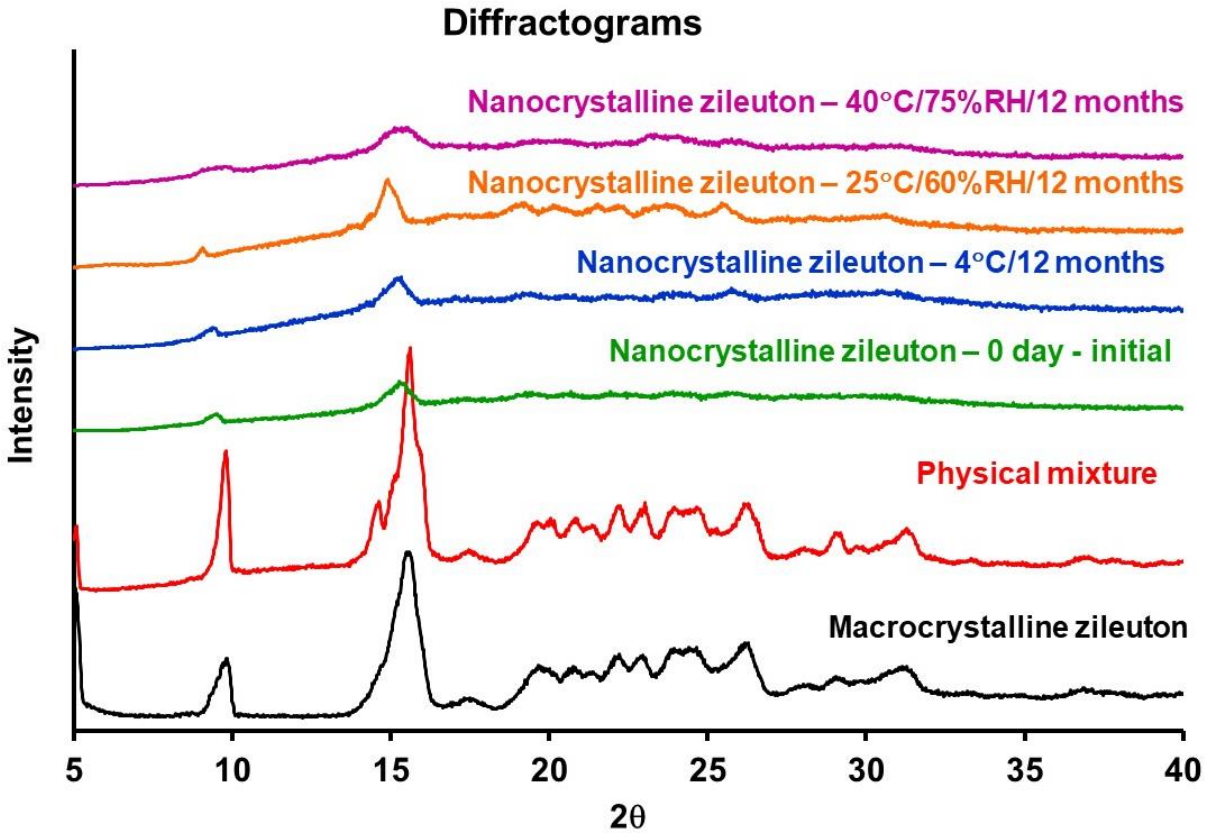

Figure 4.14. PXRD diffraction profiles of the neat macrocrystalline zileuton (raw crystalline drug), physical mixture of the drug (zileuton), polymer (KollidonVA64 fine), surfactant (Dowfax2A1) and sugar (trehalose) and the optimized spray-dried nanocrystalline zileuton formulation (initial and formulations stored for 12 months at 4°C, 25°C/60% RH and 40°C/75% RH)

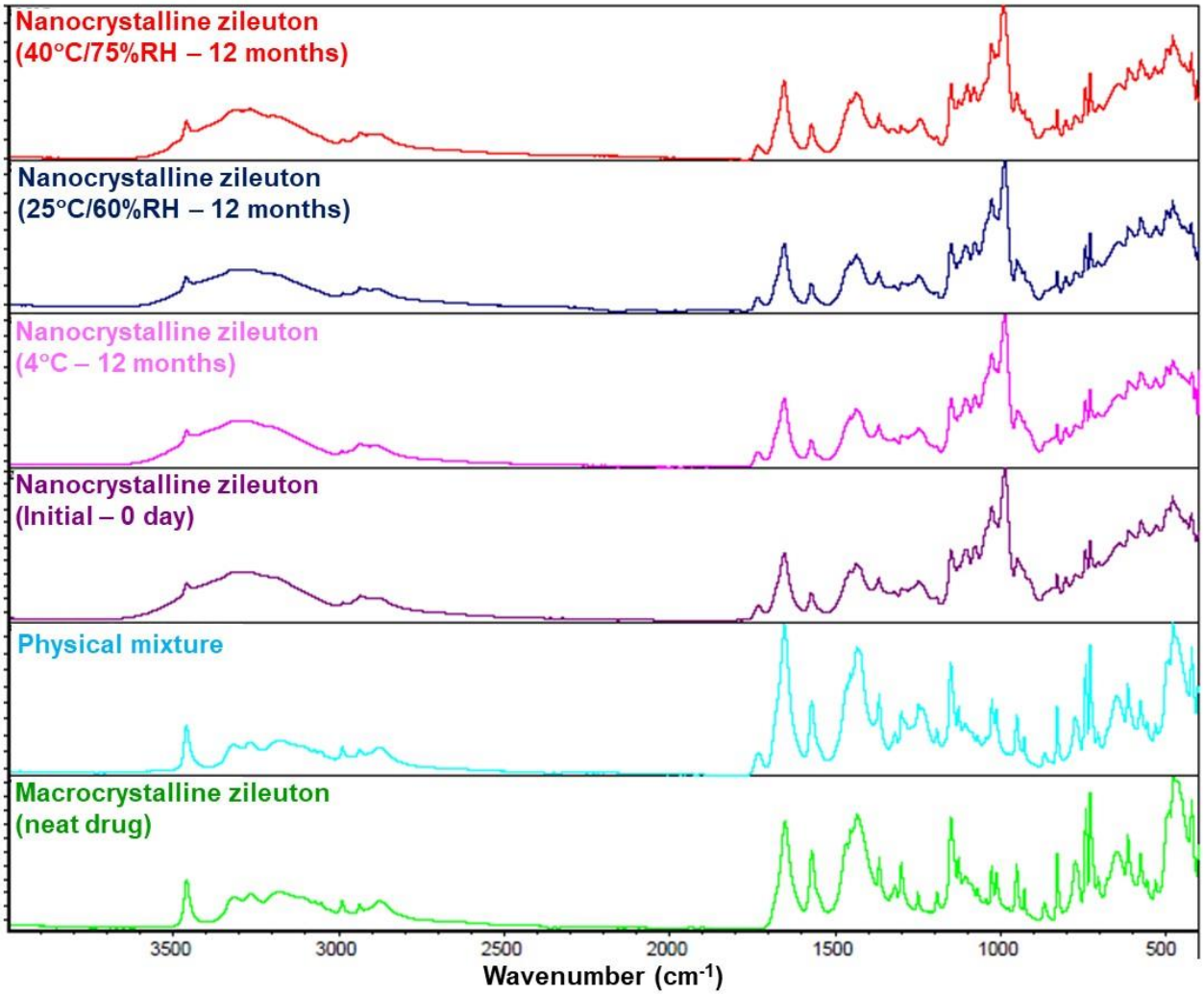

Figure 4.15a. ATR-FTIR full spectra overlay of the neat macrocrystalline zileuton (raw crystalline drug), physical mixture of the drug (zileuton), polymer (KollidonVA64 fine), surfactant (Dowfax2A1) and sugar (trehalose) and the optimized spray-dried nanocrystalline zileuton formulations (at day zero and those stored for 12 months at 4°C, 25°C/60% RH and 40°C/75% RH)

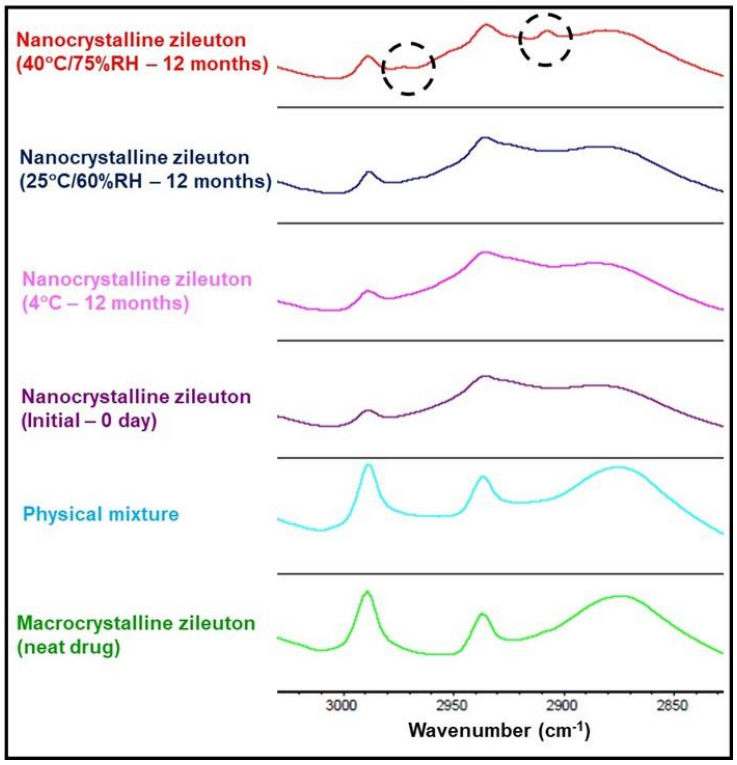

Figure 4.15b. ATR-FTIR spectra (3000-2850 cm^{-1}) overlay of the neat macrocrystalline zileuton (raw crystalline drug), physical mixture of the drug (zileuton), polymer (KollidonVA64 fine), surfactant (Dowfax2A1) and sugar (trehalose) and the optimized spray-dried nanocrystalline zileuton formulations (at day zero and those stored for 12 months at 4°C, 25°C/60% RH and 40°C/75% RH)

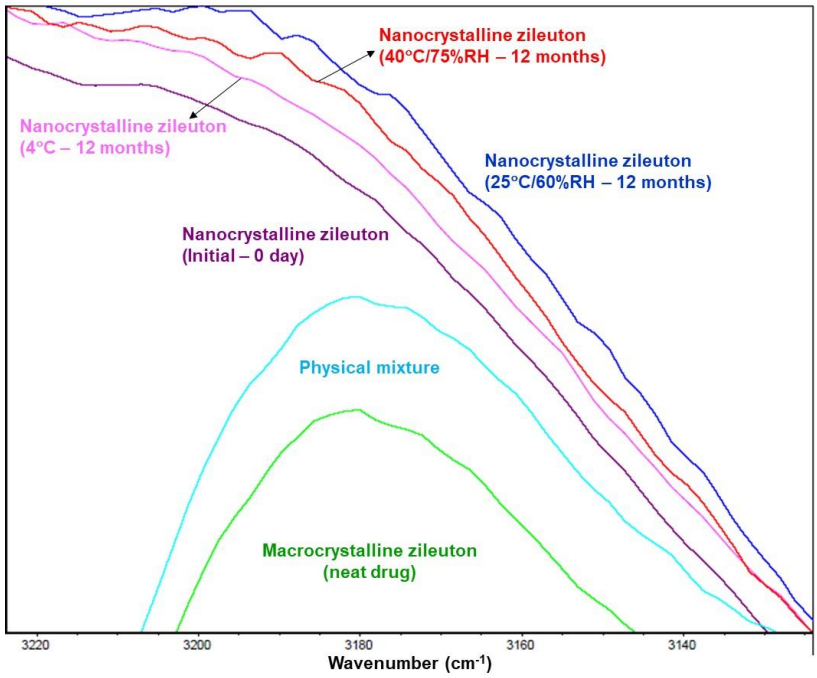

Figure 4.15c. ATR-FTIR spectra (3220-3140 cm^{-1}) overlay of the neat macrocrystalline zileuton (raw crystalline drug), physical mixture of the drug (zileuton), polymer (KollidonVA64 fine), surfactant (Dowfax2A1) and sugar (trehalose) and the optimized spray-dried nanocrystalline zileuton formulations (at day zero and those stored for 12 months at 4°C, 25°C/60% RH and 40°C/75% RH).

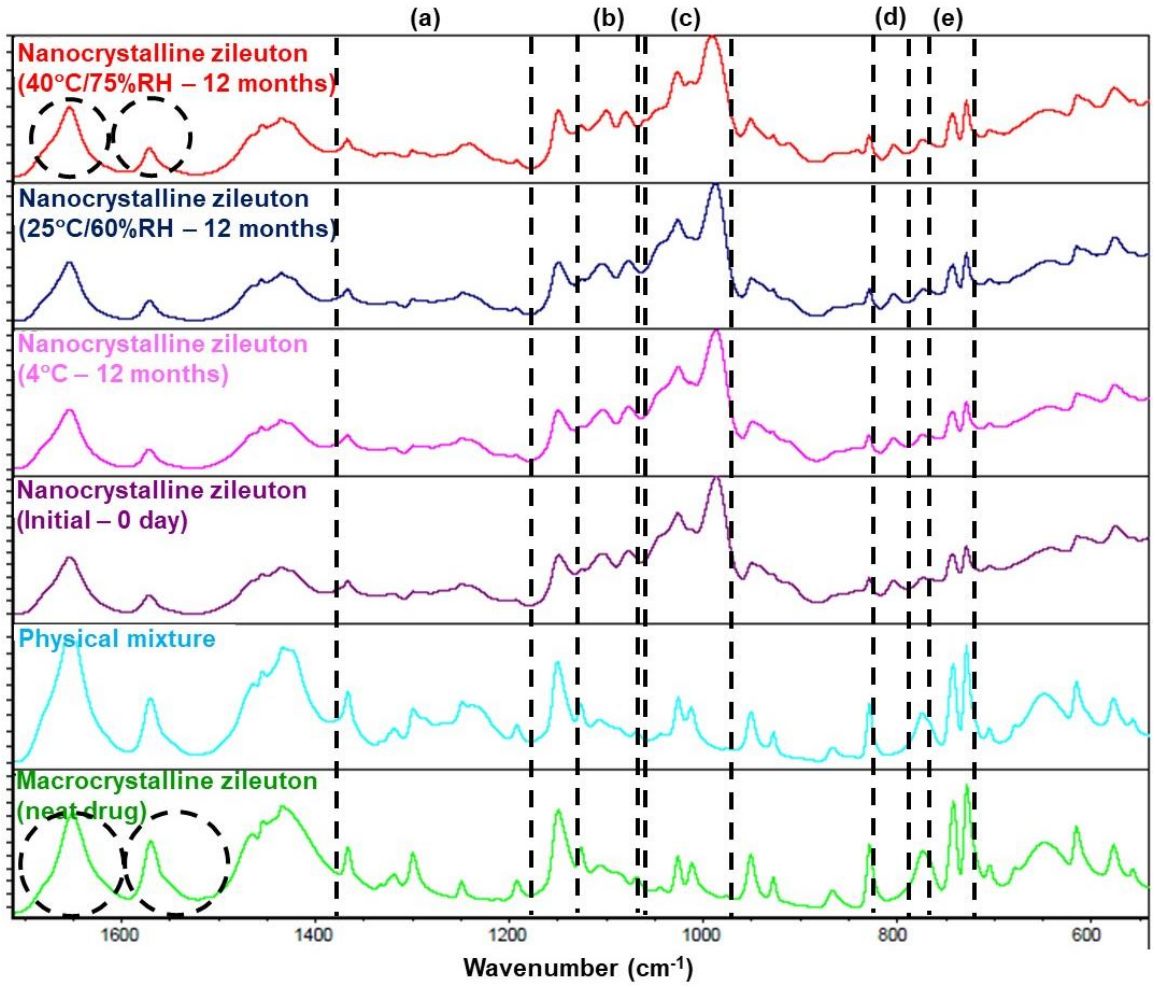

Figure 4.15d. ATR-FTIR spectra (1700-550 cm^{-1}) overlay of the macrocrystalline zileuton (neat drug), physical mixture (zileuton, KollidonVA64 fine, Dowfax2A1 and trehalose) and the optimized spray-dried nanocrystalline zileuton formulations (at day zero and those stored for 12 months at 4°C, 25°C/60% RH and 40°C/75% RH).

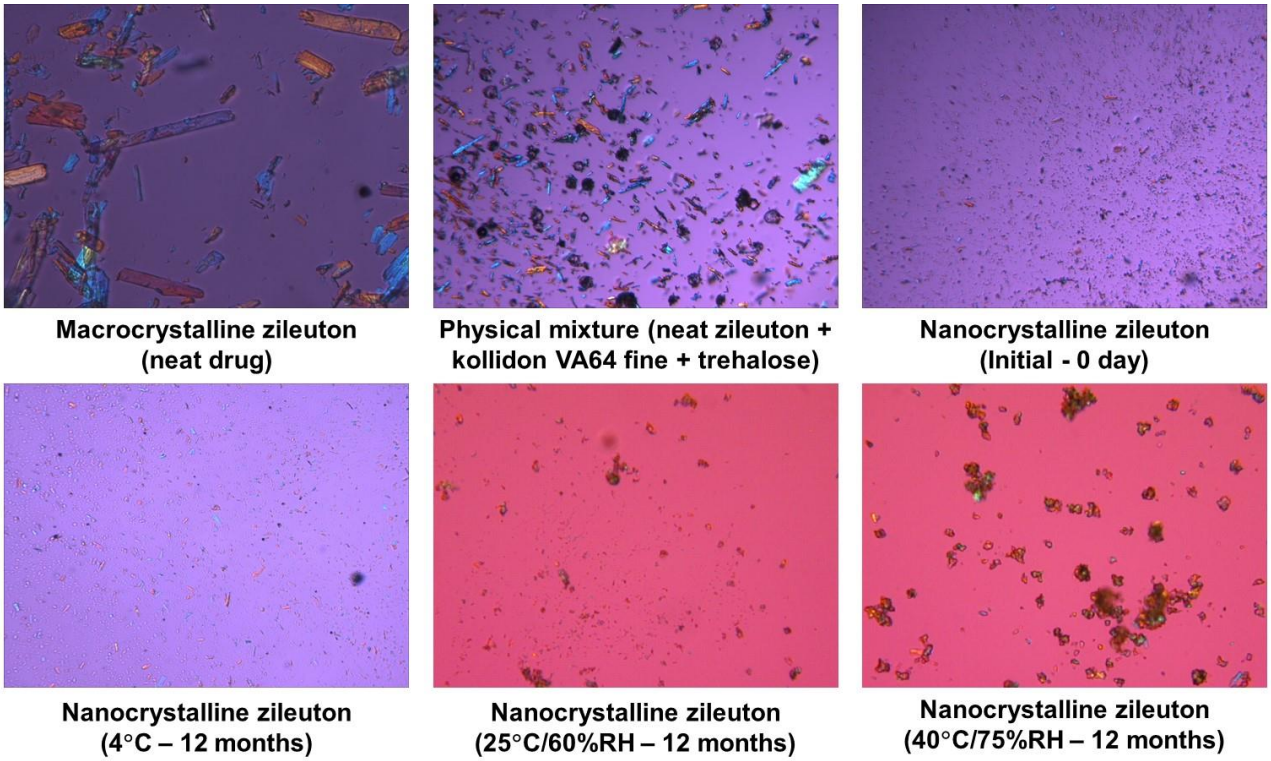

Figure 4.16. PLM images of the neat macrocrystalline zileuton (raw crystalline drug), physical mixture (zileuton, KollidonVA64 fine, Dowfax2A1 and trehalose) and the optimized spray-dried nanocrystalline zileuton formulations (day zero and those stored for 12 months at 4°C, 25°C/60% RH and 40°C/75% RH). **Note**: All images are of 10X magnification.

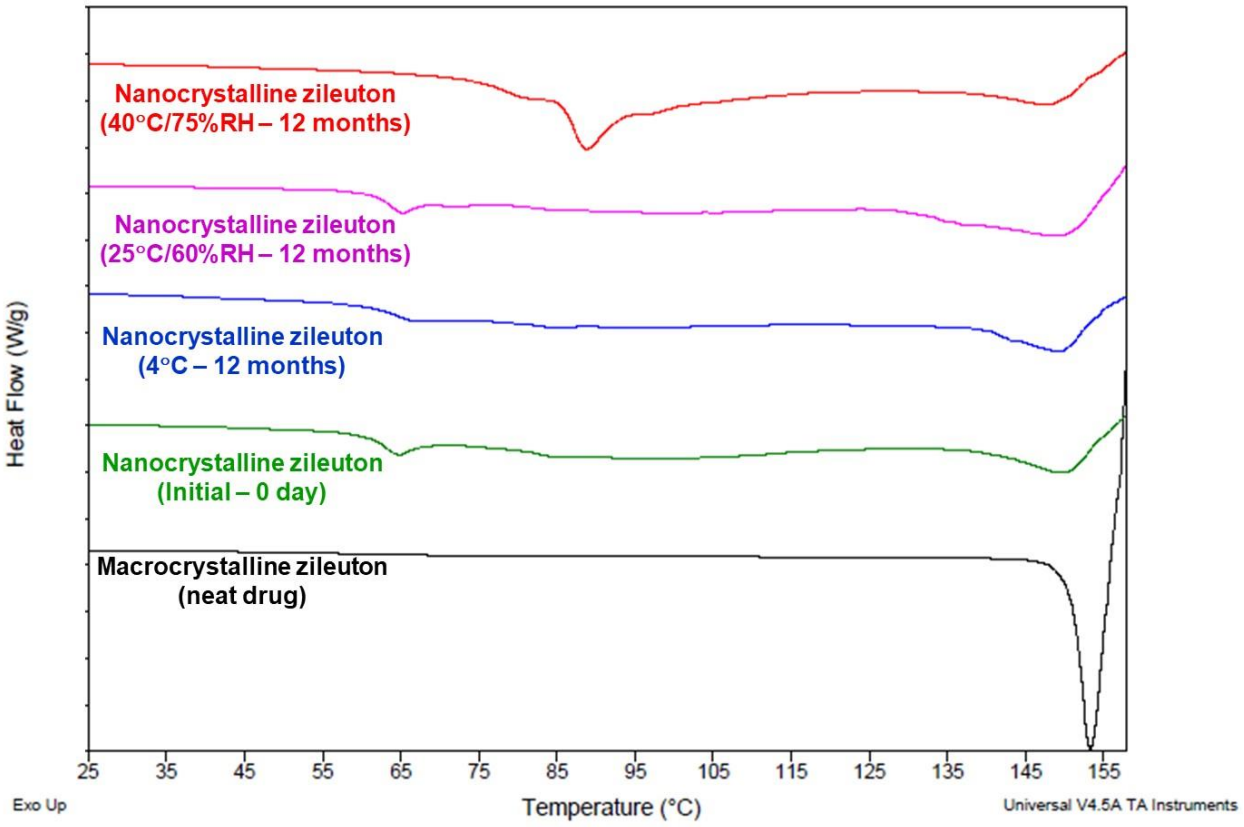

Figure 4.17. DSC thermogram of neat macrocrystalline zileuton (raw crystalline drug), and the optimized spray-dried nanocrystalline zileuton formulations (initial as well as those stored for 12 months at 4°C, 25°C/60% RH and 40°C/75% RH).

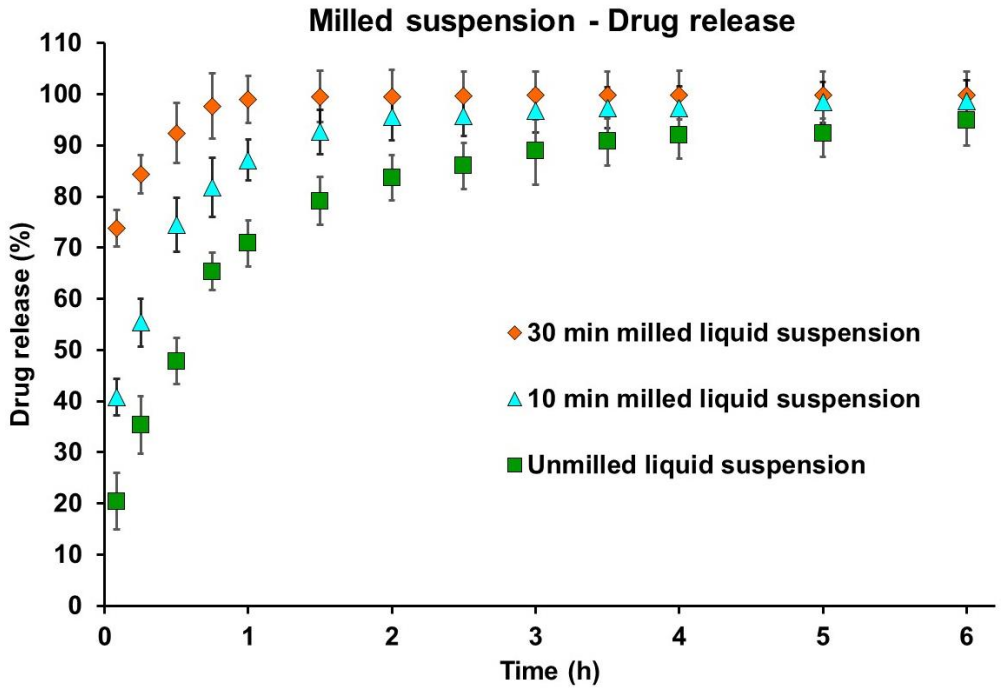

Figure 4.18a. *In vitro* drug release testing of different sized (30 min milled, 10 min milled, and unmilled) crystalline liquid suspension formulations. (USP apparatus II with paddle at 100 rpm, pH 6.8, phosphate buffer, n = 6)

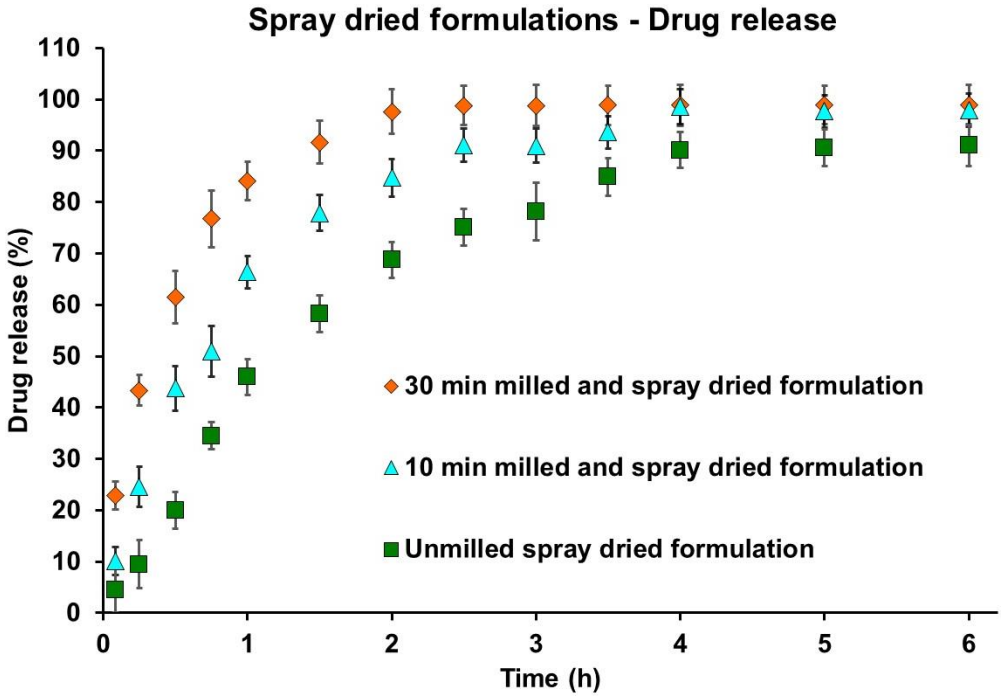

Figure 4.18b. *In vitro* drug release testing of different sized (30 min milled, 10 min milled, and unmilled) crystalline spray dried formulations as capsules. (USP apparatus I with basket at 100 rpm, pH 6.8, phosphate buffer, n = 6)

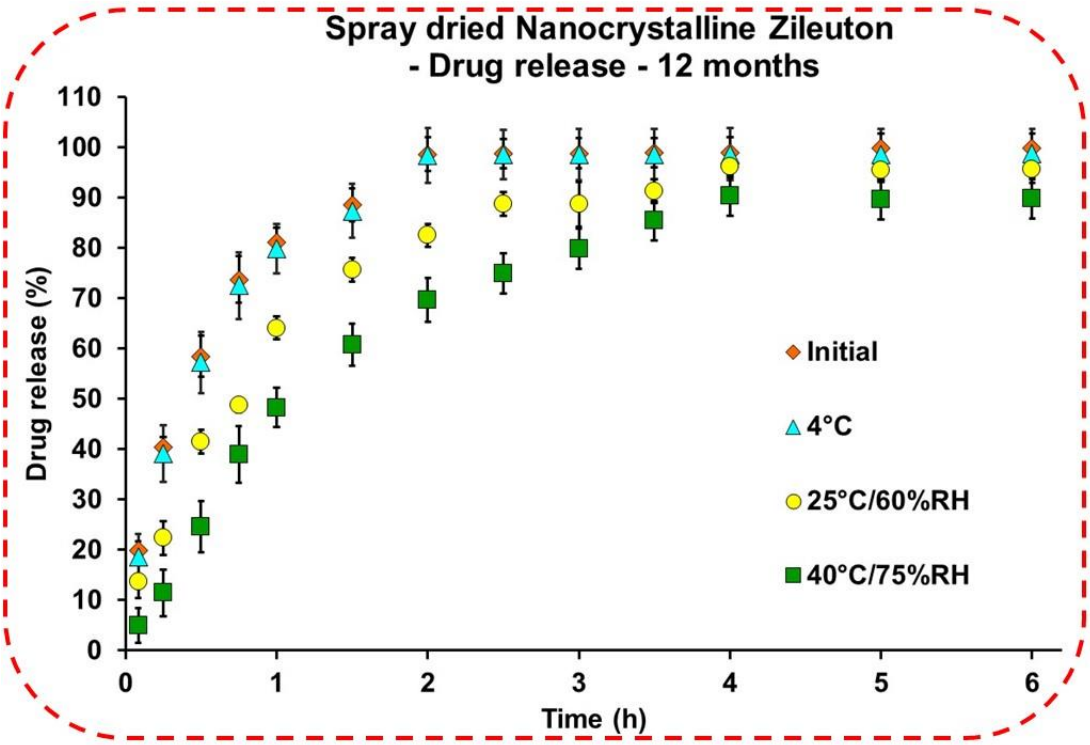

Figure 4.18c. *In vitro* drug release testing of spray dried nanocrystalline zileuton comparing freshly prepared formulations with those stored at 4°C, 25°C/60% RH and 40°C/75% RH for twelve months in capsules. (USP apparatus I with basket at 100 rpm, pH 6.8, phosphate buffer, n=6)

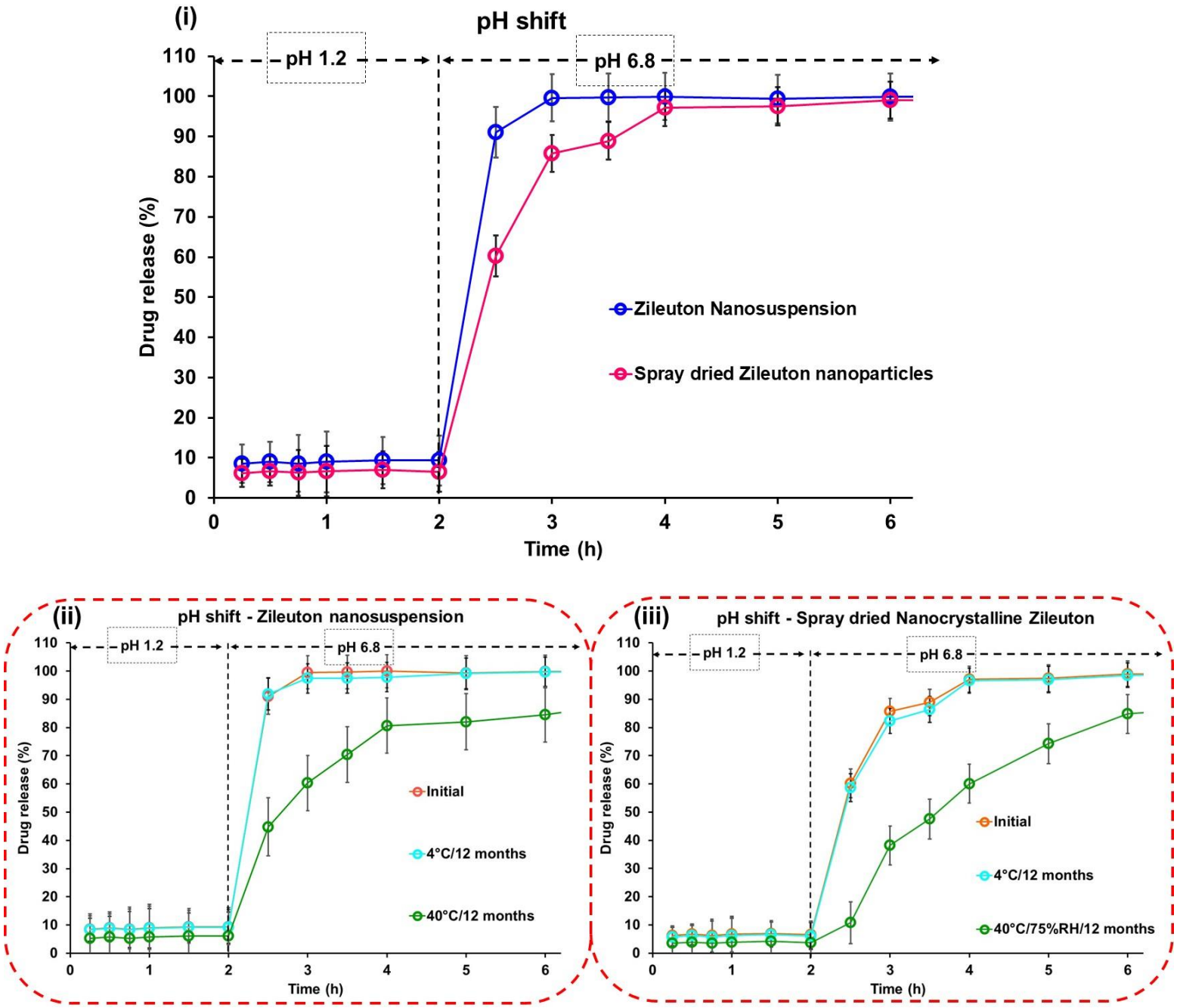

Figure 4.18d. *In vitro* drug release testing with a pH shift from pH 1.2 for the initial 2 h to pH 6.8 for next 4 h (USP apparatus II with paddle at 100 rpm, n = 6) comparing: **(i)** zileuton nanosuspensions *vs.* spray dried nanocrystalline zileuton powder (at day zero); **(ii)** zileuton nanosuspension formulations stored at different stability conditions (day zero, 4°C /12 months and 40°C/12 months); and **(iii)** spray dried nanocrystalline zileuton formulations

stored at different stability conditions (day zero, 4°C /12 months and 40°C/75% RH/12 months).

4.8 REFERENCES

[1]Terblanche N. S., 2008. New pharmaceutical product development: Barriers to overcome and opportunities to exploit. Journal of Commercial Biotechnology. 14, 201-212.

[2]Bountra C., Lee W. H., Lezaun J. and New A. L., 2017. A New Pharmaceutical Commons: Transforming Drug Discovery. Oxford Martin. .

[3]Seufert K., 2014. The New Dawn of Pharmaceutical Manufacturing: Innovative Solutions for Unprecedented Challenges. American Pharmaceutical Review. .

[4]Cardinal L. B., 2001. Technological innovation in the pharmaceutical industry: The use of organizational control in managing research and development. Organization science. 12, 19-36.

[5]Maravelias C. T. and Grossmann I. E., 2001. Simultaneous planning for new product development and batch manufacturing facilities. Industrial & engineering chemistry research. 40, 6147-6164.

[6]Kline S. J. and Rosenberg N., 2010. An overview of innovation. Studies On Science And The Innovation Process: Selected Works of Nathan Rosenberg. World Scientific. 173-203.

[7]Blau G. E., Pekny J. F., Varma V. A. and Bunch P. R., 2004. Managing a portfolio of interdependent new product candidates in the pharmaceutical industry. Journal of Product Innovation Management. 21, 227-245.

[8]Bhaskaran S. R. and Krishnan V., 2009. Effort, revenue, and cost sharing mechanisms for collaborative new product development. Management Science. 55, 1152-1169.

[9]Peterson J. J., Snee R. D., McAllister P. R., Schofield T. L. and Carella A. J., 2009. Statistics in pharmaceutical development and manufacturing. Journal of Quality Technology. 41, 111-134.

[10]Weissman S. A. and Anderson N. G., 2014. Design of experiments (DoE) and process optimization. A review of recent publications. Organic Process Research & Development. 19, 1605-1633.

[11]Rogers A. and Ierapetritou M., 2015. Challenges and opportunities in modeling pharmaceutical manufacturing processes. Computers & Chemical Engineering. 81, 32-39.
[12]Khurana A. and Rosenthal S. R., 1998. Towards holistic “front ends” in new product development. Journal of product innovation management. 15, 57-74.
[13]Junker B., Zablackis E., Verch T., Schofield T. and Douette P., 2015. Quality-by-Design: as related to analytical concepts, control and qualification. Vaccine Analysis: Strategies, Principles, and Control. Springer. 479-520.
[14]Rathore A. S. and Winkle H., 2009. Quality by design for biopharmaceuticals. Nature biotechnology. 27, 26.
[15]Lawrence X. Y., 2008. Pharmaceutical quality by design: product and process development, understanding, and control. Pharmaceutical research. 25, 781-791.
[16]Pramod K., Tahir M. A., Charoo N. A., Ansari S. H. and Ali J., 2016. Pharmaceutical product development: A quality by design approach. International journal of pharmaceutical investigation. 6, 129.
[17]Singh B., Kapil R., Nandi M. and Ahuja N., 2011. Developing oral drug delivery systems using formulation by design: vital precepts, retrospect and prospects. Expert opinion on drug delivery. 8, 1341-1360.
[18]Haleem R. M., Salem M. Y., Fatahallah F. A. and Abdelfattah L. E., 2015. Quality in the pharmaceutical industry–A literature review. Saudi Pharmaceutical Journal. 23, 463-469.
[19]Drennen J. K., 2007. Quality by design—What does it really mean? Journal of Pharmaceutical Innovation. 2, 65-66.
[20]International Conference on Harmonization (ICH) of Technical Requirements for Registration of Pharmaceuticals for Human Use, 2005, Q8 Pharmaceutical development Current step. 4, 11.
[21]Peterson J. J. and Lief K., 2010. The ICH Q8 definition of design space: A comparison of the overlapping means and the Bayesian predictive approaches. Statistics in Biopharmaceutical Research. 2, 249-259.
[22]Singh L. and Sharma V., 2015. Quality by Design (QbD) Approach in Pharmaceuticals: Status, Challenges and Next Steps. Drug Delivery Letters. 5, 2-8.

[23]Zhang L. and Mao S., 2017. Application of quality by design in the current drug development. asian journal of pharmaceutical sciences. 12, 1-8.
[24]Freeman T., Birkmire A. and Armstrong B., 2015. A QbD approach to continuous tablet manufacture. Procedia engineering. 102, 443-449.
[25]Lopes M. S. d. T. P., 2014. Critical parameters in manufacturing process validation of different forms of pharmaceutical injectable products to assess products´ risk framework. .
[26]Stegemann S., Connolly P., Matthews W., Barnett R., Aylott M., Schrooten K., Cadé D., Taylor A. and Bresciani M., 2014. Application of QbD principles for the evaluation of empty hard capsules as an input parameter in formulation development and manufacturing. AAPS PharmSciTech. 15, 542-549.
[27]Kumar S., Gokhale R. and Burgess D. J., 2014. Quality by design approach to spray drying processing of crystalline nanosuspensions. International journal of pharmaceutics. 464, 234-242.
[28]Xu X., Khan M. A. and Burgess D. J., 2011. A quality by design (QbD) case study on liposomes containing hydrophilic API: I. Formulation, processing design and risk assessment. International journal of pharmaceutics. 419, 52-59.
[29]Kumar S., Jog R., Shen J., Zolnik B., Sadrieh N. and Burgess D. J., 2015. In vitro and in vivo performance of different sized spray-dried crystalline itraconazole. Journal of pharmaceutical sciences. 104, 3018-3028.
[30]Jog R., Unachukwu K. and Burgess D. J., 2016. Formulation design space for stable, pH sensitive crystalline nifedipine nanoparticles. International journal of pharmaceutics. 514, 81-92.
[31]Kumar S., Jog R., Shen J., Zolnik B., Sadrieh N. and Burgess D. J., 2015. Formulation and performance of danazol nano-crystalline suspensions and spray dried powders. Pharmaceutical research. 32, 1694-1703.
[32]Xu X., Costa A. P., Khan M. A. and Burgess D. J., 2012. Application of quality by design to formulation and processing of protein liposomes. International journal of pharmaceutics. 434, 349-359.

[33]Qiu Y., He X., Zhu L. and Chen B., 2017. Product and Process Development of Solid Oral Dosage Forms. Developing Solid Oral Dosage Forms (Second Edition). Elsevier. 555-591.

[34]Amidon G. L., Lennernas H., Shah V. P. and Crison J. R., 1995. A theoretical basis for a biopharmaceutic drug classification: the correlation of in vitro drug product dissolution and in vivo bioavailability. Pharmaceutical research. 12, 413-420.

[35]Wolk O., Agbaria R. and Dahan A., 2014. Provisional in-silico biopharmaceutics classification (BCS) to guide oral drug product development. Drug design, development and therapy. 8, 1563.

[36]Dahan A., Miller J. M. and Amidon G. L., 2009. Prediction of solubility and permeability class membership: provisional BCS classification of the world's top oral drugs. The AAPS journal. 11, 740-746.

[37]Jog R. and Burgess D. J., 2017. Pharmaceutical amorphous nanoparticles. Journal of pharmaceutical sciences. 106, 39-65.

[38]Jog R., Kumar S., Shen J., Jugade N., Tan D. C. T., Gokhale R. and Burgess D. J., 2016. Formulation design and evaluation of amorphous ABT-102 nanoparticles. International journal of pharmaceutics. 498, 153-169.

[39]Muller R. H., Gohla S. and Keck C. M., 2011. State of the art of nanocrystals–special features, production, nanotoxicology aspects and intracellular delivery. European Journal of Pharmaceutics and Biopharmaceutics. 78, 1-9.

[40]Merisko-Liversidge E., Liversidge G. G. and Cooper E. R., 2003. Nanosizing: a formulation approach for poorly-water-soluble compounds. European Journal of Pharmaceutical Sciences. 18, 113-120.

[41]Buckton G. and Beezer A. E., 1992. The relationship between particle size and solubility. International journal of pharmaceutics. 82, R7-R10.

[42]Moschwitzer J. and Muller R. H., 2006. Spray coated pellets as carrier system for mucoadhesive drug nanocrystals. European journal of pharmaceutics and biopharmaceutics. 62, 282-287.

[43]Hecq J., Deleers M., Fanara D., Vranckx H. and Amighi K., 2005. Preparation and characterization of nanocrystals for solubility and dissolution rate enhancement of nifedipine. International journal of pharmaceutics. 299, 167-177.

[44]Keck C. M. and Müller R. H., 2013. Nanotoxicological classification system (NCS)–a guide for the risk-benefit assessment of nanoparticulate drug delivery systems. European Journal of Pharmaceutics and Biopharmaceutics. 84, 445-448.
[45]Baldinger A., Clerdent L., Rantanen J., Yang M. and Grohganz H., 2012. Quality by design approach in the optimization of the spray-drying process. Pharmaceutical development and technology. 17, 389-397.
[46]Beg S., Sandhu P. S., Batra R. S., Khurana R. K. and Singh B., 2015. QbD-based systematic development of novel optimized solid self-nanoemulsifying drug delivery systems (SNEDDS) of lovastatin with enhanced biopharmaceutical performance. Drug delivery. 22, 765-784.
[47]Casian T., Iurian S., Bogdan C., Rus L., Moldovan M. and Tomuta I., 2017. QbD for pediatric oral lyophilisates development: risk assessment followed by screening and optimization. Drug development and industrial pharmacy. 43, 1932-1944.
[48]Ghosh I., Schenck D., Bose S., Liu F. and Motto M., 2013. Identification of critical process parameters and its interplay with nanosuspension formulation prepared by top down media milling technology–a QbD perspective. Pharmaceutical development and technology. 18, 719-729.
[49]Yerlikaya F., Ozgen A., Vural I., Guven O., Karaagaoglu E., Khan M. A. and Capan Y., 2013. Development and evaluation of paclitaxel nanoparticles using a quality-by-design approach. Journal of pharmaceutical sciences. 102, 3748-3761.
[50]Pallagi E., Ambrus R., Szabo-Revesz P. and Csoka I., 2015. Adaptation of the quality by design concept in early pharmaceutical development of an intranasal nanosized formulation. International journal of pharmaceutics. 491, 384-392.
[51]Bell R., Young P., Albert D., Lanni C., Summers J., Brooks D., Rubin P. and Carter G., 1992. The discovery and development of zileuton: an orally active 5-lipoxygenase inhibitor. International journal of immunopharmacology. 14, 505-510.
[52]Carter G. W., Young P. R., Albert D. H., Bouska J., Dyer R., Bell R. L., Summers J. B. and Brooks D., 1991. 5-lipoxygenase inhibitory activity of zileuton. Journal of Pharmacology and Experimental Therapeutics. 256, 929-937.
[53]https://www.netzsch-grinding.com/en/products-solutions/wet-grinding/miniseries-microseries-laboratory-mills/.

[54]https://www.buchi.com/us-en/products/spray-drying-and-encapsulation/mini-spray-dryer-b-290.
[55]Bosch S., De Beaurepaire L., Allard M., Mosser M., Heichette C., Chrétien D., Jegou D. and Bach J.-M., 2016. Trehalose prevents aggregation of exosomes and cryodamage. Scientific reports. 6, 36162.
[56]Caputo F., Mameli M., Sienkiewicz A., Licoccia S., Stellacci F., Ghibelli L. and Traversa E., 2017. A novel synthetic approach of cerium oxide nanoparticles with improved biomedical activity. Scientific reports. 7, 4636.
[57]Workman Jr J. and Weyer L., 2007. Practical guide to interpretive near-infrared spectroscopy, CRC press. .
[58]Coates J., 2000. Interpretation of infrared spectra, a practical approach. Encyclopedia of analytical chemistry. .
[59]Vivekanandan J., Ponnusamy V., Mahudeswaran A. and Vijayanand P., 2011. Synthesis, characterization and conductivity study of polyaniline prepared by chemical oxidative and electrochemical methods. Archives of Applied Science Research. 3, 147-153.
[60]Bansal S. S., Kaushal A. M. and Bansal A. K., 2007. Molecular and thermodynamic aspects of solubility advantage from solid dispersions. Molecular pharmaceutics. 4, 794-802.
[61]Baird J. A. and Taylor L. S., 2012. Evaluation of amorphous solid dispersion properties using thermal analysis techniques. Advanced drug delivery reviews. 64, 396-421.

Chapter 5

Nanoamorphous Drug Products – Design and Development

ABSTRACT

Most of the recent drug compounds coming out of the drug discovery pipeline are labile (multiple polymorphs), and need to be developed into robust marketed oral drug formulations. There are only 22 oral macroamorphous drug products approved by FDA and till date no oral nanoamorphous drug products. However, there are several oral nanoamorphous drug formulations (including both labile and non-labile drugs) being researched and a few of these are in the clinical trials. Due to the labile nature of these drug compounds, there is a need to utilize a controlled strategy for design and development of robust nanoamorphous drug formulations in order to prevent any physicochemical instability. The present research focuses on the use of a novel *integrated* critical process parameters and critical formulation parameters (*i*CPP-CFPs) DoE approach for the design and development of stable nanoamorphous spironolactone (BCS class II compound with eight polymorphic forms). There are possibilities of the interconversion of these polymorphic forms during processing (manufacturing nanoamorphous particles) and during storage. In the present study, polymorphic transitions (amorphous to crystalline and anhydrous to hydrate) were carefully monitored *via* orthogonal solid-state characterization tools. Significant polymorphic transitions were observed in the formulations stored at 40°C/75% RH over six months, however the formulations stored at 4°C were stable. The significant *i*CPP-CFPs (solvent-to-antisolvent ratio, drug concentration and inlet temperature of the spray dryer) were critically investigated for their influence on different CQAs (critical quality attributes). Solvent-to-antisolvent ratio and inlet temperature were identified to be the significant *i*CPP-CFPs. Particle size and total product yield were identified to be the significant CQAs. Lab-scale manufacturing of the spray dried nanoamorphous spironolactone resulted in a remarkably high total product yield (82.4±3.91% w/w) with a uniform and homogenous particle size (244.2±23.32 nm). Furthermore, the physicochemical attributes and the drug release criteria of the nanoamorphous spironolactone were compared with two marketed products (spironolactone tablets, USP 100 mg (Pfizer and Mylan)) and other in-house formulations.

In addition, nanoamorphous spironolactone showed a significantly superior kinetic solubility/dissolution rate (10-fold) with a longer supersaturation time (~6 h) compared to the in-house formulations and marketed drug products.

5.1. INTRODUCTION

Pharmaceutical drug products are mostly administered *via* the oral route as this is most convenient and acceptable to patients [1, 2]. The use of nanoamorphous drug particles is an emerging strategy to allow oral administration of BCS class II and II/IV drugs (poorly soluble compounds) [3-5]. Amorphous nanoparticles have significantly enhanced solubility and bioavailability through a combination of enhanced dissolution rates (due to nano-size range and amorphous solid-state form) and increased supersaturation levels (due to amorphous solid-state form). Amorphous nanoparticles are solid dispersions in the colloidal size range (100 to 1000 nm) and are typically stabilized *via* crystallization inhibitors (polymers, surfactants, sugars or their combinations) [5]. The mechanisms by which these crystallization inhibitors stabilizes the drug in the amorphous nanoparticles are: *(1)* significant reduction in the molecular motion of the dispersed drug; *(2)* inhibition of the solution facilitated crystal growth and nucleation of the dissolved drug, maintaining the supersaturation level for a long period of time; and *(3)* improvement in the storage stability by inhibition of the recrystallization of amorphous drug [6].

Nanoamorphous amphotericin and glibenclamide prepared using the stabilizers Tween 80/poloxamer 188 and HPMC, respectively have been reported to have 13-fold and 10-fold enhancement in the kinetic solubility/dissolution rate compared to the macrocrystalline drug [7, 8]. More importantly, nanoamorphous itraconazole has been reported to have 2.5-fold and 18-fold increase in oral bioavailability compared to macroamorphous and macrocrystalline formulations, respectively [3]. Nanocrystalline itraconazole showed a similar increase in oral bioavailability to the nanoamorphous formulation, however, there was a significant delay in the C_{max} from the 4 h to 8 h due to the reduced solubility of the crystalline form. These and previous studies have used relatively stable APIs (with zero or a few polymorphic forms). However, most of the drugs coming out of the drug discovery pipeline are comparatively labile (with multiple polymorphic forms) [9]. Such labile drugs suffers from physical instability issues (polymorphic transition, drug crystallization and

nanoparticle aggregation) during processing and/or storage stability studies. When considering nanoamorphous formulations there are additional instability issues due to their small particle size (nanoparticle aggregation and increased probability of polymorphic transition) compared to macroamorphous counterparts. The present research focuses on investigating and inhibiting aggregation and polymorphic transition for nanoamorphous formulations of labile drugs during manufacturing and accelerated stability studies. Spironolactone (labile molecule with eight polymorphic forms) was used as a model BCS class II drug [10]. Spironolactone is a diuretic steroidal aldosterone agonist with an average molecular weight - 416.6 g/mol and an aqueous solubility ~ 28 μg/mL [11].

In the present research, an *integrated* critical process parameter-critical formulation parameters (*i*CPP-CFPs) DoE approach was used to develop nanoamorphous spironolactone formulations. Sonoprecipitation followed by spray drying were utilized to manufacture solid nanoamorphous spironolactone. The effect of solvent-to-antisolvent ratio, drug concentration, surfactant concentration and inlet temperature of the spray dryer were evaluated. The important CQAs investigated were particle size; drug loading; zeta potential; and total product yield. Dowfax2A1 (anionic surfactant) and trehalose (high Tg sugar) were used as auxiliary stabilizers to achieve non-crystallizing, non-aggregating spray-dried nanoamorphous spironolactone powders. *In vitro* dissolution testing was conducted on the optimized nanoamorphous spironolactone formulations as well as storage stability formulations (40°C/75% RH, 25°C/60% RH and 4°C for 6 months). The marketed spironolactone products (RLD – Aldactone®, spironolactone USP 100 mg tablets (Pfizer) and generic –spironolactone USP 100 mg tablets (Mylan)) were also investigated. To the best of our knowledge, this is the first study to develop a nanoamorphous drug product *via* an *i*CPP-CFPs DoE approach using a labile drug (multiple polymorphic forms). In addition, the effect of temperature and humidity on the physicochemical attributes of the spray dried nanoamorphous spironolactone was critically evaluated *via* storage stability studies (40°C/75% RH, 25°C/60% RH and 4°C for 6 months). The optimized nanoamorphous spironolactone and the marketed drug products were analyzed *via* an array of solid-state tools (PLM, PXRD, DSC, FTIR and AFM) to investigate any critical polymorphic transitions.

5.2. MATERIALS

Crystalline spironolactone (greater than 99% purity) was purchased from Beijing Mesochem Technology Co. Ltd., China. Trehalose was gifted by Gattefose. Dowfax 2A1 was gifted by Dow Chemical Company. Marketed spironolactone tablets (Aldactone®, Spironolactone tablets, USP 100 mg (RLD) and Spironolactone Tablets, USP 100 mg (Generic) were purchased from G.D. Searle (Division of Pfizer Inc.) and Mylan Pharmaceuticals Inc., respectively. The chemical structures of the ingredients used in the optimized spray-dried nanoamorphous spironolactone formulation are shown in Table 5.1. HPLC grade solvents were purchased from Fisher Scientific. Inspire C18 column (4.6 mm x 100 mm, 5µm) was gifted by Dikma Technologies Inc.

5.3. METHODS

Based on the pre-formulation studies, it was observed that the spray drying and the freeze drying were the most feasible drying techniques. Furthermore, at drug-stabilizer weight ratios 3:1 and 1:1, w/w, it was observed that PVP K12 and HPMC E3 resulted in lowest interaction parameter value (towards negative) and a high negative free energy of mixing indicating a strong interaction (hydrogen bonding) between these stabilizers and the drug (Figure A, B and C). Accordingly, these polymers were considered for the formulation development. However, preliminary trials showed a stable formulations is obtained at a low concentration of surfactant (Dowfax2A1) and at 1:3, w/w drug:trehalose. Therefore, the *i*CPP-CFPs DoEs were performed using only these two excipients.

5.3.1 Manufacturing of nanoamorphous spironolactone powder

5.3.1.1 Spironolactone nanoemulsions via sonoprecipitation

Spironolactone nanoemulsions were manufactured *via* the sonoprecipitation technique. Sonoprecitation is a combination of solvent-antisolvent precipitation and ultrasonication. Briefly, crystalline spironolactone was completely dissolved in dichloromethane (DCM) at different concentrations as detailed in the DoE section below (5.3.3). 1 mL drug solution in DCM ("solvent") was injected (using a syringe with a 22.1G needle) in different volumes of distilled water containing stabilizer (anionic surfactant – Dowfax2A1) ("antisolvent") at a rate of 10 mL/min under ultrasonication (probe sonication). Different surfactant

concentrations and solvent-to-antisolvent ratios were investigated as detailed in the DoE section below (5.3.3). A sonic dismembrator (Fisher scientific model 550) using a probe tip diameter of 13 mm at a frequency of 20 kHz was used for ultrasonication. The probe tip was immersed a distance of 5 mm in the antisolvent solution and sonication was carried out for the optimized time of 1 min 40 s and at the optimized speed 3.5 units to obtain nano-sized precipitates. The entire process was performed at 2-8°C to prevent thermal degradation of the drug. The resultant nanoemulsions were kept under magnetic stirring for 1 hour under vacuum for organic solvent removal.

5.3.1.2 Nanoamorphous spironolactone via spray drying

The spironolactone nanoemulsions prepared *via* sonoprecipitation were mixed with sugar stabilizer (trehalose) and spray dried to obtain nanoamorphous spironolactone powder (Figure 5.1). Spironolactone nanoemulsions were spray-dried using a benchtop B-290 spray dryer (Buchi Labortechhnik AG, Flawil, Switzerland) based on the DoE detailed in section (3.3). The spray dryer was equilibrated using distilled water. Once the spray dryer was equilibrated, distilled water was changed to the nanoemulsions formulations. The nanoemulsion formulations were pumped using a peristaltic pump at a pump rate of 15 % and at a feed flow rate of 5 mL/min. The aspirator rate was 80% (air volume flow (32.5 m^3/h)). Based on the preliminary study, it was observed that the inlet temperature is a critical spray drying process parameter which can significantly influence different CQAs (particle size, particle morphology, total product yield and crystallinity) [3, 4, 12, 13]. Thus, the inlet temperature was one of the critical process parameters investigated as detailed in the DoE section below (5.3.3). Gas flow (atomizing air) was kept constant at 40 mm Hg (air flow approximately 600 L/h) for all the formulations. Each formulation was spray-dried using trehalose as an excipient [drug:trehalose (1:3, w/w)] to prevent nanoparticle aggregation. Spray-dried powders were collected from the collection chamber and immediately analyzed for the CQAs (particle size, total product yield and crystallinity).

5.3.2 Design of experiments (DoE)

According to the preliminary investigation (data not shown), an integrated critical process and critical formulation parameters DoE (*i*CPP-CFPs) was implemented. Four different *i*CPP-CFPs were selected to analyze their effect on different CQAs of the spray dried

nanoamorphous spironolactone powders (particle size, polydispersity index, zeta potential, moisture content, drug loading and total product yield). These *i*CPP-CFPs were: drug concentration (in solvent), solvent-to-antisolvent ratio, surfactant concentration and inlet temperature of the spray dryer. The ranges of these factors were: drug concentration (0.1 – 0.6 %w/v), solvent-to-antisolvent ratio (1:2 – 1:25 v/v), surfactant concentration (0.05 – 0.5 %w/v) and inlet temperature (110 – 130 °C). A response surface methodology with a cubic centered design was utilized to investigate these factors. The design space is provided in Table 5.2. Design Expert and Minitab® 18.0 software were utilized for the experimental design and detailed analysis of the different CQAs.

5.3.3 Characterization of the nanoamorphous spironolactone

5.3.3.1 Particle size measurement

Particle size measurements were performed using a Zetasizer Nano ZS90 (Malvern Instruments). Briefly, the spray-dried formulations were suspended in a saturated and filtered (0.2 μm PVDF membrane filter) solution of spironolactone in 30% glycerin solution to avoid any discrepancy resulting from dissolution of the nano-particles during measurement. The viscosity of this dispersant solution was measured *via* a Brookfield viscometer (Model DV-III) and used to calculate the particle size of the re-dispersed nanoamorphous spironolactone. Zeta potential of these re-dispersed formulations were measured in the folded capillary zeta cells using the same instrument. All formulations were analyzed in triplicate and the results were reported as the mean value of these runs.

5.3.3.2 Powder X-Ray Diffraction (PXRD)

PXRD was utilized to determine any presence of crystallinity in the spray-dried formulations. X-ray diffraction patterns were obtained using an X-ray diffractometer (Model D5005, Bruker AXS Inc., Madison, WI) with Cu-kα radiation, a voltage of 40 kV, and a current of 40 mA. All the scans were performed with a scanning rate of 2°/minute with steps of 0.02° from 5° to 40° at 2θ ranges.

5.3.3.3 HPLC analytical method

The quantification of spironolactone was conducted using an Agilent-HPLC system with a UV detector. The absorbance wavelength was set at 254 nm. The mobile phase was a

mixture of distilled water and methanol at a 34:64 %v/v ratio. A C18 Inspire 5µ analytical column (4.6 mm × 100 mm) was used with a flow rate of 1 ml/min and the column temperature was maintained at 40°C using a column heater.

5.3.3.4 Attenuated Total Reflectance - Fourier Transform Infrared Spectroscopy (ATR-FTIR)

IR spectroscopy was performed using a Nicolet FTIR (iS5 FTIR, Thermo Scientific) spectrometer with an attenuated total reflectance (ATR) accessory. Spray-dried powders were placed on the crystal window (Germanium) and compressed lightly using a pressure clamp. Spectra were recorded over a range of 400–4000 cm^{-1} with a resolution of 4 cm^{-1}, for 128 parallel scans. Data analysis was performed on Omnic® 6.0a software (Thermo Nicolet Corporation).

5.3.3.5 Polarized Light Microscopy (PLM)

The spray-dried formulations were dispersed in the immersion oil and placed on microscope slides. The samples were analyzed using an Olympus BH2 polarized microscope with a Q-imaging camera, accessories and software. All images were obtained at 10X resolution.

5.3.3.6 Differential Scanning Calorimetry (DSC)

DSC was performed using a TA Q1000 (TA instruments, New Castle, DE) calorimeter and calibrated using indium and sapphire discs. Approximately 5–10 mg of spray-dried formulations and neat drug (control) were sealed in hermetic pans and analyzed. The heating rate was maintained at 5 °C/min and the temperature was increased from room temperature to 190 °C. Nitrogen gas was used for purging at a flow rate of 50 mL/min. The data were analyzed using TA universal analysis software.

5.3.3.7 Atomic Force Microscopy (AFM)

The spray dried nanoformulations, drug powders and tablets were mounted using double sided tape on a glass slide and placed under the AFM microscope. Images were captured using an Asylum Research MFP-3D atomic force microscope using AC Air topography mode. Silicon probe OMCL-AC160TS-W2 (Olympus) cantilevers with a nominal spring

constant of 42 N/m were used to image the surface topography of the powders and the tablets. Images were taken with a deflection set-point of 1 V and an integral gain between 3 and 22, depending on the sample and the size of the image. Images up to 10-15 microns were collected with scan rates between 0.1 and 0.5 Hz. All measurements were performed at room temperature and images were analyzed using Igor Pro 6.36 software with Asylum Research version 12 software.

5.3.3.8 In vitro dissolution testing

USP apparatus II (AT7 smart, Sotax AG Switzerland) was utilized for the *in vitro* dissolution experiments. The dissolution testing of the spray-dried powders was performed under non-sink conditions. All the dissolution experiments were conducted at 37°C in 900 mL of pH 1.2 hydrochloric acid (0.1 N) at a speed of 75 rpm. At each time point, 2 mL samples were withdrawn from the dissolution chamber and replaced with fresh dissolution media. The samples were filtered using 0.1 μm PVDF filters to avoid any erroneous results from un-dissolved nano-particulates. All samples were analyzed using the HPLC method as described above. The samples were analyzed on day zero and after storing at different conditions 4°C, 25°C/60% RH and 40°C/75% RH for one, three and six month/s. The marketed tablets were tested at the same conditions. All formulations were analyzed in sextuplet and the results were reported as the mean value of these runs.

5.3.4 Stability testing

All the spray-dried powder formulations were stored at three different storage conditions *i.e.* 4°C, 25°C/60% RH and 40°C/75% RH for 6 months. Samples were withdrawn at 1, 3 and 6 month/s and analyzed for particle size distribution, zeta potential, moisture content, crystallinity and *in vitro* dissolution testing.

5.4. Reference listed drug product and generic drug product

The spray dried nanoamorphous spironolactone formulations were characterized and compared against two marketed spironolactone drug products: Aldactone® (Spironolactone tablets, USP 100 mg) – Pfizer (RLD) and Spironolactone tablets, USP 100 mg – Mylan (Generic). All of the above analytical and solid-state characterization tools were used to test these marketed drug products. Furthermore, these marketed drug products were stored

at different accelerated stability conditions along with the spray dried nanoamorphous spironolactone formulations to compare the effect of temperature and humidity.

5.5. Miscellaneous in-house spironolactone formulations

Different in-house spironolactone formulations (macro-amorphous, macro-crystalline and nanocrystalline) were prepared and used as a controls for comparison against the spray dried nanoamorphous spironolactone formulations and marketed drug products.

5.5.1 Macroamorphous spironolactone

Amorphous spironolactone (micron-size amorphous) was prepared by spray drying. The required quantity of spironolactone and the stabilizer excipients (trehalose and Dowfax2A1) mixed in the same ratio as the optimized spray dried formulations were dissolved in methanol and spray dried. The spray dried macro-amorphous formulations were used as controls.

5.5.2 Nanocrystalline spironolactone

Spironolactone (0.4% w/v) was suspended in the aqueous stabilizer solution (*i.e.* 0.13% w/v Dowfax2A1). The prepared suspension was stirred for 30 minutes for complete wetting of the drug by the stabilizer solution. The suspension (80 mL) was milled using a Netzsch media mill (Netzsch, Exton, PA) at a fixed milling intensity of 1500 rpm in the continuous mode. The suspension formulation was continuously milled for 40 minutes. The temperature of the sample was maintained at 2-8°C using two cooling bath re-circulators. The nano-crystalline suspension was spray-dried using trehalose as an auxiliary excipient [drug:trehalose (1:3, w/w)]. The nanocrystalline spironolactone formulations were used as controls.

5.5.3 Macrocrystalline spironolactone

Crystalline spironolactone (micron-sized crystalline) were prepared by serial dilution. The required quantity of spironolactone and the stabilizer excipients (trehalose and Dowfax2A1) in the same ratio as the optimized spray dried formulations were mixed *via* serial dilution. The macrocrystalline spironolactone formulations were used as controls.

5.6. RESULTS & DISCUSSION

5.6.1. Influence of *i*CPP-CFPs on different CQAs of spray-dried nanoamorphous spironolactone

The iCPP-CFPs DoE was performed according to the CCD design space and the results are shown in Table 5.3. It was observed that surfactant concentration had a negligible influence on all CQAs.

5.6.1.1. Particle size

The drug concentration and inlet temperature were determined to be the critical parameters for the particle size. Before spray drying, the particle size of nanoamorphous spironolactone was <200 nm at drug concentrations and solvent-to-antisolvent ratios in the range of 0.2-0.5% w/v and 1:5 to 1:25 v/v, respectively (Figure 5.2a). At drug concentrations above 0.5% w/v and below 0.15% w/v, the nanoparticles were significantly larger in size (>400 nm). After spray drying, the particle size of nanoamorphous spironolactone was <200 nm at drug concentrations in the range of 0.15-0.5% w/v and at spray dryer inlet temperatures of ≤115°C (Figure 5.2b). At inlet temperatures above 120°C, the particle size of spray-dried nanoamorphous spironolactone was >400 nm. At inlet temperatures below 120°C, the atomized droplets formed from the spray dryer are uniform and homogenous in terms of particle size. Moreover, at inlet temperatures below 120°C, the particle size is maintained at <200 nm, due to the stabilizing effects of the surfactant (Dowfax2A1) and sugar (trehalose). As the inlet temperature increases above 120°C, the cosolvents (DCM and water) are rapidly evaporated, causing increase in the viscosity of the atomized droplets, which results in nanoparticle aggregation (nanoparticles sticking to one another or to the glass walls of the spray dryer) leading to significant increase in particle size. In addition, above 120°C, the surfactant and sugar lose their stabilizing effect on the drug in the nanoemulsion due to rapid drying resulting in nanoparticle aggregation and result in increase in particle size (>400 nm). Solvent-to-antisolvent ratio and surfactant concentration had a negligible influence on the particle size. A plot showing predictive particle size (theoretically predicted from the model) and actual/observed particle size (experimental based on DoE) is represented in Figure 5.2c. The main effect plot, pareto

chart of the standardized effects and the interaction plots for particle size of nanoamorphous spironolactone are shown in Figure 5.2d.

ANOVA and multiple linear regression were performed on the particle size data and a predictive surface reduced cubic model was generated. The final equation based on the three *i*CPP-CFPs (drug concentration, solvent-to-antisolvent ratio and inlet temperature) and the interaction terms for the prediction of the particle size are provided in Table 5.4. It is evident that the surface reduced cubic model was significant and the lack of fit for this model was not significant, indicating that the model was significant for the CQA.

5.6.1.2. Total product yield

The drug concentration, solvent-to-antisolvent ratio and inlet temperature were determined to be the critical parameters for the total product yield. The total product yield of nanoamorphous spironolactone increased from 60 to 80% w/w with increase in the drug concentrations from 0.1 to 0.6% w/v and increase in the solvent-to-antisolvent ratio from 1:5 to 1:25 v/v (Figure 5.3a). At low drug concentrations (0.1-0.2% w/v), and at low solvent-to-antisolvent ratio (1:5 v/v), the nanoparticles formed were large in size (>400 nm). During sonoprecipitation, these large size nanoparticles stick to the walls of the sonicator or the manufacturing vessel, resulting in low total product yield (60% w/w). In addition, a low antisolvent phase (1:5 v/v) (surfactant in distilled water) provides less dispersibility to the nanodroplets of the solvent phase (drug in DCM) compared to a high antisolvent phase (1:25 v/v). Thus, the nanodroplets are uniformly dispersed at a high solvent-to-antisolvent ratio (1:25 v/v), which dries rapidly upon atomization with low moisture content, preventing any loss of the spray-dried powder resulting in high total product yield (80-85% w/w).

The total product yield of nanoamorphous spironolactone increased from 70 to 85% w/w with an increase in the drug concentration from 0.1 to 0.35% w/v and an increase in the spray drying inlet temperature from 110°C to 125°C (Figure 5.3b). Insufficient drying at low inlet temperatures (<115°C) causes increase in the moisture content of the spray-dried powder, which causes invariable sticking of the nanoparticles to the glass walls of the spray dryer resulting in low yield (≤70% w/w). Increase in the inlet temperature from 115°C to

125°C leads to rapid drying of the atomized droplets of the nanoemulsion resulting in formation of spray-dried powder with minimal moisture content avoiding sticking problem, thereby providing high yield (85-90% w/w). A plot showing predictive (based on theoretically predicted from the model) and actual/observed (experimental based on DoE) total product yield is represented in Figure 5.3c. Figure 5.3d shows the main effect plot, pareto chart of the standardized effects and the interaction plot for the total product yield of nanoamorphous spironolactone.

ANOVA and multiple linear regression were performed on the results of the total product yield and a predictive surface reduced cubic model was generated. The final equation based on the three *i*CPP-CFPs (drug concentration, solvent-to-antisolvent ratio and inlet temperature) and the interaction terms for the prediction of the total product yield of the nanoamorphous spironolactone are provided in Table 5.5. As can be observed in Table 5.5, it is evident that the surface reduced cubic model was significant and the lack of fit for this model was not significant, indicating that the model was significant for the CQA (*i.e.* total product yield of the spray-dried nanoamorphous spironolactone).

5.6.1.3. Zeta potential

The drug concentration, solvent-to-antisolvent ratio and inlet temperature were determined to be the critical parameters for the zeta potential. The zeta potential of nanoamorphous spironolactone increased from -90 to -40 mV with the increase in the drug concentrations from 0.1 to 0.6% w/v and decrease in the solvent-to-antisolvent ratio from 1:25 to 1:5 v/v (Figure 5.4a). The increase in zeta potential was due to stabilizing effect of the surfactant molecules on the drug particles. At high solvent-to-antisolvent ratio (1:25 v/v) and at low drug concentrations (<0.25% w/v), the surfactant concentration is very high compared to the drug molecules, a low zeta potential value (-90 mV) is due to the presence excess surfactant molecules remaining after stabilizing the drug molecules. With the increase in drug concentration (towards 0.6% w/v) and decrease in solvent-to-antisolvent ratio (towards 1:5 v/v), these excess surfactant molecules stabilizes the drug molecules, thereby reducing the surfactant concentration and leading to a high zeta potential value (-40 mV).

The zeta potential of nanoamorphous spironolactone increased from -90 to -40 mV with the increase in the drug concentrations from 0.1 to 0.6% w/v and increase in the spray

drying inlet temperatures from 110°C to 130°C (Figure 5.4b). At low drug concentration (0.1% w/v) and low inlet temperature (110°C), there is incomplete coating of the drug nanoparticles by sugar, exposing the negatively charged surfactant on the surface of the drug nanoparticles, resulting in low zeta potential (-90 mV). With the gradual increase in the drug concentrations (0.1 to 0.6% w/v) and increase in the inlet temperatures (110°C to 130°C), the atomized droplets formed at end of the two fluid nozzle of the spray dryer experiences rapid drying causing uniform coating of the sugar molecules to the drug-surfactant nanoparticles minimizing the exposure of the negatively charged surfactant and resulting in the increase in zeta potential values (-90 to -40 mV). A contour plot and a 3D surface plot shows the effect of drug concentrations, solvent-to-antisolvent ratios and inlet temperatures of spray dryer on zeta potential (Figure 5.4a and 5.4b). A plot showing predictive (based on theoretically predicted from the model) and actual/observed (experimental based on DoE) is represented in Figure 5.4c. Figure 5.4d shows the main effect plot, pareto chart of the standardized effects and interaction plot for zeta potential of nanoamorphous spironolactone.

ANOVA and multiple linear regression were performed on the results of the zeta potential and a predictive surface reduced cubic model was generated. The final equation based on the three iCPP-CFPs (drug concentration, solvent-to-antisolvent ratio and inlet temperature) and the interaction terms for the prediction of the zeta potential of the nanoamorphous spironolactone are provided in Table 5.6. As can be observed in Table 5.6, it is evident that the surface reduced cubic model was significant and the lack of fit for this model was not significant, indicating that the model was significant for the CQA (i.e. zeta potential of the spray-dried nanoamorphous spironolactone).

5.6.1.4. Drug loading

The drug concentration, solvent-to-antisolvent ratio and inlet temperature were determined to be the critical parameters for the drug loading. The drug loading of nanoamorphous spironolactone decreased from 20 to 15% w/w with the increase in the drug concentrations from 0.1 to 0.6% w/v and increase in the solvent-to-antisolvent ratio from 1:5 to 1:25 v/v (Figure 5.5a). At low solvent-to-antisolvent ratio (1:5 v/v) and at low drug concentrations (0.1 – 0.2% w/v), the solvent phase (drug in DCM) has limited antisolvent phase (surfactant

in distilled water) to disperse in, as a result most of the surfactant molecules strongly stabilizes all drug molecules, minimizing the drug loss (either due to sticking to the walls of the ultrasonicator or walls of the manufacturing vessel), resulting in high drug loading (20% w/w). With the increase in drug concentrations (0.2 – 0.6% w/v) and increase in the solvent-to-antisolvent ratios (1:5 – 1:25 v/v), the solvent phase has large volumes of the antisolvent phase to disperse in, as a result the surfactant molecules fails to provide strong stability to the drug molecules, making the drug molecules vulnerable to the sticking and aggregation (as observed with the increase in particle size), resulting in decrease in drug loading (20 – 15% w/w).

With the increase in the drug concentrations (0.1 – 0.6% w/v) and increase in the inlet temperatures of the spray dryer (110°C - 130°C), the drug loading decreases (20 – 16% w/w) (Figure 5.5b). At low spray dryer inlet temperatures between 110°C - 125°C and low drug concentrations (0.1 – 0.2% w/v), the dried nanoparticles formed at the point of the atomization from the two fluid nozzle of the spray dryer has uniform and homogenous particle size and limited moisture content, and due to rapid drying the sugar-surfactant complex provides strong stabilizing effect to the drug nanoparticles, preventing any drug loss (either due to drug molecules phasing out of the sugar-surfactant coating or due to sticking to the glass walls of the spray dryer), resulting in high drug loading (≥20% w/w). At high inlet temperatures (≥130°C) and high drug concentrations (0.3 – 0.6% w/v), there is high level of rapid drying of the nanoparticles which causes the drug molecules to phase out of the drug nanoparticles (drug molecules coated with surfactant-sugar) due to the inability of the surfactant and sugar in stabilizing the drug nanoparticles at high drug concentrations. The drug molecules which phase out after passing through the two fluid nozzle atomizes into minute droplets and rapidly dry out with significant drug loss due to two main reasons: *(1)* the moisture content is very high in the dried drug particles which causes the drug molecules (that has phase out from the stabilizers) to stick to the glass walls of the spray dryer; and/or *(2)* the dried drug particles formed at the point of the atomization of the two fluid nozzle are very small in size which due to the rapid convective gas current in the spray dryer are subsequently carried directly to the filter compartment from which it is difficult to retrieve the dried particles. As a result of these two way mechanisms of drug

loss leading to only dried blank surfactant-sugar nanoparticles mixed with less dried drug-surfactant-sugar nanoparticles being accumulated in the collection chamber of the spray dryer, there is significant decrease in the drug loading of the spray-dried formulations. A plot showing predictive drug loading (based on theoretically predicted from the model) and actual/observed drug loading (experimental based on DoE) is shown in Figure 5.5c. A contour plot and a 3D surface plot shows the effect of drug concentrations, solvent-to-antisolvent ratios and inlet temperatures of spray dryer on drug loading (Figure 5.5a and 5.5b). Figure 5.5d shows the main effect plot, pareto chart of the standardized effects and interaction plot for drug loading.

ANOVA and multiple linear regression were performed on the results of the drug loading and a predictive surface reduced cubic model was generated. The final equation based on the three iCPP-CFPs (drug concentration, solvent-to-antisolvent ratio and inlet temperature) and the interaction terms for the prediction of the drug loading of the nanoamorphous spironolactone are provided in Table 5.7. As can be observed in Table 5.7, it is evident that the surface reduced cubic model was significant and the lack of fit for this model was not significant, indicating that the model was significant for the CQA (i.e. drug loading of the spray-dried nanoamorphous spironolactone).

Following the *i*CPP-CFPs DoE studies, the optimized contour plots (Figure 5.6a and 5.6b) based on the DoE models were considered to predict the optimized *i*CPP-CFPs and CQAs (Table 5.8). The predicted *i*CPP-CFPs were applied for the validation of the DoE studies.

5.6.2. Validation of DoE studies and Stability studies

The *i*CPP-CFPs DoE studies were validated by applying the statistically predicted parameters to prepare sextuplets batches (n=6) of nanoamorphous spironolactone formulations and the average experimental physicochemical properties (Table 5.9) of the sextuplet formulations was compared with the statistically predicted CQAs (Table 5.8). The optimized nanoamorphous spironolactone formulations (experimental total product yield: 82.4% w/w) prepared based on the statistically predicted parameters obtained from the *i*CPP-CFPs DoE studies (described in Table 5.8) were stored at three different stability conditions (4°C, 25°C/60% RH and 40°C/75% RH for one, three and six month/s). At each time-point, the formulations were analyzed for particle size distribution, moisture content,

drug loading and zeta potential. Additionally, the nanoamorphous spironolactone formulations were also analyzed using DSC and PXRD (to monitor any polymorphic transformation *i.e.* conversion of one crystalline form to other), AFM (to understand the surface topology and interaction between drug and stabilizer), ATR-FTIR (to investigate interaction between drug and stabilizer), PLM (to monitor any generation of non-crystallinity or amorphous particles) and *in vitro* dissolution testing (to study the effect of particle size, solid-state form, temperature and humidity on drug release).

5.6.3 Particle size distribution and Moisture content

As shown in Table 5.9 and Figure 5.7, the particle size, PDI and moisture content of the prepared spray-dried nanoamorphous spironolactone increased following one, three and six month/s storage under both conditions: 25°C/60% RH and 40°C/75% RH. The moisture content significantly increased for the formulations stored at 25°C/60% RH and 40°C/75% RH (to 3.5 and 4.25%, respectively) after six months. This can be compared to the formulations stored at 4°C which had the same moisture content as the initial formulations (1.5%). It was observed that at the high relative humidity (60% and 75%), the nanoamorphous (thermodynamically metastable form) converted to the crystalline form (thermodynamically stable) due to plasticization caused by high moisture. This physical instability was observed as a result of significant aggregation (increase in particle size) in nanoamorphous spironolactone formulations stored at 25°C/60% RH and 40°C/75% RH conditions (at all timepoints). On the other hand, the optimized formulations stored at 4°C were determined to be stable in terms of particle size distribution, moisture content and zeta potential over the six month storage stability.

5.6.4 Powder X-ray diffraction

The characteristic diffraction peaks of neat macrocrystalline spironolactone (most stable - polymorphic form II) were 9.5°, 11.9°, 12.7°, 17.05°, 18.7°, 20.5°, 23.1°, 26.3°, 29.6°, and 35.4° [11]. All formulations and marketed drug products showed characteristic PXRD diffraction peaks similar to the form II of spironolactone indicating their crystalline nature, except for the macro- and nanoamorphous spironolactone (Figure 5.8a). The macro- and nanoamorphous spironolactone displayed a halo pattern indicating their amorphous nature.

Additionally the marketed drug products, especially the RLD showed reduced intensity and less number of crystalline diffraction peaks due to the presence of multiple excipients in the drug products, which shadows the drug's crystalline diffraction peaks.

It was observed that the spray-dried nanoamorphous spironolactone formulations displayed a halo pattern for day zero, one and six month/s at 4°C indicating a stable amorphous form (Figure 5.8b). However, the formulations stored at 25°C/60% RH and 40°C/75% RH after one month showed the appearance of crystalline diffraction peaks (conversion of amorphous to crystalline form) which sharpened and increased in intensity after six months. The thermodynamically metastable amorphous form plasticized in the presence of high humidity (60% RH and 75% RH) and converted to the stable crystalline form.

Multiple crystalline diffraction peaks were observed at all conditions for the generic spironolactone drug product compared to the neat drug due to the presence of multiple excipients in addition to the drug (Figure 5.8c). However, most of the crystalline diffraction peaks relevant to the form II of the drug were clearly identified at all stability conditions for the generic spironolactone. Additionally, the generic drug product stored at 25°C/60% RH and 40°C/75% RH (1 and 6 month/s) showed reduced intensity diffraction peaks compared to that stored at 4°C (1 and 6 months) and day zero. The conversion of the form II anhydrous to the form II hydrate in the presence of high humidity is considered to be the reason for the reduced intensity in the diffraction peaks for the generic drug product stored at 25°C/60% RH and 40°C/75% RH (1 and 6 month/s).

The crystalline diffraction peaks observed for all conditions in the RLD spironolactone are scarce and with reduced intensity due to multiple excipients present in the drug product which shadows the drug's crystalline diffraction peaks (Figure 5.8d). Additionally, the low intensity diffraction profiles of the RLD is due to the presence of a mixture of crystalline and amorphous drug forms.

5.6.5 Attenuated total reflectance – Fourier transform infrared spectroscopy

Spironolactone has three carbonyl groups which show characteristics absorbance in FTIR (carbonyl stretching bond of the lactone (C=O) – 1670 cm^{-1}, 6-membered ring (C=O) – 1690 cm^{-1} and thioacetyl (C=O) – 1765 cm^{-1}) [14-16]. In addition, the drug also shows

characteristic absorbance at 1618 cm^{-1} due to –C=C– stretching of the α, β-unsaturated ring and at 2950 cm^{-1} due to –C=H stretching. Any interaction (hydrogen bonding or hydrophobic) of the drug with the stabilizer can significantly influence these peaks (either shift in the wavenumber or change (increase/decrease) in the intensity) [17].

A broad band was observed between 3000-3500 cm^{-1} in the FTIR spectra for the spray-dried nanoamorphous spironolactone which was missing in the neat drug and the physical mixture (Figure 5.9a and 5.9b). Additionally, the generic and RLD spironolactone showed this broad band with two peaks at 3400 cm^{-1} and 3500 cm^{-1}. The band broadening is considered to be due to hydrogen bonding between the: *(1)* –C=O moiety of the drug and the –OH group of the sugar; and *(2)* –SH moiety of the drug and the –OH group of the sugar. The three carbonyl (–C=O) moieties and one sulfhydryl (–SH) group of spironolactone form hydrogen bonding with the multiple hydroxyl (–OH) groups of the trehalose.

All three carbonyl groups of the drug were significantly affected *via* interaction (H-bonding) between the drug and the stabilizers (Figure 5.9c). This caused reduction in the absorbance intensity of the characteristic carbonyl peaks (1670, 1690 and 1765 cm^{-1}) in the nanoamorphous, generic and RLD spironolactone compared to the strong intensity of these peaks in the neat drug and the physical mixture. The peaks at 1670 and 1690 cm^{-1} were absent in the nanoamorphous spironolactone. In addition there is significant reduction in peak intensity (1618 cm^{-1} related to –C=C– stretching) in the nanoamorphous and generic spironolactone compared to the rest of the samples.

The neat drug and the physical mixture showed a medium intensity absorbance peak at 1440 cm-1 (due to CH_2 bending, CH_3 bending and OH bending) which is not present in the nanoamorphous, generic and RLD spironolactone (Figure 5.9d). A strong intensity absorbance peak at 1380 cm-1 (due to C-H bending, S=O stretching, OH bending) was observed in the neat drug and physical mixture samples which was not observed in the other samples. Three strong intensity absorbance peaks (1350 cm-1 (CH3 bending, SO stretching, C-O stretching), 1330 cm-1 (OH bending) and 1265 cm-1(C-O stretching)) were observed in the neat drug and physical mixture which were reduced in intensity (1265 cm-

1 and 1330 cm-1) or absent (1350 cm-1) in the nanoamorphous, generic and RLD spironolactone (Figure 5.9e).

The absence or reduced intensity of this peaks in the nanoamorphous, generic and RLD spironolactone could be possibly due to strong interaction between the drug and the stabilizers. The nanoamorphous spironolactone is prepared via sonoprecipitation followed by spray drying. The generic and RLD spironolactone are also prepared by one of the amorphous solid dispersion manufacturing process. Amorphous solid dispersions are dispersions of solid amorphous drug which is in the molecularly dispersed state (homogenous glass solution) in the amorphous stabilizer matrix with strong interactions (H-bonding and hydrophobic interactions) between the drug and the stabilizers.

In the stability formulations, the strong interaction (hydrogen bonding) between the neat drug and the stabilizers (Dowfax2A1 and trehalose) in the nanoamorphous formulations results in a broad band between 3600-3000 cm^{-1} (Figure 5.10a). Furthermore, the FTIR finger print was completely different for the neat drug and the nanoamorphous spironolactone formulations in the 1950-500 cm^{-1} region.

An additional peak was observed at 3500 cm^{-1} in the nanoamorphous spironolactone stored at 40°C/75% RH post six months which was absent in all other formulations as well as the neat drug (Figure 5.10b). Furthermore, there was a peak shift from 1765 cm^{-1} (neat drug and nanoamorphous spironolactone (day zero and 4°C/6 months)) to 1775 cm^{-1} (formulations stored at 25°C/60% RH and 40°C/75% RH for six months) (Figure 5.10c). The appearance of the new peak and the peak shift was due to the polymorphic transition (amorphous anhydrate form II to crystalline hydrate form II) in the nano-formulations stored at high humidity (60 and 75% RH) post six months.

5.6.6 Polarized light microscopy

It is required that spironolactone nanoemulsions should be completely amorphous before spray drying. All nanoemulsions were observed under PLM and no birefringence (crystallinity) was observed before spray drying (data not shown). After spray drying, the crystallinity was critically monitored for all formulations and this is discussed below.

All images (Figure 5.11a) showed sharp birefringence (shiny colored crystals), except the nanoamorphous spironolactone which lacked the birefringence (dull black particles). The large rod, plate and prism shaped crystals (sharp birefringence) were observed for the neat drug (macrocrystalline spironolactone - 20μ particle size) (Figure 5.11b). The physical mixture (spironolactone, Dowfax2A1 and trehalose in the same ratios as the optimized formulations) showed sharp birefringence. The spray-dried nanoamorphous spironolactone formulations (day zero and 4°C/6 months) showed lack of birefringence (dull black particles) due to the complete amorphous nature of the formulations.

The large rod, plate and prism shaped crystalline drug macroparticles are broken down to amorphous nanoparticles stabilized *via* the surfactant (during sonoprecipitation) which are further stabilized with the sugar (during spray drying). The stabilizers (surfactant-sugar complex) maintain the nanoamorphous nature of the formulation with specific morphology throughout the manufacturing process. Spray-dried nanoamorphous spironolactone formulations stored at 25°C/60% RH showed the appearance of limited birefringence after six months which is corroborated by the PXRD diffraction profiles. Furthermore, prominent birefringence was observed after six months in the spray-dried nanoamorphous spironolactone formulations stored at 40°C/75% RH. The amorphous form of the drug converts into the crystalline form due to plasticization effect as a result of increase in the relative humidity leading to nanoparticle aggregation (verified by the particle size increase observed in the formulations stored at high humidity (60% RH and 75% RH)) for six months. There is increase in the free volume of the amorphous nanoparticles due to the presence of high moisture/high humidity (plasticization effect of water) resulting in an increase in the molecular mobility [18]. This results in a decrease in the viscosity and glass transition temperature (Tg) of the nanoamorphous particles leading to an increased possibility of nucleation followed by crystallization. From the DSC analysis, it was observed that the nanoamorphous spironolactone showed a single uniform glass transition temperature at 91°C (no melting endotherm) indicating a homogenous amorphous nature of the drug and the excipients in the solid dispersion. The high humidity during the storage stability (60% RH and 75% RH) results in a polymorphic transition (amorphous to crystalline) leading to the appearance of multiple glass transition peaks due to separation of the amorphous sugar-surfactant stabilizer complex from the amorphous drug.

5.6.7 Atomic Force Microscopy

Based on the AFM analysis, the spray dried nanoamorphous spironolactone was homogenous with spherical shape and uniform particle size (200-300 nm) compared to the neat drug which possesses angular and prism shaped crystals (Figure 5.12). The generic and RLD spironolactone displayed macrocrystalline and irregular shaped crystals.

5.6.8 *In vitro* dissolution testing

The spray dried nanoamorphous powder showed superior *in vitro* release characteristics compared to the macroamorphous as well as the nanocrystalline and macrocrystalline spironolactone powder formulations (Figure 5.13). The nanoamorphous spironolactone reached maximum saturation concentration (*i.e.* approximately 20 μg/mL) within 30 minutes compared to the macroamorphous spironolactone (approximately 12 μm), which took almost 10 h to reach maximum drug concentration. The nanocrystalline and macrocrystalline spironolactone powder formulations took approximately 12 and 24 h, respectively to reach equilibrium solubility (*i.e.* 20 μg/mL). Following 2 h of *in vitro* dissolution testing, the nanocrystalline (784 nm), macroamorphous (12 μm) and nanoamorphous spironolactone (251 nm) formulations showed a 2-fold, 4.5-fold and 10-fold increase in the saturation solubility compared to the macrocrystalline spironolactone (20 μm). The nanoamorphous spironolactone showed superior *in vitro* release characteristics (90% in 15 min) compared to the marketed products (90% in 45-60 min). Additionally, the generic and RLD spironolactone showed faster dissolution rates compared to the macrocrystalline, macroamorphous and nanocrystalline spironolactone (Figure 5.13).

The nanoamorphous spironolactone formulations (day zero and those stored for six months at 4°C) maintained the supersaturation of the drug during 6 h of *in vitro* dissolution testing (Figure 5.14). At high humidity (60% RH and 75% RH) there was a polymorphic transition (amorphous to crystalline) due to the plasticization effect of the moisture on the nanoamorphous formulations. This significantly affected the dissolution profiles of the nanoamorphous formulations stored for six months (25°C/60% RH and 40°C/75% RH). The drug release was reduced significantly to approximately 70% and 40% for the nano-

formulations stored at 25°C/60% RH and 40°C/75% RH, respectively. There was a drop in the supersaturation for these nano-formulations within 45-60 min. The formulations stored for 25°C/60% RH and 40°C/75% RH (six months) failed to maintain the supersaturation which can significantly impact drug absorption. The optimized nanoamorphous spironolactone formulations (stored at 4°C for six months) maintained the supersaturation for 6 h, within which the drug can be released and absorbed in the stomach and/or small intestine and reach the systemic circulation to provide the required therapeutic effect [19, 20].

5.7. CONCLUSIONS

This is the first study to develop a robust nanoamorphous drug formulation *via* an *i*CPP-CFPs DoE approach using a labile drug spironolactone (multiple polymorphic forms). This nanoamorphous formulation was stable during both accelerated and long term stability conditions over a six months period. Dowfax2A1 and trehalose were determined to be the best excipients to provide strong stabilization of spironolactone (*via* hydrogen bonding and hydrophobic interaction). The present research shows that the use of orthogonal solid-state tools is extremely important since no single solid-state technique can generate all the necessary critical information on the physicochemical instabilities (nanoparticle aggregation, drug crystallization, polymorphic transition) of nanoamorphous formulations. Using these orthogonal research tools, two critical polymorphic transitions (anhydrous to hydrate and amorphous to crystalline) were identified which may occur during the processing and storage stability studies of labile BCS class II ad II/IV drugs. The nanoamorphous spironolactone prepared *via* an *i*CPP-CFPs DoE approach showed superior supersaturation and faster drug dissolution rate (90% in 15 min) compared to the marketed drug products (RLD and generic) (90% in 45-60 min). In the present research, 80-90% w/w of the total product yield of spray-dried nanoamorphous spironolactone was achieved. For a lab-scale spray dryer, total product yield above 80% w/w is remarkable since industrial pilot level spray dryers have maximum total product yield of 50-55% w/w. This study will aid formulation scientists to apply novel strategies to develop nanoamorphous products of labile drugs compared to the conventional trial and error techniques utilized currently in drug product development.

The present research provides important information on: *(1)* selection of suitable crystallization inhibitors (stabilizing excipients); *(2)* selection of appropriate manufacturing techniques; and *(3)* critical process and product controls that significantly impact the physicochemical attributes of the nanoamorphous drug products. In addition, exposure of the nanoamorphous drug products to high relative humidity/ high moisture should be avoided to ensure complete product stability throughout the shelf life. Therefore, it is necessary to take precautionary handling measures for labile APIs from the first step to the last step of the product development. The present research can be applied to the other labile BCS class II and II/IV drugs.

5.8. Tables

Table 5.1. Chemical structures of the active pharmaceutical ingredient and excipients

Materials	Chemical structures
Zileuton	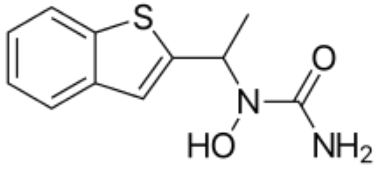
KollidonVA64 fine	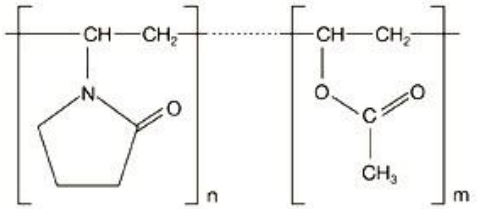
Dowfax 2A1	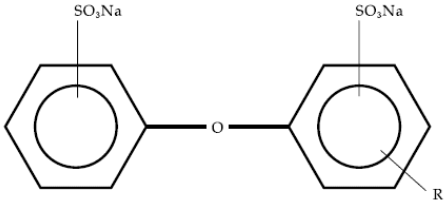
Trehalose	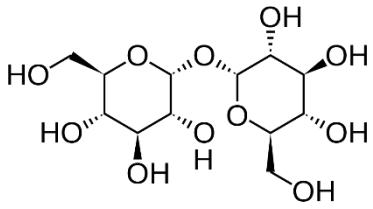

Table 5.2. A DoE Design space for optimization of the wet media milling critical process parameters for the preparation of stable nanocrystalline zileuton.

No.	CPPs (wet media milling)		
	Milling speed	Pump speed	Milling time
	rpm	rpm	min
-	500-1500	80-120	15-30
1	159	100	22.5
2	1500	80	30
3	1500	120	15
4	1500	120	30
5	1500	80	15
6	1000	100	22.5
7	1000	100	10
8	1000	100	22.5
9	1000	100	22.5
10	1000	134	22.5
11	1000	66	22.5
12	1841	100	22.5
13	500	120	15
14	1000	100	22.5
15	1000	100	35

16	500	120	30
17	1000	100	22.5
18	500	80	30
19	1000	100	22.5
20	500	80	15

Table 5.3a. A DoE Design space for optimization of the spray drying critical process parameters for the preparation of stable nanocrystalline zileuton using **mannitol** as the sugar stabilizer (drug:sugar – 1:1, w/w).

No.	CPPs (spray drying with mannitol)		
	Inlet temperature	Aspirator rate	Feed flow rate
	°C	%	%
-	**105-125**	**70-90**	**10-25**
1	115	80	18
2	132	80	18
3	115	80	18
4	105	70	25
5	115	80	18
6	115	80	30
7	105	90	25
8	115	63	18
9	105	70	10
10	115	80	18
11	115	80	5
12	98	80	18
13	125	70	25
14	105	90	10
15	125	90	25
16	115	80	18
17	115	80	18
18	115	97	18
19	125	90	10
20	125	70	10

Table 5.3b. A DoE Design space for optimization of the spray drying critical process parameters for the preparation of stable nanocrystalline zileuton using **trehalose** as the sugar stabilizer (drug:sugar – 1:1, w/w).

No.	CPPs (spray drying with trehalose)		
	Inlet temperature	Aspirator rate	Feed flow rate
	°C	%	%
-	**105-125**	**70-90**	**10-25**
1	115	80	18
2	132	80	18
3	115	80	18
4	105	70	25
5	115	80	18
6	115	80	30
7	105	90	25
8	115	63	18
9	105	70	10

10	115	80	18
11	115	80	5
12	98	80	18
13	125	70	25
14	105	90	10
15	125	90	25
16	115	80	18
17	115	80	18
18	115	97	18
19	125	90	10
20	125	70	10

Table 5.4a. A DoE Design space for the optimization of critical formulation parameters for the preparation of stable nanocrystalline zileuton post wet media milling.

No.	CFPs		
	Drug concentration	**Polymer concentration**	**Surfactant concentration**
	% w/v	**% w/v**	**% w/v**
-	**0.35-1**	**0.3-0.8**	**0.03-0.08**
1	1	0.3	0.08
2	0.675	0.55	0.005
3	1.325	0.55	0.055
4	0.675	0.55	0.055
5	1	0.3	0.08
6	1	0.3	0.03
7	0.675	1.05	0.055
8	0.675	0.55	0.055
9	0.675	0.55	0.055
10	0.35	0.8	0.08
11	0.675	0.55	0.055
12	1	0.8	0.08
13	0.675	0.55	0.055
14	0.675	0.55	0.105
15	0.35	0.3	0.03
16	0.675	0.05	0.055
17	0.35	0.8	0.08
18	1	0.8	0.03
19	0.35	0.8	0.03
20	0.35	0.3	0.08
21	0.35	0.3	0.03
22	0.025	0.55	0.055
23	0.675	0.55	0.055
24	0.35	0.8	0.03
25	1	0.3	0.03
26	1	0.8	0.08
27	0.35	0.3	0.08
28	0.675	0.55	0.055
29	0.675	0.55	0.055
30	1	0.8	0.03

Table 5.4b. A DoE Design space for the optimization of critical formulation parameters for the preparation of stable nanocrystalline zileuton post spray drying.

No.	CFPs			
	Drug concentration	**Polymer concentration**	**Surfactant concentration**	**Sugar amount**
	% w/v	**% w/v**	**% w/v**	**mg**
-	**0.35-1**	**0.3-0.8**	**0.03-0.08**	**850-2000**
1	1	0.8	0.03	2000
2	0.35	0.3	0.03	2000
3	0.35	0.3	0.08	850
4	0.675	0.55	0.055	1425
5	0.35	0.8	0.03	2000
6	0.35	0.3	0.03	850
7	1	0.3	0.03	2000
8	1	0.8	0.08	850
9	0.675	0.05	0.055	1425
10	0.675	0.55	0.055	2575
11	1	0.8	0.08	2000
12	0.675	0.55	0.055	1425
13	0.675	1.05	0.055	1425
14	0.35	0.8	0.08	2000
15	0.35	0.3	0.08	2000
16	0.675	0.55	0.055	1425
17	1	0.3	0.03	850
18	1	0.3	0.08	2000
19	0.675	0.55	0.055	275
20	0.35	0.8	0.08	850
21	0.675	0.55	0.105	1425
22	0.675	0.55	0.055	1425
23	1	0.3	0.08	850
24	0.675	0.55	0.055	1425
25	0.675	0.55	0.055	1425
26	1	0.8	0.03	850
27	0.025	0.55	0.055	1425
28	1.325	0.55	0.055	1425
29	0.35	0.8	0.03	850
30	0.675	0.55	0.005	1425

Table 5.5. Solubility of zileuton in different excipient solutions

Sample Number	Excipient solution (0.2% w/v)	Type of Stabilizer	Zileuton solubility (µg/mL)	Solubility (times X)
1	No excipient	N/A	130.2	-
2	Dowfax2A1	Anionic surfactant	165.2	1
3	SLS	Anionic surfactant	144.43	
4	Poloxamer P407	Nonionic surfactant	165.2	
5	Poloxamer 188	Nonionic surfactant	135.12	
6	EC 10	Nonionic polymer	187.905	1.5
7	Kolliphor SLS fine	Anionic surfactant	184.78	
8	Kollidon CLM	Nonionic polymer	197.97	
9	PVP K17	Nonionic polymer	241.41	2
10	PVP K25	Nonionic polymer	262.52	
11	PVP K30	Nonionic polymer	258.35	
12	PVP K90	Nonionic polymer	282.75	
13	HPMC K3	Nonionic polymer	258.94	
14	KollidonVA64	Nonionic polymer	254.74	
15	KollidonVA64 fine	Nonionic polymer	242.55	
16	HPMC E3	Nonionic polymer	319.32	2.5
17	HPMC E5	Nonionic polymer	327.01	
18	HPMC E15	Nonionic polymer	338.45	
19	HPMC E50	Nonionic polymer	344.9	
20	MC A15	Nonionic polymer	346.68	
21	Soluplus	Nonionic polymer	391.64	3

Table 5.6a. Results of DoE runs for optimization of the wet media milling critical process parameters for the preparation of stable nanocrystalline zileuton (3 CPPs x 3 CQAs).

Wet media milling DoE						
No.	CPPs			CQAs		
	Milling speed	Pump speed	Milling time	Particle size	PDI	Zeta potential
	rpm	rpm	min	nm	units	mV
-	500-1500	80-120	15-30			
1	159	100	22.5	212.3	0.26	-78.3
2	1500	80	30	29.16	0.322	-62.1
3	1500	120	15	135	0.235	-66.8
4	1500	120	30	65.7	0.156	-57.4
5	1500	80	15	85.24	0.145	-63.6
6	1000	100	22.5	214.5	0.187	-71.9
7	1000	100	10	431.3	0.112	-76.3
8	1000	100	22.5	200.4	0.237	-64.6
9	1000	100	22.5	214.3	0.136	-57.1

10	1000	134	22.5	130.5	0.219	-68.8
11	1000	66	22.5	174.2	0.121	-69.3
12	1841	100	22.5	37.13	0.228	-42.2
13	500	120	15	306	0.136	-82.9
14	1000	100	22.5	157.1	0.163	-72.8
15	1000	100	35	145.9	0.17	-74.9
16	500	120	30	182.1	0.13	-73.7
17	1000	100	22.5	245.4	0.459	-74.7
18	500	80	30	274.2	0.197	-47.2
19	1000	100	22.5	271.5	0.218	-77.6
20	500	80	15	269	0.136	-82

Table 5.6b. ANOVA table for CQA: Particle size of nanocrystalline zileuton post wet media milling

Particle size ➔ ANOVA for Response Surface Quadratic model						
Source	**Sum of Squares**	**df**	**Mean Square**	**F Value**	**p-value Prob > F**	
Model	1.563E+005	9	17362.87	6.73	0.0032	**significant**
A-Milling speed	74813.42	1	74813.42	28.99	0.0003	R^2=0.9519, Adjusted R^2=0.9478
B-Pump speed	130.98	1	130.98	0.051	0.8263	
C-Milling time	38388.65	1	38388.65	14.88	0.0032	
AB	2499.25	1	2499.25	0.97	0.3483	
AC	5.58	1	5.58	2.162E-003	0.9638	
BC	2531.87	1	2531.87	0.98	0.3453	
A^2	19311.12	1	19311.12	7.48	0.0210	
B^2	10378.25	1	10378.25	4.02	0.0727	
C^2	6560.44	1	6560.44	2.54	0.1419	
Lack of Fit	18150.64	5	3630.13	2.37	0.1826	***not significant***
Particle size (nm) = +217.80 – 74.01A – 3.1B – 53.02C + 17.68AB – 0.83AC – 17.79BC – 36.61A^2 – 26.84B^2 + 21.34C^2						

Table 5.6c. Statistically predicted CPPs and CQAs based on the wet media milling DoE studies

CPPs			**CQAs**			**Desirability**
Milling speed (rpm)	**Milling time (min)**	**Pump speed (rpm)**	**Particle size (nm)**	**PDI (units)**	**Zeta potential (mV)**	
1200	30	92	225	0.198	-67.99	0.898

Table 5.7a. Results of DoE runs for optimization of the spray drying critical process parameters (stabilizer: mannitol) for the preparation of stable nanocrystalline zileuton (3 CPPs x 7 CQAs).

Spray drying DoE (Stabilizer: Mannitol)										
No.	**CPPs**			**CQAs**						
	Inlet temperature	**Aspirator rate**	**Feed flow rate**	**Outlet temperature**	**Particle size**	**PDI**	**Zeta potential**	**Drug loading**	**Yield**	**Moisture content**
	°C	**%**	**%**	**°C**	**nm**	**units**	**mV**	**% (w/w)**	**% (w/w)**	**%**
-	**105-125**	**70-90**	**10-25**							
1	115	80	18	51	1084.00	0.098	-95.200	38.554	64.174	0.850
2	132	80	18	60	1285.00	0.140	-73.600	33.764	66.957	0.745
3	115	80	18	48	748.30	0.521	-11.000	33.582	61.739	0.745
4	105	70	25	40	7259.00	0.866	-25.000	39.163	58.696	0.592
5	115	80	18	51	222.50	0.257	-20.000	35.611	56.348	1.013
6	115	80	30	46	169.50	0.125	-85.300	39.513	60.174	1.252
7	105	90	25	48	165.50	0.205	-99.600	40.656	64.348	0.684
8	115	63	18	47	180.70	0.289	-12.000	35.928	62.000	0.774
9	105	70	10	60	167.40	0.164	-13.000	43.318	75.478	0.828
10	115	80	18	51	1144.00	0.539	-24.000	35.656	62.696	0.980
11	115	80	5	74	1131.00	0.373	-20.000	34.833	67.043	0.518
12	98	80	18	37	5779.00	0.901	-36.000	37.959	60.174	0.767
13	125	70	25	51	515.00	0.509	-42.000	41.774	54.174	0.711
14	105	90	10	67	266.60	0.523	-37.000	37.438	84.000	0.815
15	125	90	25	58	158.50	0.241	-11.000	41.575	60.609	0.683
16	115	80	18	51	586.40	0.329	-15.000	36.752	74.522	1.208
17	115	80	18	50	1071.00	0.967	-19.000	40.331	57.391	1.133
18	115	97	18	60	172.70	0.306	-21.000	36.959	87.739	0.639
19	125	90	10	74	356.70	0.613	-35.000	42.574	75.652	0.424
20	125	70	10	68	191.10	0.421	-22.000	38.324	85.913	0.480

Table 5.7b. ANOVA table for CQA: Total product yield of nanocrystalline zileuton (solid powder) post spray drying (with mannitol)

Total product yield ➔ ANOVA for Response Surface Reduced Cubic model						
Source	**Sum of Squares**	**df**	**Mean Square**	**F Value**	**p-value Prob > F**	
Model	1684.42	10	168.44	5.94	0.0066	**significant**
A-Inlet temperature	23.00	1	23.00	0.81	0.3913	R^2=0.9694, Adjusted R^2=0.9622
B-Aspirator rate	331.25	1	331.25	11.68	0.0077	
C-Feed flow rate	23.60	1	23.60	0.83	0.3855	
AB	40.50	1	40.50	1.43	0.2626	
BC	23.90	1	23.90	0.84	0.3826	
B^2	310.54	1	310.54	10.95	0.0091	
ABC	47.85	1	47.85	1.69	0.2263	
A^2B	133.99	1	133.99	4.72	0.0578	
A^2C	231.58	1	231.58	8.17	0.0189	
AB^2	25.76	1	25.76	0.91	0.3654	
Lack of Fit	43.94	4	10.98	0.26	0.8919	***not significant***
Total product yield (% w/w) = +63.85 + 2.02A + 7.65B – 2.04C – 2.25AB +1.73BC +4.6B^2 + 2.45ABC – 6.36A^2B – 8.36A^2C – 2.79AB^2						

Table 5.8a. Results of DoE runs for optimization of the spray drying critical process parameters (stabilizer:trehalose) for the preparation of stable nanocrystalline zileuton (3 CPPs x 7 CQAs).

Spray drying DoE (Stabilizer:Trehalose)										
No.	**CPPs**			**CQAs**						
	Inlet temperature	**Aspirator rate**	**Feed flow rate**	**Outlet temperature**	**Particle size**	**PDI**	**Zeta potential**	**Drug loading**	**Yield**	**Moisture content**
	°C	**%**	**%**	**°C**	**nm**	**units**	**mV**	**% (w/w)**	**% (w/w)**	**%**
-	**105-125**	**70-90**	**10-25**							
1	115	80	18	54	161.70	0.216	-27.00	40.00	59.57	3.36
2	132	80	18	65	231.80	0.517	-29.00	41.25	67.57	3.21
3	115	80	18	56	200.30	0.743	-19.00	36.27	58.61	3.47
4	105	70	25	39	588.10	0.747	-33.00	40.31	58.96	3.45
5	115	80	18	55	152.90	0.235	-11.00	43.06	64.96	3.42
6	115	80	30	50	1316.00	0.779	-17.00	40.04	56.61	4.06
7	105	90	25	50	3646.00	0.569	-19.00	43.64	51.91	3.42
8	115	63	18	53	3069.00	0.741	-10.00	40.64	64.35	3.61
9	105	70	10	60	3223.00	1.000	-16.00	42.23	63.65	3.93
10	115	80	18	55	175.70	0.188	-20.00	45.30	63.30	3.78
11	115	80	5	73	423.20	0.454	-58.60	40.02	59.39	3.07
12	98	80	18	50	1523.00	0.351	-80.20	37.18	45.22	3.87
13	125	70	25	50	1248.00	0.611	-23.00	44.57	60.87	3.31
14	105	90	10	65	1054.00	0.681	-16.00	44.63	74.61	2.71
15	125	90	25	60	964.00	0.930	-14.00	42.83	58.26	3.19
16	115	80	18	55	117.70	0.485	-11.00	42.83	65.39	3.51
17	115	80	18	56	148.10	0.231	-29.00	44.99	70.09	3.37
18	115	97	18	60	284.30	0.595	-12.00	39.64	72.70	3.29
19	125	90	10	75	1221.00	0.424	-88.40	41.24	50.00	2.79
20	125	70	10	70	809.40	0.934	-15.00	38.22	60.00	2.98

Table 5.8b. ANOVA table for CQA: Total product yield of nanocrystalline zileuton (solid powder) post spray drying (with trehalose)

Total product yield ➔ ANOVA for Response Surface Reduced Cubic model						
Source	**Sum of Squares**	**df**	**Mean Square**	**F Value**	**p-value Prob > F**	
Model	907.60	13	69.82	4.57	0.0363	**significant**
A-Inlet temperature	249.71	1	249.71	16.33	0.0068	R^2=0.9082, Adjusted R^2=0.8993
B-Aspirator rate	34.84	1	34.84	2.28	0.1819	
C-Feed flow rate	3.87	1	3.87	0.25	0.6328	
AB	34.12	1	34.12	2.23	0.1859	
AC	166.73	1	166.73	10.90	0.0164	
BC	14.07	1	14.07	0.92	0.3745	
A^2	111.66	1	111.66	7.30	0.0355	
B^2	32.65	1	32.65	2.14	0.1943	
C^2	70.69	1	70.69	4.62	0.0751	
ABC	80.59	1	80.59	5.27	0.0615	
A^2B	42.20	1	42.20	2.76	0.1477	
A^2C	7.02	1	7.02	0.46	0.5234	
AB^2	277.07	1	277.07	18.12	0.0053	

Lack of Fit	3.36	1	3.36	0.19	0.6810	***not significant***
Total product yield (% w/w) = $+63.69 + 6.64A + 2.48B - 0.83C - 2.07AB + 4.57AC - 1.33BC - 2.78A^2 + 1.51B^2 - 2.21C^2 + 3.17ABC - 3.57A^2B - 1.46A^2C - 9.41AB^2$						

Table 5.8c. Statistically predicted CPPs and CQAs based on the spray drying DoE studies

Spray drying DoE (drug:sugar-1:1, w/w)		**Mannitol**	**Trehalose**
CPPs	**Inlet temperature (°C)**	125	118
	Aspirator rate (%)	90	90
	Feed flow rate (%)	10	10
CQAs	**Outlet temperature (°C)**	70	67
	Particle size (nm)	499.24	326.97
	PDI (units)	0.28	0.12
	Zeta potential (mV)	-27.66	-58.18
	Drug loading (% w/w)	41.15	41.28
	Total yield (% w/w)	72.95	63.05
	Moisture content (%)	2.85	0.47
Desirability		0.807	0.967

Table 5.9a. Results of DoE runs for optimization of the critical formulation parameters (wet media milling) for the preparation of stable nanocrystalline zileuton (3 CFPs x 3 CQAs).

Formulation DoE (Wet Media Milling)						
No.	**CFPs**			**CQAs**		
	Drug concentration	**Polymer concentration**	**Surfactant concentration**	**Particle size**	**PDI**	**Zeta potential**
	% w/v	**% w/v**	**% w/v**	**nm**	**units**	**mV**
-	**0.35-1**	**0.3-0.8**	**0.03-0.08**			
1	1	0.3	0.08	174.1	0.266	-71.7
2	0.675	0.55	0.005	346.5	0.336	-68.1
3	1.325	0.55	0.055	125.8	0.224	-69.9
4	0.675	0.55	0.055	383.3	0.263	-79.2
5	1	0.3	0.08	182.8	0.277	-77.6
6	1	0.3	0.03	212.6	0.316	-80.6
7	0.675	1.05	0.055	356.8	0.499	-9.1
8	0.675	0.55	0.055	497.5	0.315	-81
9	0.675	0.55	0.055	397	0.213	-83.7
10	0.35	0.8	0.08	746.1	0.885	-83.2
11	0.675	0.55	0.055	426.6	0.313	-90.1
12	1	0.8	0.08	230.7	0.176	-59
13	0.675	0.55	0.055	434	0.202	-69.1
14	0.675	0.55	0.105	526.7	0.319	-89.8
15	0.35	0.3	0.03	732.8	0.394	-98.1
16	0.675	0.05	0.055	286.3	0.166	-129
17	0.35	0.8	0.08	621	0.462	-74.2
18	1	0.8	0.03	207.6	0.181	-69
19	0.35	0.8	0.03	703.3	0.483	-80.1
20	0.35	0.3	0.08	748.5	0.5	-109
21	0.35	0.3	0.03	613	0.419	-96.3
22	0.025	0.55	0.055	1536	0.45	-112
23	0.675	0.55	0.055	366.3	0.282	-81.3

24	0.35	0.8	0.03	756.2	0.478	-78.1
25	1	0.3	0.03	108.5	0.167	-78.2
26	1	0.8	0.08	133.3	0.225	-55.4
27	0.35	0.3	0.08	667.1	0.434	-107
28	0.675	0.55	0.055	230.9	0.363	-75.8
29	0.675	0.55	0.055	234.1	0.253	-82.6
30	1	0.8	0.03	117.3	0.278	-64.5

Table 5.9b. ANOVA table for CQA: Particle size of nanocrystalline zileuton post wet media milling

Particle size ➔ ANOVA for Response Surface Cubic model						
Source	**Sum of Squares**	**df**	**Mean Square**	**F Value**	**p-value Prob > F**	
Model	2.551E+006	22	1.160E+005	16.86	0.0004	**significant**
A-Drug concentration	9.943E+005	1	9.943E+005	144.60	< 0.0001	R^2=0.9815, Adjusted R^2=0.9233
B-Polymer concentration	2485.13	1	2485.13	0.36	0.5667	
C-Surfactant concentration	16236.02	1	16236.02	2.36	0.1683	
AB	184.28	1	184.28	0.027	0.8746	
AC	594.14	1	594.14	0.086	0.7773	
BC	1578.08	1	1578.08	0.23	0.6465	
A^2	2.911E+005	1	2.911E+005	42.33	0.0003	
B^2	16219.91	1	16219.91	2.36	0.1685	
C2	541.88	1	541.88	0.079	0.7870	
ABC	1711.89	1	1711.89	0.25	0.6331	
A^2B	883.23	1	883.23	0.13	0.7306	
A^2C	9310.26	1	9310.26	1.35	0.2827	
AB^2	41990.59	1	41990.59	6.11	0.0428	
Lack of Fit	8427.93	2	4213.97	0.53	0.6180	***not significant***
Particle size (nm) = +392.58 – 352.55A + 17.62B + 45.05C – 3.39AB + 6.09AC – 9.93BC +103.02A^2 – 24.32B^2 + 4.44C^2 + 10.34ABC – 12.87A^2B – 41.78A^2C + 88.73AB^2						

Table 5.10a. Results of DoE runs for optimization of critical formulation parameters (spray drying) for the preparation of stable nanocrystalline zileuton (4 CFPs x 7 CQAs).

Formulation DoE (spray drying)											
No.	CFPs				CQAs						
	Drug concentration	Polymer concentration	Surfactant concentration	Sugar amount	Outlet temperature	Particle size	PDI	Zeta potential	Drug loading	Total Yield	Moisture content
	% w/v	% w/v	% w/v	mg	°C	nm	units	mV	%	%	%
-	0.35-1	0.3-0.8	0.03-0.08	850-2000							
1	1	0.8	0.03	2000	72	494.1	1	-117	11.75377	48.69	3.68
2	0.35	0.3	0.03	2000	71	1718	0.065	-103	6.539006	63.69	3.456
3	0.35	0.3	0.08	850	68	1756	0.291	-113	12.5826	75.40	3.214
4	0.675	0.55	0.055	1425	68	1472	1	-109	11.98958	54.30	3.18
5	0.35	0.8	0.03	2000	71	658.7	0.855	-106	6.510985	49.85	3.649
6	0.35	0.3	0.03	850	71	1735	0.2	-99.1	10.98196	68.35	3.404
7	1	0.3	0.03	2000	68	1004	0.877	-123	11.00261	59.29	3.457
8	1	0.8	0.08	850	72	694.8	0.781	-107	21.56875	58.25	2.703
9	0.675	0.05	0.055	1425	70	1551	0.679	-101	16.41053	82.69	2.668
10	0.675	0.55	0.055	2575	70	1668	0.927	-114	14.89958	46.00	4.431
11	1	0.8	0.08	2000	72	137.9	0.323	-103	9.036766	52.06	3.82
12	0.675	0.55	0.055	1425	71	1668	0.927	-113	14.21775	65.96	3.611
13	0.675	1.05	0.055	1425	68	1593	1	-94.1	10.57662	40.16	3.858
14	0.35	0.8	0.08	2000	68	2880	0.956	-108	5.346451	42.95	3.729
15	0.35	0.3	0.08	2000	76	852.2	0.233	-99.9	5.612018	58.18	3.663
16	0.675	0.55	0.055	1425	70	1668	0.927	-50.2	11.90832	72.29	3.323
17	1	0.3	0.03	850	68	273.3	0.663	-94.7	31.19071	83.51	2.806
18	1	0.3	0.08	2000	70	171.9	0.177	-130	18.74133	64.15	3.433
19	0.675	0.55	0.055	275	71	1668	0.927	-91	12.25046	65.57	2.857
20	0.35	0.8	0.08	850	68	969.1	0.367	-80.3	9.417043	61.06	3.108
21	0.675	0.55	0.105	1425	68	102.4	0.692	-103	15.849	70.65	3.607
22	0.675	0.55	0.055	1425	71	1582	1	-101	16.11059	55.99	3.499
23	1	0.3	0.08	850	72	146.1	0.414	-43.2	14.40945	85.07	2.98
24	0.675	0.55	0.055	1425	72	898.7	0.786	-76.3	37.93154	52.89	2.728
25	0.675	0.55	0.055	1425	67	317.9	0.642	-90.7	16.26445	54.00	3.003
26	1	0.8	0.03	850	69	368.5	0.697	-86.9	27.06975	59.85	3.17
27	0.025	0.55	0.055	1425	71	3440	0.735	-111	2.75378	48.84	4.421
28	1.325	0.55	0.055	1425	71	196.9	0.455	-102	21.35168	49.52	3.146
29	0.35	0.8	0.03	850	75	1990	0.729	-92.8	8.798703	65.44	4.334
30	0.675	0.55	0.005	1425	72	1718	0.0656	-103	15.95752	73.25	3.166

Table 5.10b. ANOVA table for CQA: Total product yield of nanocrystalline zileuton (solid powder) post spray drying (with trehalose)

Total product yield ➔ ANOVA for Response Surface Quadratic model						
Source	**Sum of Squares**	**df**	**Mean Square**	**F Value**	**p-value Prob > F**	
Model	3492.06	14	249.43	6.19	0.0006	**significant**
A-Drug concentration	31.14	1	31.14	0.77	0.3931	R^2=0.9525, Adjusted R^2=0.9149
B-Polymer concentration	1743.67	1	1743.67	43.29	< 0.0001	
C-Surfactant concentration	1.90	1	1.90	0.047	0.8310	
D-Amount of sugar	1029.61	1	1029.61	25.56	0.0001	
AB	45.14	1	45.14	1.12	0.3065	
AC	20.07	1	20.07	0.50	0.4910	
AD	2.99	1	2.99	0.074	0.7890	
BC	19.09	1	19.09	0.47	0.5016	
BD	15.94	1	15.94	0.40	0.5387	
CD	2.90	1	2.90	0.072	0.7920	
A^2	117.96	1	117.96	2.93	0.1076	
B^2	26.79	1	26.79	0.67	0.4275	
C^2	359.40	1	359.40	8.92	0.0092	
D^2	4.88	1	4.88	0.12	0.7326	
Lack of Fit	285.94	10	28.59	0.45	0.8681	***not significant***
Total product yield (% w/w) = +59.24 + 1.14A – 8.52B – 0.28C – 6.55D – 1.68AB + 1.12AC – 0.43AD – 1.09BC + 1.00BD – 0.43CD – $2.07A^2$ + $0.99B^2$ + $3.62C^2$ – $0.42D^2$						

Table 5.11. Statistically predicted CPPs, CFPs and CQAs based on the formulation DoE

Comprehensive DoEs					
Wet media milling (CPPs)		**Spray drying (CPPs)**		**Formulation (CFPs)**	
Milling speed (rpm)	1200	**Inlet temperature (°C)**	118	**Drug concentration (% w/v)**	1
Milling time (min)	30	**Aspirator rate (%)**	90	**Polymer concentration (% w/v)**	0.3
Pump speed (rpm)	92	**Feed flow rate (%)**	10	**Surfactant concentration (% w/v)**	0.06
				Amount of sugar (mg)	850

CQAs	**Outlet temperature (°C)**	69
	Particle size (nm)	300.03
	PDI (units)	0.126
	Zeta potential (mV)	-80.84
	Drug loading (% w/w)	22.31
	Total yield (% w/w)	77.66
	Moisture content (%)	1.66
Desirability		0.904

Table 5.12. Physicochemical properties of the optimized spray-dried nanocrystalline zileuton formulations following one, six and twelve month/s exposure under different storage conditions.

Testing formulation : Optimized spray-dried nanocrystalline zileuton		**Particle size (nm)**	**PDI (units)**	**Zeta potential (mV)**	**Moisture content (%)**	**Drug loading (% w/w)**
Predicted values		**300.03**	**0.126**	**-80.84**	**1.66**	**22.31**
Experimental values						
0 month	**Initial (n=6)**	**276.4**	**0.109**	**-91.4**	**1.09**	**23.8**
1 month	**4°C**	273.1	0.115	-81.5	0.990	23.71
	25°C/60% RH	619.5	0.589	-103	1.17	23.25
	40°C/75% RH	996.4	0.791	-92.6	1.29	23.31
6 months	**4°C**	275.43	0.12	-79.63	0.994	23.84
	25°C/60% RH	648.91	0.723	-97.64	2.79	23.41
	40°C/75% RH	1013.19	0.817	-94.61	3.29	23.61
12 months	**4°C**	274.16	0.118	-81.2	0.989	23.82
	25°C/60% RH	694.37	0.653	-102	3.19	23.28
	40°C/75% RH	1209.43	0.923	-96.39	4.55	23.81

5.9. Figures

GRAPHICAL ABSTRACT

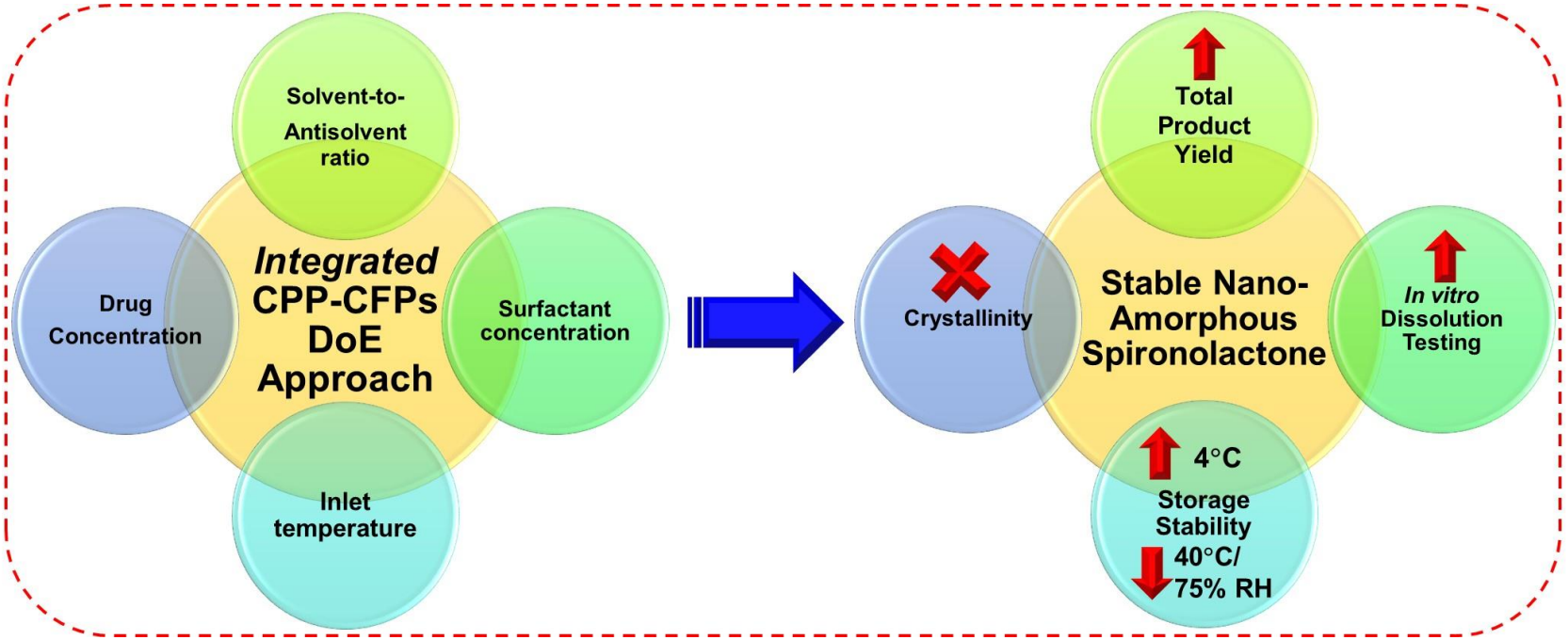

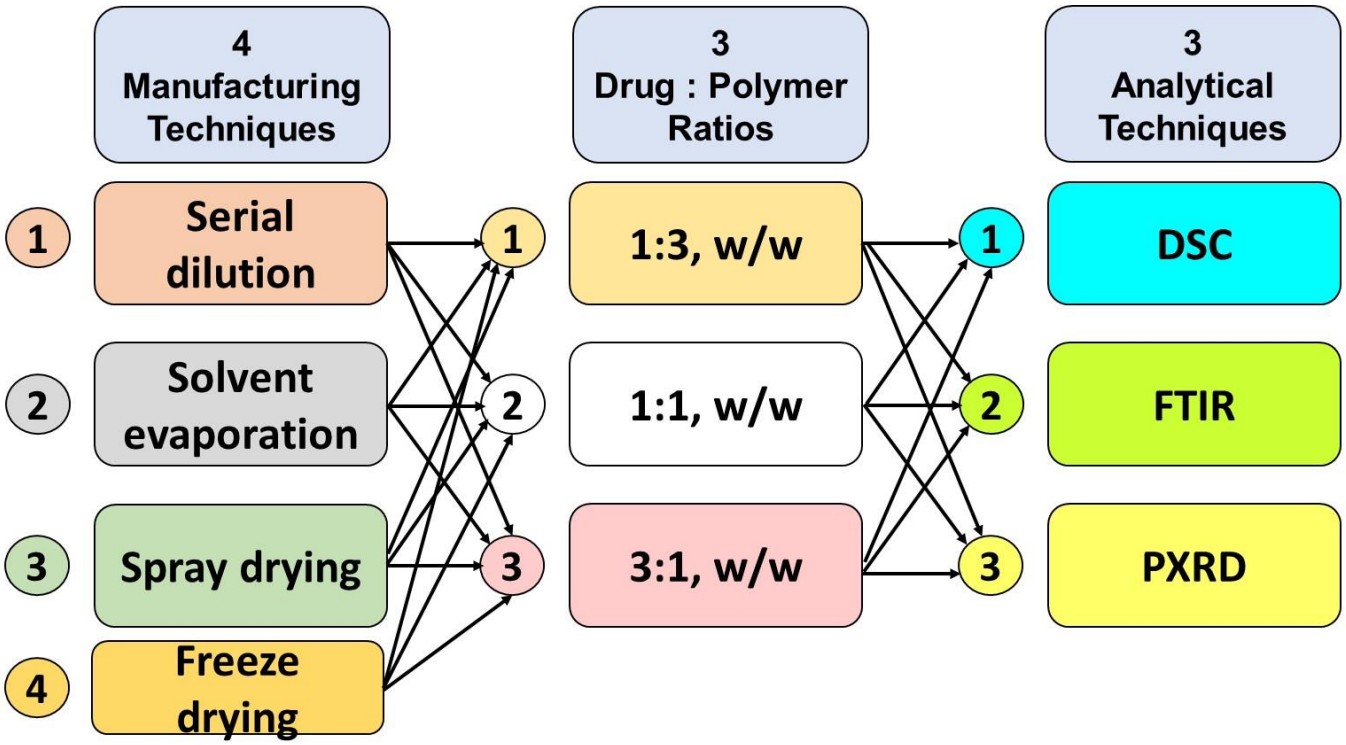

Figure A: Design of Experiments for drug-stabilizer interaction studies (4 manufacturing techniques, 3 drug-stabilizer weight ratios and 3 orthogonal solid-state techniques).

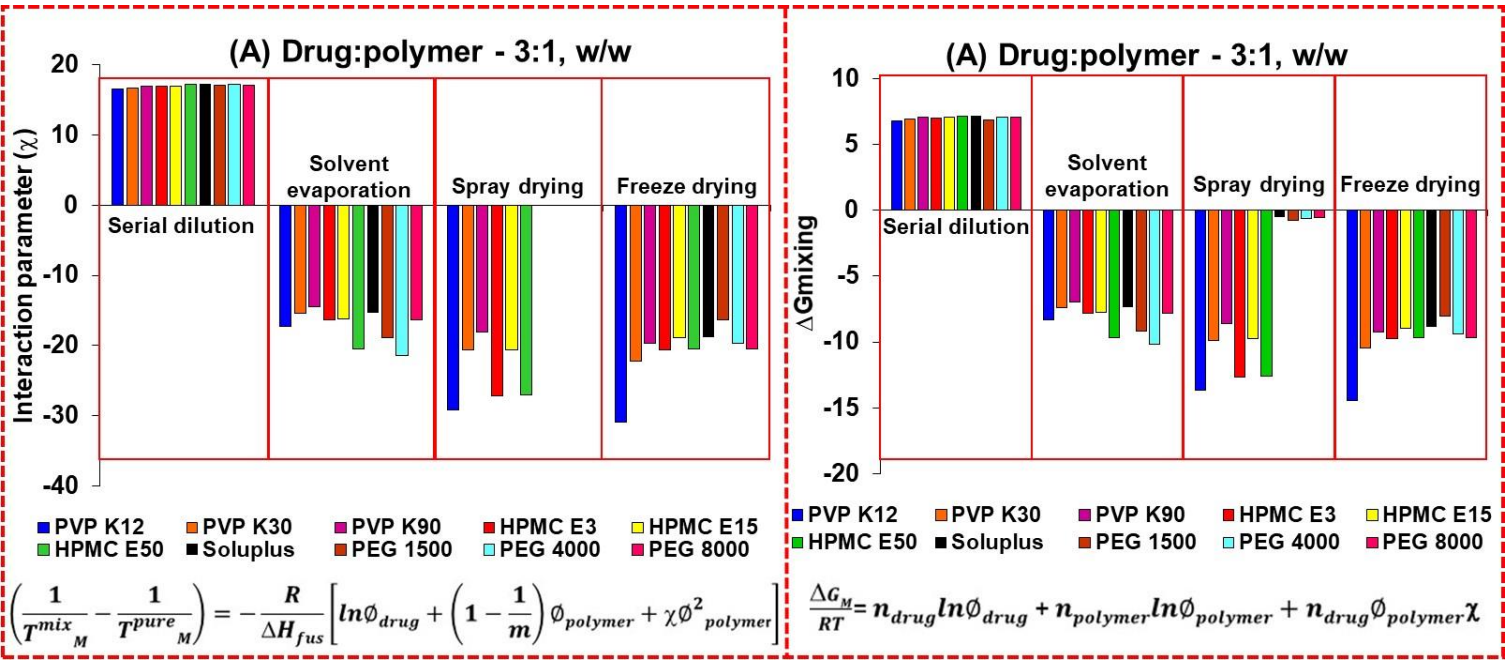

$$\left(\frac{1}{T^{mix}{}_M} - \frac{1}{T^{pure}{}_M}\right) = -\frac{R}{\Delta H_{fus}}\left[ln\emptyset_{drug} + \left(1 - \frac{1}{m}\right)\emptyset_{polymer} + \chi\emptyset^2{}_{polymer}\right]$$

$$\frac{\Delta G_M}{RT} = n_{drug} ln\emptyset_{drug} + n_{polymer} ln\emptyset_{polymer} + n_{drug}\emptyset_{polymer}\chi$$

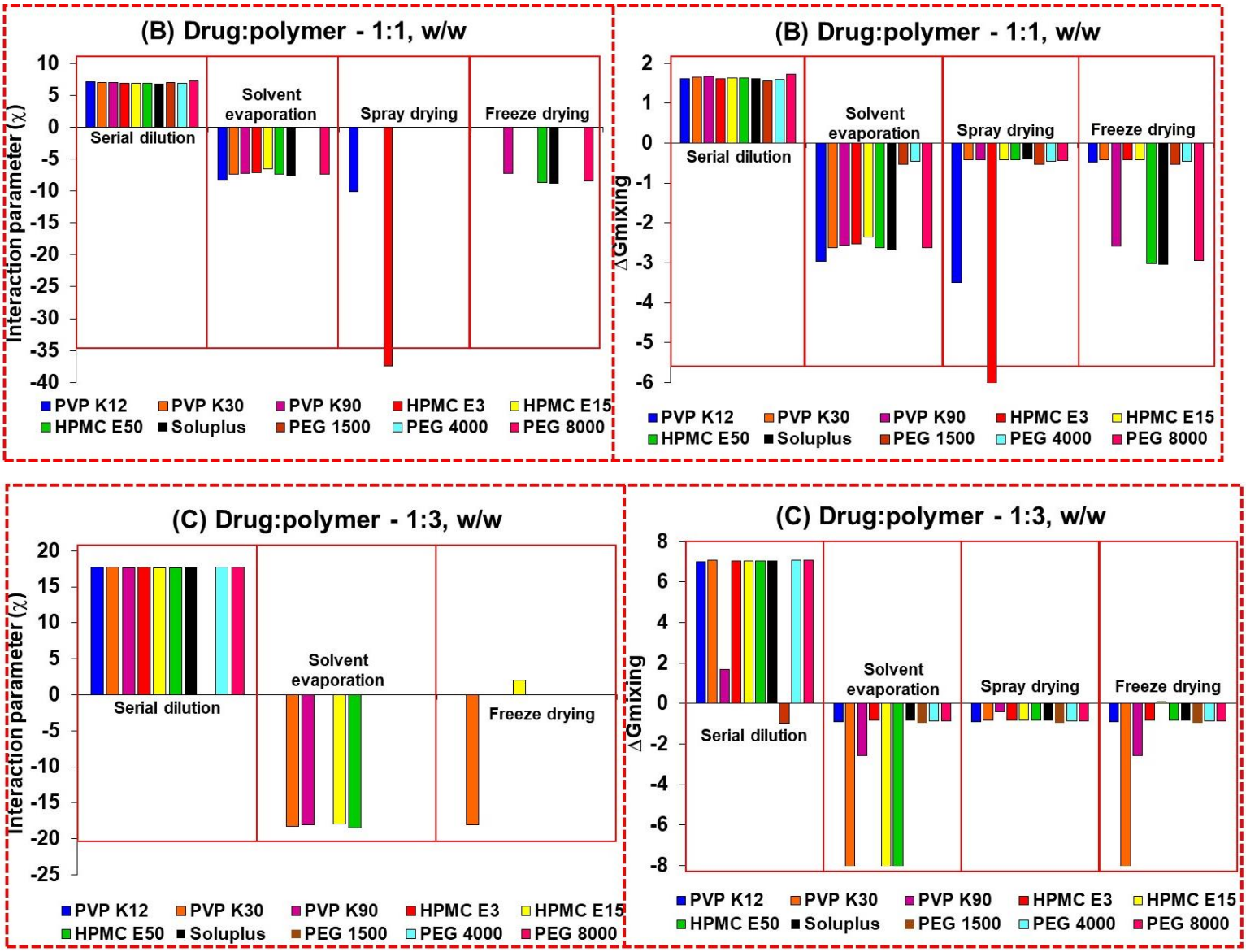

Figure B: Interaction parameter (χ) *vs.* different manufacturing techniques (left) and Free energy of mixing (ΔGm) *vs.* different manufacturing techniques (right) for drug:stabilizer weight ratios: (A) 3:1, w/w; (B) 1:1, w/w; and (C) 1:3, w/w.

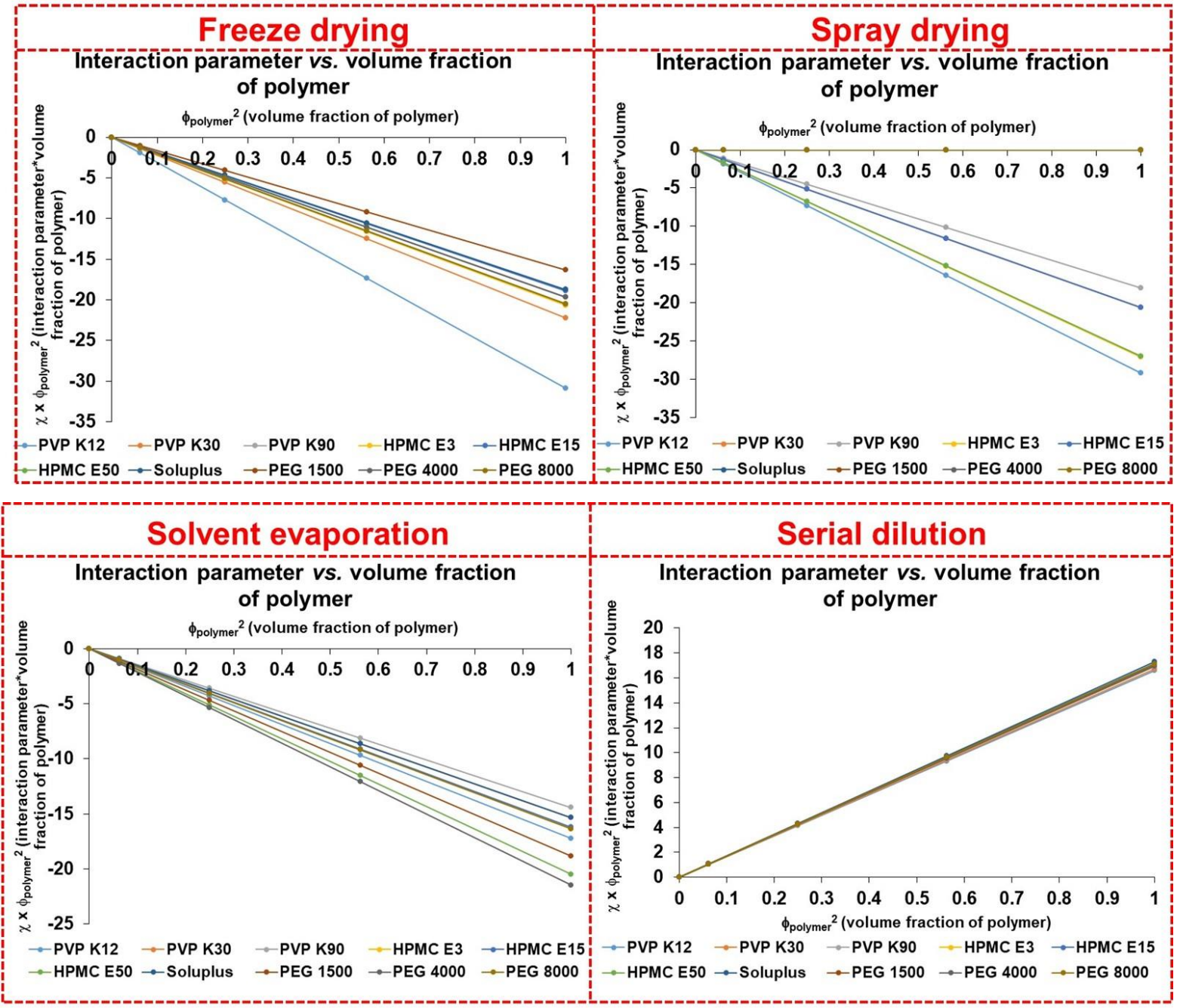

Figure C: Interaction parameter (χ) *vs.* volume fraction of stabilizer (top left – Freeze drying, top right – spray drying, bottom left – solvent evaporation and bottom right – serial dilution).

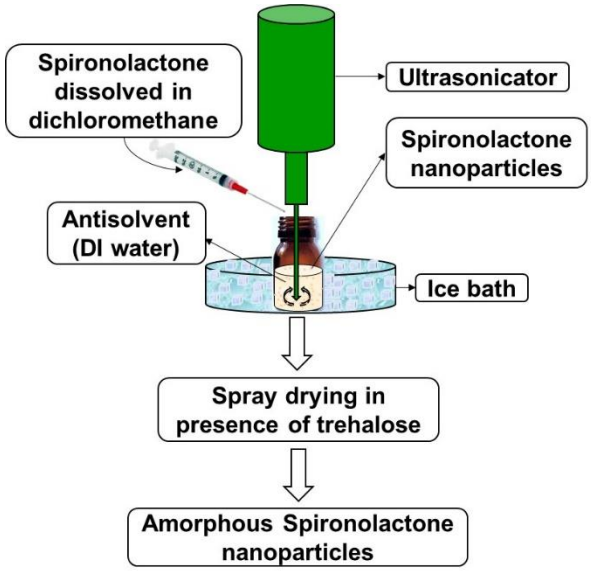

Figure 5.1: Flow diagram for the manufacturing of nano-amorphous spironolactone formulations

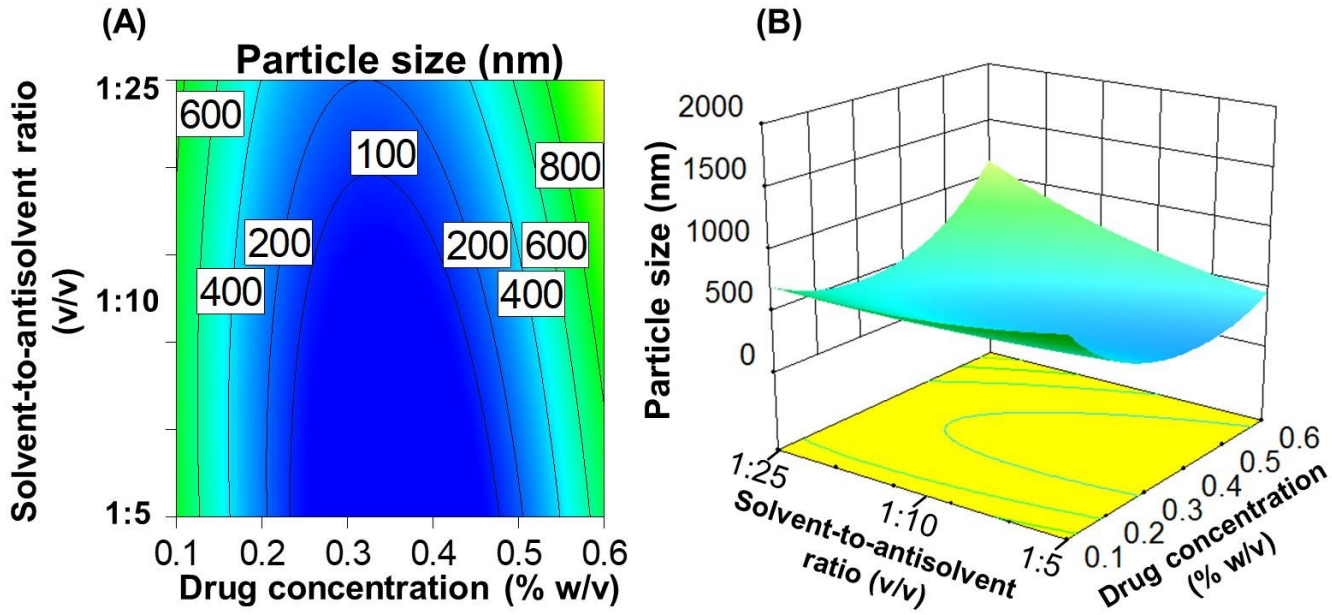

Figure 5.2a. (A) Contour plots and **(B)** 3D surface plots comparing effect of solvent-to-antisolvent ratio and drug concentration on the particle size of nanoamorphous spironolactone.

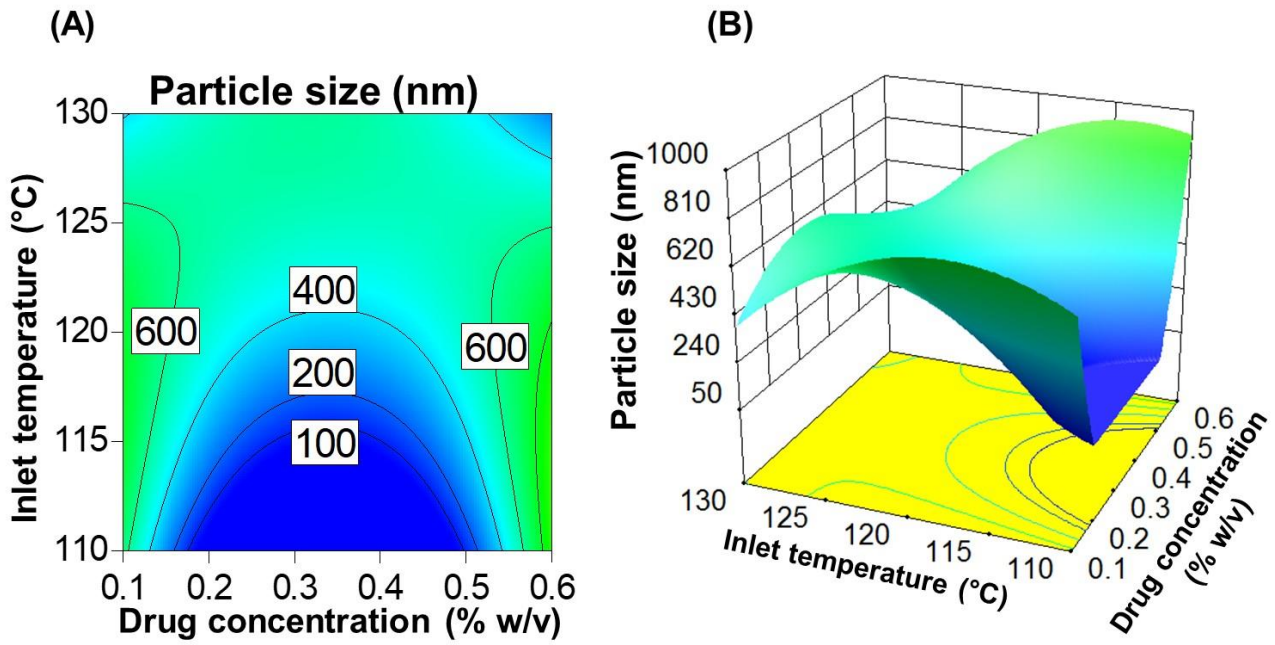

Figure 5.2b. (A) Contour plots and **(B)** 3D surface plots comparing effect of inlet temperature of spray dryer and drug concentration on the particle size of nanoamorphous spironolactone.

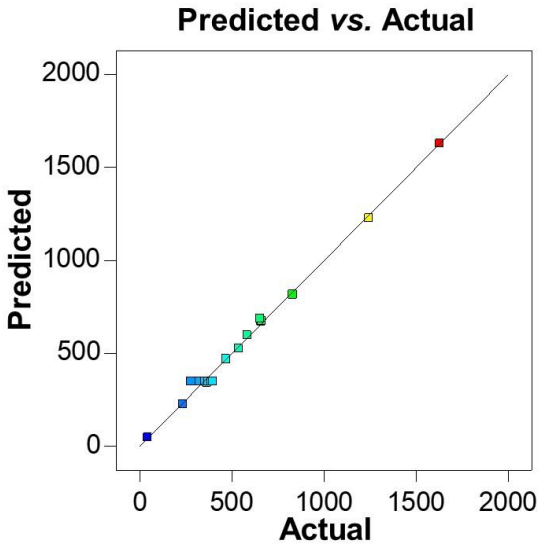

Figure 5.2c. Graph showing model predicted *vs.* actual values of the experiments.

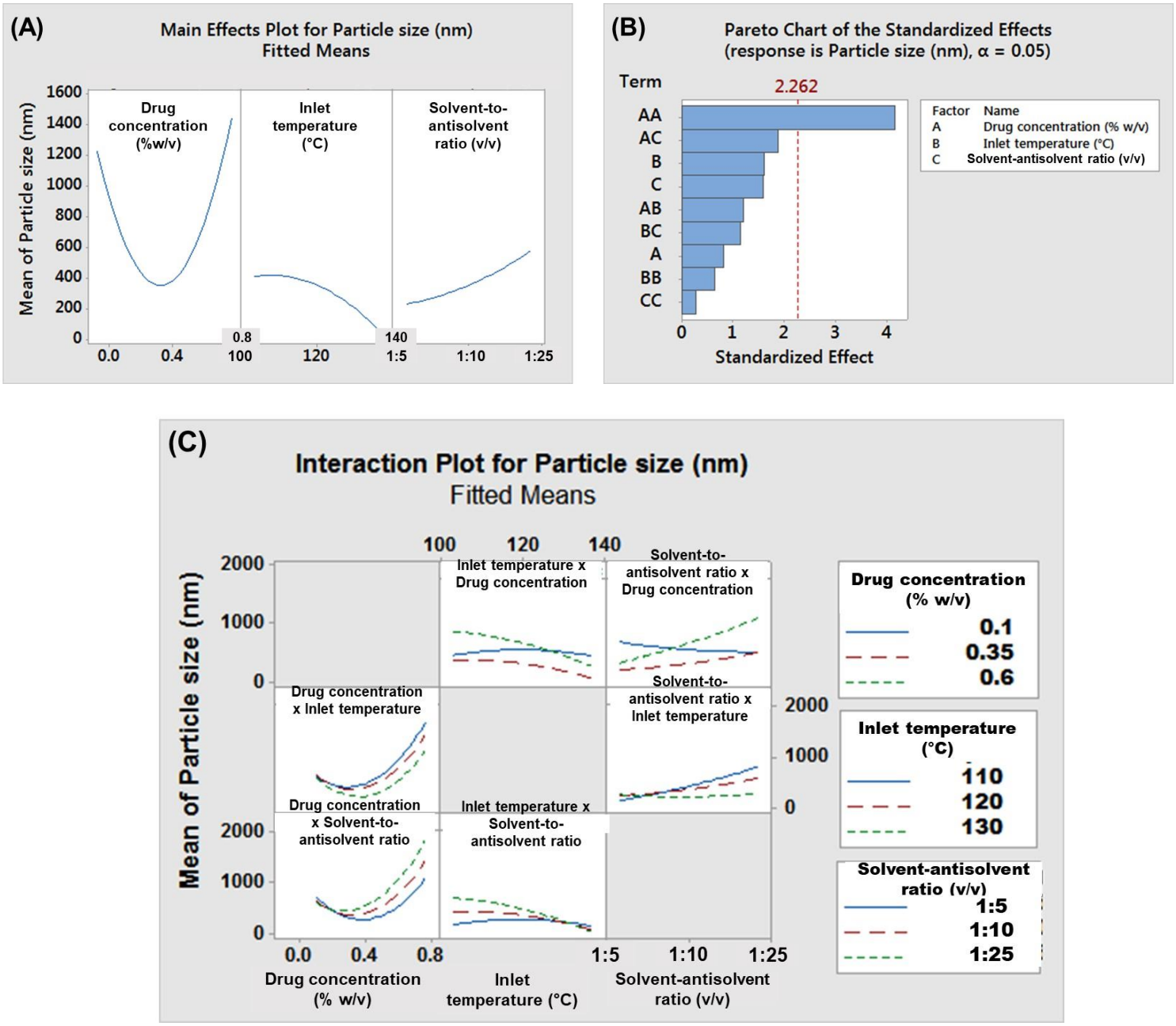

Figure 5.2d. (A) Main effect plot **(B)** Pareto chart and **(C)** Interaction plot for mean particle size of nanoamorphous spironolactone.

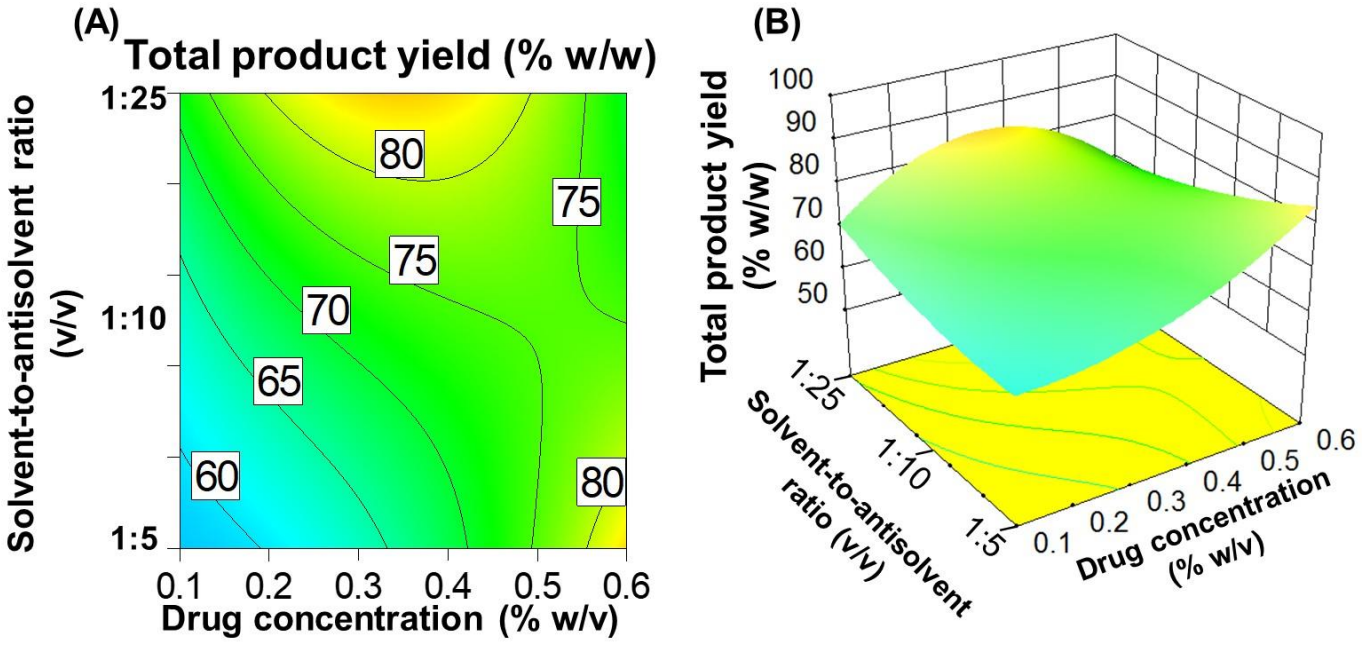

Figure 5.3a. (A) Contour plots and **(B)** 3D surface plots comparing effect of solvent-to-antisolvent ratio and drug concentration on the total product yield of nanoamorphous spironolactone.

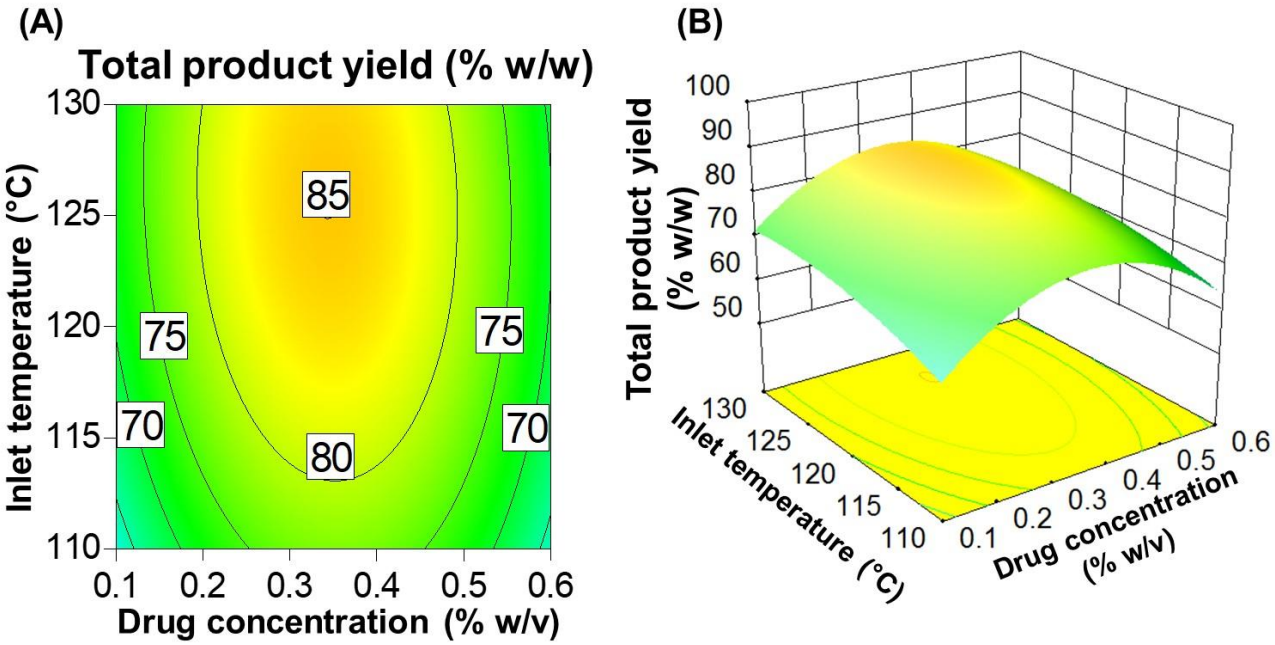

Figure 5.3b. (A) Contour plots and **(B)** 3D surface plots comparing effect of inlet temperature of spray dryer and drug concentration on the total product yield of nanoamorphous spironolactone.

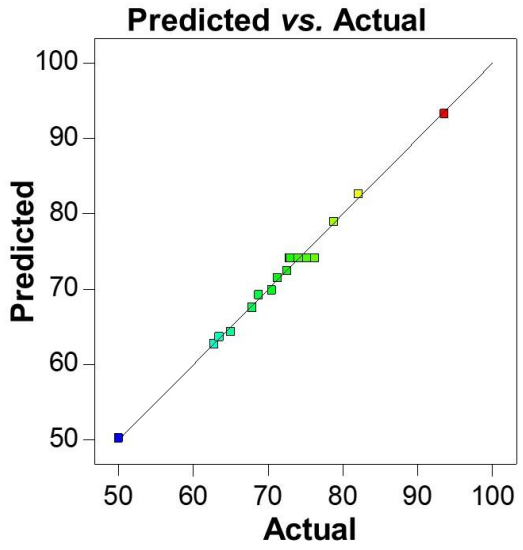

Figure 5.3c. Graph showing model predicted *vs.* actual values of the experiments.

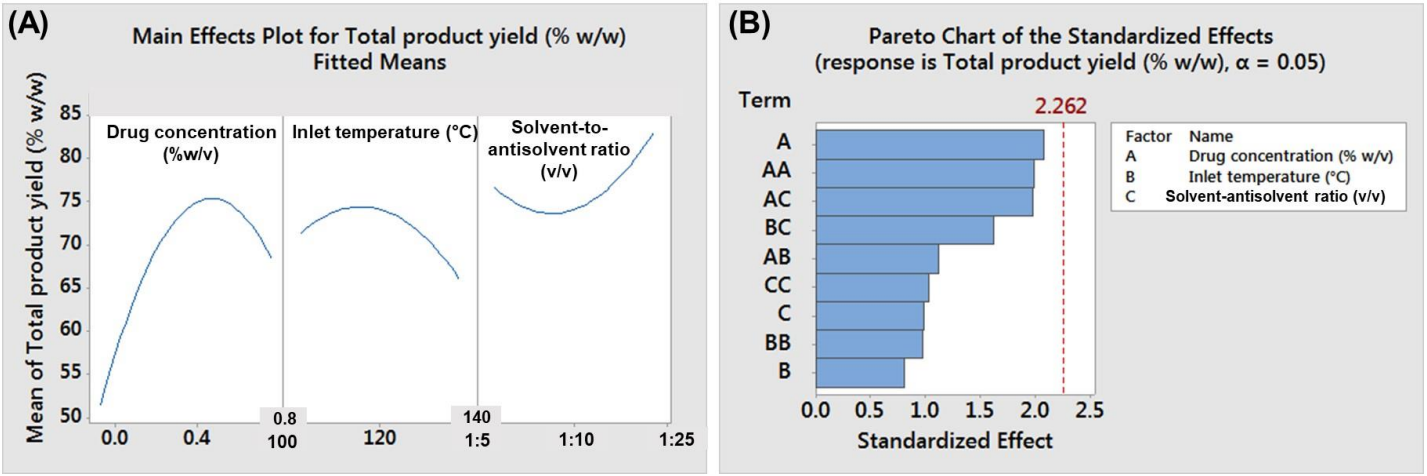

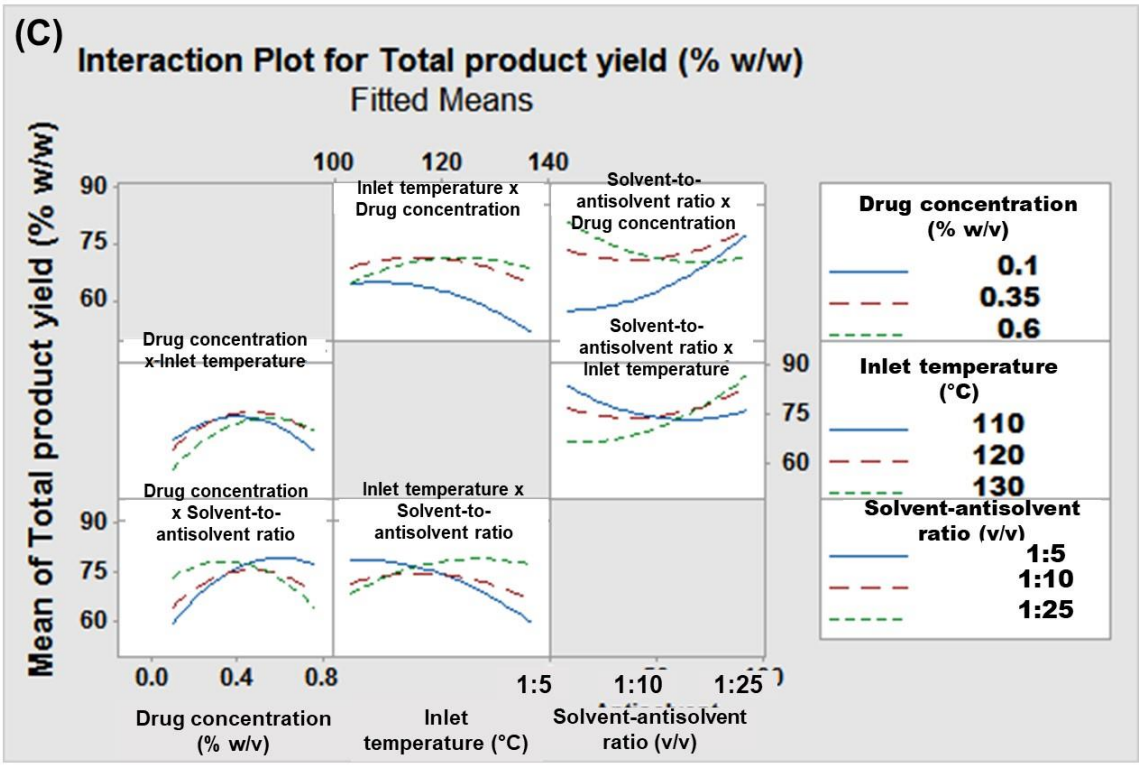

Figure 5.3d. (A) Main effect plot **(B)** Pareto chart and **(C)** Interaction plot for mean total product yield of nanoamorphous spironolactone.

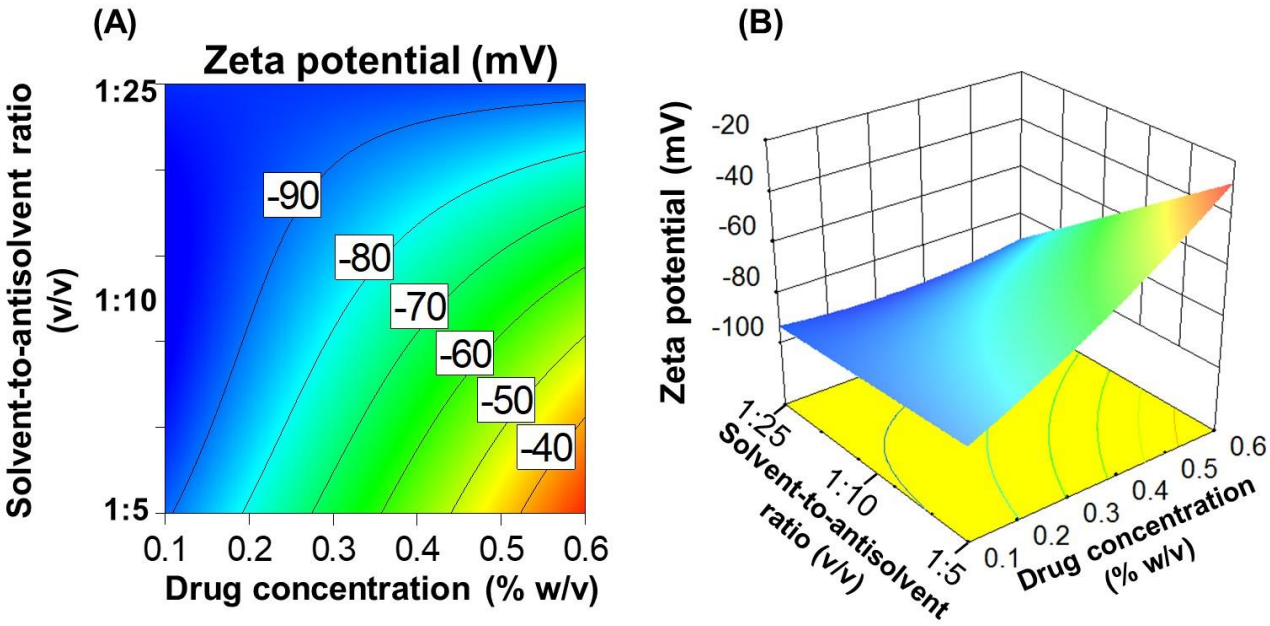

Figure 5.4a. (A) Contour plots and **(B)** 3D surface plots comparing effect of solvent-to-antisolvent ratio and drug concentration on the zeta potential of nanoamorphous spironolactone.

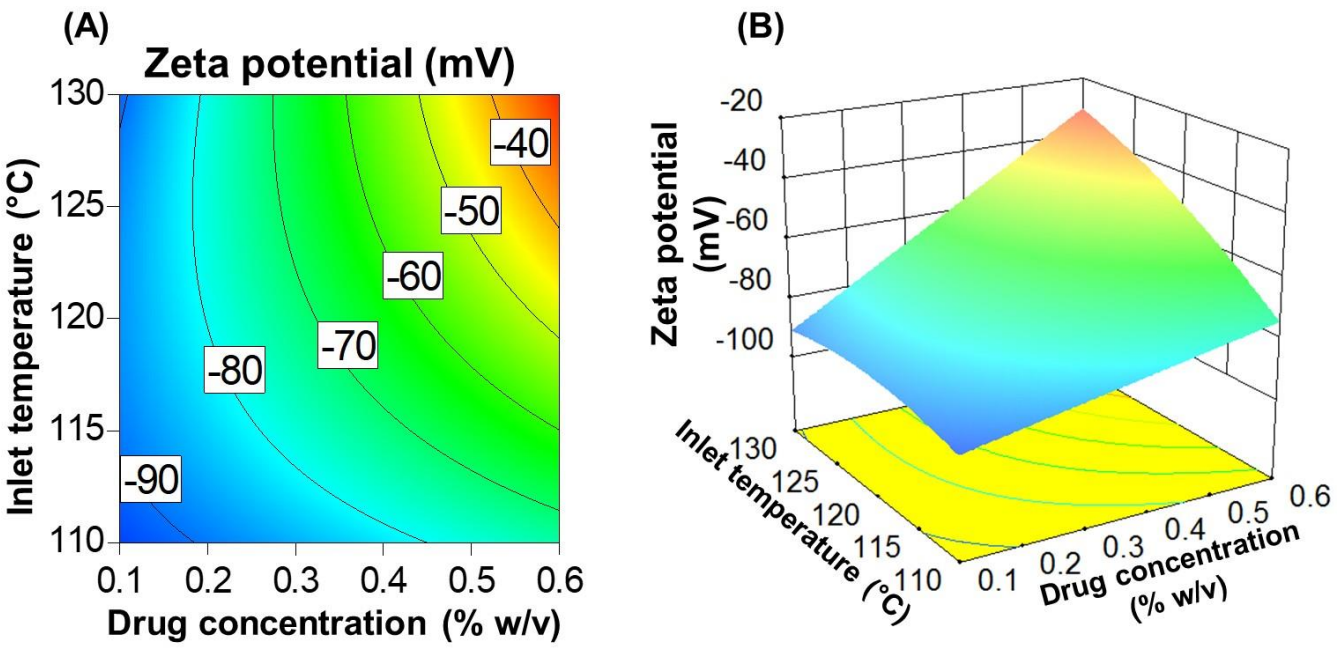

Figure 5.4b. (A) Contour plots and **(B)** 3D surface plots comparing effect of inlet temperature of spray dryer and drug concentration on the zeta potential of nanoamorphous spironolactone.

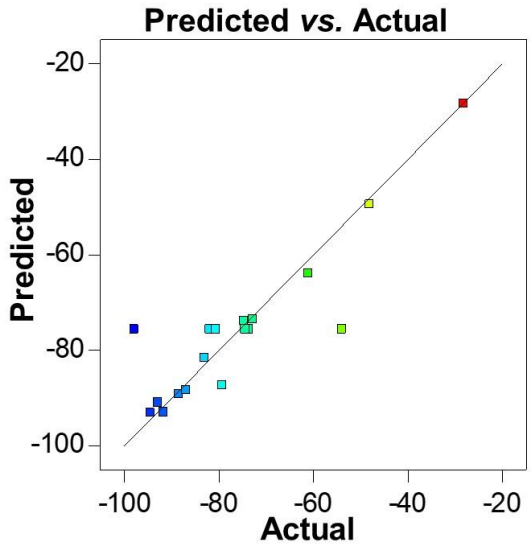

Figure 5.4c. Graph showing model predicted *vs.* actual values of the experiments.

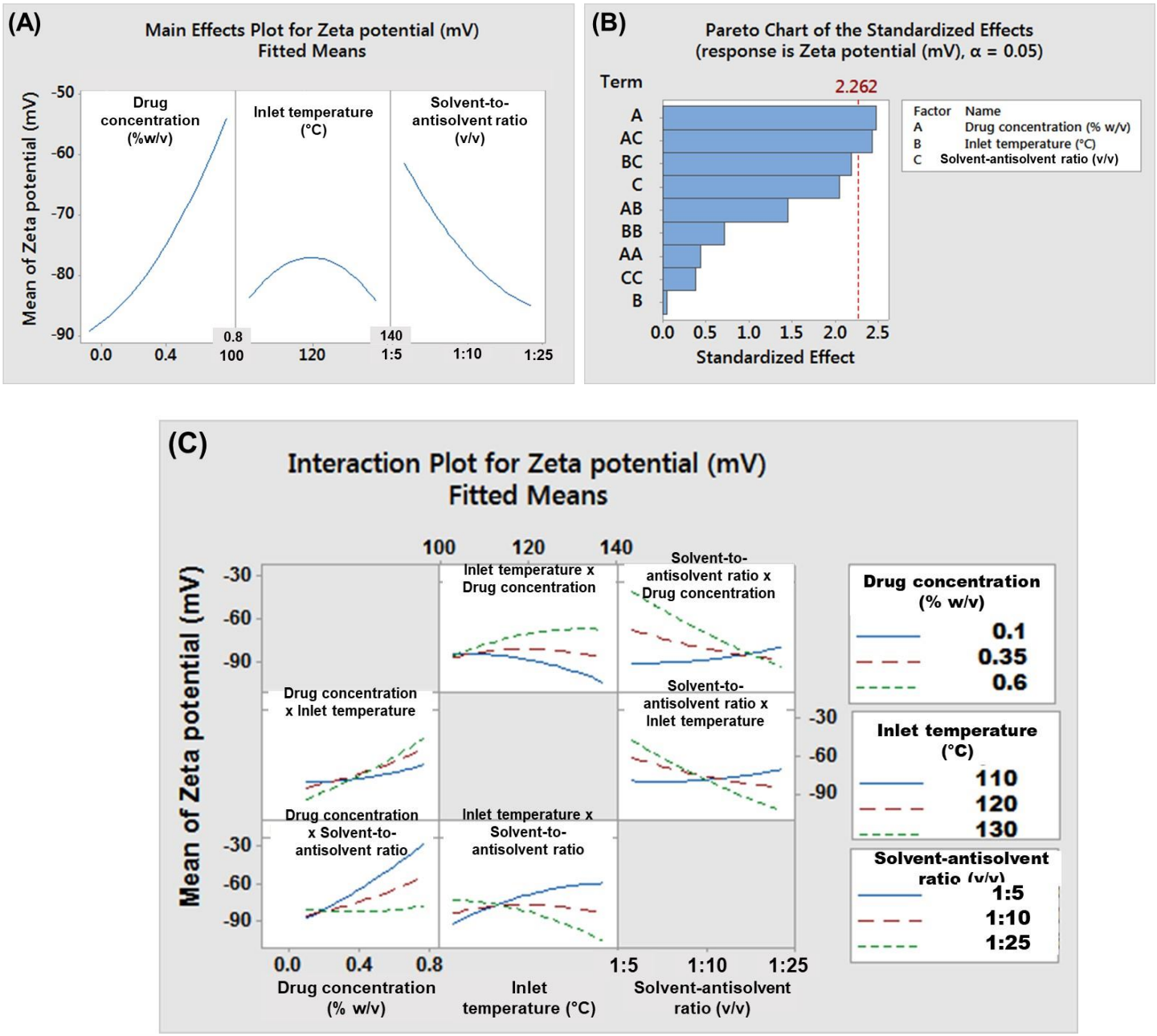

Figure 5.4d. (A) Main effect plot **(B)** Pareto chart and **(C)** Interaction plot for mean zeta potential of nanoamorphous spironolactone.

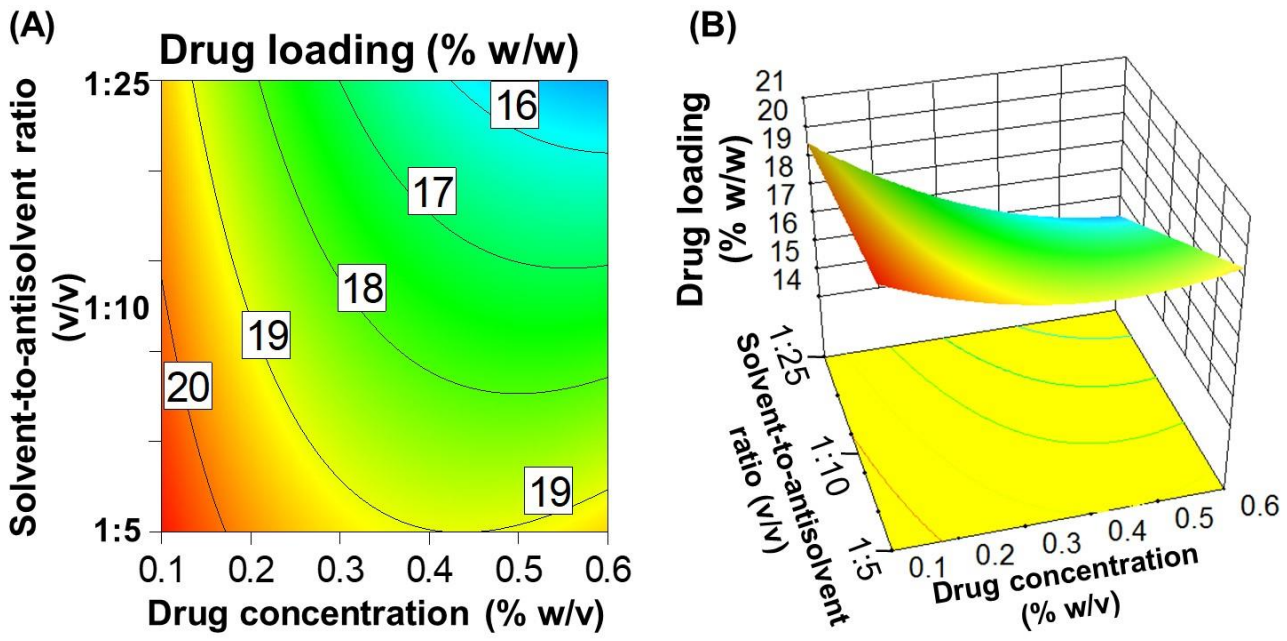

Figure 5.5a. (A) Contour plots and **(B)** 3D surface plots comparing effect of solvent-to-antisolvent ratio and drug concentration on the drug loading of the nanoamorphous spironolactone.

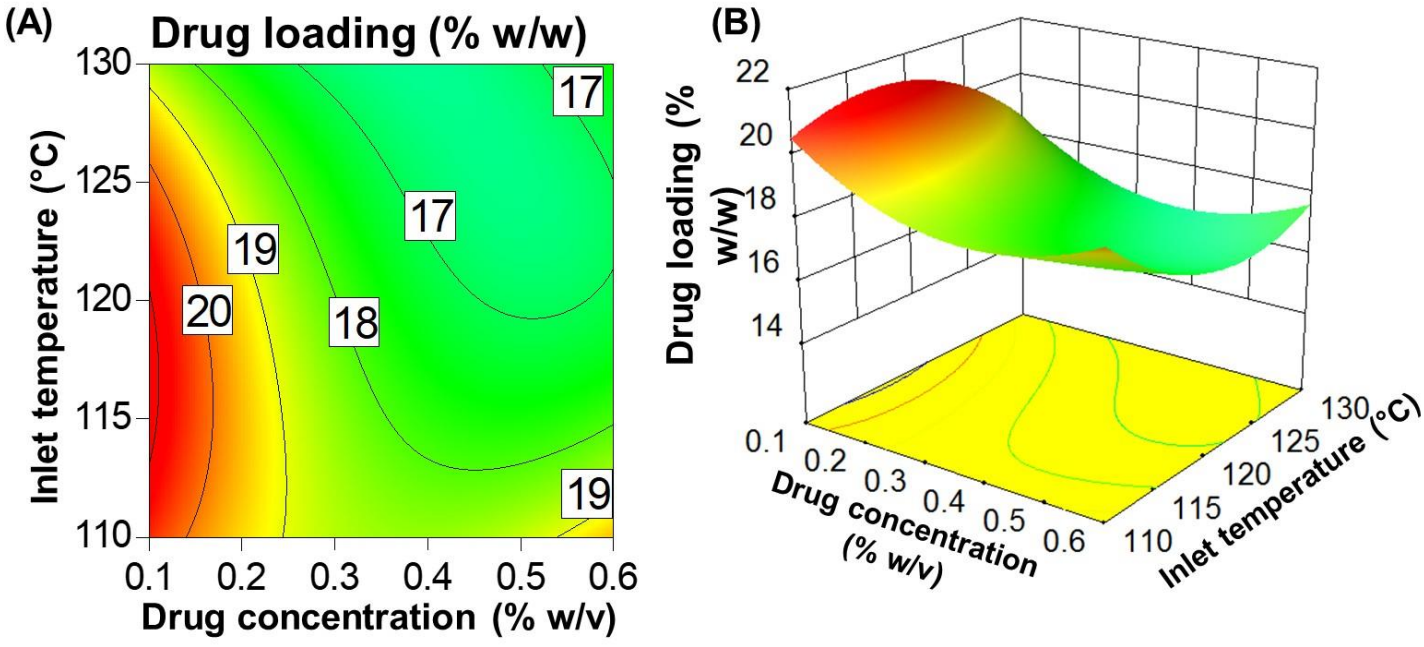

Figure 5.5b. (A) Contour plots and **(B)** 3D surface plots comparing effect of inlet temperature of spray dryer and drug concentration on the drug loading of the nanoamorphous spironolactone.

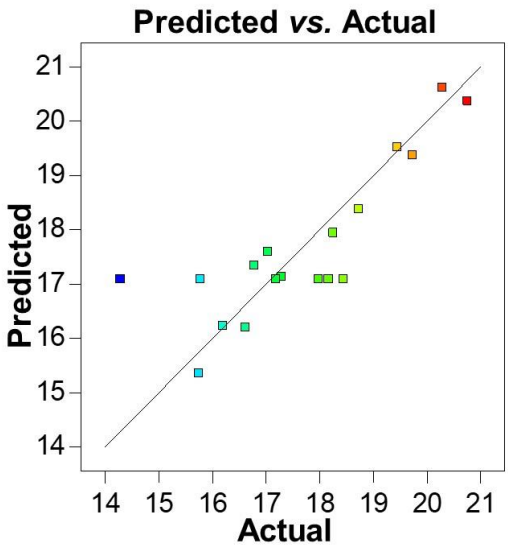

Figure 5.5c. Graph showing model predicted *vs.* actual values of the experiments.

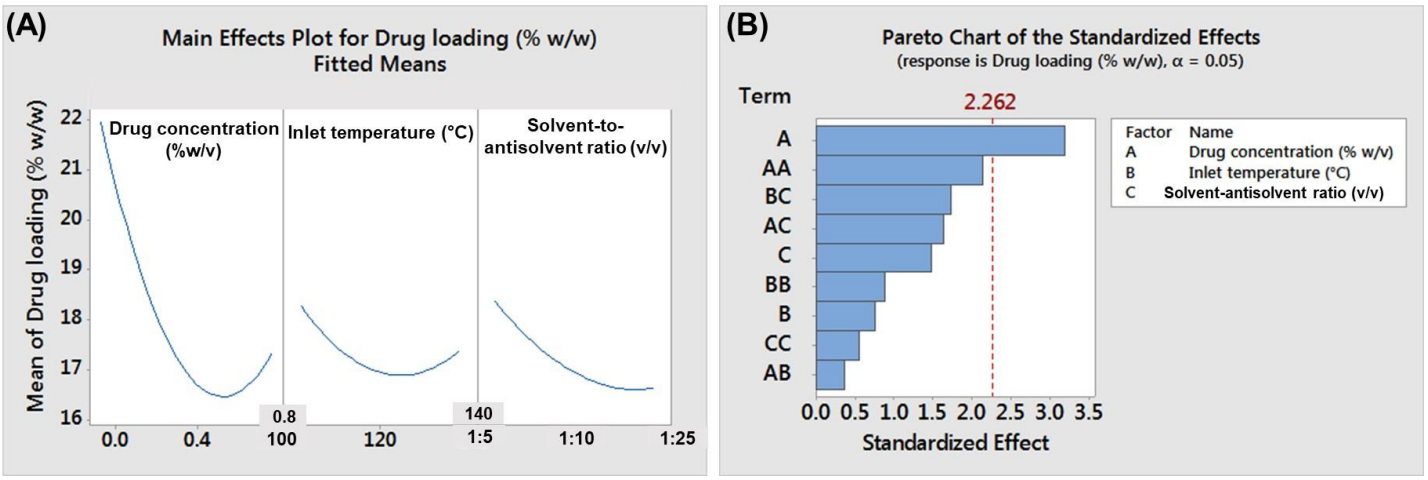

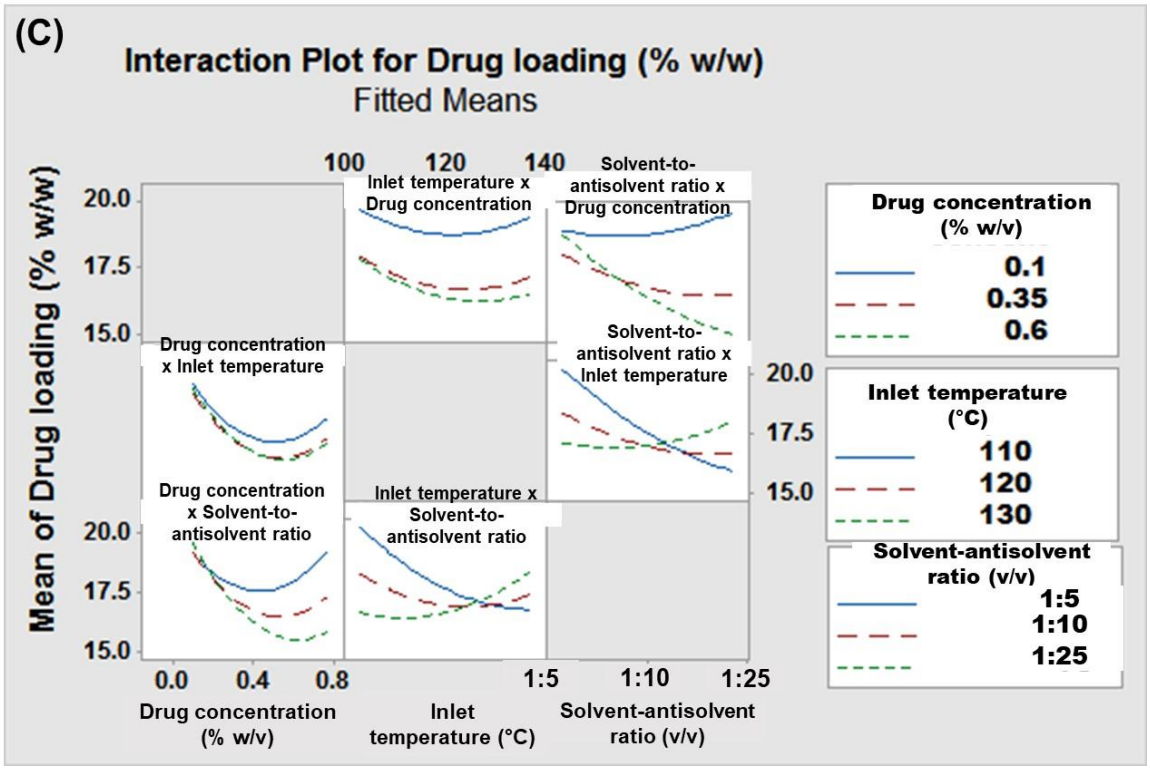

Figure 5.5d. (A) Main effect plot **(B)** Pareto chart and **(C)** Interaction plot for mean drug loading of nanoamorphous spironolactone.

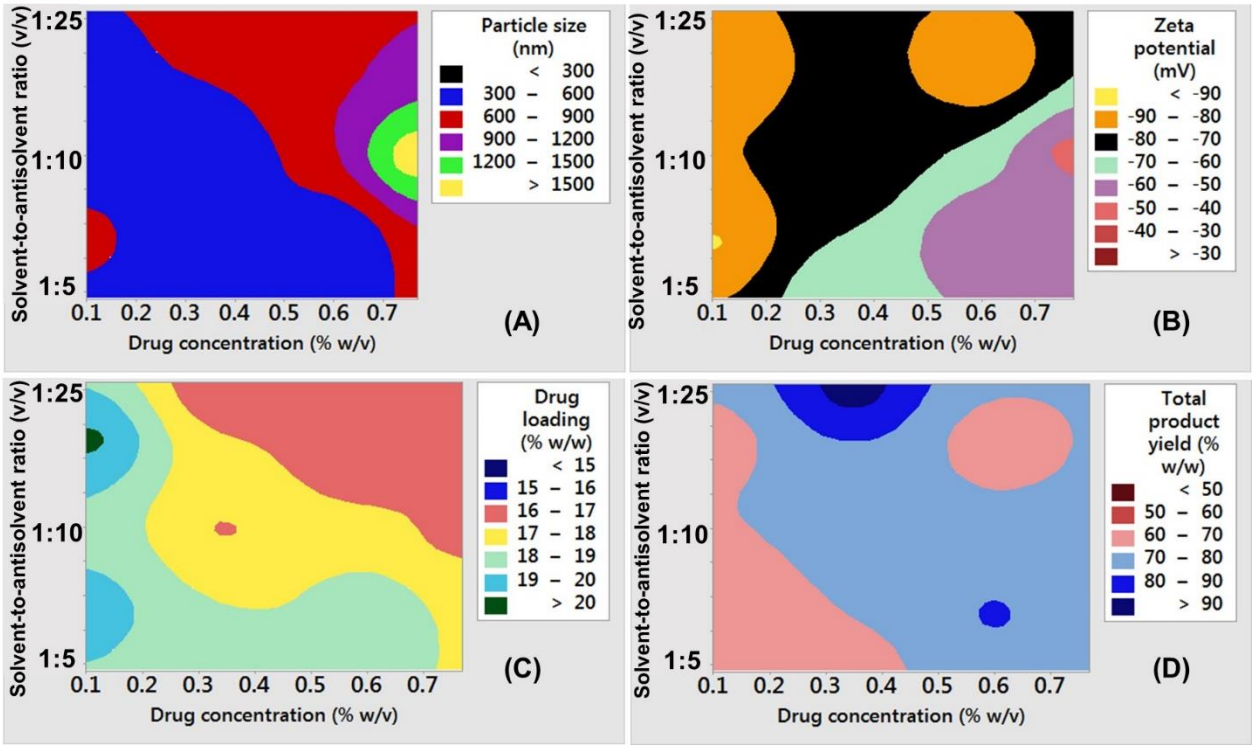

Figure 5.6a. The optimized contour plots comparing effect of drug concentration and solvent-to-antisolvent ratio on different CQAs: (A) Particle size; (B) Zeta potential; (C) Drug loading; and (D) Total product yield of nanoamorphous spironolactone.

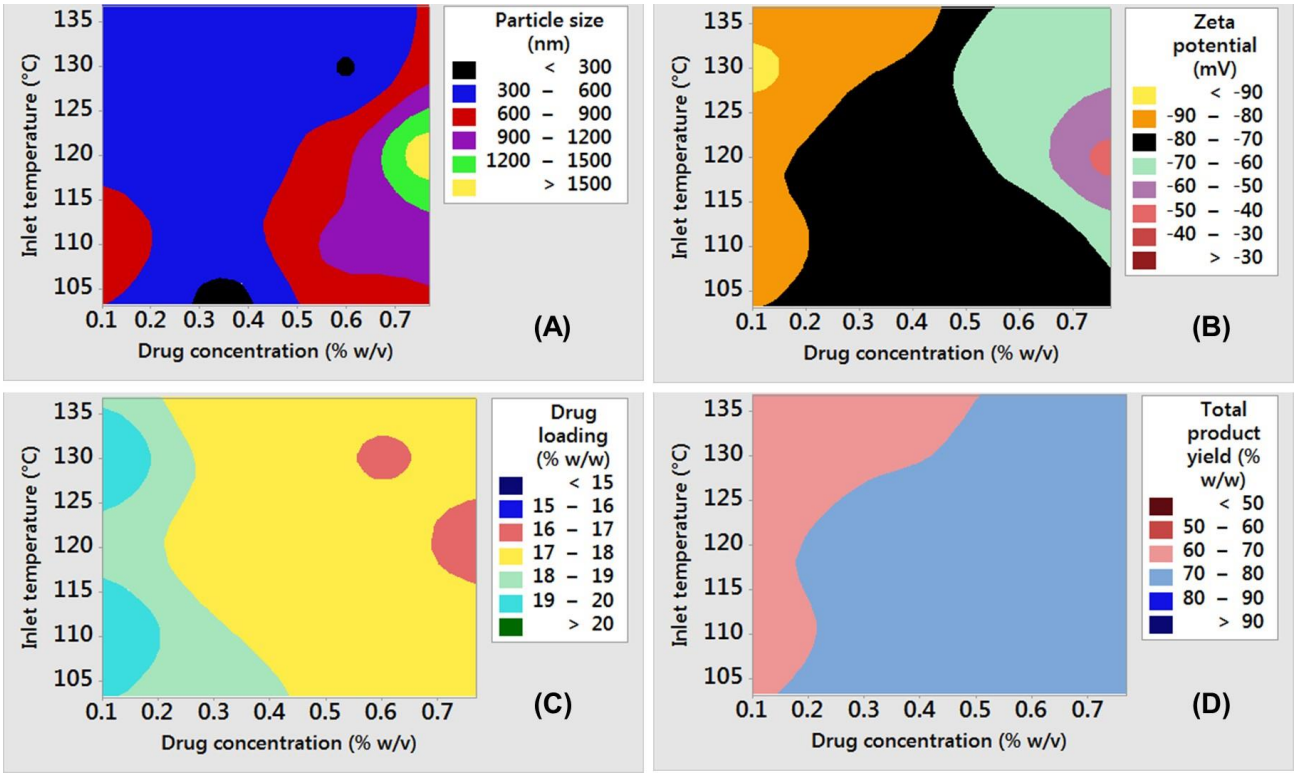

Figure 5.6b. The optimized contour plots comparing effect of drug concentration and spray dryer inlet temperature on different CQAs: (A) Particle size; (B) Zeta potential; (C) Drug loading; and (D) Total product yield of nanoamorphous spironolactone.

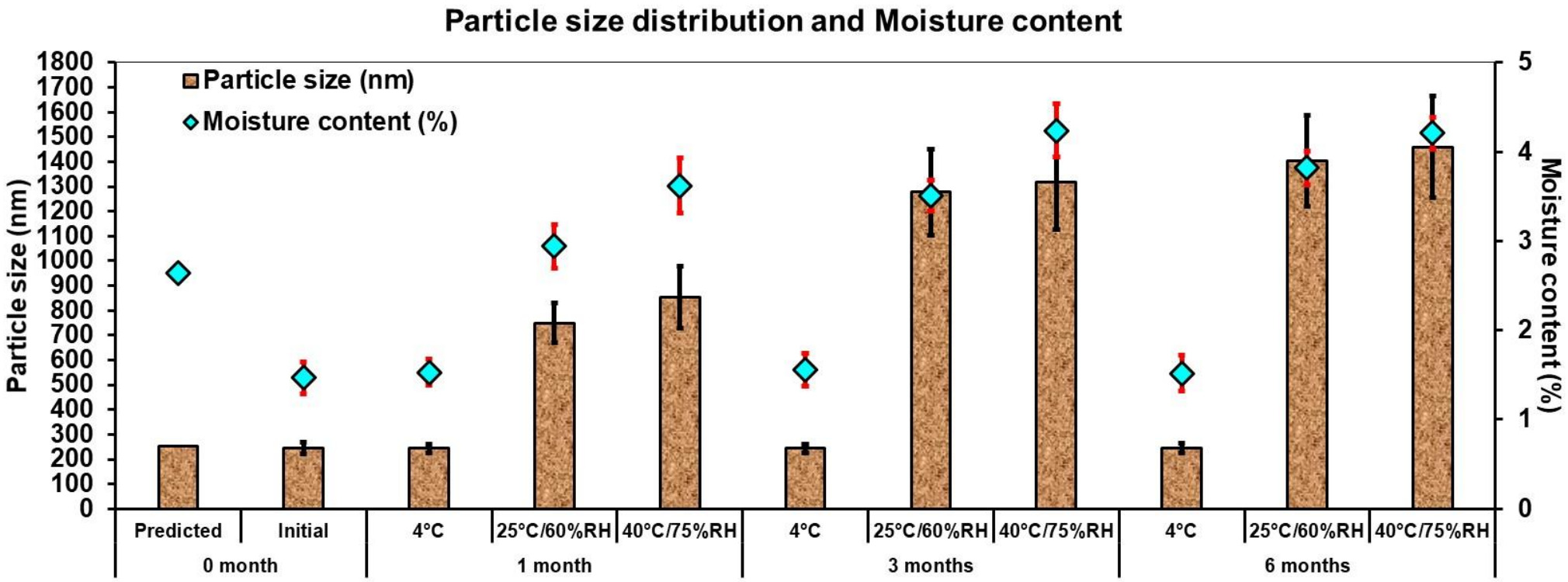

Figure 5.7. Particle size distribution and moisture content of the optimized spray-dried nanoamorphous spironolactone formulations stored for 1, 3 and 6 month/s at (a) 4°C (b) 25°C/60% RH (c) 40°C/75% RH compared with zero month formulations.

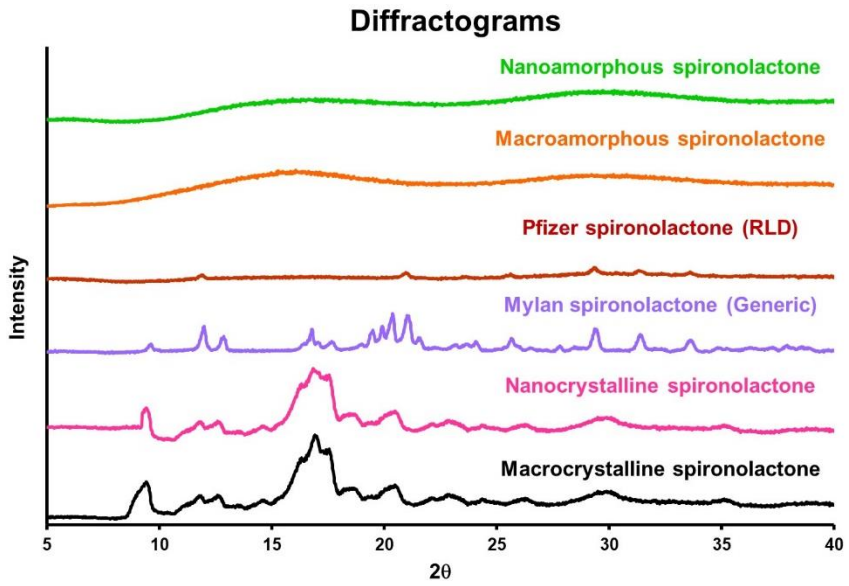

Figure 5.8a. PXRD diffraction profiles of the macrocrystalline spironolactone (neat crystalline drug), nanocrystalline spironolactone, Generic spironolactone (Mylan), RLD spironolactone (Pfizer), macroamorphous spironolactone and nanoamorphous spironolactone

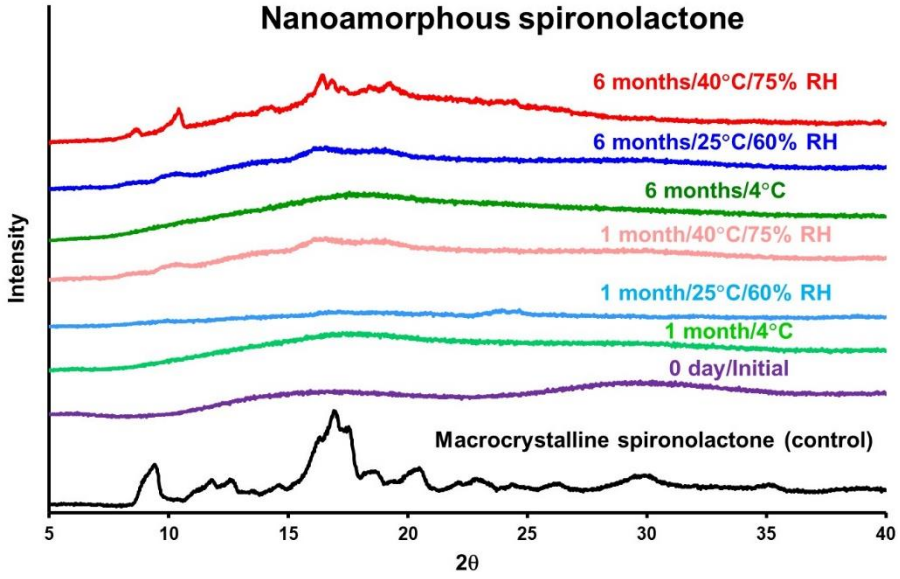

Figure 5.8b. PXRD diffraction profiles of the optimized spray-dried nanoamorphous spironolactone formulations (initial (0 day) and formulations stored for 1 and 6 month/s at 4°C, 25°C/60%RH and 40°C/75%RH)

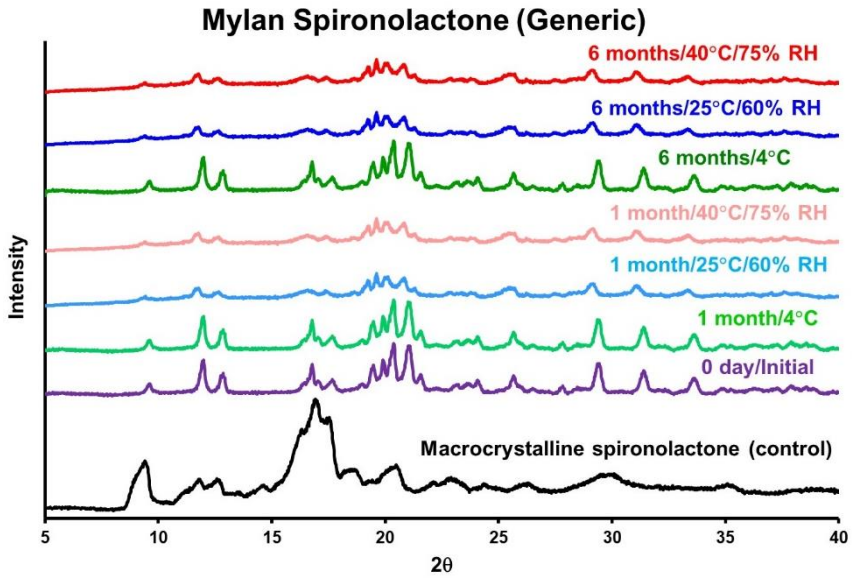

Figure 5.8c. PXRD diffraction profiles of the Generic spironolactone drug product (Mylan) (day zero and those stored for 1 and 6 month/s at 4°C, 25°C/60%RH and 40°C/75%RH)

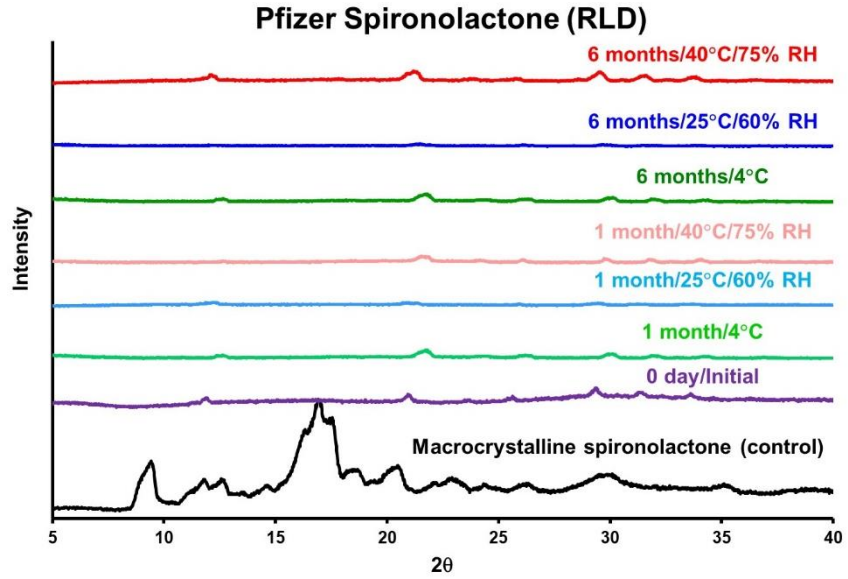

Figure 5.8d. PXRD diffraction profiles of the RLD spironolactone drug product (Pfizer) (day zero and those stored for 1 and 6 month/s at 4°C, 25°C/60%RH and 40°C/75%RH)

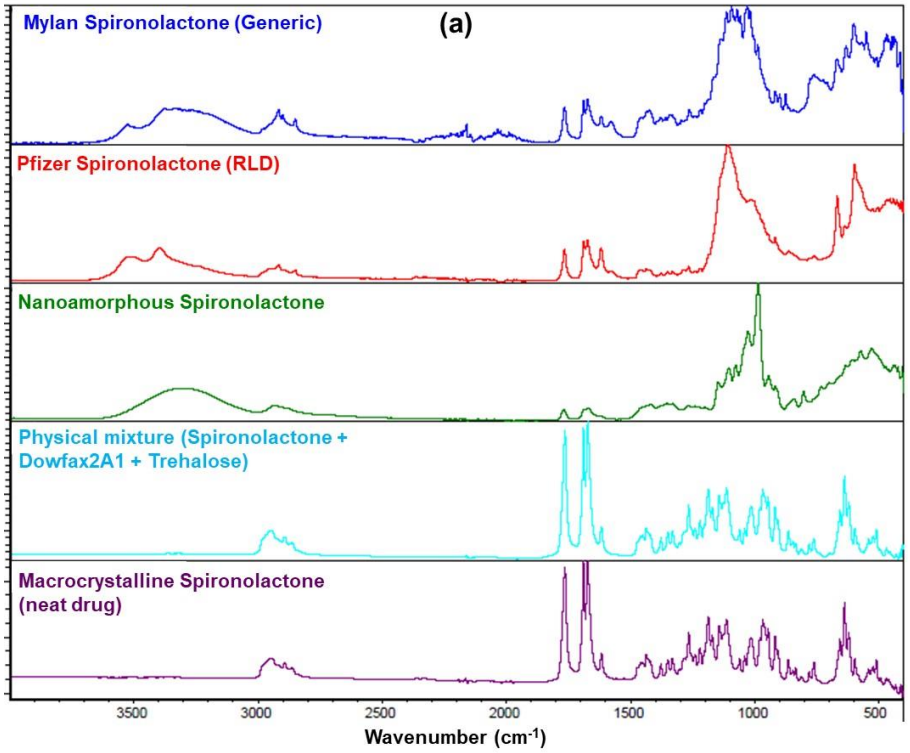

Figure 5.9(a). ATR-FTIR full spectra (4000-500 cm^{-1}) overlay of the macrocrystalline spironolactone (neat drug), physical mixture (neat drug, surfactant (Dowfax2A1) and sugar (trehalose)), nanoamorphous spironolactone, RLD spironolactone (Pfizer) and Generic spironolactone (Mylan).

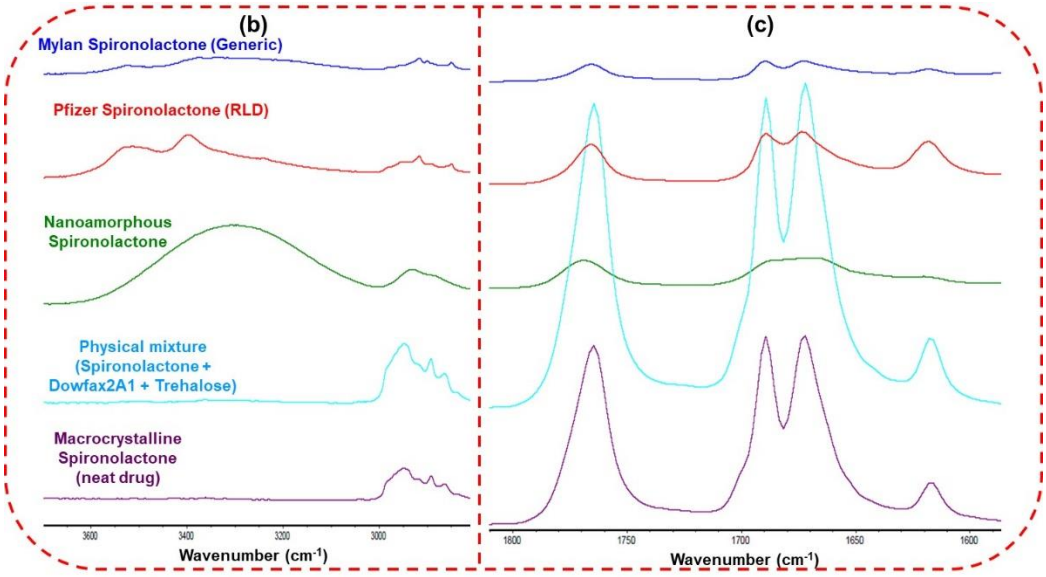

Figure 5.9(b) - 3700-2800 cm^{-1}, **(c)** - 1800-1600 cm^{-1} - ATR-FTIR spectra overlay of the macrocrystalline spironolactone (neat drug), physical mixture (neat drug, surfactant (Dowfax2A1) and sugar (trehalose)), nanoamorphous spironolactone, RLD spironolactone (Pfizer) and Generic spironolactone (Mylan).

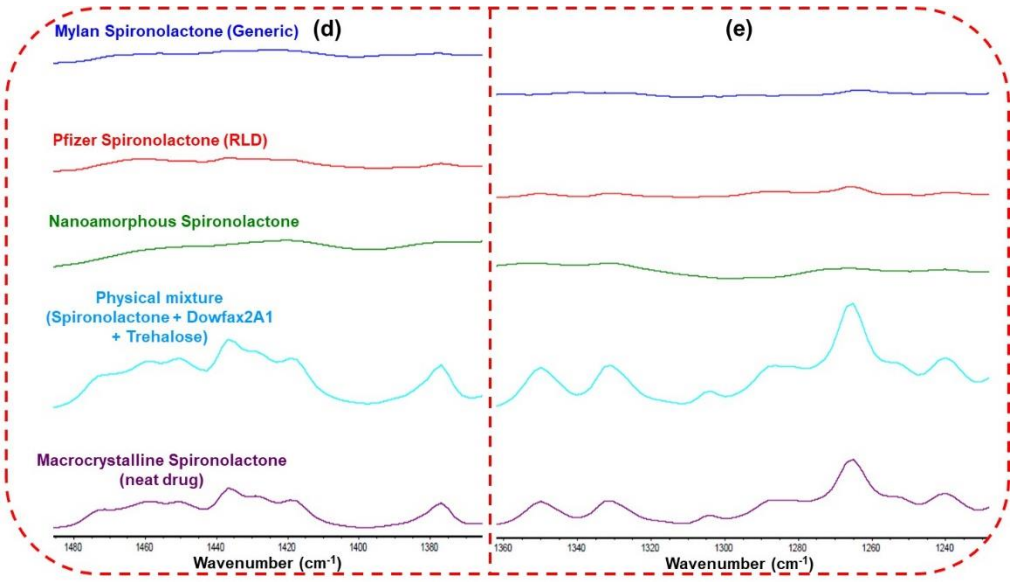

Figure 5.9(d) - 1480-1370 cm^{-1}, **(e)** – 1360-1230 cm^{-1} - ATR-FTIR spectra overlay of the macrocrystalline spironolactone (neat drug), physical mixture (neat drug, surfactant (Dowfax2A1) and sugar (trehalose)), nanoamorphous spironolactone, RLD spironolactone (Pfizer) and Generic spironolactone (Mylan).

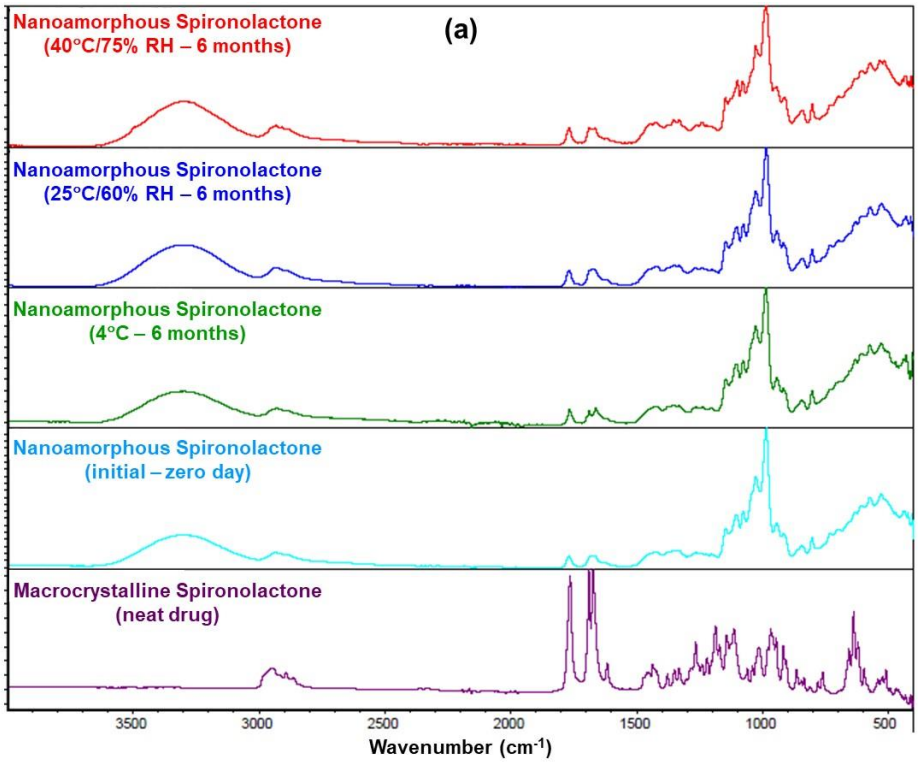

Figure 5.10(a). ATR-FTIR full spectra (4000-500 cm^{-1}) overlay of the macrocrystalline spironolactone (neat drug) and nanoamorphous spironolactone (day zero and those stored for six months at 4°C, 25°C/60%RH and 40°C/75%RH).

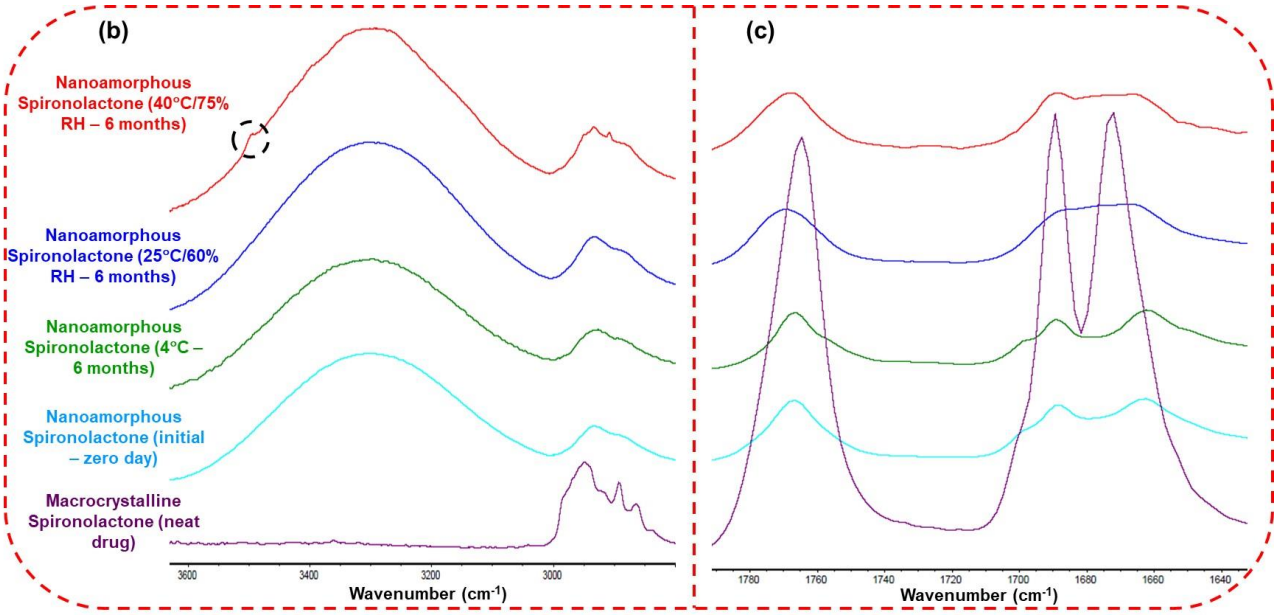

Figure 5.10(b) – 3600-2800 cm^{-1}, **(c)** – 1780-1640 cm^{-1} - ATR-FTIR overlay of the macrocrystalline spironolactone (neat drug) and nanoamorphous spironolactone (day zero and those stored for six months at 4°C, 25°C/60%RH and 40°C/75%RH).

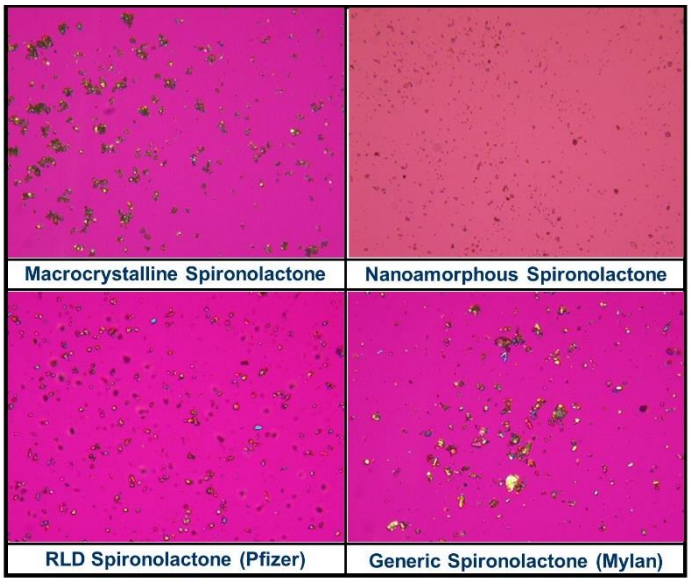

Figure 5.11a. PLM images of macrocrystalline spironolactone (neat drug), nanoamorphous spironolactone, Generic spironolactone (Mylan), RLD spironolactone (Pfizer). **Note**: All images are of 10X magnification.

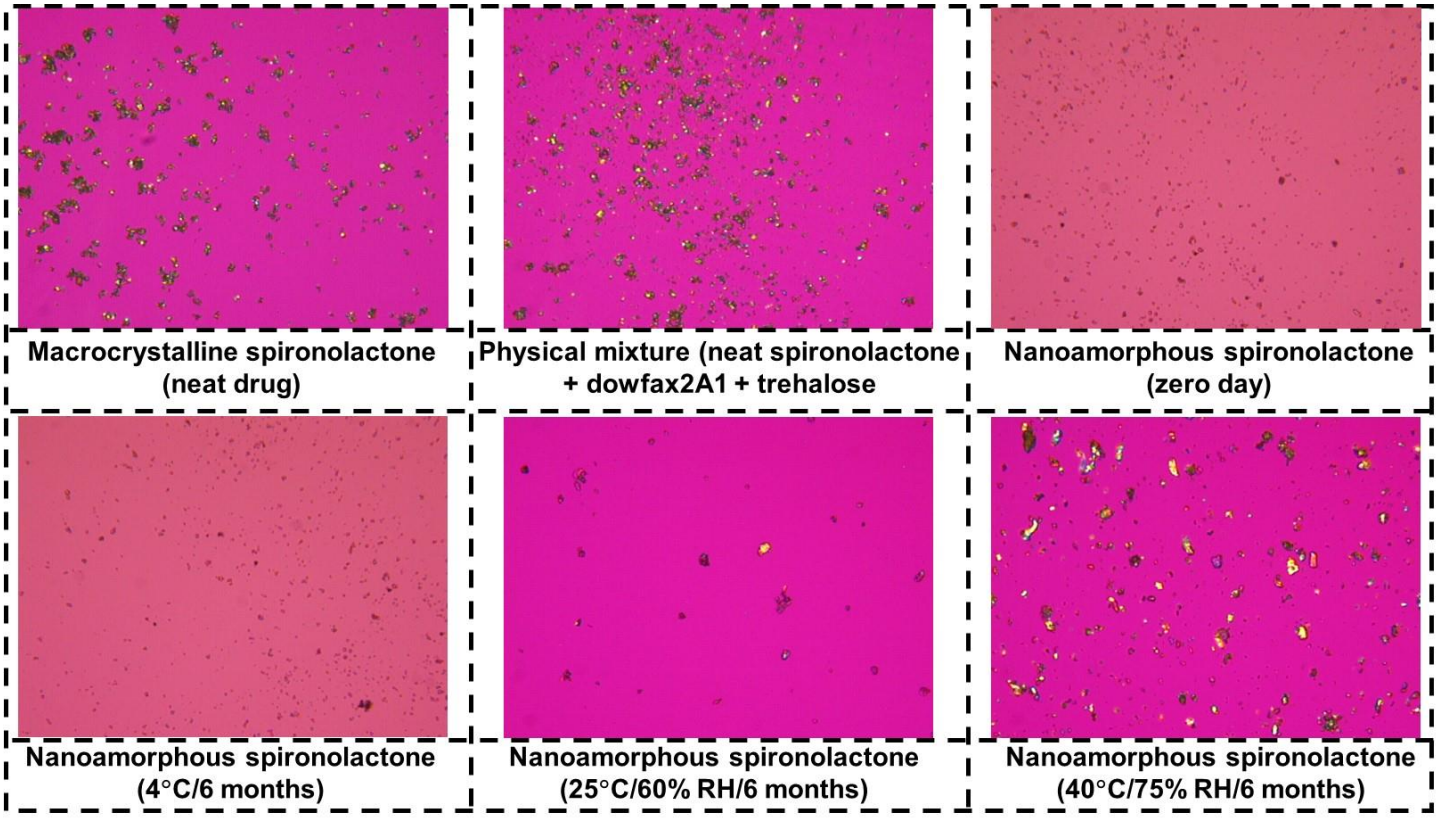

Figure 5.11b. PLM images of the macrocrystalline spironolactone (neat drug), physical mixture (spironolactone, Dowfax2A1 and trehalose) and the optimized spray-dried nanoamorphous spironolactone formulations (day zero and those stored for 6 months at 4°C, 25°C/60% RH and 40°C/75% RH). **Note**: All images are of 10X magnification.

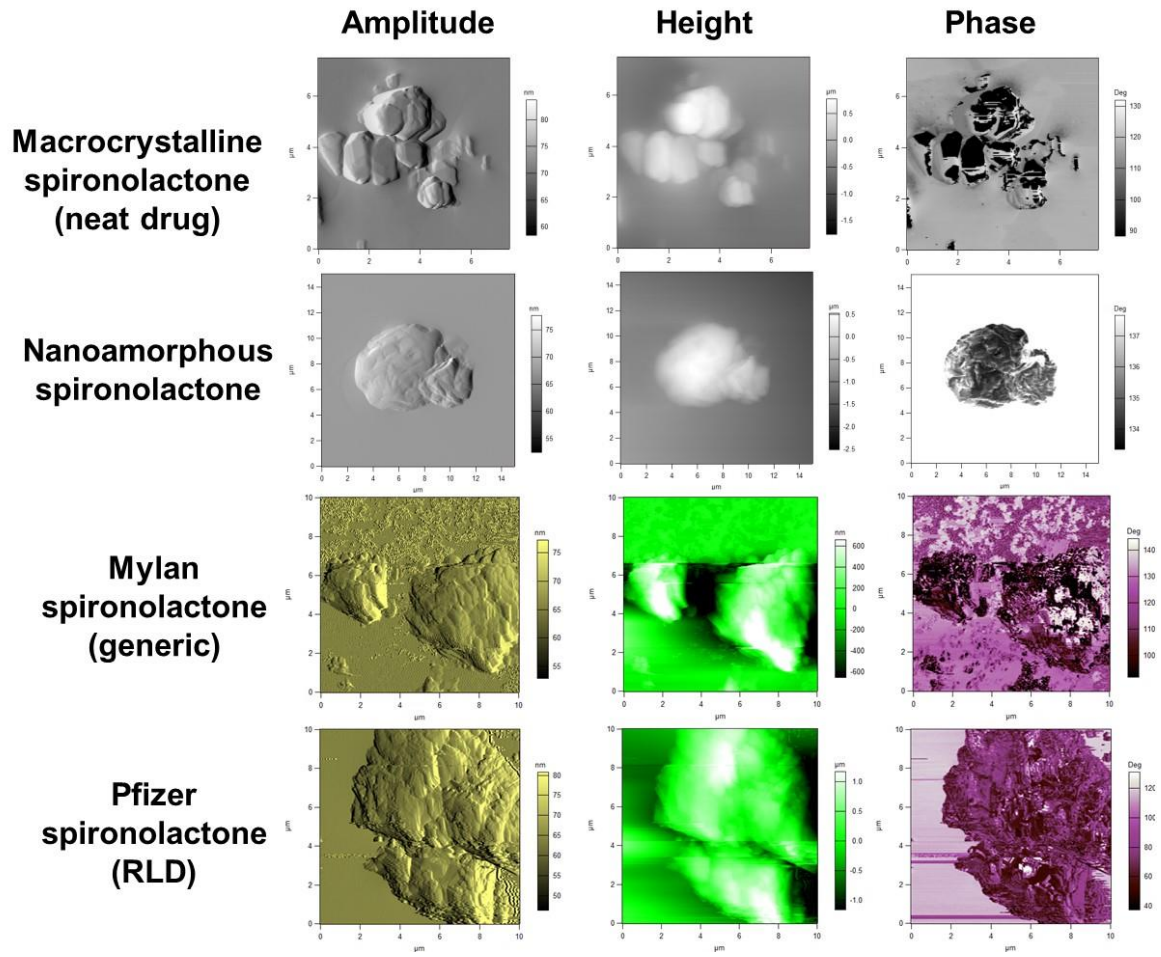

Figure 5.12. AFM images (amplitude images – left, height images – center and phase images – right) of the macrocrystalline spironolactone (neat drug), nanoamorphous spironolactone, Generic spironolactone (Mylan) and RLD spironolactone (Pfizer).

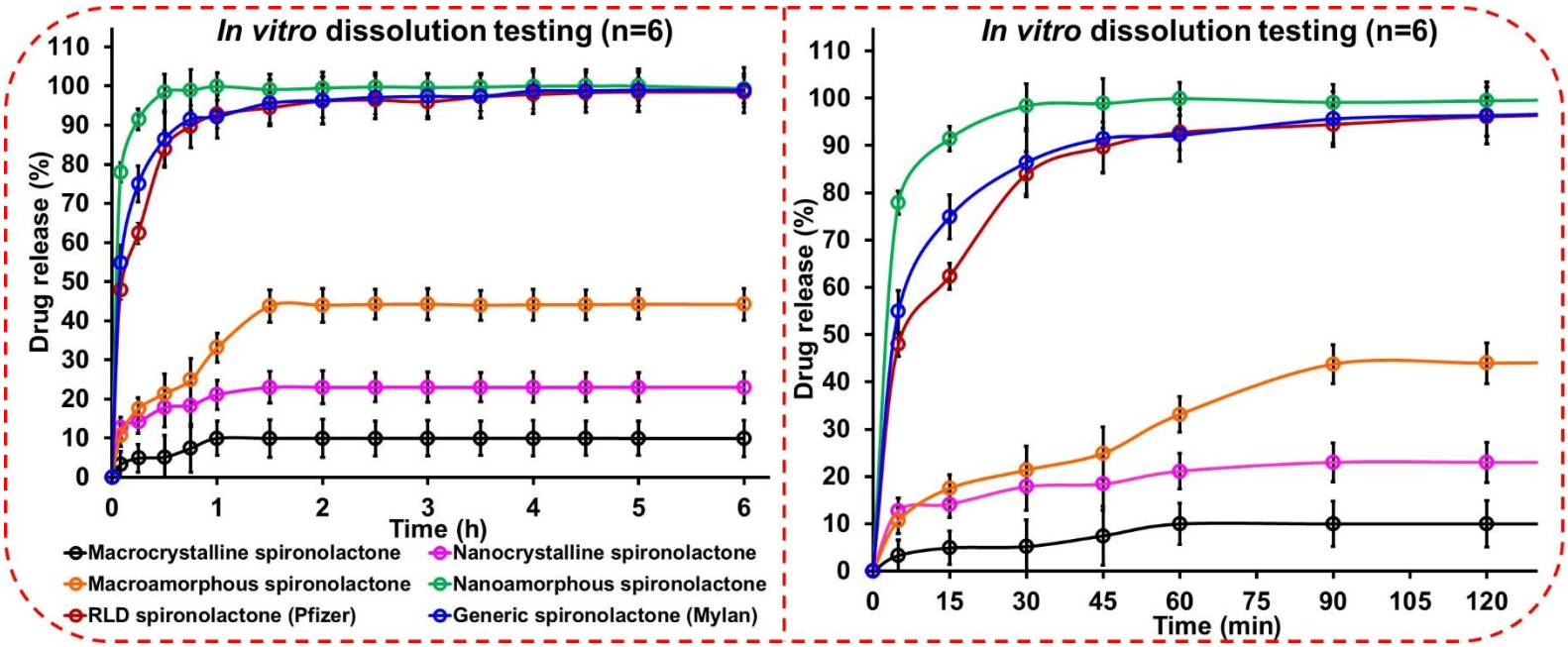

Figure 5.13. *In vitro* drug release testing of macrocrystalline spironolactone (neat drug), nanocrystalline spironolactone, macroamorphous spironolactone, nanoamorphous spironolactone, Generic spironolactone (Mylan) and RLD spironolactone (Pfizer).

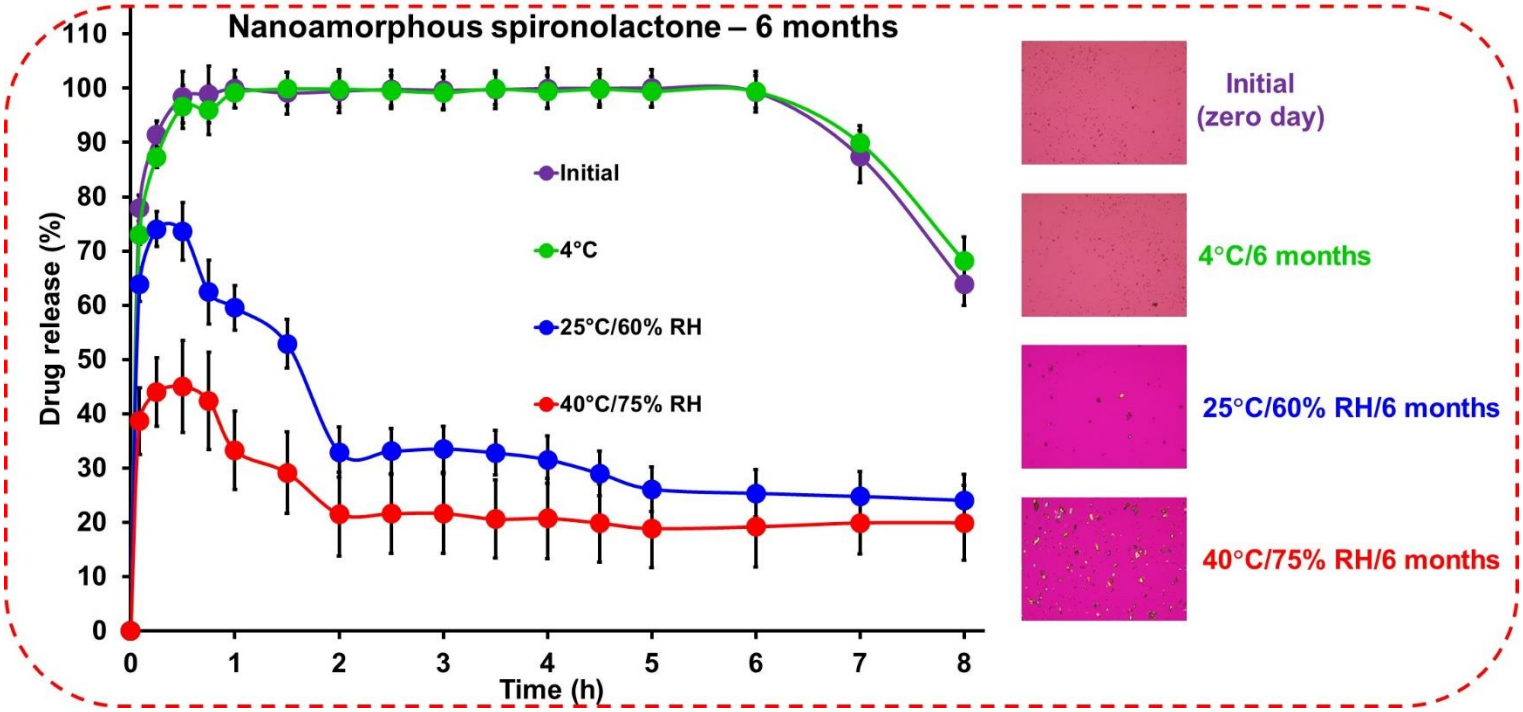

Figure 5.14. *In vitro* drug release testing of macrocrystalline spironolactone (neat drug) and the optimized spray-dried nanoamorphous spironolactone formulations (day zero and those stored for 6 months at 4°C, 25°C/60% RH and 40°C/75% RH).

5.10. REFERENCES

[1]Shah R. B., Ahsan F. and Khan M. A., 2002. Oral delivery of proteins: progress and prognostication. Critical Reviews™ in Therapeutic Drug Carrier Systems. 19.

[2]Brown L. R., 2005. Commercial challenges of protein drug delivery. Expert opinion on drug delivery. 2, 29-42.

[3]Kumar S., Shen J. and Burgess D. J., 2014. Nano-amorphous spray dried powder to improve oral bioavailability of itraconazole. Journal of Controlled Release. 192, 95-102.

[4]Jog R., Kumar S., Shen J., Jugade N., Tan D. C. T., Gokhale R. and Burgess D. J., 2016. Formulation design and evaluation of amorphous ABT-102 nanoparticles. International journal of pharmaceutics. 498, 153-169.

[5]Jog R. and Burgess D. J., 2017. Pharmaceutical amorphous nanoparticles. Journal of pharmaceutical sciences. 106, 39-65.

[6]Lindfors L., Skantze P., Skantze U., Rasmusson M., Zackrisson A. and Olsson U., 2006. Amorphous drug nanosuspensions. 1. Inhibition of Ostwald ripening. Langmuir. 22, 906-910.

[7]Yu L., Li C., Le Y., Chen J.-F. and Zou H., 2011. Stabilized amorphous glibenclamide nanoparticles by high-gravity technique. Materials Chemistry and Physics. 130, 361-366.

[8]Zu Y., Sun W., Zhao X., Wang W., Li Y., Ge Y., Liu Y. and Wang K., 2014. Preparation and characterization of amorphous amphotericin B nanoparticles for oral administration through liquid antisolvent precipitation. European Journal of Pharmaceutical Sciences. 53, 109-117.

[9]Lee E. H., 2014. A practical guide to pharmaceutical polymorph screening & selection. asian journal of pharmaceutical sciences. 9, 163-175.

[10]Salole E. and Al-Sarraj F., 1985. Spironolactone crystal forms. Drug Development and Industrial Pharmacy. 11, 855-864.

[11]Sutter, J. L., and Lan, E. P. K.: Spironolactone, in Florey, K., editor: Analytical profiles of drug substances, New York, 1975, Academic Press, Inc., voL 4, p. 441.

[12]Kumar S., Jog R., Shen J., Zolnik B., Sadrieh N. and Burgess D. J., 2015. In vitro and in vivo performance of different sized spray-dried crystalline itraconazole. Journal of pharmaceutical sciences. 104, 3018-3028.

[13]Kumar S., Jog R., Shen J., Zolnik B., Sadrieh N. and Burgess D. J., 2015. Formulation and performance of danazol nano-crystalline suspensions and spray dried powders. Pharmaceutical research. 32, 1694-1703.

[14]Wray P., Chan K. A., Kimber J. and Kazarian S. G., 2008. Compaction of pharmaceutical tablets with different polymer matrices studied by FTIR imaging and X-ray microtomography. Journal of pharmaceutical sciences. 97, 4269-4277.
[15]Dong Y., Ng W. K., Shen S., Kim S. and Tan R. B., 2009. Preparation and characterization of spironolactone nanoparticles by antisolvent precipitation. International journal of pharmaceutics. 375, 84-88.
[16]Jiang C., Yan J., Wang Y., Zhang J., Wang G., Yang J. and Hao H., 2015. Isolation Strategies and Transformation Behaviors of Spironolactone Forms. Industrial & Engineering Chemistry Research. 54, 11222-11229.
[17]Jog R., Gokhale R. and Burgess D. J., 2016. Solid state drug-polymer miscibility studies using the model drug ABT-102. International journal of pharmaceutics. 509, 285-295.
[18]Mehta M., Kothari K., Ragoonanan V. and Suryanarayanan R., 2016. Effect of water on molecular mobility and physical stability of amorphous pharmaceuticals. Molecular pharmaceutics. 13, 1339-1346.
[19]Sun D. D. and Lee P. I., 2013. Evolution of supersaturation of amorphous pharmaceuticals: the effect of rate of supersaturation generation. Molecular pharmaceutics. 10, 4330-4346.
[20]Takano R., Takata N., Saito R., Furumoto K., Higo S., Hayashi Y., Machida M., Aso Y. and Yamashita S., 2010. Quantitative analysis of the effect of supersaturation on in vivo drug absorption. Molecular pharmaceutics. 7, 1431-1440.

Chapter 6

Conclusions and Future studies

6.1. Summary and conclusions

The novelty of the present research is the application of a comprehensive QbD approach for the identification, optimization, validation and control of the critical processes parameters and critical formulation parameters *via* multiple DoE models. Till date, individual DoEs (either process or formulation) have been investigated for the development of nanocrystalline and nanoamorphous drug products. These isolated DoEs can resolve a specific physicochemical property (one or two) of the drug product, however, the optimized formulation composition or process parameters cannot be assured, since all possible process and formulation interactions are not investigated. The QbD approach utilized in this research are examples of how these studies can be applied to obtain precise design space for CQAs of nanocrystalline and nanoamorphous powders of water insoluble drugs. This research can be applied to other BCS class II and II/IV drugs for the successful development of robust spray-dried nanocrystalline and nanoamorphous drug products.

Typically, lab-scale spray dryers have total product yield in the range of ~50-60% w/w, however based on this research, the total product yield of the nanocrystalline zileuton and nanoamorphous spironolactone solid powder was in the range of ~70-80% w/w. This remarkably high total product yield was obtained following the comprehensive QbD approach. Such high yield is difficult to achieve when using individual DoEs or in the industrial setup where there is no time for optimization. Trehalose compared to mannitol was determined to be a better stabilizer preventing nanoparticle aggregation during the spray drying process which is in agreement with previous reports on nanoparticle aggregation. Soluplus/PVPK-25 were determined to be better crystallization inhibitors for long term stabilization of the nanoamorphous formulations. Based on the stability data, it is concluded that the spray-dried nanocrystalline and nanoamorphous drug products should be stored and transported at 4°C to avoid any physicochemical instability. In addition, the manufacturing of such nanocrystalline and nanoamorphous drug products (lab-scale and pilot scale) requires strict temperature control (2-8°C) to prevent nanoparticle physicochemical instability as well as any API associated instability.

Furthermore, this research utilized a mechanistic approach to understand drug-stabilizer interactions. The interaction parameters and free energy of mixing obtained using the Flory Huggins principle and the melting point depression approach confirmed that the solid dispersions prepared *via* spray drying and freeze drying resulted in the strongest miscibility between drugs: ABT-102/spironolactone and the polymers compared to the solvent evaporation and serial dilution method. FTIR data showed that the C=O/O-H moieties of the polymers/sugars interacted with the N-H/S-H moieties of the drug *via* hydrogen bonding to facilitate nanoparticle stabilization. This study will aid pre-formulation scientists in screening stabilizers for formulation development of similar solid dispersion formulations compared to the conventional trial and error methods. PLM was a better solid state characterization tool compared to PXRD for analysis of the nanoamorphous formulations (ABT-102, spironolactone) stability. This study shows that nanoamorphous formulations prepared using sonoprecipitation followed by spray drying have an enhanced dissolution rate and may have enhance bioavailability compared to macro-crystalline drug. Nanoamorphous spironolactone prepared *via* the comprehensive QbD approach showed longer supersaturation time (~6 h) and faster drug dissolution rate (90% in 15 min) compared to the marketed drug products (RLD and generic spironolactone) (90% in 45-60 min).

In addition, the present research provides important information on: (1) selection of suitable crystallization inhibitors (stabilizing excipients) for nanoamorphous drug products; (2) selection of appropriate manufacturing techniques; and (3) critical process and product controls that significantly impact the physicochemical attributes of the nanocrystalline and nanoamorphous drug products. In addition, exposure of the nanoamorphous drug products to high relative humidity/high moisture should be avoided to ensure complete product stability throughout the shelf life. Therefore, it is necessary to take precautionary handling measures for labile APIs from the first to the last step of the product development process.

6.2. Future studies

Nanoamorphous and nanocrystalline formulations were superior in their dissolution performance compared to the macro-sized formulations. In addition, *in vivo* studies should be performed to develop an IVIVC correlation for these solid nanoformulations.

There are several drying techniques available which impacts the physicochemical attributes of the solid nanoformulations. It will be important to investigate different drying techniques such as

freeze drying, spray-freeze drying, vacuum drying, solvent evaporation, microwave drying, *etc.* to understand the impact of drying processing conditions on different CQAs (such as particle size, solid-state form, moisture content, and total product yield) of nanoamorphous and nanocrystalline formulations.

The focus of the present research was to develop stable solid nanoformulations for small molecules (~200-400 g/mol) *via* a comprehensive QbD approach. Until now, only a few oral protein formulations are approved by FDA. With the advancement in personalized medicine and genetic engineering, proteins and peptides are extensively investigated due to their chemical diversity and non-toxicity. Stability of such biomolecules during processing is an important concern. It will be interesting to investigate critical process (such as spray drying, freeze drying) and formulations parameters (protein/peptide/stabilizer compositions) that significantly impact different CQAs (such as activity, size, and any structural change) for these large molecular weight compounds *via* a QbD approach. Developing robust oral protein/peptide drug products with enhanced bioavailability and activity will aid formulation scientists to gain important insights on their stability aspects. Furthermore, comprehensive QbD approach can be applied to other pharmaceuticals (such as microspheres, hydrogels and liposomes) to investigate critical process and formulation parameters involved during manufacturing of these complex dug products.